Dissertation zur Erlangung des Doktorgrades
der Fakultät für Chemie und Pharmazie
der Ludwig-Maximilians-Universität München

Mass Spectrometric Approaches to Study the Composition and Assembly of Centromere-Associated Complexes

Götz-Norman Karl Hagemann

aus

Offenbach am Main

2020

Erklärung

Diese Dissertation wurde im Sinne von § 7 der Promotionsordnung vom 28. November 2011 von Herrn Dr. Franz Herzog betreut.

Eidesstattliche Versicherung

Diese Dissertation wurde eigenständig und ohne unerlaubte Hilfe erarbeitet.

München, 17.11.20 .....

Götz-Norman Hagemann

Dissertation eingereicht am: 17.11.2020

1. Gutachter: Dr. Franz Herzog

2. Gutachter: Prof. Dr. Stefan Westermann

Mündliche Prüfung am: 16.12.2020

Table of Contents

1. Summary

Mitosis is the process of dividing a eukaryotic cell into two identical daughter cells. This part of the cell cycle executes the faithful propagation of the genome. A prerequisite for maintaining genome stability is the assembly of the conserved kinetochore structure at chromosomal loci called centromeres. The kinetochore is a macromolecular protein complex that physically links chromosomes to spindle microtubules. Aberrations in chromosome segregation cause aneuploidy, which has been associated with tumorigenesis, trisomy, and age-related pathologies. To ensure the accurate segregation of sister chromatids, their kinetochores have to be attached to microtubules emanating from opposite spindle poles, a configuration which is known as biorientation of chromosomes. The kinetochore is composed of more than 80 proteins, which are organized in stable subcomplexes and follow a conserved hierarchy of assembly from centromeric chromatin to microtubules: the centromere proximal inner kinetochore or Constitutive Centromere Associated Network (CCAN), the microtubule binding KMN (KNL1/MIS12/NDC80) network at the outer kinetochore and the fibrous corona. The proteins of the CCAN complex build the interface between centromeric chromatin and the microtubule-binding unit. Several kinetochore proteins are conserved among eukaryotes. In contrast, the underlying centromeric chromatin is highly divergent and epigenetically specified. The major epigenetic mark of the centromere are nucleosomes that have H3 replaced by centromere specific histone variant CENP-A. Interestingly, the levels of CENP-A are halved during DNA replication by equally distributing CENP-A between sister chromatids. Cells pass through mitosis with half-maximal CENP-A levels until they are replenished during mitotic exit. The underlying molecular pathways of histone redistribution during DNA replication and CENP-A replenishment in the early G1-phase remain largely unknown. In this thesis, I analyzed the protein composition of the human centromere in a time-resolved manner to study the quantitative changes in protein interactions of CENP-A containing oligo-nucleosomes. This proteomic screen detected several proteins that are associated with the centromere in a cell cycle-dependent manner and identified candidates that may regulate CENP-A distribution to the leading and lagging DNA strands subsequent to replication. Besides chromatin-associated proteins, histone remodelers, and readers and writers of histone post-translational modifications (PTMs), I identified an uncharacterized protein. This transcription

factor-like protein was selectively associated with CENP-A at levels comparable to CCAN proteins throughout the entire cell cycle, indicating that this protein may have a structural role at the centromere or inner kinetochore.

Spatial restraints derived from the mass spectrometric analysis of crosslinked proteins (XLMS) are widely applied in integrative structural biology approaches to determine protein connectivity. I used label-free quantification of crosslink spectral data to show the dependence of crosslink distances and intensities, which facilitated the estimation of protein dissociation constants and aided the prediction of interfaces of budding yeast subunit contacts. The load-bearing link of chromosomes to microtubules through the kinetochore is stabilized through phosphorylation of CCAN and KMN proteins by mitotic kinases. Titration of the assembly of up to 11 budding yeast kinetochore proteins in vitro indicated that phosphorylation of CCAN and KMN proteins induces cooperative stabilization of the kinetochore at the centromeric nucleosome, which is required to withstand the pulling forces of depolymerizing microtubules. Phosphorylation of distinct sites at the outer kinetochore subunit Dsn1 by AuroraB^{Ipl1}, and at the inner kinetochore protein Mif2, mediated cooperativity of the kinetochore assembly. These phosphorylation events decreased the KD values of the kinetochore protein-interactions to the centromeric nucleosome by ~200-fold, which was essential for cell viability. This work demonstrates the potential of quantitative XLMS for characterizing mechanistic effects on protein assemblies upon post-translational modifications or cofactor interaction and for biological modeling.

2. Preface

This study was performed in the laboratory of Dr. Franz Herzog. From November 2014 to November 2020, I was working on two main projects described in this thesis. A detailed description based on the state of the art will introduce both projects as both deals with the investigation of the cell cycle regulation of centromeric chromatin and kinetochore assembly.

The thesis was split into two parts, each of which will be introduced separately. The results of my first project will be summarized as a manuscript with the title: "Quantitative Crosslinking and Mass Spectrometry Determine Binding Interfaces and Affinities Mediating Kinetochore Stabilization" that was submitted. Parts of these results were presented in an international conference: EMBO workshop "Chromosome segregation and aneuploidy" from May 11-15th 2019 in Cascais, Portugal; Poster title: "Measuring Cooperativity in Multi-Protein Complex Assemblies by Quantitative Crosslinking Mass Spectrometry." An extended discussion follows the results part in which I discuss the topics of the manuscripts in more detail, as well as future research directions for the field.

> **Hagemann G***, Solis-Mezarino V*, Singh S, Potocnjak M, Kumar C, Herzog F. (2020) Quantitative Crosslinking and Mass Spectrometry Determine Binding Interfaces and Affinities Mediating Kinetochore Stabilization. *(in revision)*

The second part contains my research on the human centromere-specific histone H3 variant CENP-A. This second part will be introduced, based on the main introduction and further specified on human centromeres and centromeric chromatin. The results of this part will be discussed based on the latest research giving future directions of the project.

Several collaborative projects were performed with coworkers from the laboratories of Prof. Dr. Stefan Westermann (ZMB, Essen) and Dr. Kevin D. Corbett (Ludwig Institute for Cancer Research, University of California, San Diego). These projects are not subject to this work.

Publications

1) Ye Q, Kim DH, Dereli I, Rosenberg SC, **Hagemann G**, Herzog F, Tóth A, Cleveland DW, Corbett KD. (2017) The AAA+ ATPase TRIP13 remodels HORMA domains through N-terminal engagement and unfolding. *EMBO J*. doi: 10.15252/embj.201797291.

2) West AM, Rosenberg SC, Ur SN, Lehmer MK, Ye Q, **Hagemann G**, Caballero I, Usón I, MacQueen AJ, Herzog F, Corbett KD. (2019) A Conserved Filamentous Assembly Underlies the Structure of the Meiotic Chromosome Axis. *Elife* doi: 10.7554/eLife.40372.

3) Fischböck-Halwachs J, Singh S, Potocnjak M, **Hagemann G**, Solis-Mezarino V, Woike S, Ghodgaonkar-Steger M, Weissmann F, Gallego LD, Rojas J, Andreani J, Köhler A, Herzog F. (2019) The COMA Complex Interacts With Cse4 and Positions Sli15/Ipl1 at the Budding Yeast Inner Kinetochore. *Elife* doi: 10.7554/eLife.42879.

4) Killinger K, Böhm M, Steinbach P, **Hagemann G**, Blüggel M, Jänen K, Hohoff S, Bayer P, Herzog F, Westermann S. (2020) Auto-inhibition of Mif2/CENP-C Ensures Centromere-Dependent Kinetochore Assembly in Budding Yeast. *EMBO J. doi: 10.15252/embj.2019102938*

5) Ghodgaonkar-Steger M, Potocnjak M, Zimniak T, Fischböck-Halwachs J, Solis-Mezarino V, Singh S, Speljko T, **Hagemann G**, Herzog F. (2020) C-terminal motifs of the MTW1 complex cooperatively stabilize outer kinetochore assembly in budding yeast. *Cell Rep*. doi: 10.1016/j.celrep.2020.108190.

3. Main Introduction

3.1 Introduction

The proliferation of all eukaryotes depends on the equal and accurate segregation of chromosomes during cell division. The foundation of this process is the duplication of the DNA sequence and its dynamic organization by nucleoproteins into chromatin throughout the progression of the cell cycle. The nucleosome, as the basic unit of chromatin, comprises a core particle with 147 bp of DNA wrapped ~1.7 times around a histone octamer. Two molecules, each of the core histones H2A, H2B, H3, and H4, form a canonical histone octamer (Luger et al., 1997). Still, the nucleosome remains a highly versatile and modular structure. Changes in composition by incorporating various histone variants and the addition of multiple posttranslational-modifications (PTMs) can modulate the packaging and accessibility of DNA and adapt it to various needs to read and regulate expression or transmission of the genetic information (Ahmad and Henikoff, 2002, Kamakaka and Biggins, 2005, Probst et al., 2009).

Consequently, the nucleosome make-up provides the basis of chromatin organization and orchestrates all DNA-templated processes, like transcriptional regulation, DNA repair, or dense packing of DNA chromosome protection (Rieder et al., 2012, Malik and Henikoff, 2003). Chromatin assembly and quality control are tightly aligned with DNA replication for reliable maintenance of chromatin organization. Reassembly of chromatin after DNA replication occurs either by recycling modified parental histones or by the deposition of newly synthesized ones (Gunjan et al., 2005, Marzluff and Duronio, 2002). The propagation of chromatin domains is dependent on these mechanisms (Ransom et al., 2010, Alabert and Groth, 2012, Probst et al., 2009). Accordingly, the current perspective proposes two models of histone mark propagation (Stellfox et al., 2013). In the first model, chromatin formation after replication happens randomly out of a pool of old and new histones (De Rop et al., 2012). Although easy to implement for the cell, there are some disadvantages. Random incorporation of histones would result in the dilution of PTMs and, consequently, in a loss of significance of the defined chromatin domains (Dunleavy et al., 2011). Also, the histone distribution relative to the DNA sequence is likely to change, which causes a change of transcription

patterns (Margueron and Reinberg, 2010, Probst et al., 2009). The second model proposes a semi-conservative distribution of histone dimers by a histone deposition machinery (Xu et al., 2010). However, proof of this model is still a matter of active research, and hence, the precise mechanism remains elusive. A key factor of this machinery could be the proliferating cell nuclear antigen (PCNA), a DNA clamp protein involved in DNA replication (Stillman, 1986, Smith and Stillman, 1989, Shibahara and Stillman, 1999, Stewart-Morgan et al., 2020). Several studies showed its capability to recruit DNA polymerase along with chromatin remodeling factors, cell-cycle regulators, and helicases (Gerard et al., 2006). Up to now, a remodeling complex necessary for the incorporation of parental histone dimers, has not yet been identified. A detailed analysis of the CENP-A associated protein complexes will help us to understand the molecular mechanism of CENP-A deposition that propagates chromatin organization and epigenetic inheritance. Histone recycling by distribution onto sister DNAs after replication is vital for maintaining chromatin organization and the identity of specialized chromatin domains like centromeres.

3.2 Centromere Size and Composition

Centromeres are specialized chromatin domains that establish the molecular basis for genomic stability. After DNA condensation, centromeres are visible as primary constrictions of the mammalian metaphase chromosomes and are the sites of kinetochore formation where spindle microtubules are attached to mediate chromosome segregation during mitosis and meiosis. Kinetochores facilitate the segregation of bivalents in the reductional division, known as meiosis, and the distribution of sister chromatids to obtain two identical daughter cells in mitosis. They have to withstand DNA replication stress, topological constraints, and pulling forces of depolymerizing microtubules during anaphase (Manuelidis, 1978, Vissel and Choo, 1987, Henikoff et al., 2001). Despite the high phylogenetic conservation of centromere function, the complexity, placement, and density are quite diverse among different species (Willard and Waye, 1987, Grady et al., 1992, Cleveland et al., 2003, Plohl et al., 2014, Schueler et al., 2001). In budding yeast, the centromere consists of a 125bp DNA sequence sufficient to define centromere function (Clarke and Carbon, 1980). The simplicity of these ‘point centromeres’ (CEN) enabled intense studying of the minimally required proteins for chromosome segregation. These centromeres organize into three distinct

'centromere DNA elements' (CDE) (Clarke and Carbon, 1980). CDEI is only partially conserved and 8bp long (Cumberledge and Carbon, 1987). CDEII is an AT-rich 78-86bp sequence; CDEIII consists of a palindromic sequence and is essential for kinetochore assembly (McGrew et al., 1986, Ng and Carbon, 1987, Cumberledge and Carbon, 1987). However, most eukaryotic species have 'regional centromeres,' which are complex assemblies of simple repeated DNA sequences (Fukagawa and Earnshaw, 2014, Kursel and Malik, 2016). As shown in multiple species like the orangutan, horse, chicken, mice, or human, a specific pattern of repeated DNA elements defining centromere identity has not been identified (Wade et al., 2009, Locke et al., 2011, Piras et al., 2010, Shang et al., 2010). Despite the efforts on finding a centromere consensus DNA sequence in metazoans, neither a consensus nor a defined order of sequences can be described, which demonstrates a satellite higher-order repeat (HORs) structure (Vissel and Choo, 1987, Alkan et al., 2011).

Human centromeres are composed of centromeric chromatin flanked by pericentromeric heterochromatin (Schueler and Sullivan, 2006). The core centromere contains an array of higher-order repeats of 171 bp α-satellite DNA (Alexandrov et al., 2001, Choo et al., 1991, Waye and Willard, 1987). While higher-order α-satellite DNA sequences at centromeres slightly differ between chromosomes, all chromosomes, except the Y-chromosome, contain a 17 bp motif termed CENP-B box (Ikeno et al., 1994). This sequence is explicitly recognized and bound by the centromeric protein CENP-B, which is the only human kinetochore protein with DNA sequence specificity (Hemmerich et al., 2008). In contrast, monomeric α-satellite DNA, which resides in the pericentromeric region, varies significantly in sequence and lacks a higher-order organization (Schueler and Sullivan, 2006). This species-specific enrichment of a characteristic repetitive sequence, like the α-satellite DNA in humans repeats, is not strictly required for kinetochore formation (Ohzeki et al., 2002).

Centromeres are epigenetically defined by the presence of the centromere-specific histone H3 variant CENP-A, except budding yeast point centromeres, that are specified by a distinct DNA sequence (Palmer et al., 1987, Yoda et al., 2000, Furuyama and Biggins, 2007). Unlike the distinct spatial organization of DNA sequence-specific point centromeres in budding yeasts, the regional centromeres of other eukaryotes span several hundred kilobases to several megabases (Aldrup-Macdonald and Sullivan, 2014). Here, all active centromeres harbor large arrays

of CENP-A nucleosomes interspersed by those carrying histone H3 (Westhorpe et al., 2015). However, number and distribution vary between species ranging from a single CENP-A^{Cse4} containing nucleosome in budding yeast to ~200 CENP-A nucleosomes per centromere in humans (Lawrimore et al., 2011, Black and Cleveland, 2011, Hasson et al., 2013). The incorporation of CENP-A histones into centromeric chromatin is essential in all organisms (Blower and Karpen, 2001, Howman et al., 2000, Goshima et al., 2003, Oegema et al., 2001, Regnier et al., 2005, Stoler et al., 1995, Takahashi et al., 2000). As new centromeres (i.e., neocentromeres) are known to establish at chromosomal loci that do not have any sequence similarity to canonical centromeres but are solely characterized by the presence of CENP-A nucleosomes, CENP-A deposition is the most upstream event of centromere formation, which results in the recruitment of most known centromere and kinetochore proteins (Ishii et al., 2008, Ketel et al., 2009, Shang et al., 2013, Heun et al., 2006, Olszak et al., 2011). Artificial tethering of LacI tagged CENP-A to DNA containing the Lac operator sequence was sufficient for centromere formation and for the recruitment of all kinetochore proteins to stably attach to spindle microtubules (Mendiburo et al., 2011, Gascoigne et al., 2011). Importantly the site of neocentromere self-propagated even after the loss of LacI-CENP-A tethering (Hori et al., 2013). This finding has supported the assumption that epigenetic events define centromeres, although repetitive alphoid DNA can induce centromere formation in humans (Barnhart et al., 2011, Guse et al., 2011).

The centromeric chromatin domain is present throughout the cell cycle. It acts as a platform for the transient assembly of the kinetochore, which builds up a microtubule binding unit in mitosis just in time before chromosomes are attached and biorientated (Hegemann and Fleig, 1993, Pluta et al., 1995, Clarke, 1998). Aberrations in chromosome segregation can lead to aneuploidy, which has been associated with congenital disabilities, infertility, cancer, and aging (Ly et al., 2019).

3.3 Inner Kinetochore Composition and Specification.

CENP-A specifies the recruitment of several proteins to build up functional kinetochores. Kinetochores are highly conserved and composed of approximately 100 proteins (in humans) organized in distinct subcomplexes and assemble in a defined hierarchy from centromeric DNA to microtubules (Tipton et al., 2012).

The centromere-proximal or inner kinetochore complex includes at least 16 proteins, which are organized in subcomplexes that identify as constitutive centromere associated network 'CCAN' (organized in subcomplexes as CENP-C; CENP-L/-N; CENP-H/-I/-K/-M; CENP-O/-P/-Q/-U/-R; CENP-T/-W/-S/-X) (Figure 1) (Cheeseman and Desai, 2008). Besides CENP-A, CENP-C is an essential CCAN component that directly interacts with CENP-A containing nucleosomes (Falk et al., 2015, Falk et al., 2016, Kato et al., 2013). CENP-C was initially identified in patients with CREST syndrome (Earnshaw and Rothfield, 1985). Like CENP-A, most organisms have functional CENP-C homologs, although the overall sequence homology between human CENP-C and the yeast ortholog Mif2 is low (Brown, 1995, Meluh and Koshland, 1995). Its depletion causes severe chromosome defects resulting in cell death (Saitoh et al., 1992, Brown et al., 1993, Brown, 1995, Tomkiel et al., 1994, Meluh and Koshland, 1995, Fukagawa and Brown, 1997, Fukagawa et al., 1999, Holland et al., 2005, Heeger et al., 2005, Moore and Roth, 2001).

Particular domains are well conserved between yeast and humans, and protein sequence analysis of CENP-C and its orthologs suggests that most of the protein is intrinsically disordered (Kato et al., 2013, Holland et al., 2005, Klare et al., 2015, Nagpal et al., 2015, Screpanti et al., 2011). The CENP-C N-terminus provides an interaction site for the microtubule-proximal outer kinetochore subcomplexes (Screpanti et al., 2011, Przewloka et al., 2011). Ectopic targeting of this domain induces the assembly of a functional kinetochore lacking other CCAN proteins (Hori et al., 2013). Along the carboxy-terminal half of the protein are two related short motifs (central domain and CENP-C motif) required to interact with centromeric chromatin (Nagpal et al., 2015, Klare et al., 2015). At the very C-terminus resides a cupin fold domain, which induces dimerization (Cohen et al., 2008). Another critical domain of vertebrate CENP-C is the PEST-rich domain that was shown to interact with CENP-H and CENP-L/N proteins of the CCAN (Nagpal et al., 2015, Klare et al., 2015). While CENP-C provides a direct link of centromeric chromatin to the microtubule-binding outer kinetochore, it is the dynamically modulated cornerstone of faithful chromosome segregation (Klare et al., 2015, Nagpal et al., 2015). Notably, the depletion of CENP-C in chicken DT40 cells did not result in the loss of other CCAN proteins (Fukagawa et al., 2001, Hori et al., 2008, Kwon et al., 2007). The interactions of CENP-C with other CCAN subunits and how these affect kinetochore assembly and stabilization was further investigated in this work.

The three CCAN subcomplexes (CENP-L/-N; CENP-H/-I/-K/-M; CENP-O/-P/-Q/-U/-R) form a 'Y'-shaped structure that was obtained from cryo electron microscopy reconstructions from recombinant *S. cerevisiae* proteins (Hinshaw and Harrison, 2019, Yan et al., 2019). Like their human orthologs, the yeast proteins co-purify in *in vivo* pull-downs and are interdependent for kinetochore localization (Foltz et al., 2006, Akiyoshi et al., 2009). Despite the similarities in connectivity and assembly of CCAN proteins between budding yeast and vertebrates, not all CCAN proteins have orthologs in humans (Figure 1) (Cheeseman and Desai, 2008). Notably, almost all human CCAN proteins are required for mitosis, while only CENP-Q^{Okp1} and CENP-U^{Ame1} together with CENP-C^{Mif2} are essential in budding yeast (Hornung et al., 2014, De Wulf et al., 2003). Depletion of human CENP-U and CENP-Q result in comparably mild phenotypes (Foltz et al., 2006, Hornung et al., 2014). This striking difference could point to a different organization of budding yeast and human kinetochores, yet sequence conservation and domain arrangement of the orthologous proteins indicate substantial architectural similarity (Hinshaw and Harrison, 2019, Yan et al., 2019). Notably, subunit connectivity differences may reflect the requirement for linking microtubules to point or regional centromeres in budding yeast and humans, respectively. In humans, CENP-N binds selectively and directly to the L1-loop in the CENP-A targeting domain (CATD) of CENP-A (Pentakota et al., 2017). This second axis of kinetochore attachment is more interlaced with the other CCAN components and probably underlies a dynamic regulation (Pentakota et al., 2017). Likewise, CENP-N, despite its direct binding to CENP-A containing nucleosomes, needs to simultaneously interact with other CCAN components for stabilization (Weir et al., 2016, Pentakota et al., 2017). CENP-N forms a heterodimeric complex with CENP-L, which directly binds to the CENP-H/-I/-K/-M subcomplex and CENP-C (McKinley et al., 2015, Weir et al., 2016). In the assembly process, CENP-N and CENP-C can bind CENP-A simultaneously at different binding sites (Weir et al., 2016, Pentakota et al., 2017). CENP-H/-I/-K/-M form a stable complex that is important for chromosome alignment, segregation, and viability by maintaining the integrity and stability of the CCAN (Basilico et al., 2014, Weir et al., 2016). Human CENP-M has a pseudo GTPase activity of unknown function and lacks an ortholog in yeast (Basilico et al., 2014). The yeast orthologs of CENP-N/-L, Chl4/Iml3 do not interact with the CENP-A^{Cse4} nucleosome but reside more central in the 'Y'-shaped structure of the CCAN (Hinshaw and Harrison, 2019, Yan et al., 2019). Even though CENP-N^{Chl4} is

required for faithful chromosome segregation in yeast, it remains elusive how its position in the kinetochore and its contacts with other CCAN proteins can contribute to this function without affecting viability (Hinshaw and Harrison, 2019, Yan et al., 2019, Carroll et al., 2009). CENP-L^{Iml3} forms the interface with CENP-H ^{Mcm16}/-I ^{Ctf3}/-K ^{Mcm22} along with CENP-T ^{Cnn1}/-W ^{Wip1} and generates one arm of the 'Y' (Hinshaw and Harrison, 2019, Yan et al., 2019). Several studies suggested that the vertebrate CENP-T/-W/-S/-X subcomplex forms a nucleosome-like complex that binds to 80-100 bp of DNA and introduces positive supercoils into DNA *in vitro* (Takeuchi et al., 2014). In contrast, in budding yeast, CENP-T^{Cnn1} /CENP-W^{Wip1} were found to co-localize with centromeric chromatin in a CENP-I^{Ctf3} dependent manner (Pekgoz Altunkaya et al., 2016). CENP-S and CENP-X are neither necessary for viability nor conserved between budding yeast and vertebrates (Hori et al., 2008). The N-terminus of budding yeast CENP-T^{Cnn1}, similar to the vertebrate CENP-T, directly binds to the microtubule-binding Ndc80 complex in a phosphorylation-dependent manner. Hence CENP-T offers an additional scaffold for microtubule-binding (Pekgoz Altunkaya et al., 2016, Malvezzi et al., 2013). Due to its centered position, CENP-N^{Chl4} interacts on one side with the more elongated CENP-P/-Q/-O/-U (Ctf19, Okp1, Mcm21, Ame1 in yeast: COMA complex) subcomplex that generates the opposite arm and stem of the 'Y'-shape (Hinshaw and Harrison, 2019, Yan et al., 2019). Notably, the CENP-U^{Ame1}/CENP-Q^{Okp1} heterodimer of the COMA complex is a direct and selective interactor of the N-terminal tail of CENP-A^{Cse4} (Anedchenko et al., 2019, Fischbock-Halwachs et al., 2019). Remarkably, the Okp1 core domain (AA163–187) interacts with AA34-46 of CENP-A^{Cse4} (Fischbock-Halwachs et al., 2019).

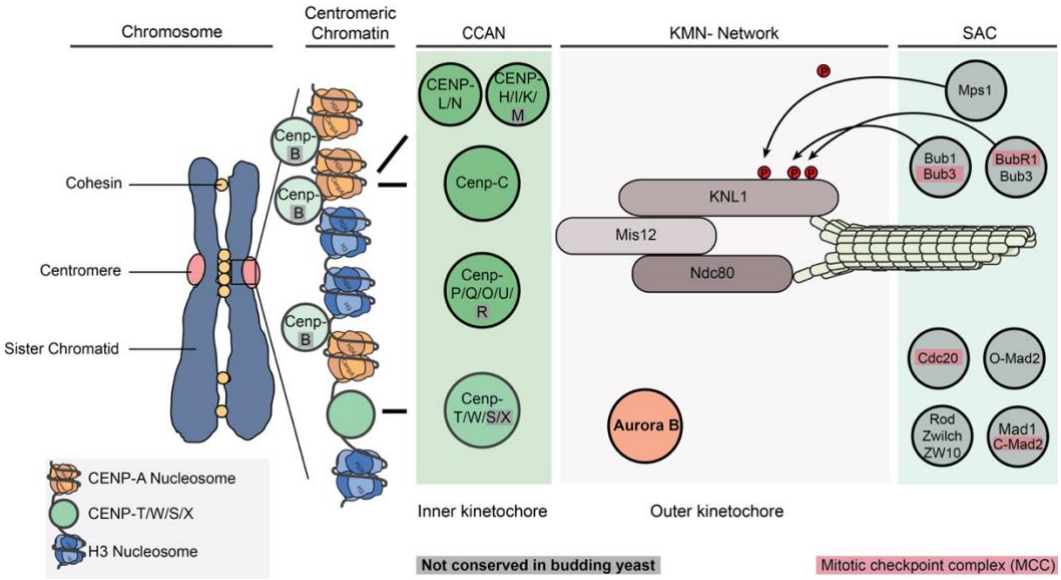

Figure 1. Schematic Representation of the Human Kinetochore Topology.

The highly conserved hierarchy of kinetochore modules is depicted from centromeric chromatin to the microtubule binding interface. Proteins that are not conserved in budding yeast are grayed out. Centromeric chromatin is composed of CENP-A containing nucleosomes (orange) interspersed by patches of H3 containing nucleosomes (blue). The first assembly step is the interaction of the proteins that build the centromeric chromatin and the constitutive centromere associated network (CCAN). Proteins of the CCAN are constitutively bound to CENP-A containing nucleosomes. This module recruits the outer kinetochore complexes of the KMN network by forming protein contacts between CENP-C and the MIS12 complex and CENP-T and the NDC80 complex. The binding of NDC80 to microtubules from opposing spindle poles is monitored by a surveillance mechanism called the spindle assembly checkpoint (SAC). The SAC delays cell cycle progression until an AuroraB kinase-mediated correction mechanism resolves all improper attachments.

Even though the enormous efforts in reconstituting vertebrate and yeast kinetochores expand our understanding of the molecular interactions, the complicated features of their interaction network and their interdependency for centromere localization are not entirely understood. Especially the dynamics of transient protein interactions and their influence on dynamic alterations of single CCAN interactions throughout the cell cycle are particularly intriguing. How PTM events influence kinetochore assembly dynamics has been challenging to explore

and will be addressed in this work. Gaining insights into the architecture of the centromere-proximal subcomplexes of the kinetochores and the interactome of centromeric chromatin will significantly improve our understanding of cell cycle regulation, mitotic checkpoint establishment, and chromatin dynamics.

3.4 Composition of the Microtubule-Binding Outer Kinetochore

On the microtubule-proximal site, the outer kinetochore forms a load-bearing link between the CCAN proteins and the plus ends of the spindle microtubules. The highly conserved framework of the outer kinetochore is a 10-subunit protein assembly known as KMN-network (KNL1-, MIS12- and NDC80-complex) (Cheeseman et al., 2004). The primary microtubule receptor at the kinetochore is the four-subunit NDC80 complex (NDC80 [Hec1 in humans], Nuf2, Spc24, Spc25) (Figure 1) (Ciferri et al., 2008). The large coiled coils, flanked by globular domains, resulting in a dumbbell-like structure, dominate the morphology of the complex (Ciferri et al., 2008, Wei et al., 2007, Wei et al., 2005). Its primary function, microtubule-binding, is mediated by the N-terminal side of the structure, built by Ndc80 and Nuf2 (Wan et al., 2009). Structural analysis has shown that a pair of tightly packed calponin-homology (CH) domains in Nuf2 and Ndc80 impart direct interaction with microtubules (Ciferri et al., 2008, Wei et al., 2007, Wei et al., 2005). Besides the CH domains, two basic patches in the unstructured N-terminal tail of Ndc80 showed microtubule-binding capabilities *in vitro* (Ciferri et al., 2008). Interestingly, only the deletion of the CH domains and not the basic segments in the N-terminal tail resulted in a loss of microtubule interaction (Ciferri et al., 2008). Whether these segments mediate an intermolecular interaction of NDC80-complexes or promote a cooperative binding effect by forming NDC80-complex clusters of microtubules is highly controversial. However, microtubule interaction of Ndc80 is dynamically regulated by phosphorylation events that antagonize the intrinsic positive charge, which results in a marked decrease in the binding affinity (DeLuca et al., 2006). AuroraB^{Ipl1} mediates this phosphorylation (DeLuca et al., 2006, Guimaraes et al., 2008). C-terminally, the RWD-domains of the NDC80-complex subunits Spc24 and Spc25 directly interact with the CCAN protein CENP-T (Malvezzi et al., 2013). Within the KMN-network, the MIS12-complex, consisting of Mis12, Pmf1, Dsn1, Nsl1, or MIND-/MTW1-complex (Mtw1, Nnf1, Dsn1, Nsl1) in budding yeast, acts as a

central interaction hub to facilitate the assembly and attach the KMN to the CCAN by interaction with CENP-C, CENP-T (in most organisms), and CENP-U^{Ame1}/-Q^{Okp1} (only in yeast) (Malvezzi et al., 2013, Dimitrova et al., 2016). The MIS12-complex is, like all members of the KMN-network, highly conserved between human and yeast and organized as a four-protein rod-shaped structure that seems to extend the Ndc80-complex (Dimitrova et al., 2016). The stable subcomplexes Mis12/ Pmf1 and Dsn1/Nsl1 meet in the central stalk domain, whereby the C-termini of the Dsn1/ Nsl1 subcomplex provide binding sites for the RWD domains of the Spc24/25 subunits of the Ndc80-complex (Hornung et al., 2011, Maskell et al., 2010, Petrovic et al., 2010). The C-terminal end of Nsl1, together with the stalk domain, also provides a binding interface for the two-member KNL1-complex (KNL1/Zwint) (Hornung et al., 2011, Maskell et al., 2010, Petrovic et al., 2010). Besides its C-terminus that contains RWD-domains, KNL1 is vastly disordered and has some microtubule-binding affinity (Krenn et al., 2014, Lampert and Westermann, 2011). However, cell biological and biochemical work has shown that it has several conserved protein-binding motifs (Zhang et al., 2014, Vleugel et al., 2013, Krenn et al., 2014). The very N-terminus harbors a protein phosphatase1 (PP1) binding domain, followed by multiple MELT-repeats (Met, Glu, Leu, Thr) (Krenn et al., 2014). Mps1 kinase phosphorylates the Thr of the MELT-repeats, forming a binding hub for the spindle assembly checkpoint (SAC) protein complex consisting of Bub1 and Bub3 (Krenn et al., 2014).

The NDC80 complex, along with the KNL1 complex, builds an elaborate microtubule-binding site (Lampert and Westermann, 2011). In particular, the NDC80 complex supports load-bearing microtubule attachments *in vitro* (Lampert and Westermann, 2011). The depletion of any KMN component leads to an aberrant kinetochore structure and, in the worst case, to a complete lack of kinetochore-microtubule attachments in all eukaryotes. Factually, spindle attachment is the crucial step of mitosis. Therefore, sister chromatids and their kinetochores are monitored by tight surveillance systems, whose components -in case of an error- interact with the kinetochore architecture most likely provided by KNL1 (Lara-Gonzalez et al., 2012).

3.5 Regulation of Kinetochore Microtubule Attachments and the Spindle Assembly Checkpoint

Kinetochores not only mediate the proper attachment of spindle microtubules but detect unattached kinetochores by their tension state and regulate the progression of mitosis by the SAC (Welburn et al., 2010). Although the essential components of the SAC have been identified, the precise signaling mechanism remains enigmatic and remains a matter of ongoing research (Lampson and Cheeseman, 2011). An important turning point in mitosis is the transition from metaphase to anaphase (Lampson and Cheeseman, 2011). Before the onset of anaphase, all sister chromatid kinetochores are attached to microtubules of opposing spindle poles (Gordon et al., 2012). After achieving bi-oriented microtubule attachment, the Anaphase-Promoting Complex/Cyclosome (APC/C), an E3-ubiquitin ligase, promotes the degradation of several substrates, like B-type cyclins, and securin by ubiquitination for degradation by the 26S proteasome (Peters, 2006). Securin inhibits separase, the protease which - once activated - cleaves a subunit of the cohesin complexes that hold bi-oriented sister chromosomes together (Cohen-Fix et al., 1996, Funabiki et al., 1996, Holloway et al., 1993, King et al., 1995, Sudakin et al., 1995). Hence, inhibition of APC/C activity delays the onset of anaphase and therefore is the principal target of the SAC (Glotzer et al., 1991). In particular, the four-protein mitotic checkpoint complex (MCC) directly binds and inhibits the APC/C by incorporating the coactivator Cdc20 (Foe et al., 2011, Foster and Morgan, 2012, Pan and Chen, 2004).

The assembly of the MCC eventuates at unattached kinetochores (Sudakin et al., 2001, Fraschini et al., 2001, Kim and Burke, 2008, Malureanu et al., 2009). Here, the MELT repeats in KNL1 are phosphorylated by Mps1 (Krenn et al., 2014). MELT-(p) recruits the SAC proteins Bub3, Bub1, and its paralog BubR1 (Krenn et al., 2014). Bub1 serves as the primary hub and recruits other SAC components (Rischitor et al., 2007, Vanoosthuyse et al., 2004). After Bub1 and BubR1 bind Bub3 through their so-called GLEBS motifs, the proteins bind the MELT-(p) motif (Krenn et al., 2014, Overlack et al., 2017). For Cdc20 co-inhibition, Mad2 has to be recruited to the kinetochore (Musacchio and Salmon, 2007, Luo and Yu, 2008). In higher eukaryotes, Mad2 recruitment is most likely achieved by the interaction of Mad1/Mad2 with the RZZ-complex (Rod, Zwilch, ZW10) (Kops et al., 2005, Musacchio and Salmon, 2007). Here the conformation of Mad2 changes from a

soluble O-Mad2 (open) to a C-Mad2 (closed) state, which is capable of binding Cdc20 (Luo and Yu, 2008). The mature MCC consists of Bub3, BubR1, C-Mad2, and Cdc20 that can signal a single unattached kinetochore to prevent anaphase onset (Musacchio and Salmon, 2007). Mps1 recruitment to the kinetochore is key to SAC-signaling and the onset of anaphase (Maciejowski et al., 2010, Hewitt et al., 2010, Santaguida et al., 2010). Although the critical determinant of Mps1 recruitment is the Ndc80 complex, the coordination of Mps1 within the kinetochore remains unknown.

Before anaphase onset, microtubule-binding requires to be such dynamic that erroneous microtubule attachments can be corrected while bi-oriented attachments on chromosomes remain stable during anaphase (Lampson et al., 2004, Pinsky et al., 2006). Balancing these two conflicting requirements is regulated in part by reversible phosphorylation of the KMN-network (Foley and Kapoor, 2013). The conserved main effector proteins in this error-correction mechanism are the kinase Aurora B (Ipl1 in yeast) and the phosphatase B56-PP2A (Lampson and Cheeseman, 2011). Aurora B^{Ipl1}, together with INCENP, Survivin, and Borealin (Sli15, Bir1, and Nbl1 respectively in yeast), form the chromosomal passenger complex (CPC) that is targeted to centromeric chromatin and acts as a molecular ruler in a tension-sensing manner (Lampson and Cheeseman, 2011). In brief, the tension on erroneously attached kinetochores is lower compared to bi-oriented kinetochores (Figure 2) (Yoo et al., 2018). When the tension is low, the distance between the kinetochore and centromere is small and within the reach of Aurora B, destabilizing microtubule attachments by phosphorylation (Lampson and Cheeseman, 2011). If the tension increases, the spatial distance of the microtubule attachment also increases and eventually exceeds the range of Aurora B activity (Lampson et al., 2004). Recent publications found several pools of Aurora B acting independently of the CPC framework (Fischbock-Halwachs et al., 2019, Campbell and Desai, 2013). Accordingly, misaligned chromosomes display enriched Aurora B levels at centromeres and kinetochores (Salimian et al., 2011).

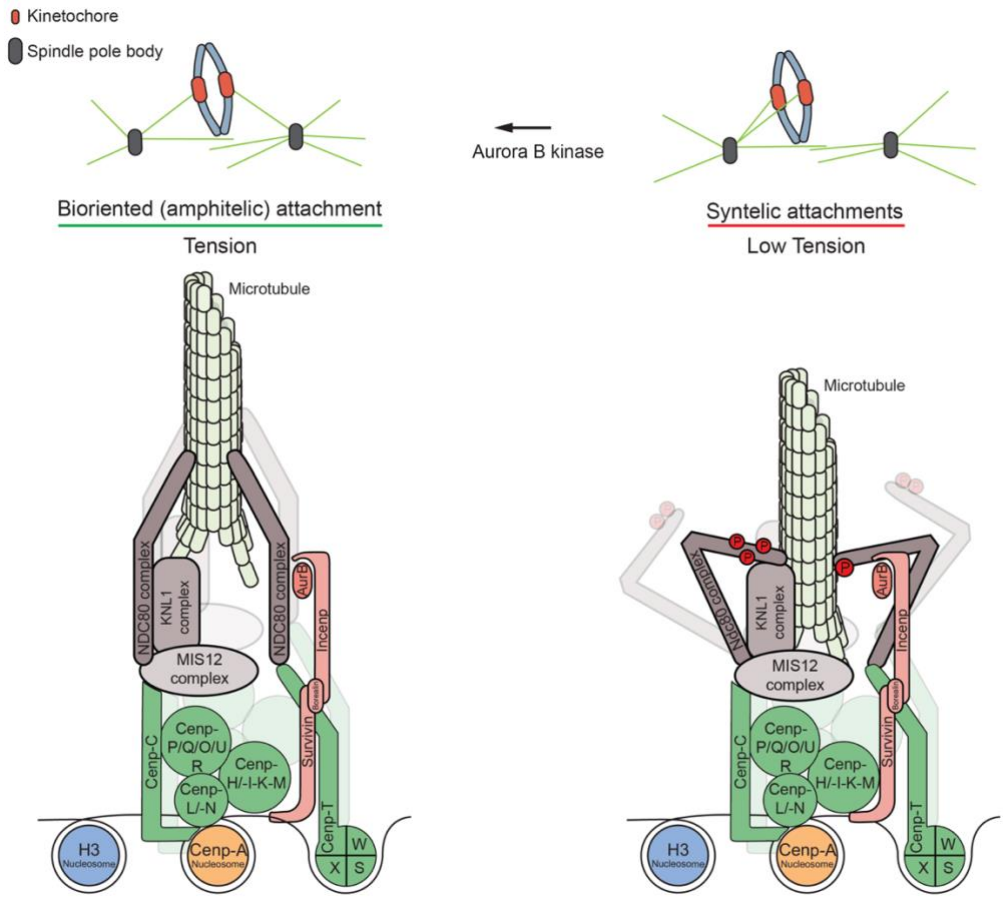

Figure 2. Schematic Representation of Tension Induced Error Correction.

A single incorrectly attached kinetochore can prevent cell cycle progression. Incorrect microtubule attachments occur quite frequently and are corrected in a tension sensing process. When microtubules depolymerize, the applied tension leads to intra- and inter-kinetochore stretching. The lack of tension in incorrect microtubule attachments results in AuroraB phosphorylation of the microtubule binding interface and the recruitment of the spindle assembly checkpoint (SAC) to the kinetochore. This enables the correction of microtubule attachments. Here the chromosomal passenger complex (CPC) acts as a 'molecular ruler' that detaches the microtubules from the kinetochore. The SAC is recruited to unattached kinetochores and halts cell cycle progression by inhibiting APC/C activity. When tension across centromeres is achieved by bioriented (amphitelic) microtubule attachment, the SAC is deactivated, and the cell cycle progresses.

After correct kinetochore-microtubule attachment, the phosphorylation of the KMN-network is decreased by the antagonizing phosphatase B56-PP2A (Foley

and Kapoor, 2013). Regulation of kinetochore-microtubule attachments depends on an interlinked and sophisticated network of SAC proteins, Aurora B, and additional proteins, including Polo-like kinase 1 (Plk1) (Suijkerbuijk et al., 2012). Polo-like kinases are a conserved subfamily of serine/threonine protein kinases that play a substantial role throughout the cell cycle (Combes et al., 2017, Liu et al., 2017). Plk1 is recruited via its polo box domain (PBD) to the CCAN protein CENP-U which is phosphorylated by Plk1 (Kang et al., 2006). In addition, the PBD of Plk1 interacts with multiple components of the outer and inner kinetochore (Combes et al., 2017). However, the mechanism underlying the recruitment of Plk1 to these sites is mostly unclear. Without sufficient Plk1 activity, cells suffer severe chromosome misalignment and kinetochore instabilities (Lera et al., 2019). Hence, this kinase is an essential regulator of microtubule-kinetochore attachments and kinetochore robustness (Lera et al., 2019). The substrate specificities of Plk1 and Mps1 are largely overlapping as both can phosphorylate the MELT repeats of KNL1 (von Schubert et al., 2015).

Furthermore, there is tight crosstalk between Plk1 and Aurora B, which affects their activities at the kinetochore (Joukov and De Nicolo, 2018). Additionally, Plk1 is often deregulated in a multitude of human cancers and targeted in therapeutic cancer drugs (Liu et al., 2017). How these mitotic protein kinases interact in the spatiotemporal context of the kinetochore to guide various mitotic events is key to our understanding of the coordination of chromosome segregation.

4. Quantitative Crosslinking and Mass Spectrometry Determine Binding Interfaces and Affinities Mediating Kinetochore Stabilization

4.1 Introduction

The importance of the timely assembly of the macromolecular kinetochore complex to ensure accurate chromosome segregation in eukaryotes raises the important questions of how it is built up and what are the underlying regulatory mechanisms controlling the formation of this high-affinity linkage between centromeric nucleosomes and microtubules? Notably, the role of internal stabilization of the CCAN and the KMN through phosphorylation to generate stable microtubule attachment and biorientation remains elusive. Various protein kinases coordinate kinetochore functions (Saurin, 2018). As mentioned earlier, Mps1 initiates the mitotic checkpoint, BubR1 controls microtubule attachment, AuroraB corrects erroneous microtubule attachments, Haspin kinase helps to align chromosomes, and Plk1 serves several purposes, including the stabilization of end-on microtubule attachments (Saurin, 2018). The localization of each kinase reflects their distinct roles within the structure of the kinetochore (Saurin, 2018). Plk1 phosphorylates substrates throughout the entire kinetochore, either by binding them directly or through adjacent proteins (Lera et al., 2016, Saurin, 2018). Many interaction partners are crucial, as Plk1 is tethered to distinct proteins within the kinetochore; it can solely phosphorylate in the vicinity of this kinetochore subcompartment (Lera et al., 2016, Saurin, 2018, Qi et al., 2006). Most Plk1 interacting proteins are found at the KMN network (Saurin, 2018). However, Plk1 localization at the CCAN and centromeric chromatin has been shown to be essential for proper alignment and faithful chromosome segregation, but the corresponding substrates remain unclear (Kang et al., 2006).

Several studies reported the cooperative binding of kinetochore proteins (Hornung et al., 2014, Dimitrova et al., 2016, Weir et al., 2016, Pesenti et al., 2018). Thus far, there is only speculation about why kinetochore proteins act in

cooperative binding networks. The size and complexity of the kinetochore limit the possibility of studying all interactions and their modulations that happen. The use of hybrid structural approaches might overcome these limitations.

4.1.1 Identification of Protein-Protein Interactions

Protein-protein interactions (PPIs) and their fundamental essence in biology led to the development of multiple sophisticated methods to analyze the protein interactome. Despite most of the techniques like co-immunoprecipitation, affinity purification in combination with mass spectrometry (AP-MS), proximity-dependent biotin identification (BioID), or conventional yeast two-hybrid screening (Y2H) are successfully used to map protein interactions, - each has its deficiencies (Smits and Vermeulen, 2016). Besides requiring tedious genetic modifications, most of the techniques have time-consuming experimental workflows and conceivably result in alteration of structural properties of the proteins (Smits and Vermeulen, 2016). Furthermore, the ability to gain quantitative information on protein complex abundance and composition from AP-MS experiments is limited (Smits and Vermeulen, 2016).

In the field of proteomics, liquid chromatography coupled with mass spectrometry (LC-MS) is the primary protein analytics technology. Mass spectrometry (MS) examines molecules based on their mass to charge ratio (m/z) (Eliuk and Makarov, 2015). In combination with chromatography and ionization methods, MS can resolve proteins and peptides after ionization and sort them based on their masses (Domon and Aebersold, 2006). The information enables the quantification of the peptides and fragmentation into smaller molecules (Domon and Aebersold, 2006). Reconciling the derived masses with theoretical databases enables identifying the proteins in a sample (Cox and Mann, 2008). A typical workflow in this approach, also known as shotgun-proteomics, begins with the extraction and purification of proteins from the cell or any other biological sample (Domon and Aebersold, 2006, Cox and Mann, 2008). The isolated proteins are digested into peptides by endopeptidases with particular cleavage specificity (e.g., trypsin) (Olsen et al., 2004). Subsequently, the peptides are separated by chromatography based on their hydrophobicity charged by an ionization source, focused further by the mass spectrometer based on their m/z ratios and identified by a detector within the machine (Aebersold and Mann, 2003). These peaks result in the first spectral data or MS1 spectrum. Some of these peptides qualify for fragmentation

into smaller molecules. Here their masses are again analyzed and stored in a spectrum (MS2 spectrum).

During fragmentation of a peptide, the bondage break occurs at the amino acid backbone of the sequence (Ong and Mann, 2005). Thus, the MS2 spectrum of a peptide contains masses of its complete sequence and fragments (Ong and Mann, 2005). Protein candidates from a sequence database are cleaved *in silico* to their theoretical peptides following the rules of the endopeptidase of choice (e.g., trypsin) (Cox and Mann, 2008). Finally, the experimental spectra are checked against the theoretical database to match the masses' best identification for the protein identity (Cox and Mann, 2008).

The spectra also contain quantitative information as the MS1 spectral intensity corresponds to the relative abundance of peptides in the sample (Ong and Mann, 2005). As the peak intensity is not in direct proportion to the protein abundance, MS is not intrinsically a quantitative method, which led to the development of several quantification methods (Ong and Mann, 2005). Some are reliant on protein labeling techniques either through metabolic (e.g., SILAC) or chemical approaches (e.g., TMT) (Ong et al., 2003, Thompson et al., 2003). These tags allow mixing and analyzing different cell or protein populations simultaneously, as the labeling-introduced mass-shift enables the discrimination between each population (Ong et al., 2003, Thompson et al., 2003). Under distinct experimental conditions, the relative changes in peptide intensities infer differences in protein abundance (Bantscheff et al., 2007). Alternatively, label-free approaches utilize computational strategies to obtain quantitative information on MS derived spectral data (Bantscheff et al., 2007). These are either based on the count of peptide fragmentation (spectral counting) or the sum of intensities obtained from all precursor peptide scans (Bantscheff et al., 2007). Both approaches have assets and drawbacks, but label-free quantification is, in general, less precise, yet less tedious and expensive (Bantscheff et al., 2007). Besides improvements in these methods, neither can discriminate between direct and indirect protein interactions nor determine the topology or dynamics of protein complexes.

4.1.2 Quantitative Chemical Cross-Linking followed by Mass Spectrometry

The combination of chemical cross-linking and mass spectrometry (XLMS) facilitates the characterization of large protein complexes and has emerged over the past two decades as a versatile tool for identifying protein connectivity and topology (O'Reilly and Rappsilber, 2018). Typically, protein cross-linking is implemented by using homo-bi-functional *N-Hydroxysuccinimide* (NHS)-esters (O'Reilly and Rappsilber, 2018). The reactive groups form bridges between the ε-ammonium groups of the lysines nearby. Thereby varying the spacer length between the functional groups controls the range of interaction (O'Reilly and Rappsilber, 2018). The covalent linkages between the protein's lysines enable to analyze the interactions, which happen within distances beneath the spatial restraint of the linker length (O'Reilly and Rappsilber, 2018). Cross-link derived distance restraints identify interactions at peptide resolution and allow to pinpoint sites of interaction.

A cross-link sample contains several moieties of peptide species, whereby the dominating amount is linear peptides, but also several cross-linking products (Holding, 2015). Most interesting are inter- and intra-protein cross-links, which harbor most structural information (Holding, 2015, Leitner, 2016). Besides, two more cross-links species occur that are generally less informative — Loop-links form when the endopeptidase is not cleaving between the cross-link residues (Holding, 2015). Moreover, mono-links occur when one side of the cross-linker is inactive by either hydrolysis or amination (Holding, 2015, Leitner, 2016).

A comprehensive characterization of protein complexes goes beyond determining its members and their stoichiometry. Furthermore, the binding interfaces and the affinities their interactions establish within the protein complex play a significant role. High-resolution structural methods cannot characterize the majority of known protein complexes, either by the limitation of resolving flexible regions of the protein or due to their sheer size (Chavez and Bruce, 2019). Therefore, most protein domain interactions remain unexplored for the lack of structural information (Chavez and Bruce, 2019, Schmidt and Urlaub, 2017). Even low-resolution structural data would be sufficient to characterize such interactions more comprehensively (Leitner, 2016, Schmidt and Urlaub, 2017). However, these experimental approaches that necessitate mutagenesis of specific amino acid

residues are either arduous or have low accuracy (e.g., hydrogen/deuterium exchange [HXD]) and XLMS) (Leitner, 2016). Computational approaches have low specificity and are not suitable to make sophisticated statements about protein complexes (Xue et al., 2011). Combining the advantages of both methods might deliver the best results.

Indeed, quantification of cross-link intensities bears excellent possibilities to understand protein-protein binding events on a peptide level (Solis-Mezarino, 2019). Recent developments of bioinformatics pipelines for the label-free quantification of cross-links now allow the detection of conformational changes within protein complexes and will allow the weighted use of distance restraints in integrative modeling (Walzthoeni et al., 2015, Solis-Mezarino, 2019, Schmidt et al., 2013, Fischer et al., 2013).

For this purpose, we established a bioinformatics pipeline, which is based on modified tools from the OpenMS framework, which was described earlier (Solis-Mezarino, 2019). We observed a linear dependency of cross-link peak intensity and Euclidean lysine-lysine distance (Solis-Mezarino, 2019). This not only bears the potential to identify interaction sites within protein complexes but might guide computational modeling even for *de novo* protein structure prediction. Based on this observation, we used statistical modeling to estimate apparent binding affinities of *in vitro* reconstituted yeast kinetochore protein complexes expressed in *E. coli* or insect cells. The results of this project are presented in the format of a manuscript (in revision) and will be further discussed in a separate section.

4.2 Aims of the Work

As previously demonstrated by Victor Solis-Mezarino in his thesis (Solis-Mezarino, 2019), the quantification of cross-links by mass spectrometry (qXLMS) aids the determination of binding interfaces and facilitates the estimation of binding affinities of several subunit in contacts in protein complexes. Hence, quantitative crosslink data provide a measure for the kinetic description of the assembly and stabilization of protein complexes and how post-translational modifications and ligand binding may affect the molecular mechanism of protein complexes.

The formation of interactions is described by the apparent constant of dissociation (K_D) and is critical to characterize complex formation. However, standard methods for K_D measurements almost exclusively assess binary interactions and have limitations with respect to protein concentration, size, and sample amounts. This pipeline has the potential to measure multiple protein interactions simultaneously that are necessary to establish macromolecular complexes. I applied this pipeline to study the interactions of a minimal budding yeast kinetochore assembled on a CENP-A^{Cse4} containing nucleosome by qXLMS. The *in vitro* reconstitution of CCAN and KMN complexes interacting with CENP-A^{Cse4} containing nucleosomes was expected to provide insights into the assembly of a high-affinity CENP-A^{Cse4} nucleosome binding complex and how it is stabilized by phosphorylation. Ultimately, I aimed to address the following questions:

- What is the dynamic range of estimating apparent K_D values by qXLMS?

- What are the interfaces of key interactions that mediate the cooperative stabilization of the kinetochore at CENP-A^{Cse4} containing nucleosomes?

- What are the specific phosphorylation sites that mediate the cooperative stabilization of the kinetochore resulting in a high-affinity kinetochore complex that resists the pulling forces of depolymerizing microtubules in mitosis?

4.3 Results

Quantitative Crosslinking and Mass Spectrometry Determine Binding Interfaces and Affinities Mediating Kinetochore Stabilization

Goetz Hagemann[1†], Victor Solis-Mezarino[1†], Sylvia Singh[1], Mia Potocnjak[1], Chandni Kumar[1] and Franz Herzog[1*].

1 Gene Center and Department of Biochemistry, Ludwig-Maximilians-Universität München, Munich 81377, Germany.

* Correspondence to: herzog@genzentrum.lmu.de (F.H.)

†These Authors contributed equally to this work.

Abstract

Crosslinking and mass spectrometry (XLMS) are used in integrative structural biology to acquire spatial restraints. We found a dependency between crosslink distances and intensities and developed a quantitative workflow to simultaneously estimate apparent dissociation constants (K_D) of contacts within multi-subunit complexes and to aid interface prediction. Quantitative XLMS was applied to study the assembly of the macromolecular kinetochore complex, which is built on centromeric chromatin and establishes a stable link to spindle microtubules in order to segregate chromosomes during cell division. Inter-protein crosslink intensities facilitated determination of phosphorylation-induced binding interfaces and affinity changes. Phosphorylation of outer and inner kinetochore proteins mediated cooperative kinetochore stabilization and decreased the K_D values of its interactions to the centromeric nucleosome by ~200-fold, which was essential for cell viability. This work demonstrates the potential of quantitative XLMS for characterizing mechanistic effects on protein assemblies upon post-translational modifications or cofactor interaction and for biological modeling.

Main

Distance restraints derived from the mass spectrometric identification of crosslinked amino acids (XLMS) are widely applied in integrative approaches to determine protein connectivity (O'Reilly and Rappsilber, 2018) and to model the topology of proteins and their domains in a complex (Rout and Sali, 2019). Quantification of crosslinks has been initially implemented to detect conformational changes and domain interactions (Fischer et al., 2013, Schmidt et al., 2013, Walzthoeni et al., 2015). Besides structure, the critical determinant of the molecular mechanism of a complex is the interaction strength of its subunit contacts, which can be modulated through cofactors or post-translational modifications to execute its biological function on time. Several biophysical methods (Rossi and Taylor, 2011) are available to measure protein-protein affinity through estimation of the apparent dissociation constant (K_D), but the individual methods mainly analyze binary interactions and require high protein concentrations, protein engineering, immobilization or labeling which may affect the integrity of complexes. We reasoned that crosslink intensities provide a quantitative measure for the formed complex and the free subunits at the equilibrium state. Thus, we investigated whether crosslink intensities facilitate the simultaneous estimation of individual protein-protein affinities within kinetochore multi-subunit complexes.

The kinetochore is a macromolecular protein complex assembled at centromeric chromatin that ensures the fidelity of chromosome segregation by connecting chromosomes and spindle microtubules and by integrating feedback control mechanisms (Biggins, 2013, Musacchio and Desai, 2017). In order to bi-orient chromosomes on the mitotic spindle the budding yeast kinetochore has to transmit forces of ~10 pN (Akiyoshi et al., 2009, Powers et al., 2009) by forming a load-bearing attachment to spindle microtubules and a high-affinity link to the centromeric nucleosome, marked by the histone H3 variant $Cse4^{CENP\text{-}A}$ (human orthologs are superscripted if appropriate). The kinetochore subunits are largely conserved between budding yeast and humans (Schleiffer et al., 2012, van Hooff et al., 2017) and form stable subcomplexes, which are organized in two layers of the kinetochore architecture. The outer kinetochore, a 10-subunit network that is built up on the inner kinetochore, forms the microtubule binding site. The inner kinetochore is assembled by at least 15 proteins on centromeric chromatin with Mif2 and Ame1/Okp1 directly linking the outer kinetochore MTW1 (Mtw1/Nnf1/Dsn1/Nsl1) complex to the Cse4-NCP (Cse4 containing nucleosome

core particle) in budding yeast (Anedchenko et al., 2019, Fischbock-Halwachs et al., 2019, Xiao et al., 2017, Hornung et al., 2014). Whereas the human kinetochore assembly is temporally regulated, establishing a microtubule attachment site in mitosis, budding yeast kinetochores are built up and attached to a single microtubule almost throughout the entire cell cycle (Biggins, 2013, Gascoigne and Cheeseman, 2013, Hara and Fukagawa, 2020). In both species, phosphorylation of Dsn1^{DSN1} by the mitotic kinase Ipl1^{AuroraB} stabilizes the recruitment of the outer to the inner kinetochore (Akiyoshi et al., 2013, Dimitrova et al., 2016, Petrovic et al., 2016). In addition, phosphorylation of the human kinetochore by Plk1 has been shown to stabilize the inner kinetochore architecture at centromeric chromatin to withstand the pulling forces of depolymerizing microtubules (Lera et al., 2019).

By quantifying crosslink-derived restraints we found a dependency between crosslink distances and intensities. This relation was applied to improve the prediction of protein binding interfaces and to determine apparent K_D values of their interactions, which provided quantitative measures to capture different functional states of the kinetochore. Our approach facilitated the detection of phosphorylation-induced changes in binding affinities between the centromeric nucleosome and a minimal kinetochore assembly composed of the outer kinetochore MTW1^{MIS12} complex, the inner kinetochore Mif2^{CENP-C} and Ame1/Okp1$^{CENP-U/Q}$ proteins.

Results

Determination of Crosslink Intensity and its Dependence on Crosslink Distance

To quantify protein crosslinks, we first extracted the MS1 peak intensities of the MS2 based crosslink identifications using an in-house bioinformatics pipeline that merges the open-source software tools xQuest/xProphet (Herzog et al., 2012, Walzthoeni et al., 2012) and OpenMS (Rost et al., 2016) (Figure 3 and Methods). Protein complexes were crosslinked by modifying the α-amino groups with the isotopically labeled BS2G-d_0/d_6 reagent and crosslinked peptide fractions were analyzed by liquid chromatography coupled to tandem mass spectrometry. The raw files were processed by the xQuest/xProphet software to identify the crosslinked peptides, their precursor ion masses and retention times. This information was subsequently used for the extraction of ion chromatograms by the OpenMS software tool, which were summarized in text tables. The quantification

pipeline was benchmarked against available datasets showing that our bioinformatics workflow performs similarly to previously reported software tools in terms of signal detection rate and accuracy of quantification and is independent of the crosslinker type (Figure 9).

Quantifying the crosslinks of published multi-protein complex datasets (Iacobucci et al., 2019, Jennebach et al., 2012) and mapping the corresponding Euclidean lysine-lysine distances on available crystal structures, including those of RNA polymerase I and II, indicated that shorter Euclidean distances between the crosslinked lysines correlate with increasing crosslink intensities (a and Figure 10). We assumed that the inter-protein crosslink intensity is also affected by the physicochemical microenvironment of individual lysines as well as by a competition for the formation of intra-, inter-protein or mono-links at a specific lysine site during the crosslinking reaction. To assess whether crosslink intensities increase for lysine sites proximal to binding interfaces, we mapped the intensity values along the sequences of the RPB1-RPB2 interaction in RNA polymerase II (Figure 11a) as well as of the budding yeast kinetochore Cnn1-Spc24/25 interaction (Figure 11b). We normalized the inter-protein crosslink intensities to the sum of intensities of intra- and inter-protein crosslinks and monolinks occurring at a specific lysine residue. This normalized intensity value or 'Relative Interface Propensity Index' (RIPI) served as an indicator for putative interface sequences and was applied in an heuristic approach together with secondary structural elements, sequence conservation and other parameters to aid in the prediction of protein-protein interfaces (Figure 11 and Methods).

Estimation of protein affinities based on crosslink intensities

We further applied inter- and intra-protein crosslink intensities to estimate the concentrations of the formed complex and the free subunits according to the steady state equilibrium in solution. To assess whether crosslink intensities supported the estimation of binding affinities we purified recombinant kinetochore subunits and titrated complex formation over a range of molar ratios. First, the inner and outer kinetochore proteins $Cnn1^{1-270}$ and Spc24/25 (Malvezzi et al., 2013), respectively, were titrated by applying molar ratios from 0.05:1 to 2:1 (Figure 3, Figure 12, and Figure 13). To capture the equilibrium state of the binding reaction by crosslinking, the reaction time of the BS2G-d_0/d_6 reagent was limited to 2 minutes. Intra-protein crosslink intensities of the constant interactor facilitated the normalization between titration steps and those of the titrated interactor enabled the calculation of a linear regression of the intra-protein

intensities on the increasing input protein concentrations (Figure 12, and Figure 13). The regression model was applied to interpolate the concentration of the formed complex from the inter-protein crosslink intensities (Figure 3).

The estimation of the apparent K_D value was performed first by the *Scatchard* plot (Scatchard, 1949) (Figure 4 and Methods) that indicates the K_D value as the negative inverse of the slope. We calculated the K_D values for three different sets of inter-protein crosslinks (Figure 4). Applying either all inter-protein crosslinks to $Cnn1^{1-270}$ or only those intersecting with the structured domains of Spc24/25 resulted in K_D values of ~120 nM or ~50 nM, respectively. The subset of inter-links decorating the $Cnn1^{60-84}$ motif, that is required for mediating the interaction with Spc24/25, showed a K_D of ~15 nM which agrees with the value previously obtained by isothermal titration calorimetry (ITC) (Malvezzi et al., 2013). This observation is consistent with the notion that residues proximal to the interface may be stably positioned and thus yield relatively higher inter-protein crosslink intensities. The second method used the steady state equilibrium equation to calculate the mean of K_D values of each titration step from the concentrations of the formed complex and the free interactors (Figure 3, c). The second approach based on the steady state equilibrium equation closely reproduced the values obtained by the *Scatchard* plot. Moreover, a similar experiment was performed by titrating increasing concentrations of the $Cnn1^{60-84}$ peptide, containing the minimal binding motif, against the Spc24/25 dimer. The estimated K_D value of 2.6 μM (Figure 14, and Figure 15) agrees with previous ITC measurements (Malvezzi et al., 2013) and suggests that Cnn1 sequences outside the $Cnn1^{60-84}$ motif contribute to the stabilization of the interaction.

Phosphorylation of the inner kinetochore by $Cdc5^{Plk1}$ induces its cooperative stabilization on Cse4 nucleosomes

To determine the apparent K_D values of the individual interactions that assemble the kinetochore on the octameric Cse4 nucleosome, we *in vitro* reconstituted kinetochore complexes of up to 11 recombinant proteins (Figure 5) purified from *E. coli*, except Mif2, which was isolated from insect cells (Methods). We first reproduced the interaction of Mif2 and Ame1/Okp1 (Hornung et al., 2014), both of which directly bind Cse4-NCPs (Anedchenko et al., 2019, Fischbock-Halwachs et al., 2019, Hinshaw and Harrison, 2019), and found that this interaction was lost upon dephosphorylation of Mif2 (Figure 5b). *In vitro* phosphorylation of lambda-phosphatase-treated Mif2 by the mitotic kinases $Cdc28^{CDK1}$, $Cdc5^{PLK1}$, $Ipl1^{AuroraB}$ and $Mps1^{MPS1}$ showed that $Cdc5^{PLK1}$ restored Ame1/Okp1 binding to levels detected

at insect cell-phosphorylated Mif2 (Figure 5b). For the subsequent XLMS and binding experiments Mif2 wild-type and mutant proteins were *in vitro* phosphorylated by Cdc5 and are indicated as Mif2*.

We first estimated apparent K_D values of the individual interactions of Cse4-NCP, Mif2* and Ame1/Okp1 by titrating the Cse4-NCP with increasing concentrations of Mif2* or Ame1/Okp1 and by titrating Ame1/Okp1 with Mif2* (Figure 5c, d, e, and Figure 16). The binding affinities of these binary interactions were then compared to the K_D values of these interactions in the Mif2*:Ame1/Okp1:Cse4-NCP complex. Only intra- and inter-protein crosslinks yielding the extraction of intensities from all 3 replicates (Figure 17 - Figure 24) were applied to estimate the apparent K_D values based on the steady state equilibrium equation. The affinities of the binary interactions ranging from 3 to 6 µM were increased 6-fold for the Mif2*:Cse4-NCP interaction and 10-fold for the Ame1/Okp1:Cse4-NCP and Mif2*:Ame1/Okp1 interactions in the Mif2*:Ame1/Okp1:Cse4-NCP complex, indicating cooperative stabilization upon the phosphorylation-induced Mif2*:Ame1/Okp1 interaction (Figure 5c, d).

Similar to the K_D calculation of the Cnn1$^{1-270}$:Spc24/25 interaction, the restriction of inter-protein crosslinks to the subset intersecting with the minimal binding motif, the Mif2$^{285-311}$ signature motif (Figure 5d and e) which directly binds the CENP-A C-terminus (Kato et al., 2013, Xiao et al., 2017), resulted in lower K_D values. The K_D value of the Mif2*:Cse4-NCP complex was reduced from 3.2 to 0.9 µM which is in agreement with ITC measurements of the Mif2$^{285-311}$ peptide with the Cse4-NCP showing a K_D of 0.5 µM (Kato et al., 2013). Upon the cooperative interactions of Mif2* and Ame1/Okp1 to the Cse4-NCP the K_D dropped by a factor of ~30 from 0.6 to 0.03 µM (Figure 5d and e) demonstrating that quantitative XLMS facilitates the estimation of apparent K_D values and the detection of ~200-fold affinity changes in multi-subunit complexes.

Phosphorylation of outer and inner kinetochore proteins synergistically enhance kinetochore stabilization at the Cse4 nucleosome

The tetrameric MTW1^{MIS12} complex binds Mif2^{CENP-C} and Ame1/Okp1. This interaction is stabilized upon Dsn1^{DSN1} phosphorylation by Ipl1^{AuroraB} which releases the masking of the Mif2^{CENP-C} and Ame1/Okp1 binding sites at the MTW1^{MIS12} head I domain by Dsn1^{DSN1} (Figure 5a) (Akiyoshi et al., 2013, Dimitrova et al., 2016, Emanuele et al., 2008, Yang et al., 2008). To test whether addition of

MTW1c affected the interactions of Cse4-NCP with Mif2* and Ame1/Okp1, we titrated constant levels of Cse4-NCPs with increasing concentrations of an equimolar mixture of Mif2*:Ame1/Okp1:MTW1c which contained either wild-type Dsn1 or the phosphorylation-mimicking Dsn1^{S240D,S250D} mutant (Figure 25). The quantification of inter-protein crosslinks (Figure 26 and Figure 27) intersecting with Mif2 indicated the previously reported Mif2 interfaces to the Cse4-NCP (Hornung et al., 2014, Kato et al., 2013, Xiao et al., 2017) and to the MTW1c (Figure 28 and Figure 29a) (Musacchio and Desai, 2017). The estimation of binding affinities by the steady state equilibrium equation revealed that addition of wild-type MTW1c did not affect the K_D values of Mif2* and Ame1/Okp1 to the Cse4-NCP (Figure 5d, Figure 6a and b). In comparison, the phosphorylation-mimicking MTW1c(Dsn1^{S240D,S250D}) decreased the K_D values by ~20-fold and a similar change in affinity was observed for the Mif2:Okp1 interaction (Figure 6a and b). This indicated that in addition to the Mif2*:Okp1 interaction, putatively mediated by Cdc5, phosphorylation of Dsn1 by Ipl1 synergistically enhanced the binding affinity of Mif2* and Ame1/Okp1 to the Cse4-NCP.

The phosphorylation-induced cooperativity mediating kinetochore stabilization is essential in budding yeast

The RIPI calculated from inter-protein crosslink intensities of the Mif2*:Okp1 interaction identified Mif2$^{150-250}$ and Okp1$^{180-220}$ as the putative binding motifs (Figure 5a, Figure 6c and Figure 29b). Based on the indicated regions, mutant proteins were generated to assess the required Mif2 phosphorylation sites mediating its interaction with Ame1/Okp1 in *in vitro* binding and cell viability assays. The Mif2$^{\Delta221-240}$ mutant abrogated the Mif2*:Ame1/Okp1 interaction *in vitro* whereas Mif2$^{\Delta200-230}$ still bound (Figure 7a). By assessing the phosphorylation dependency of this interaction (Figure 5b), we found that Ame1/Okp1 binding was lost upon mutating 9 serines to alanines within Mif2$^{217-240}$ (Figure 7a and Figure 30a). Ectopic expression of the Mif2 mutants, that were impaired in Ame1/Okp1 binding, did not affect growth of budding yeast cells after nuclear depletion of endogenous Mif2 (Figure 31, Figure 32a). Similarly, the Dsn1^{S240A,S250A,S264A} mutant, which has been previously shown to affect binding of the outer kinetochore MTW1 complex to the inner kinetochore, was viable (Figure 7b) (Akiyoshi et al., 2013). Notably, ectopic expression of the Mif2 mutants as only nuclear copies in a Dsn1^{S240A,S250A,S264A} mutant background showed that the Mif2$^{217-240*9S-A}$ mutant was synthetically lethal whereas the Mif2$^{177-229*9ST-A}$ and Mif2$^{232-240*5S-A}$ mutants grew normally (Figure 7b). The synthetic growth defect of only the

phosphorylation-deficient Mif2 mutants, that did not mediate interaction with Ame1/Okp1 *in vitro*, suggests that cooperative kinetochore stabilization through phosphorylation of Dsn1 and the Mif2 region 217-240 is required for cell viability.

The putative Okp1 interface region included 2 predicted helices (Figure 29b and Figure 30b). A deletion mutant of the helix motif Okp1$^{156-188}$, which was previously reported to be essential for binding the Cse4-END (essential-N-terminal-domain) (Fischbock-Halwachs et al., 2019), was lethal but still bound Mif2* *in vitro*, whereas the Okp1$^{196-229}$ helix deletion abrogated Mif2* binding (Figure 7c and Figure 30c) and inhibited cell growth (Figure 7d and Figure 32b). Both Okp1 helices form an α-helical hairpin-like structure (Figure 8) (Hinshaw and Harrison, 2019, Yan et al., 2019) suggesting that the putative phosphorylation of the 9 serines within Mif2$^{217-240}$ establishes a cooperative high-affinity binding environment for the Cse4-NCP by bringing the Mif2$^{217-240}$:Okp1$^{196-220}$, Cse4-END:Okp1$^{156-188}$ and Mif2$^{285-311}$:Cse4$^{C\text{-}term}$ contacts into close proximity (Figure 8 and Figure 28). Moreover, Ame1/Okp1 and Mif2$^{217-240*9S\text{-}A*}$ competed for binding to Mtw1/Nnf1 (Figure 5a) (Killinger et al., 2020) but formed a nearly stoichiometric complex with *in vitro* phosphorylated wild-type Mif2*, suggesting that phosphorylation of the Mif2$^{217-240}$ motif (Figure 5b) might facilitate the simultaneous stabilization of Mif2* and Ame1 at the same MTW1c (Figure 7e and Figure 8) (Dimitrova et al., 2016).

Discussion

Our observation that increasing crosslink intensities correlate with shorter crosslink distances lead to the development of a quantitative XLMS approach, which applies inter-protein crosslinks to characterize protein binding interfaces beyond the detection of the protein connectivity. This study demonstrates the capacity of inter-protein crosslink intensities to simultaneously estimate K_D values of individual contacts in multi-protein assemblies ranging from 6 to 0.015 µM. Notably, the subset of inter-links proximal to minimal binding interfaces yielded apparent K_D values that are in good agreement with values determined by ITC (c and Figure 5d). Moreover, the distance-intensity relation was exploited in the 'Relative Interface Propensity Index' to support the prediction of putative interface sequence regions, whose physiological importance was confirmed in cell viability assays.

To demonstrate the applicability of our workflow to datasets, which were not acquired as titration experiments for the purpose of this study, we analyzed the

XLMS dataset of the histone H3 methyltransferase Polycomb repressive complex 2 (PRC2) (Figure 8b) (Kasinath et al., 2018). Based on crosslink intensities we showed that binding of methylated JARID2 increases the relative affinity of the second cofactor AEBP2 to the PRC2 complex (Figure 8c, d), which is consistent with the observation of a compact active state upon methylation of JARID2 by electron microscopy (Kasinath et al., 2018). In addition, the sequence areas, indicated by the RIPI blot, are in good agreement with the binding interfaces of the PRC2 subunit SUZ12 with the cofactors, JARID2 and AEBP2, which were obtained from electron microscopy density maps (Figure 8e, f) (Kasinath et al., 2018).

By applying the quantitative XLMS method to analyze the budding yeast kinetochore assembly at centromeric nucleosomes, we identified the interface of the phosphorylation-dependent Mif2:Ame1/Okp1 interaction at the inner kinetochore (Figure 5a and b). The phosphorylation sites within the Mif2$^{217-240}$ motif established the Mif2:Ame1/Okp1 interaction *in vitro* (Figure 7a) and were required not only to generate a hub of Cse4 nucleosome binding motifs but might also induce the switch-like stabilization of Mif2 and Ame1 at the outer kinetochore MTW1 complex phosphorylated at the Dsn1 subunit (Figure 5a, Figure 7e and Figure 8). Together, phosphorylation of the outer kinetochore Dsn1 and the inner kinetochore Mif2 proteins resulted in a ~200-fold increase in Cse4 nucleosome binding affinity *in vitro* (Figure 5 and Figure 6) and expression of phosphorylation-ablative mutants resulted in synthetic lethality suggesting that the phosphorylation-induced cooperativity is important for kinetochore stabilization *in vivo*. This highlights the capacity of quantitative XLMS to detect the impact of two phosphorylation events on the cooperative stabilization of a macromolecular assembly by a sharp increase in binding affinities.

Although human and budding yeast kinetochores differ in subunit connectivity (Musacchio and Desai, 2017), the human orthologue of the MTW1 complex, MIS12c, has been implicated in CENP-A stabilization at centromeres (Kline et al., 2006). Moreover, we found that the Mif2:Okp1 interface is partially conserved in their human orthologues CENP-C:CENP-Q (Figure 33) and the CENP-C residue T667, which corresponds to Mif2 S226, shows a single nucleotide polymorphism, T667K, in malignant hepatic cancer cells (Wu et al., 2014).

We demonstrated that quantitative XLMS facilitated the mechanistic characterization of protein complexes beyond a structural description by estimating protein affinities and their relative changes upon protein modification

or ligand interaction. This quantitative XLMS method will significantly contribute to biological modeling at the molecular and cellular level and holds great promise for the development of diagnostic tools for studying the effects of drug interactions on protein complexes and the characterization of epitopes for protein therapeutics.

Acknowledgements

We thank Ruedi Aebersold, Stefan Westermann and Alexander Leitner for comments on the manuscript. GH and CK were funded by the Graduate School (GRK 1721) and MP was supported by the Graduate School (Quantitative Biosciences Munich) of the German Research Foundation (DFG). FH was supported by the European Research Council (ERC-StG no. 638218), the Human Frontier Science Program (RGP0008/2015), by the Bavarian Research Center of Molecular Biosystems and by an LMU excellent junior grant.

Data and materials availability: The mass spectrometry raw data was uploaded to the PRIDE Archive. The access information for reviewers is Project Name: Quantitative Crosslinking and Mass Spectrometry Detects Phosphorylation-Induced Kinetochore Stabilization, Project accession: PXD020094, Username: reviewer83353@ebi.ac.uk, Password: JFeuElbD.

Figure 3

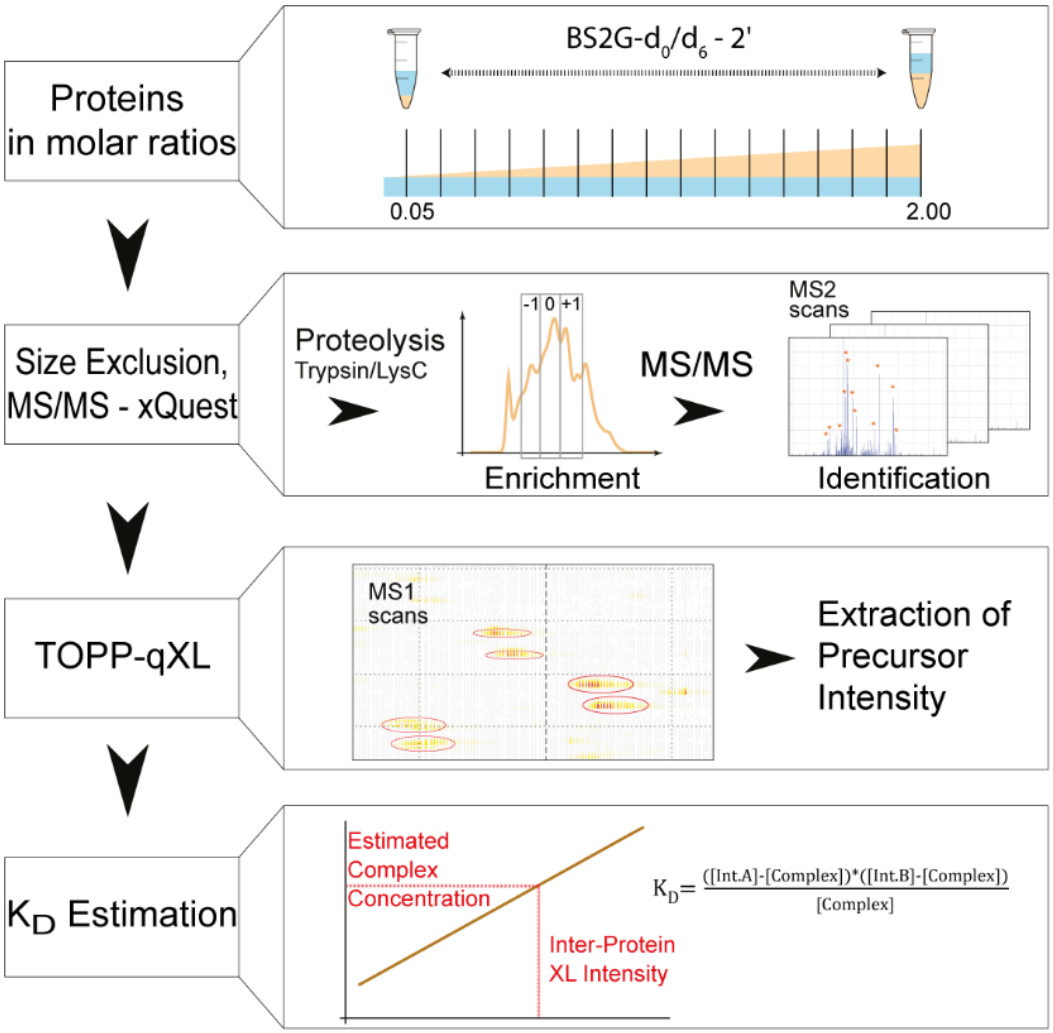

Figure 3. Schematic Workflow of Estimating Protein Affinities by Quantitative XLMS.

The binding partners were titrated by increasing the molar ratio of one interactor. Crosslinked proteins were proteolytically digested, enriched by size exclusion chromatography and linked peptides were identified by tandem mass spectrometry and the software xQuest(Herzog et al., 2012, Walzthoeni et al., 2012). Precursor intensities of the crosslinks were extracted using our TOPP-qXL (The OpenMS Proteomics Pipeline-quantitative XLMS) bioinformatics workflow. The intensities of intra- and inter-protein site-site links were applied to estimate the concentration of free interactors and complex and for the statistical modeling of apparent K_D values.

Figure 4

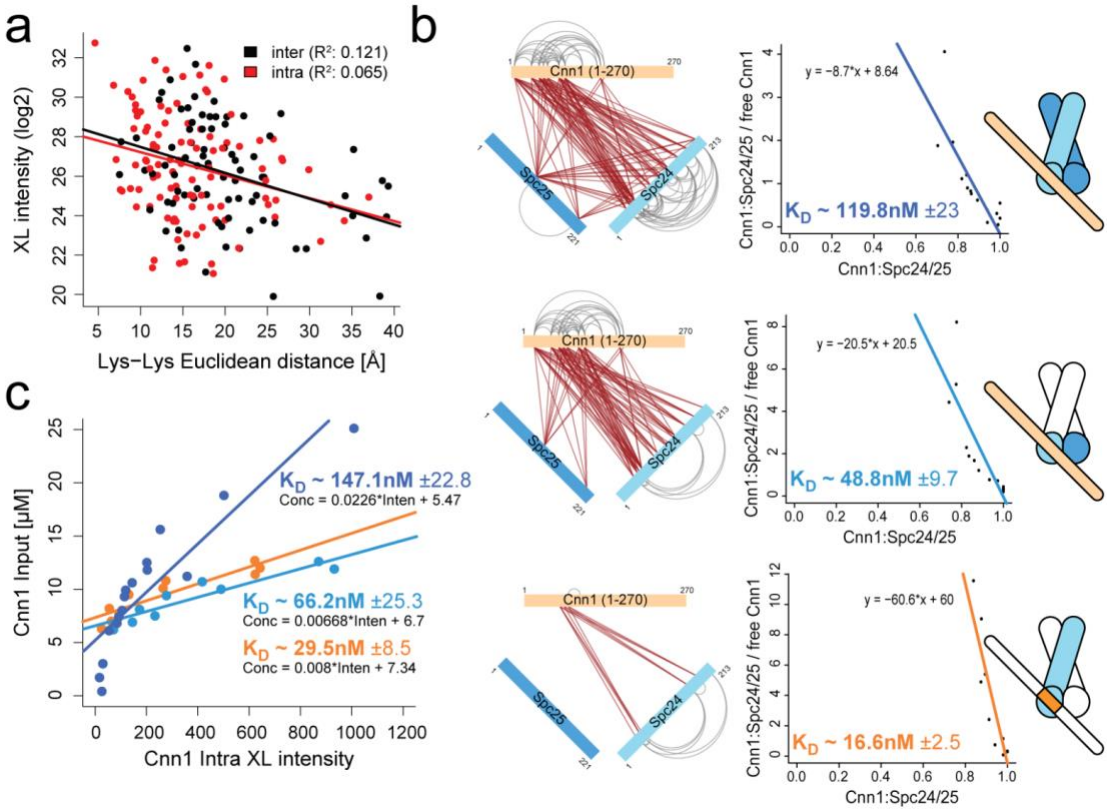

Figure 4. Estimation of apparent K_D values in protein complexes using quantitative XLMS.

a, Correlation of increasing crosslink intensities with decreasing Euclidean distances between crosslinked residues obtained from RNA polymerases analyses (Figure 10). The R-squared statistics and Fisher´s test was computed (p-value(intra)=0.00526, p-value(inter)=0.00098). **b**, Estimation of apparent K_D values of the $Cnn1^{1-270}$:Spc24/25 interaction by the *Scatchard* plot using different subsets of inter-protein crosslinks to quantify complex formation. **c**, Apparent K_D values were calculated based on the concentration of formed complex interpolated from the linear regression and averaged across molar ratios of the titration steps.

Figure 5

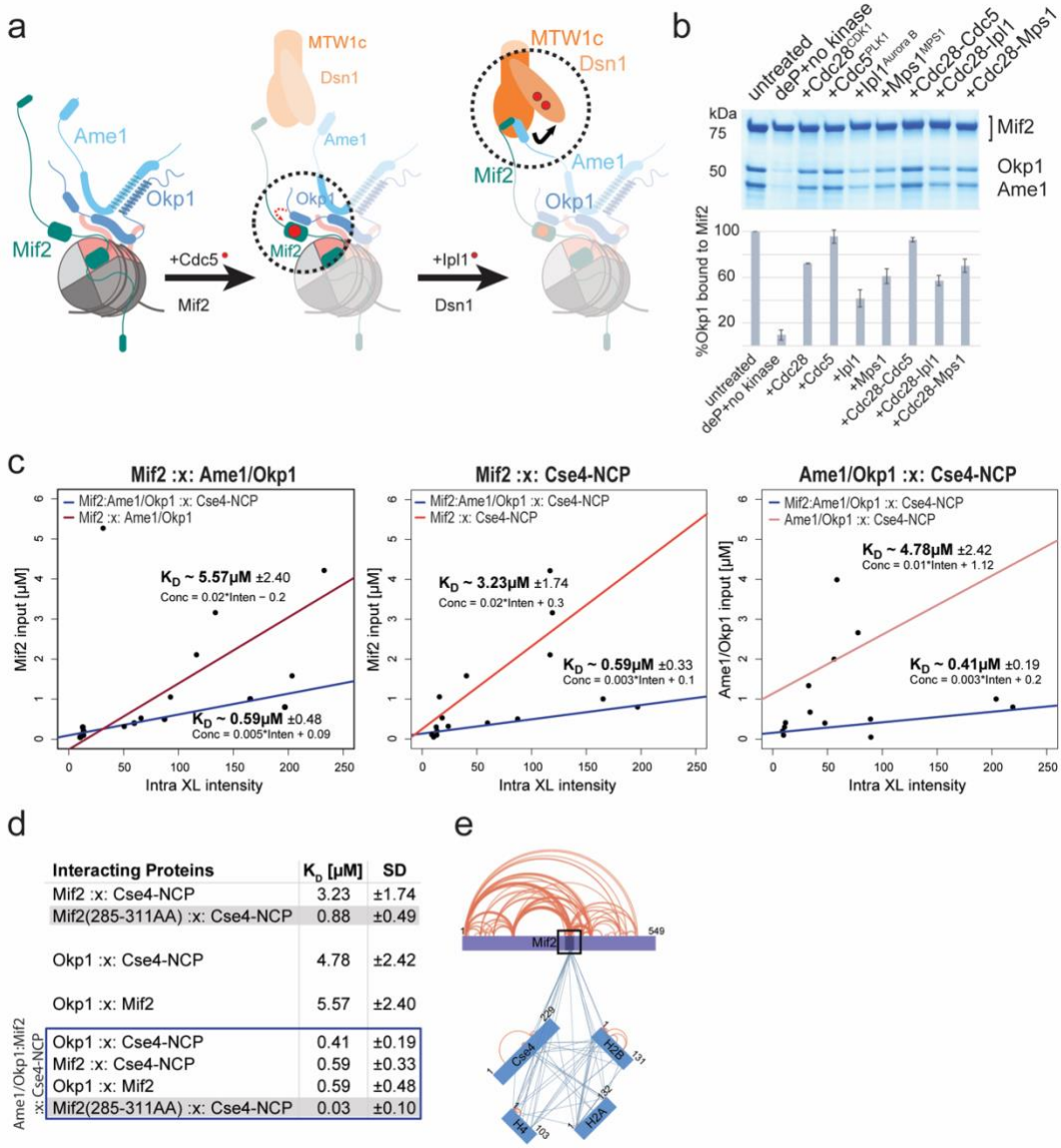

Ame1/Okp1:Mif2 :x: Cse4-NCP	Interacting Proteins	K_D [µM]	SD
	Mif2 :x: Cse4-NCP	3.23	±1.74
	Mif2(285-311AA) :x: Cse4-NCP	0.88	±0.49
	Okp1 :x: Cse4-NCP	4.78	±2.42
	Okp1 :x: Mif2	5.57	±2.40
	Okp1 :x: Cse4-NCP	0.41	±0.19
	Mif2 :x: Cse4-NCP	0.59	±0.33
	Okp1 :x: Mif2	0.59	±0.48
	Mif2(285-311AA) :x: Cse4-NCP	0.03	±0.10

Figure 5. The phosphorylation-dependent binding of Mif2* to Ame1/Okp1 cooperatively stabilizes their interactions with the Cse4-NCP.

a, Reconstitution of the Mif2:Ame1/Okp1interaction by dephosphorylation (deP) of Mif2 and subsequent *in vitro* phosphorylation with the indicated kinases (mean ±SD of 3 replicates). **b**, Schematic representation of the assembly of MTW1c, Mif2, and Ame1/Okp1 on the Cse4-NCP. **c**, Estimation of apparent K_D values from XLMS analysis of Mif2*:Ame1/Okp1, Mif2*:Cse4-NCP and Ame1/Okp1:Cse4-NCP complexes compared to the apparent K_D values within the Mif2*:Ame1/Okp1:Cse4-NCP complex (mean ±SD of 3 replicates). **d**, Summary of estimated K_D values including the K_D determination of the Mif2:Cse4-NCP interaction using the subset of inter-protein crosslinks to the Mif2$^{285\text{-}311}$ signature motif. **e**, Network plot of Mif2*:Cse4-NCP crosslinks intersecting with Mif2$^{285\text{-}311}$.

Figure 6

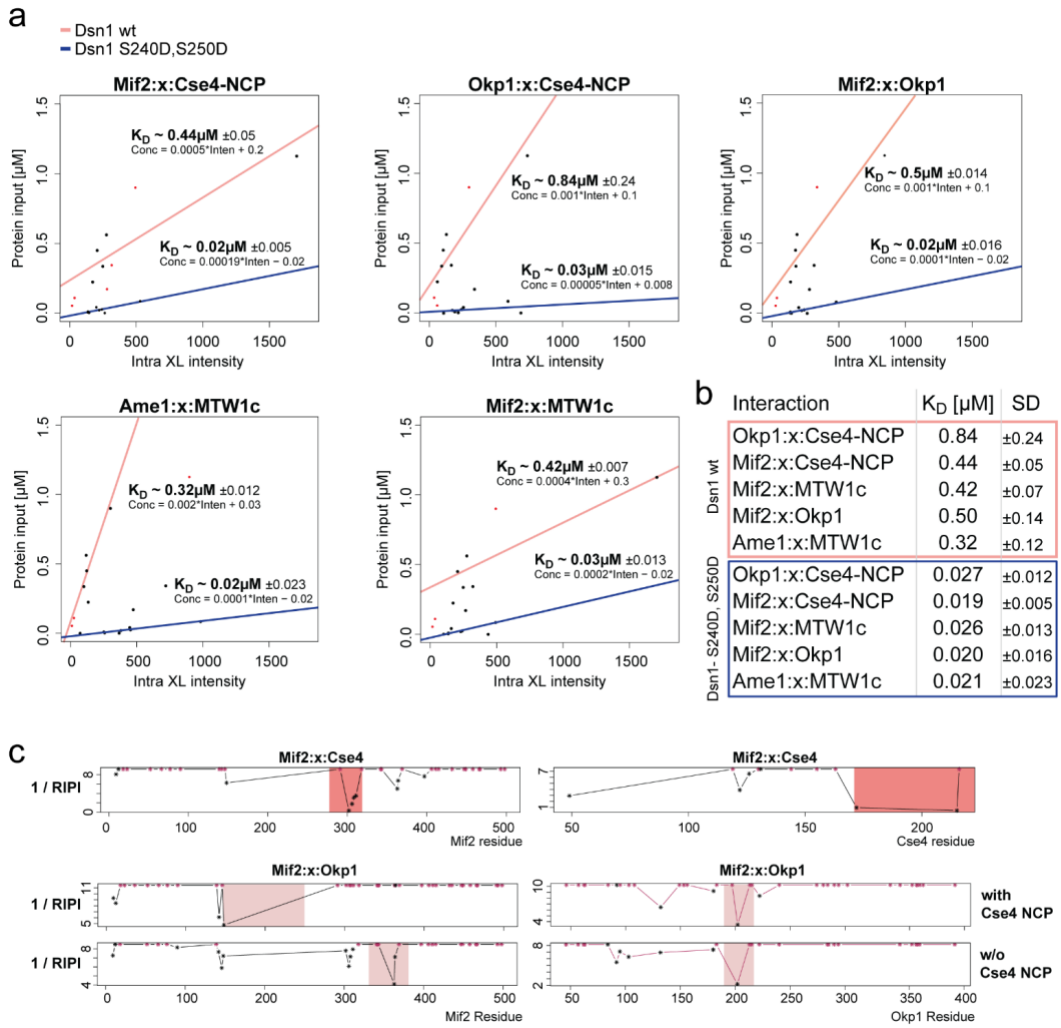

Figure 6. Binding of the MTW1c cooperatively increased the affinity of the Mif2* and Ame1/Okp1 interaction to the Cse4-NCP.

a, Estimation of apparent K_D values by titrating Cse4-NCPs with increasing concentrations of a MTW1c:Mif2*:Ame1/Okp1 complex containing either wild-type Dsn1 or phosphorylation-mimicking Dsn1^{S240D,S250D} (mean ±SD of 2 replicates). **b**, Summary of K_D values showing the effect upon binding of MTW1c(Dsn1^{S240D,S250D}). **c**, Prediction of the Mif2*:Cse4 and Mif2*:Okp1 interface by calculating the RIPI based on inter-protein crosslink intensities (Figure 10 and Methods).

Figure 7

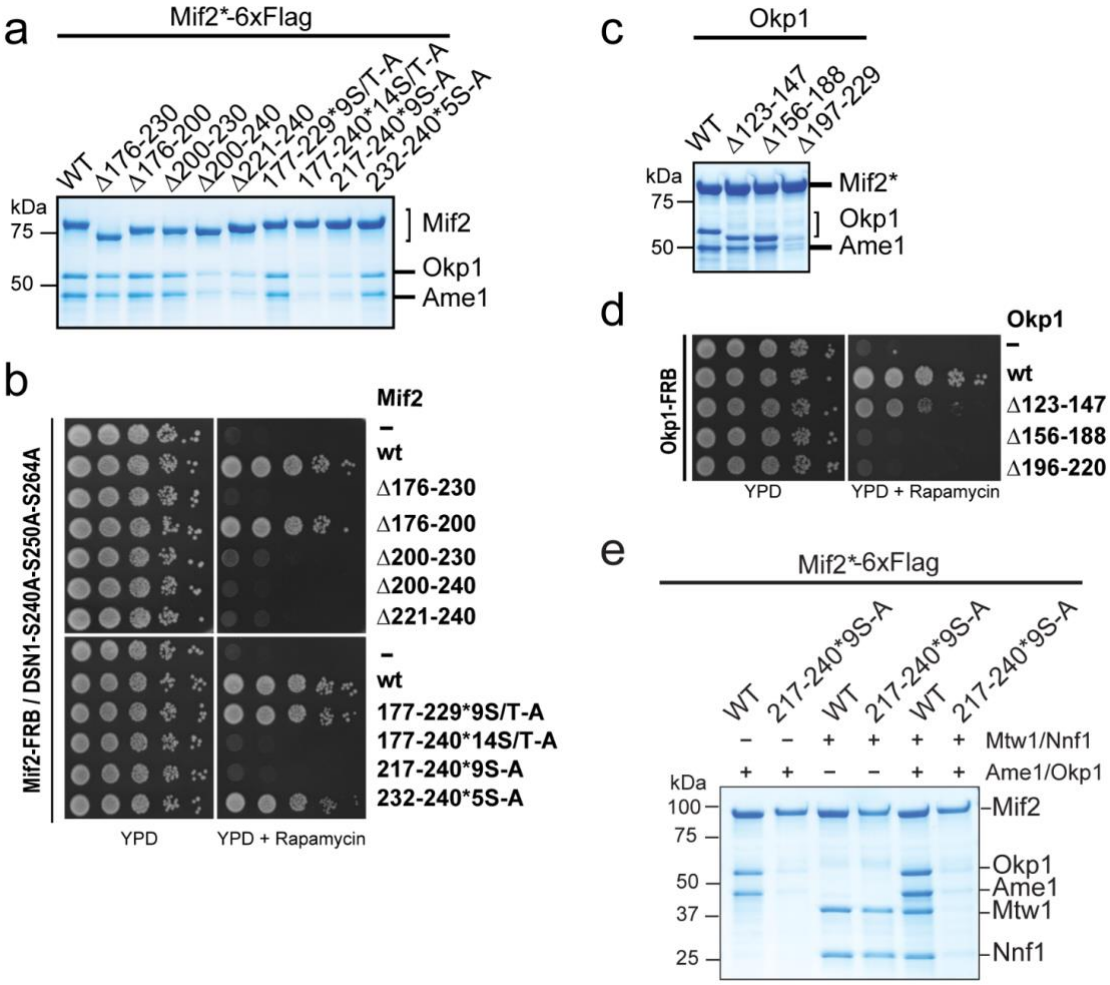

Figure 7. Phosphorylation of Mif2 and Dsn1 mediates a cooperative high-affinity link to the Cse4-NCP and is essential for cell viability. **a**, *In vitro* binding assay to identify the Ame1/Okp1 binding site on Mif2* using the indicated Mif2* deletion and phosphorylation-ablative mutants. **b**, Assay monitoring the rescue of cell growth upon nuclear depletion of Mif2 using the anchor-away method through the ectopic expression of wild-type Mif2 or its indicated deletion or phosphorylation-ablative mutants in a *Mif2-FRB/Dsn1S240A-S250A-S264A* background. **c**, Identification of the Mif2* binding site on Okp1 by assessing the binding of Okp1 deletion mutants *in vitro*. **d**, Assay of the effect of ectopically expressed Okp1 deletion mutants on cell growth in an *Okp1-FRB* anchor-away strain. **e**, *In vitro* assay to determine the effect of 9 putative phosphorylation sites within Mif2$^{217-240}$ on the interaction of Mif2 and Ame1/Okp1 with Mtw1/Nnf1.

Figure 8

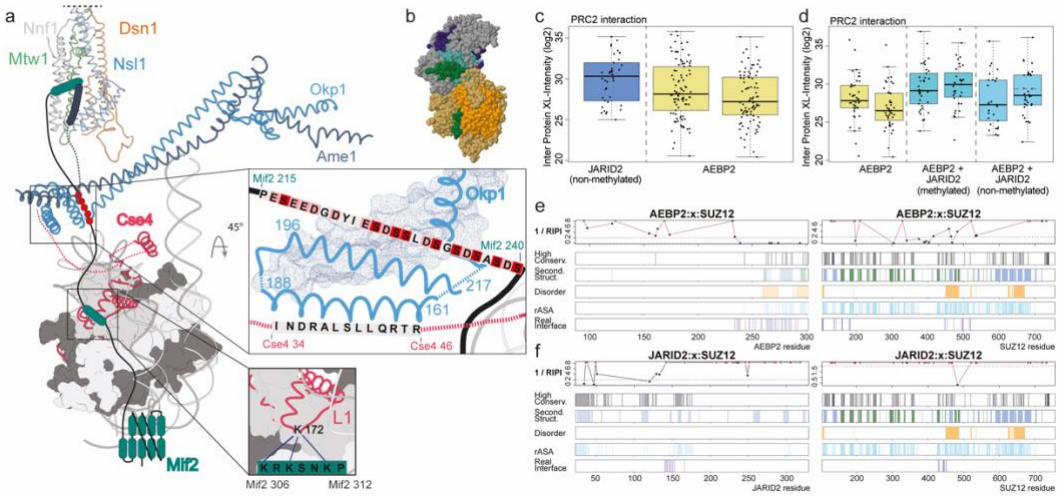

Figure 8. Summary of quantitative XLMS applications to the kinetochore and PRC2.

a, Structural model of cooperative kinetochore stabilization on the Cse4 nucleosome through phosphorylation-induced interactions. Model of the MTW1c:Mif2:Ame1/Okp1:Cse4-NCP complex based on cryo electron microscopy and crystal structures (PDB 6NUW, 6QLD, 5T58) depicting the subunit contacts essential for establishing the cooperative binding of Cse4-NCPs by Mif2 and Ame1/Okp1 upon phosphorylation of Dsn1 and Mif2(Hinshaw and Harrison, 2019, Yan et al., 2019). L1 shows Cse4 loop1. Light red and red residues within the Mif2$^{215\text{-}240}$ sequence indicate acidic and putatively phosphorylated amino acids, respectively. **b**, Cryo electron microscopy density map of the PRC2 complex with the cofactors JARID2 (dark green) and AEBP2 (cyan) (PDB 6C23) showing the subunits SUZ12 (grey), EED (orange), EZH2 (kaki) and RbAp48 (violet). **c**, Estimation of relative affinities of the cofactors AEBP2 and JARID2 to the PRC2 complex based on crosslink intensities which were extracted and quantified by the TOPP-qXL pipeline. Boxplots with the same colour indicate replicates. **d**, Relative affinity change of AEBP2 for the PRC2 complex in the presence of methylated and non-methylated JARID2. **e**, **f**, Interface sequence regions are indicated by RIPI blots, calculated from crosslink intensities, for the interactions of SUZ12 with (**e**) AEBP2 and (**f**) JARID2. Inter-protein crosslink lysines are represented as black asterisks. The top 20% conserved residues within the protein sequences are indicated. Secondary structures are shown as alpha helices (blue) and beta strands (green). Real interface residues were obtained from the PDB 6C23.

4.4 Materials and Methods

M1. Protein Expression and Purification of Spc24/25, MTW1C, Cnn1ΔHFD, Ame1/Okp1, Clb2 and Mps1 from *E. coli*

For the expression of the budding yeast Spc24/25 complex in *E. coli*, the respective genes were amplified from genomic DNA and cloned into the pETDuet-1 vector (Novagen). Expression and purification of the Spc24/25 complex were performed as described previously (Hornung et al., 2014). In brief, pETDuet1-Spc24-6xHis/Spc25 was transformed into *E. coli* strain BL21 DE3 (EMD Millipore). Bacteria were grown in selective LB-medium to an OD_{600} of 0.6 at 37 °C and protein expression was induced with 0.2 mM IPTG for 18 h at 18 °C. Cells were lysed in lysis buffer (30 mM HEPES, pH 7.5, 300 mM NaCl, 5% glycerol, 30 mM imidazole, Complete EDTA-free protease inhibitor [Roche]) and the cleared lysate was incubated with Ni-NTA agarose beads (Qiagen). The protein complex was eluted with buffer containing 30 mM HEPES pH 7.5, 150 mM NaCl, 0.01% NP-40, 2% glycerol and 250 mM imidazole and further purified on a Superdex 200 HiLoad 16/600 column (GE Healthcare) in the gel filtration buffer (30 mM HEPES pH 7.5, 150 mM KCl and 5% glycerol).

The constructs for budding yeast Mtw1/Nnf1 (pETDuet-Mtw1-Nnf1-6xHis) and Dsn1/Nsl1 (pST-39-Mtw1-Nsl1-6xHis-Dsn1) were kindly provided by S. Westermann (Hornung et al., 2014). For the phospho-mimetic version of MTW1c (Mtw1/Nnf1/Dsn1^{S240DS250D}/Nsl1), the serine residues S240 and S250 in Dsn1 were mutated to aspartic acid using the Q5 site-directed mutagenesis kit (NEB) as described previously (Akiyoshi et al., 2013, Dimitrova et al., 2016). The plasmid containing Mtw1/Nnf1 was transformed into *E. coli* Rosetta (DE3) strain (EMD Millipore), whereas Dsn1/Nsl1 was transformed into BL21 DE3 (EMD Millipore). Transformed bacteria were grown in selective LB medium at 37 °C to OD_{600} 0.6-0.8 and protein expression was induced with 0.2 mM IPTG (Mtw1/Nnf1 expression) or 0.5 mM IPTG (Dsn1/Nsl1) at 18 °C for 18 h. Cells were lysed in lysis buffer (50 mM HEPES, pH 7.5, 400 mM NaCl, 5% glycerol, 20 mM imidazole, 1 mM DTT, Complete EDTA-free protease inhibitor [Roche]) and the cleared lysate was incubated with Ni-NTA agarose beads (Qiagen). After several washing steps in wash buffer (50 mM HEPES, pH 7.5, 600 mM NaCl, 5% glycerol, 20 mM imidazole) the protein complex was recovered in elution buffer (50 mM HEPES

pH 7.5, 150 mM NaCl, 5% glycerol, 300 mM imidazole). To reconstitute the MTW1c, fractions containing pure protein sub-complexes were subjected to size-exclusion chromatography (Superose 6 increase 10/300, GE Healthcare) in 25 mM HEPES pH 7.5, 150 mM KCl, 5% glycerol and fractions containing reconstituted MTW1c were collected, flash-frozen in liquid nitrogen and stored at -80 °C.

The construct encoding Ame1-6xHis/Okp1 (pST39-Okp1-Ame1-6xHis) was kindly provided by S. Westermann (Hornung et al., 2014). Protein expression and purification in *E. coli* was essentially performed as described (Hornung et al., 2014) with the modification that 25 mM HEPES buffer was used as buffer component in all purification steps and the final gel filtration was performed on a Superdex 200 HiLoad 16/600 column (GE Healthcare) in 25 mM HEPES pH 7.5, 150 mM KCl, 5% glycerol.

For Mps1 expression and purification, the Mps1 coding sequence was cloned into pETDuet-1 with an N-terminal 6xHis-tag. Protein expression and purification was performed as described for the MTW1c and the Ni-NTA eluate was desalted using a PD10 column (GE Healthcare) in desalting buffer (50 mM HEPES pH 7.5, 150 mM NaCl, 10% glycerol, 0.5 mM DTT).

The construct for budding yeast $Cnn1^{1-270}$ (pETDuet-6xHis- $Cnn1^{1-270}$) was kindly provided by S. Westermann (Malvezzi et al., 2013) and purified as described. After elution, the protein was further purified on a Superdex 200 HiLoad 16/600 column (GE Healthcare) in gel filtration buffer (25 mM HEPES pH 7.5, 150 mM KCl and 5% glycerol).

M2. $CDC28^{CDK1}$ Complex Purification

Reconstitution of the CDC28 complex, consisting of Clb2, Cdc28 and Cks1, could not be performed by the single expression of all partners from a single baculovirus in insect cells, as Clb2 was degraded. To reconstitute the three subunit CDC28c, 1xStrep-tagged Clb2 was expressed and purified from *E. coli*, immobilized on Strep-Tactin beads (Qiagen) and incubated with cell lysate of baculovirus infected High Five™ cells expressing Cdc28 and Cks1, to assemble the three subunit CDC28c.

Full-length Clb2 was PCR amplified from budding yeast genomic DNA and cloned into pET-28 with an N-terminal 1xStrep-tag. pET28-1xStrep-Clb2 transformed *E.*

coli Rosetta (DE3) (EMD Millipore) cells were grown in selective LB medium to OD_{600} 0.6-0.8 and expression of Clb2 was induced by 0.4 mM IPTG at 18 °C for 18 h. Cells were resuspended in lysis buffer containing 50 mM HEPES pH 7.5, 150 mM KCl, 5% glycerol, 0.01% Tween, 1.5 mM $MgCl_2$, 1 mM DTT and complete EDTA-free protease inhibitor (Roche) and lysed by sonication. The cleared lysate was incubated with Strep-Tactin Superflow resin (Qiagen) for 1 h at 4 °C. Immobilized Clb2 was washed with wash buffer (50 mM HEPES pH 7.5, 150 mM KCl, 5% glycerol, 1 mM DTT) and incubated with the cleared insect cell lysates containing recombinant Cdc28 and Cks1 for one hour at 4 °C. Beads were washed and the reconstituted CDC28 complex was recovered in elution buffer (50 mM HEPES pH 7.5, 300 mM KCl, 5% glycerol, 1 mM DTT, 10 mM biotin). The eluate was dialyzed in 50 mM HEPES pH 7.5, 150 mM KCl, 10% glycerol) and flash-frozen aliquots were stored at -80 °C.

M3. Protein Expression and Purification from Insect Cells

Open reading frames encoding the respective subunits were amplified from yeast genomic DNA and cloned into the pBIG1/2 vectors for insect cell expression according to the biGBac protocol (Weissmann et al., 2016). Generation of recombinant viruses expressing single or multiple subunits was performed according to the MultiBac system (Trowitzsch et al., 2010).

Mif2-6xHis-6xFlag wild-type and mutant proteins were expressed in High Five™ cells for three days at 27 °C. Cells were lysed in lysis buffer (30 mM HEPES pH 7.5, 400 mM NaCl, 20 mM imidazole, 5% glycerol, 125 U/ml benzonase (Merck), 1 mM $MgCl_2$ and complete protease inhibitor cocktail [Roche]) using a dounce homogenizer. The cleared lysate was incubated with Ni-NTA resin (Qiagen) washed with lysis buffer (without protease inhibitor) and eluted in 30 mM HEPES pH 7.5, 150 mM NaCl, 5% glycerol and 250 mM imidazole.

6xHis-$Cdc5^{Plk1}$ was expressed and purified from insect cells as described for Mif2 with the following modifications. Cells were lysed in lysis buffer (50 mM HEPES pH 7.5, 150 mM NaCl, 5% glycerol, 125 U/ml benzonase (Merck), 1 mM $MgCl_2$ and complete protease inhibitor cocktail [Roche]) using a dounce homogenizer. The cleared lysate was incubated with Ni-NTA resin (Qiagen), washed with 50 mM HEPES pH 7.5, 300 mM NaCl, 20 mM imidazole, 5% glycerol and eluted in 50 mM HEPES pH 7.5, 150 mM NaCl, 5% glycerol and 250 mM imidazole. Peak fractions were combined, and the buffer was exchanged using a PD10 column (GE

Healthcare) in desalting buffer (50 mM HEPES pH 7.5, 120 mM NaCl, 3% glycerol).

Sli15ΔN228-2xStrep/Ipl1 complex was purified from insect cells as described previously (Fischbock-Halwachs et al., 2019).

Insect cell lysates containing expressed untagged Cdc28 and Cks1 were prepared as described above in lysis buffer (50 mM HEPES, pH 7.5, 150 mM KCl, 5 % glycerol, 0.01% Tween and complete EDTA-free protease inhibitors [Roche]) and the cleared lysates were used to assemble the trimeric CDC28 complex with 1xStrep-Clb2 purified from *E. coli*.

For *in vitro* binding and quantitative crosslinking experiments $Cdc5^{Plk1}$ phosphorylated Mif2 was generated according to the following procedure. 1 mg 6xHis-tag purified Mif2-6xHis-6xFlag was immobilized on anti-FlagM2 agarose beads (Merck) for 1 h, at 4 °C. Unbound protein was removed by washing 2x with wash buffer (30 mM HEPES pH 7.5, 150 mM NaCl, 5% glycerol). Subsequently, Mif2 was treated for 2 h at 30 °C with lambda-phosphatase (*New England Biolabs)* according to the manufacturer´s instruction. The dephosphorylation reaction was stopped by washing 1x in wash buffer supplemented with Halt™ Phosphatase Inhibitor Cocktail (Thermo Fisher) and 2x without phosphatase inhibitors. Mif2 was rephosphorylated by adding 50 µg $Cdc5^{Plk1}$ in the presence of 2.5 mM $MgCl_2$ and 1 mM ATP at 30 °C. The kinase reaction was stopped by washing 2x in wash buffer and Mif2 was recovered in elution buffer (30 mM HEPES pH 7.5, 150 mM NaCl, 5% glycerol, 1 mg/ml 3xFLAG-peptide). For quantitative crosslinking experiments the eluate was further purified on a Superdex 200 HiLoad 16/60 column (GE Healthcare) in gelfiltration buffer (30 mM HEPES pH 7.5, 150 mM KCl and 5% glycerol).

M4. *In vitro* Binding Assay of Mif2 Wild-Type and Mutant Proteins to Ame1/Okp1

To analyze the interaction of Ame1-6xHis/Okp1 with Mif2-6xHis-6xFlag wild-type and mutant proteins *in vitro*, 10 µM $Cdc5^{Plk1}$ rephosphorylated Mif2 protein (M3) was immobilized on anti-FlagM2 beads (Merck) and incubated with 25 µM Ame1/Okp1 complex in binding buffer (50 mM HEPES pH 7.5, 150 mM NaCl, 3% glycerol, 0.01% Tween 20) for 1 h at 4 °C and 1200 rpm in a thermomixer (Eppendorf). Unbound protein was removed by washing 2x with high salt buffer

(50 mM HEPES pH 7.5, 300 mM NaCl, 3% glycerol, 0.01% Tween 20) and 1x with binding buffer. Bound protein was eluted in binding buffer containing 1 mg/ml 3xFLAG peptide (Ontores).

To test the binding of Mif2 and Ame1/Okp1 to Mtw1/Nnf1, 10 µM Mif2-6xHis-6xFlag or Mif2 S217-240A-6xHis-6xFlag was incubated with 20 µM Mtw1-Nnf1-6xHis and immobilized on anti-FlagM2 beads (Merck) for 1 h at 4 °C and 1200 rpm. The beads were washed 1x with high salt buffer and 1x with binding buffer. The complex was subsequently incubated with 10 µM Ame1/Okp1 complex in binding buffer for 1 h at 4 °C and 1200 rpm. Unbound Ame1/Okp1 was removed by washing 2x with high salt buffer and 1x with binding buffer. Proteins were eluted in a buffer containing 50 mM HEPES pH 7.5, 150 mM NaCl, 5% glycerol and 1 mg/ml 3xFLAG peptide (Ontores). The input and bound fractions were separated by SDS-PAGE and proteins were visualized by Coomassie brilliant blue staining. Quantification of the ratios of bound protein to the bait was performed by using ImageJ (Schindelin et al., 2012).

To analyze the binding of untreated, dephosphorylated or rephosphorylated Mif2-6xHis-6xFlag wild-type to Ame1-6xHis/Okp1 *in vitro*, 10 µM Mif2 protein per condition was immobilized on anti-FlagM2 agarose beads (Merck) for 1 h at 4 °C and 1200 rpm in a thermomixer. The beads were washed 3x with wash buffer (50 mM HEPES pH 7.5, 150 mM NaCl, 3% glycerol, 0.01% Tween 20) and an aliquot of the untreated sample was removed. Anti-Flag immobilized Mif2-6xHis-6xFlag was then treated with lambda-phosphatase (*New England Biolabs)* according to the manufacturer´s instruction and incubated for 2 h at 30 °C and 1200 rpm in a thermomixer. The dephosphorylation reaction was stopped by washing 1x in wash buffer supplemented with Halt™ Phosphatase Inhibitor Cocktail (ThermoFisher) and 2x without phosphatase inhibitors. An aliquot of the lambda-phosphatase treated sample was removed and the rest was aliquoted and used in *in vitro* kinase assays with CDC28c, Cdc5, Sli15/Ipl1, Mps1 or combinations thereof in the presence of 2.5 mM $MgCl_2$ and 1 mM ATP for 30 min at 30 °C and 1200 rpm. The kinase reaction was stopped by washing 1x with high salt buffer and 2x with wash buffer. The binding of the untreated, dephosphorylated and rephosphorylated Mif2-6xHis-6xFlag samples to Ame1-6His/Okp1 was analyzed as described.

M5. *In vitro* Reconstitution of Cse4- and H3-Nucleosome Core Particles (NCP)

Octameric Cse4 and H3 containing nucleosomes were *in vitro* reconstituted from budding yeast histones which were recombinantly expressed in *E. coli* and assembled on the 147 bp 'Widom601' nucleosome positioning sequence according to a modified protocol (Turco et al., 2015, Shim et al., 2012).

M6. Protein Complex Titration, Chemical Crosslinking and Mass Spectrometry

The purified proteins and protein complexes were titrated applying a series of molar ratios and incubated for 45 min at room temperature to allow complex formation. For example the titration of the Cnn1$^{1-270}$-Spc24/25 complex was performed by incubating Cnn1$^{1-270}$ with the Spc24/25 dimer at molar ratios of 0.05, 0.15, 0.25, 0.55, 0.60, 0.65, 0.75, 0.80, 0.85, 0.90, 0.95, 1.0, 1.25, 1.5 and 2.0 in a final volume of 95 µl at 25 °C. Subsequently, protein complexes were crosslinked by the addition of an equimolar mixture of isotopically light (hydrogen) and heavy (deuterium) labelled bis(sulfosuccinimidyl) 2,2,4,4-glutarate (BS2G-d_0/d_6) (Creative Molecules) at a final concentration of 0.5-0.75 mM at 30 °C for 2 min. The crosslinking reaction was quenched by adding ammonium bicarbonate to a final concentration of 100 mM for 20 min at 30 °C. Proteins were diluted by adding 2 volumes of 8 M urea, reduced by 5 mM TCEP (Thermo Fisher) at 35 °C for 15 min and alkylated by incubating with 10 mM iodoacetamide (Sigma-Aldrich) at room temperature for 30 min in the dark. Proteins were digested with Lys-C (1:50 (w/w), Wako Pure Chemical Industries) for 2 h at 35°C and 1300 rpm, diluted to 1 M urea with 50 mM ammonium bicarbonate and digested with trypsin (1:50 (w/w), Promega) overnight at 35 °C and 1300 rpm. Peptides were acidified by adding trifluoroacetic acid to a final concentration of 1% and purified by reversed phase chromatography using C18 cartridges (Sep-Pak, Waters). Crosslinked peptides were enriched by size exclusion chromatography on a Superdex Peptide PC 3.2/30 column (GE Healthcare) using water/acetonitrile/TFA (77.4/22.5/0.1, v/v/v) as mobile phase at a flow rate of 50 µl/min. Fractions containing crosslinked peptides were analyzed by liquid chromatography coupled to tandem mass spectrometry (LC-MS/MS) using an EASY-nLC 1200 and an LTQ-Orbitrap Elite mass spectrometer (Thermo Fisher). Peptides were injected onto a 15 cm x 0.075 mm i.d. Acclaim™ PepMap™ C18 column (2 µm particle size, 100 Å pore

size) and separated at a flow rate of 300 nl/min using the following gradient: 0-5 min 3% B and 5-65 min 3-35%B (acetonitrile/water/formic acid, 98:2:0.1). The mass spectrometer was operated in data-dependent mode, selecting up to 10 precursors from a MS1 scan (resolution 60,000) in the range of m/z 350–1800 for collision-induced dissociation excluding singly and doubly charged precursor ions and precursors of unknown charge states. Dynamic exclusion was activated with a repeat count of 1, exclusion duration of 30 s, list size of 300, and a mass window of ±50 ppm. Fragment ions were detected at low resolution in the linear ion trap.

M7. Identification of Peptide-Peptide Crosslink Spectra

Raw spectra were converted to mzXML format using MSConvert (Chambers et al., 2012) and crosslink spectra were searched and identified using xQuest/XProphet (Walzthoeni et al., 2012). Peptide spectrum matches were performed against a database including the subunits of the respective complex (Spc24, Spc25, Cnn1 or Mif2, Ame1/Okp1, Cse4-NCP, Mtw1/Nnf1/Dsn1/Nsl1) and 22 *E. coli* decoy protein sequences. A maximum of two trypsin missed cleavages and peptide lengths between 4 and 45 amino acids were allowed. Carbamidomethyl-Cys was set as a fixed modification and a mass shift of 96.0211296 for intra-/inter-protein crosslink candidates with an additional shift of 6.03705 to account for crosslinks with the heavy version of BS2. A precursor mass tolerance of ±10 ppm was used and a tolerance of 0.2 and 0.3 Da for linear and crosslinked fragment ions, respectively. The search was performed in the 'ion-tag' mode. Identifications were filtered by applying a maximum FDR of 5%, precursor errors of ±5.0 ppm, a maximum delta score of 0.9 and a minimum of 3 fragment ion matches per peptide. The final identification tables were downloaded as xtract.csv files from the xQuest/xProphet visualization tool.

M8. Quantification of Peptide-Peptide Crosslinks and Site-Site Crosslinks

Quantification was performed with an in-house developed workflow based on the OpenMS software version 2.0 (Rost et al., 2016). All scripts as well as the xtract.csv files to run the python script ‘toppXLquant.py’ (C:/Users/…/Scripts/TOPPqXL/bin/) are provided in the ‘Scripts.zip’ folder. The pipeline starts with the conversion of the identification tables in the xtract.csv files to idXML format using our script ‘xtractToIdXML.py’. The files were saved and

the workflow 'basic_xlquant.toppas' (C:/Users/…/Scripts/TOPP-qXL/workflows) was opened in the OpenMS framework (Rost et al., 2016). The '*.idXML' files were loaded as input to (1) and '*.mzXML' files are input to (2) and the script was executed. In parallel, raw files in the mzXML format were converted to mzML using the FileConverter function with default parameters except for the filter of MS2 scans and MS1 peaks with intensities <100.0. Peak features in the mzML files and their respective profile chromatograms were extracted with a modified version of the FeatureFinderAlgorithmPicked function from OpenMS. Parameters fed to this tool are found in the file 'ffcentroided_params.ini'. Detected features were annotated with their putative peptide identifications in the idXML files using the IDMapper function with an m/z tolerance of ±7 ppm and retention time tolerance of ±10 s. Retention times between runs were aligned using the MapAlignerIdentification function with default parameters. Finally, consensus tables were generated using the FeatureLinkerUnlabeled function with default parameters and converted to .csv format with the TextExporter function. The intensities of the unique peptide-peptide crosslink ions were summarized to site-site crosslink intensities using the in-house script 'csvToToppXLqTSV.py' (provided in: C:/Users/…/ Scripts/TOPPqXL/bin).

M9. Estimation of the Apparent Equilibrium Dissociation Constant (K_D) Based on Crosslink Intensities

Site-site crosslink intensities were loaded and analyzed in the statistical environment R (https://www.r-project.org). Technical replicates were averaged with non-assigned values being ignored at this step. The intensities of peptides seen in >1 SEC fraction were summed up and peptide-peptide crosslinks were summarized to site-site crosslinks by addition of their intensities. The intensities of the subunit whose concentration was constant in all titrations were applied to normalize the intensities between runs. Finally, a linear model was fitted between the initial concentrations of the varying subunit and the median intensity of its intra-protein crosslinks. This linear relation was used to estimate the concentration of the formed complex from the median intensity of the inter-protein crosslinks. Subsequently, the K_D was calculated as:

$$Kd = \frac{\left(A_{init_{conc}} - A_{conc}\right) * \left(B_{init_{conc}} - B_{conc}\right)}{(A{:}\,x{:}\,B)_{conc}}$$

where *A* represents the subunit whose concentration varies, *B* the subunit whose concentration remains constant and *A*:x:*B* the complex. The initial concentrations of *A* and *B* were recalculated based on the linear relation of concentration and intensity. For each titration step a K_D value was calculated and the mean and standard deviation of these values were reported.

We also applied the *Scatchard plot* (Scatchard, 1949) to estimate the K_D by plotting the linear relation of 'fraction of B bound over concentration of free A' (y-axis) versus 'fraction of B bound' (x-axis). This approach indicates the K_D as the negative inverse of the slope as well as the inverse of the intersection coefficient (Figure 4b).

To calculate the apparent K_D values based on the steady state equilibrium equation the R script was run according to the following procedure. The scripts (C:/Users/.../Scripts/R-Script) were opened in the R environment. To analyze the Cnn1:x:Spc24/25 titration the 'CnnSPC_Kd_Est.R' script and for the analysis of the Mif2:Ame1/Okp1:MTW1c:x:Cse4-NCP titration the 'MTW1cMifAO_CSE4-NCP_Kd_Est.R' script were applied. The location of the input files was defined in the working directory in setwd("C:/Users/.../"). The input file name was defined in 'fname' (e.g.: fname = "1.1-MIFNUC_F restraints.tsv"). Subsequently, the default settings of the calculation parameters, as described above, can be altered by following the instructions in the code. Executing the script shows the results table ('kdtable2') which indicates the K_D values of each titration step and the mean (KD) and standard deviation (SD). At this step outliers that exceed the double SD are excluded and the mean K_D (KD2) and standard deviation (SD2) are recalculated. In addition, several exploratory plots are generated. (1) Crosslink intensities per protein:x:protein pair (median) before normalization (Figure 12, Figure 14, Figure 17, Figure 19, Figure 21, Figure 23, and Figure 26) (2) Correlation of crosslink intensities within protein:x:protein pairs. (3) Crosslink intensities per protein:x:protein pair (median) after normalization (Figure 13, Figure 18, Figure 20, Figure 22, Figure 24, and Figure 27). (4) Correlation of crosslink intensities between experiments and between crosslinks. (5) Linear regression between crosslink intensity and protein concentration. The linear regression model is used to estimate the apparent K_D values. The statistical analysis of the apparent K_D values for each interaction is summarized in 'kdtable2'.

M10. Determination of the Relative Interface Propensity Index (RIPI)

Peptide-peptide crosslink intensities were summarized to site-site intensities, by summing up all restraint intensities involving the specific lysine residue. This total sum includes mono-links, loop-links, intra- and inter-protein crosslinks. Next, the site-site intensity of the inter-protein crosslinks from a specific dimer interaction was divided by the total sum. The resulting value was called the Relative Interface Propensity Index (RIPI) of a crosslinked residue. Lysine sites, which were not identified in inter-protein crosslinks, were assigned a RIPI value equal to the minimum RIPI in the set, in order to avoid infinite values for the plotted inversed RIPIs.

Sequence conservation in the RIPI plots was computed by using PSIBlast against the UNIREF90 database. Only residue positions with conservation above the 80% quantile within the protein sequence were plotted.

Secondary structure and rASA (relative accessible surface area) were predicted using the SPIDER2 software (Yang et al., 2017) against the UNIREF90 database. The fasta protein sequences and the PSSMs (Position-Specific Scoring Matrix) obtained by PSIBlast were used as input for the SPIDER2 software. Residues were considered to have low accessibility if their rASA was below 40%. Residues were considered to have low disorder if their IUPred index was below 0.25 in a scale of 0 to 1.

Real interface residues were extracted from PDB models if applicable. Real binding interfaces were identified by a residue-residue distance between the interacting proteins of below 4.5 Å. The distances were measured from any heavy atom in one residue to any heavy atom in the other residue.

M11. Yeast Strains and Methods

All yeast strains used in this study were created in the S288c background. The generation of yeast strains and yeast methods were performed by standard procedures. The anchor-away analysis was performed as described previously (Haruki et al., 2008).

For anchor-away rescue experiments, the Mif2 promoter (1 kb) and coding sequence were PCR amplified from yeast genomic DNA and cloned with a 6xHis-

7xFlag tag PCR fragment into vector pRS313 via the Gibson assembly reaction (Gibson et al., 2009). The deletion mutants were generated using the Q5 site-directed mutagenesis kit (New England Biolabs) and phospho-ablative mutants were constructed by Gibson assembly of the corresponding mutant gene fragments (IDT). The rescue constructs were transformed into a Mif2 anchor-away strain (*Mif2-FRB*), a *Mif2-FRB/dsn1*^{S240AS250AS264A} mutant strain or a *Mif2-FRB/Δcnn1* mutant strain and cell growth was tested in 1:10 serial dilutions on YPD plates in the absence or presence of rapamycin (1 mg/ml) at 30 °C for 3 days.

M12. Western Blot Analysis

The levels of proteins ectopically expressed in yeast were probed by western blot analysis as described previously (Fischbock-Halwachs et al., 2019). For western blot analysis an equivalent of 10 OD_{600} of cells logarithmically grown in liquid culture was collected by centrifugation at 3140 x g for 5 min at room temperature and the pellet was washed once with aqua dest. For protein extraction, the pellet was resuspended in 1 ml ice-cold 10% trichloroacetic acid and incubated on ice for 1 hr. Samples were pelleted at 4°C and 20000x g for 10 min and washed twice with ice-cold 95% ethanol. Pellets were air-dried and resuspended in 100 µl 1x SDS-PAGE sample buffer containing 75 mM Tris (pH 8.8). Samples were boiled (10 min, 95°C) and centrifuged at 10800 x g for 3 min at room temperature and supernatants were separated on 10% or 15% (Cse4 containing samples) SDS-PAGE gels. Immunoblotting was performed with the following antibodies: Anti-FLAG M2 (Sigma-Aldrich), Anti-PGK1 (ThermoFisher) and visualized by HRP-conjugated anti-mouse secondary antibodies (Santa Cruz).

M13. Amino Acid Sequence Alignment

Multiple sequence alignments of *S. cerevisiae* Mif2 and Okp1 amino acid sequences with their respective mammalian orthologues CENP-C or CENP-Q were performed with Clustal Omega (Sievers et al., 2011) (https://www.ebi.ac.uk/Tools/msa/clustalo/).

4.5 Supplementary Figures

Figure 9

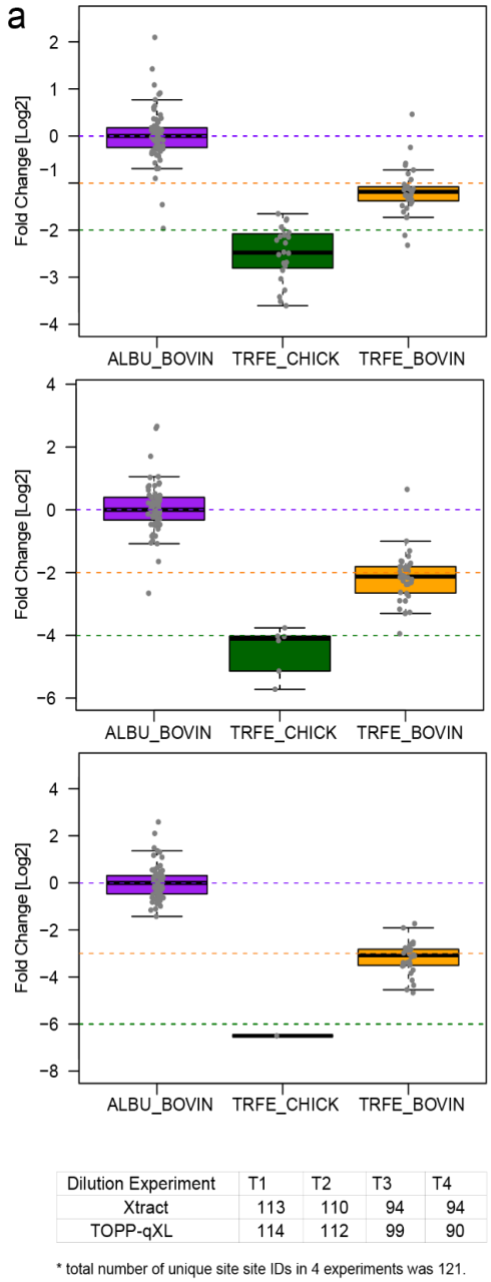

		MQ for Xlinks	TOPP-qXL
Sensitivity	(%)	68	79.07
Accuracy	(%)	88	89.04
Quantified in one of pair	(No.)	11	22
Quantified consistently	(No.)	65	65
Conflict quantitation	(No.)	16	12
Conflict quantitation & Quantified in one of pair	(No.)	0	3
Not quantified	(No.)	11	1

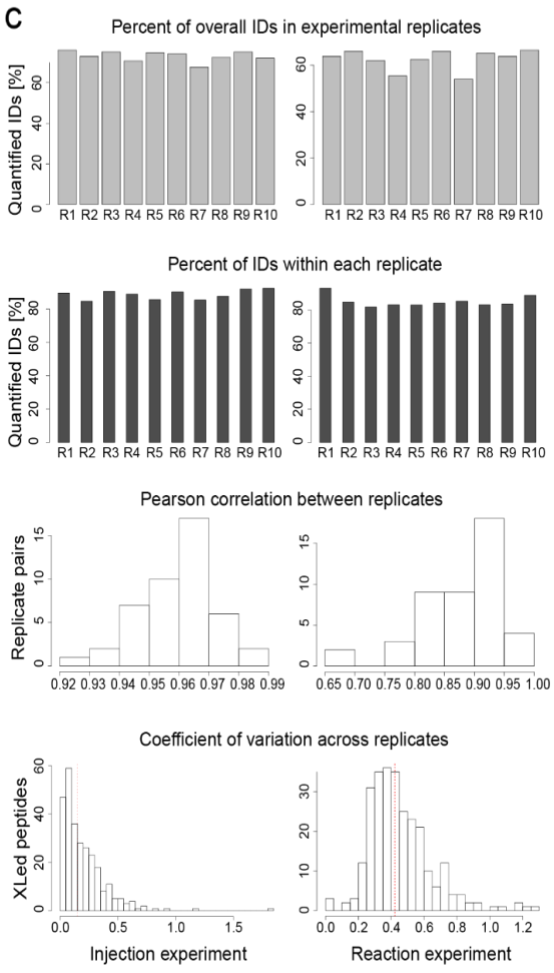

Dilution Experiment	T1	T2	T3	T4
Xtract	113	110	94	94
TOPP-qXL	114	112	99	90

* total number of unique site site IDs in 4 experiments was 121.

Figure 9. Validation of the Bioinformatic Workflow TOPP-qXL for the Extraction of Crosslink Precursor Intensities.

For validation, the performance of the TOPP-qXL pipeline was tested against published datasets which were analyzed by different extraction tools including

datasets for the development of the Xtract algorithm(Walzthoeni et al., 2015) (a) and the extraction pipelines described in (b) and (c) (Fischer et al., 2013, Muller et al., 2018).

(a) The first dataset comprises 4 dilution experiments from bovine albumin, bovine transferrin and chicken transferrin (Walzthoeni et al., 2015). Each protein was crosslinked separately and then pooled before MS acquisition. In each dilution experiment, the concentration of albumin was kept constant, whereas the transferrin concentration decreased monotonically in 2:4:8 ratios for the bovine homolog and 4:16:64 for the chicken homolog. Our pipeline is able to reproduce the dilution steps of the experimental design. In the two highest dilutions of chicken transferrin the extracted features were only detectable by the 'match-between-runs' strategy, as the protein was not identified by fragment spectra in these two dilutions. In the highest dilution experiment, the features that passed undetected by the 'match-between-runs' strategy were noisy and had missing mass traces and thus, the failure of detection was justified. Our pipeline was able to quantify a similar number of site-site crosslinks in comparison to the Xtract software, for which this dataset was created. The overall recall of site-site crosslinks was 97.5% (118/121) and the accuracy of the quantification close to the expected values.

(b) The second dataset (Fischer et al., 2013) consists of a SILAC-like experiment which used the protein C3 crosslinked in its native and cleaved form, C3b, in forward (C3-BS3d_0 and C3b-BS3d_4) and reverse labeling (C3-BS3d_4 and C3b-BS3d_0). The crosslink identifications provided by the authors were applied as feature extraction seeds and without the 'match-between-runs' strategy, as it was not applicable to this dataset. As reference extraction pipeline the authors used the Pinpoint software with manual curation of the extracted features and compared it against their proposed pipeline based on MaxQuant. We also applied Pinpoint as basis to compare the performance of their MaxQuant version tailored for crosslinking quantification against our pipeline. Our pipeline showed a 10% increase in sensitivity by recalling features not detected by MaxQuant. Moreover, our pipeline could quantify certain identifications, whose recall was not possible even with the benchmark pipeline Pinpoint. Thus, the reported sensitivity might be even higher than 79%.

(c) A third dataset, which was published for the assessment of the reproducibility of crosslink quantification (Muller et al., 2018), was also used

for benchmarking the TOPP-qXL workflow. This dataset comprises two experiments with ten replicates each. In the first dataset, human serum albumin was crosslinked in 10 crosslinking reaction replicates that were analyzed separately by mass spectrometry. For the second dataset, the 10 reaction replicates were pooled and analyzed 10 times by mass spectrometry and thus representing injection replicates. The crosslink identifications provided by the authors were matched to the MS1 peaks, which were extracted using our pipeline and a 'match-between-runs' strategy. As a result, unique crosslinks were quantified with a recall between 67-76% in the injection replicates and 55-66% in the reaction replicates in respect to the overall number of unique crosslinks in each of the two experiments (first row). Pooling all the quantifications across their replicates results in a sensitivity of 86% and 79% for the injection and reaction experiments, respectively. The sensitivities of the number of identifications within each replicate are even higher and fluctuate between 84-92% and 82-92% for the injection and reaction experiments, respectively (second row). Overall, these quantification rates indicate the high sensitivity of the proposed pipeline. Next, we calculated the correlations and coefficients of variation of the abundances at the peptide-peptide crosslink level (third and fourth row). The minimum Pearson correlation between replicates was 0.92 in the injection experiment and 0.67 in the reaction experiment. Regarding the coefficients of variation, the median value was 14.6% in the injection experiment and 42.3% in the reaction experiment. Similar coefficients of variation were observed at the unique crosslinked residues level: 15% and 43%, respectively. These values are higher than the values reported in the original publication of 14% and 32%, respectively.

Figure 10

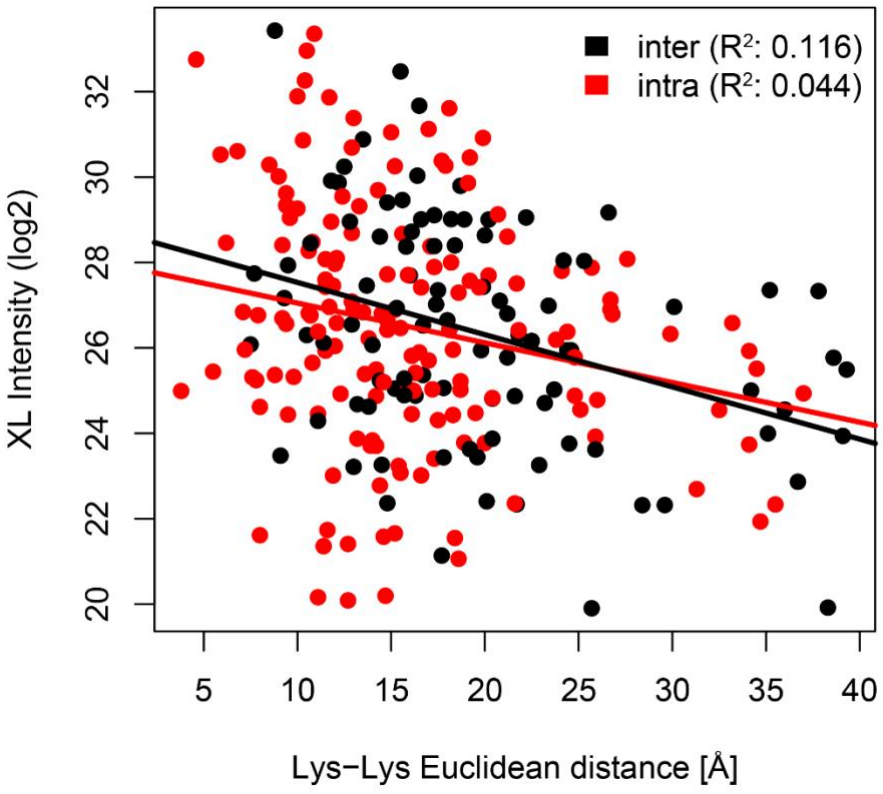

Figure 10. Correlation Between Crosslink Intensity and the Euclidean Distance of the Linked Residues.

Crosslink restraints were extracted and quantified with the in-house TOPP-qXL pipeline (Figure 9 and Methods) from RNA polymerase I and II, 26S Proteasome, XRCC5/6 and PLC (MHC-I peptide-loading complex) datasets (Blees et al., 2017, Dubois et al., 2016, Iacobucci et al., 2019, Jennebach et al., 2012, Wang et al., 2017). The Euclidean intra- and inter-protein distances were mapped on the crystal structures of RNA Polymerase I (PDB 4C2M), RNA Polymerase II (PDB 5IP7), Ku heterodimer (XRCC5/6) (PDB 1JEY) and the electron microscopy density maps of PLC (PDB 6ENY) and 26S Proteasome (PDB 5L4G; 5L4K) using the XWALK software (*49*). The Euclidean distances were plotted against the site-site crosslink intensities. To assess the dependence of crosslink intensity on Euclidean distance the R-squared statistics and the Fisher´s Exact Test were computed (p-value (intra) < 0.001 ; p-value (inter) < 0.001).

Figure 11

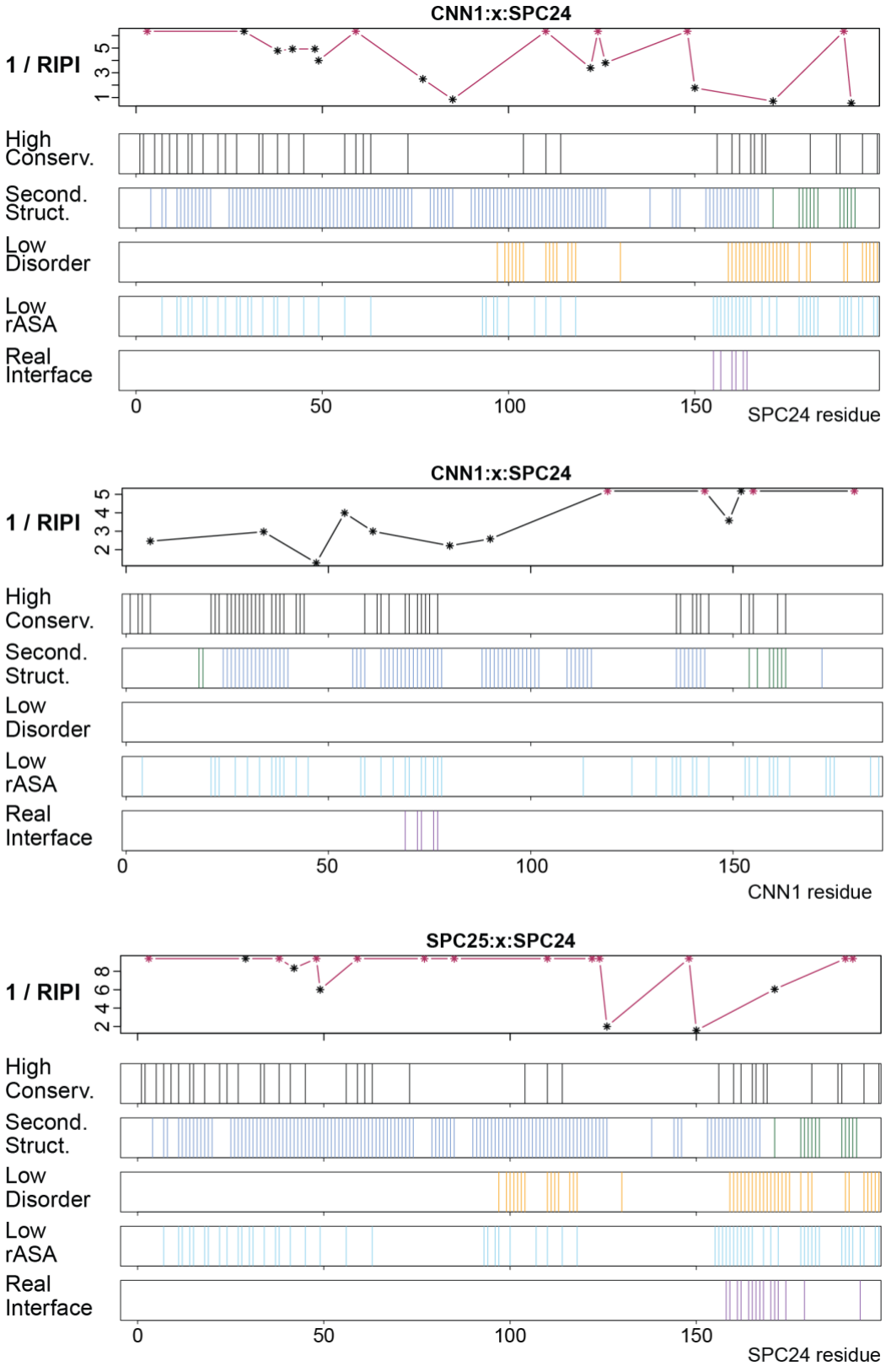
CNN1:x:SPC24
1 / RIPI
1 3 5
High Conserv.
Second. Struct.
Low Disorder
Low rASA
Real Interface
0
50
100
150
SPC24 residue
CNN1:x:SPC24
1 / RIPI
2 3 4 5
High Conserv.
Second. Struct.
Low Disorder
Low rASA
Real Interface
0
50
100
150
CNN1 residue
SPC25:x:SPC24
1 / RIPI
2 4 6 8
High Conserv.
Second. Struct.
Low Disorder
Low rASA
Real Interface
0
50
100
150
SPC24 residue

Figure 11. High RIPI (Relative Interface Propensity Index) Values Indicated the Binding Interfaces of the Cnn1$^{1-270}$:Spc24/25 Complex.

Crosslink intensities were extracted and quantified using the TOPP-qXL quantification pipeline (M8) and the RIPI was calculated as described (M10). The inverse of the RIPI is plotted in the respective first panel of each protein:protein interaction. Areas of sequence conservation, secondary structure prediction (Yang et al., 2017), state of protein disorder and the rASA are indicated by colored lines (M10). Amino acid residues establishing the binding interface (Real Interface) were retrieved from the PDB database (4GEQ). This heuristic approach was applied by interpreting a drop in 1/RIPI together with predicted secondary structures, sequence conservation and rASA in order to identify amino acid sequences that putatively establish binding interfaces and serve as candidates for mutational analysis.

Figure 12

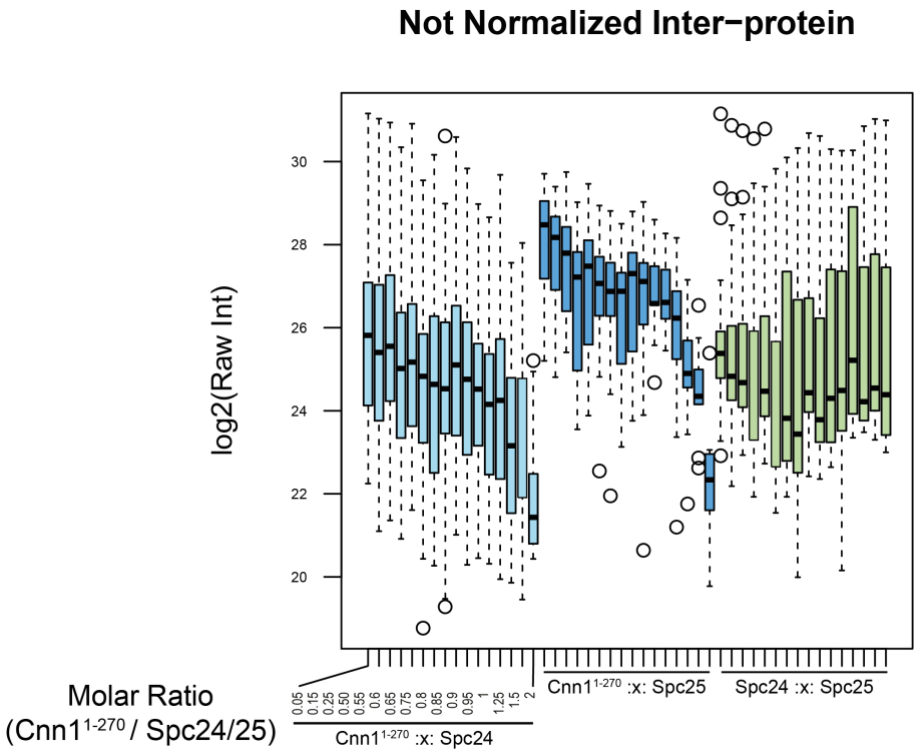
Not Normalized Inter−protein
log2(Raw Int)
30
28
26
24
22
20
Molar Ratio
(Cnn1 1-270 / Spc24/25)
0.05
0.15
0.25
0.50
0.55
0.6
0.65
0.75
0.8
0.85
0.9
0.95
1
1.25
1.5
2
Cnn1 1-270 :x: Spc24
Cnn1 1-270 :x: Spc25
Spc24 :x: Spc25

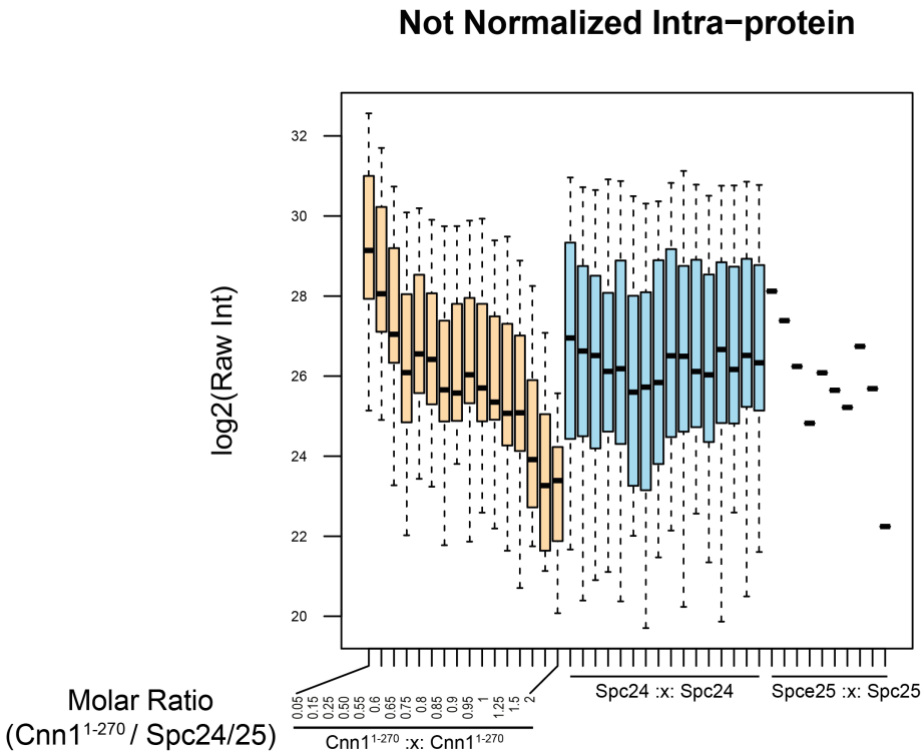
Not Normalized Intra−protein
log2(Raw Int)
32
30
28
26
24
22
20
Molar Ratio
(Cnn1 1-270 / Spc24/25)
0.05
0.15
0.25
0.50
0.55
0.6
0.65
0.75
0.8
0.85
0.9
0.95
1
1.25
1.5
2
Cnn1 1-270 :x: Cnn1 1-270
Spc24 :x: Spc24
Spce25 :x: Spc25

Figure 12. Inter- and Intra-Protein Crosslink Intensities of the Cnn1$^{1-270}$ to Spc24/25 Titration Before Normalization.

Constant levels of Spc24/25 complex were titrated with Cnn1$^{1-270}$ applying the indicated molar ratios. Crosslink intensities were extracted using the TOPP-qXL pipeline (M8). The intensities of the identified peptide-peptide crosslinks were summarized to protein site-site crosslink intensities. The intra-protein crosslink intensities of the constant interactor were used to normalize intensities between titration points and showed the reproducible quantification of the subunits across the titration series. The sum of the site-site raw intensities of the indicated intra- or inter-protein crosslinks of the individual molar ratios were plotted after normalization. The intra-protein crosslink intensities of the titrated interactor were applied to calculate a linear regression on the input concentrations. The linear regression model was used to recalculate the input concentrations and to interpolate the concentration of the formed complex from the inter-protein crosslink intensities.

Figure 13

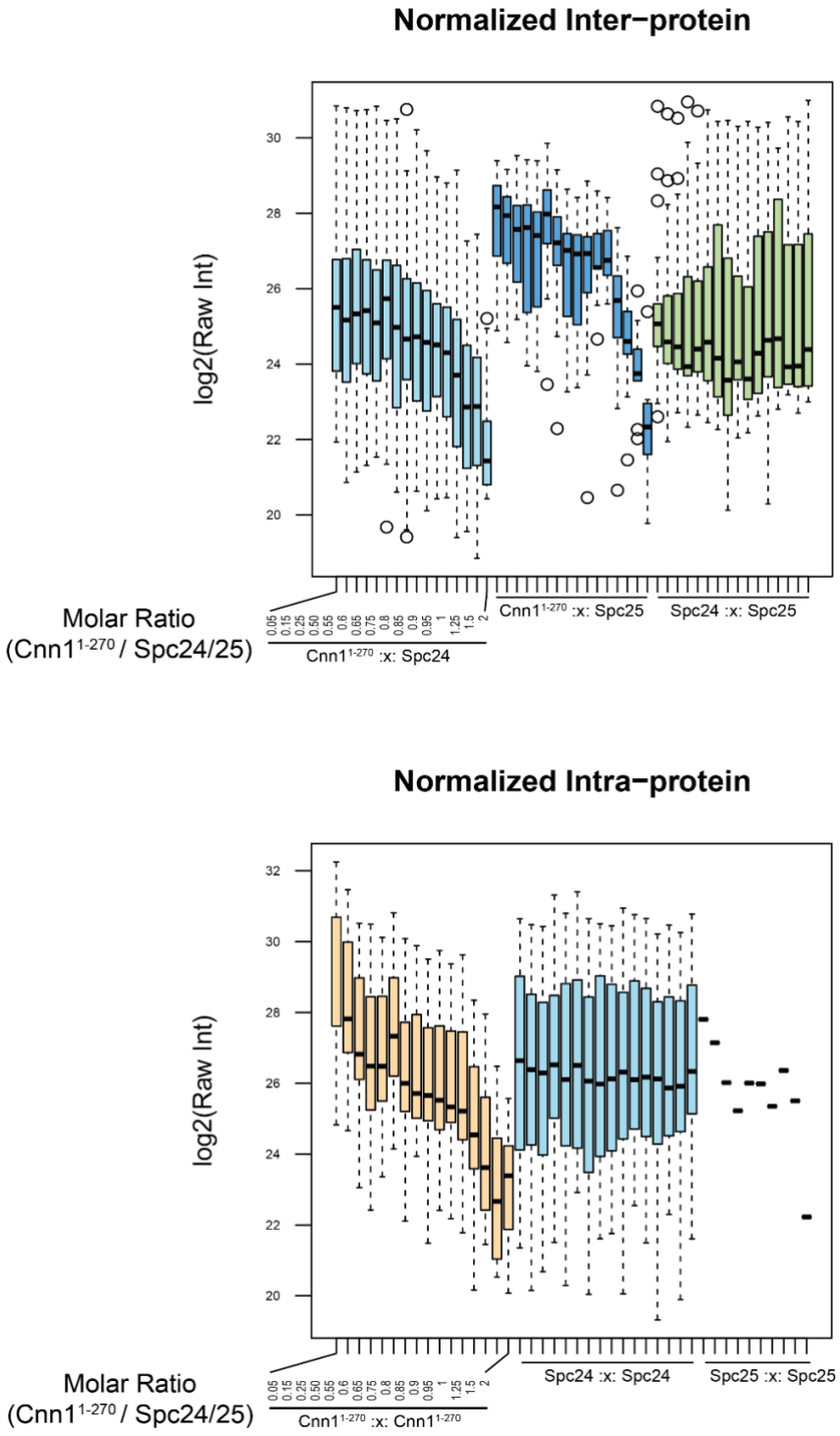

Figure 13. Inter- and Intra-Protein Crosslink Intensities of the Cnn1$^{1-270}$ to Spc24/25 Titration After Normalization.

The plot was generated as described in Figure 12.

Figure 14

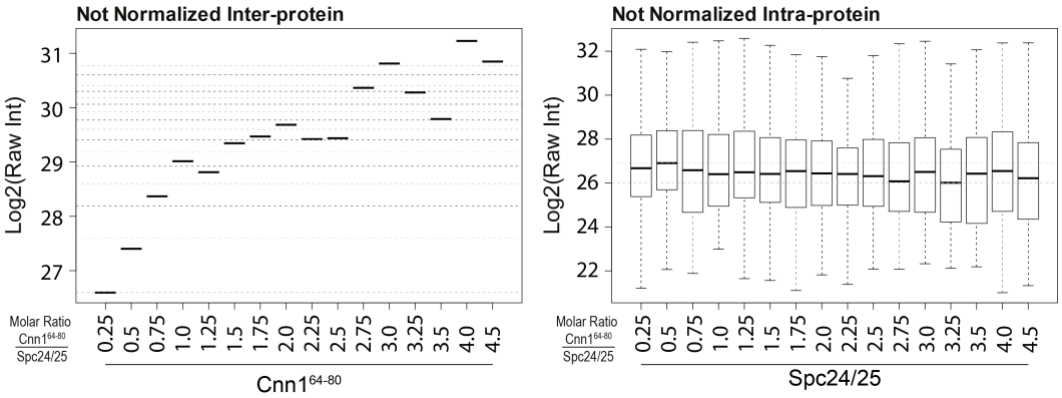

Figure 14. Intra- and Inter-Protein Crosslink Intensities of Spc24/Spc25 Titration with Cnn1$^{64-80}$ Before Normalization.

The identified peptide-peptide crosslink intensities in each of the three replicates were extracted by the TOPP-qXL pipeline (M8) and summarized to their respective site-site crosslink intensities. The intra-protein crosslink intensities of the constant interactor were used to normalize intensities between replicates and showed the reproducible quantification of the subunits across the titration series (right panel). The intra-protein crosslink intensities of Cnn1$^{64-80}$ were applied to calculate a linear regression on the input concentrations (left panel). The linear regression model was used to recalculate the input concentrations and to interpolate the concentration of the formed complex from the inter-protein crosslink intensities (Figure 15).

Figure 15

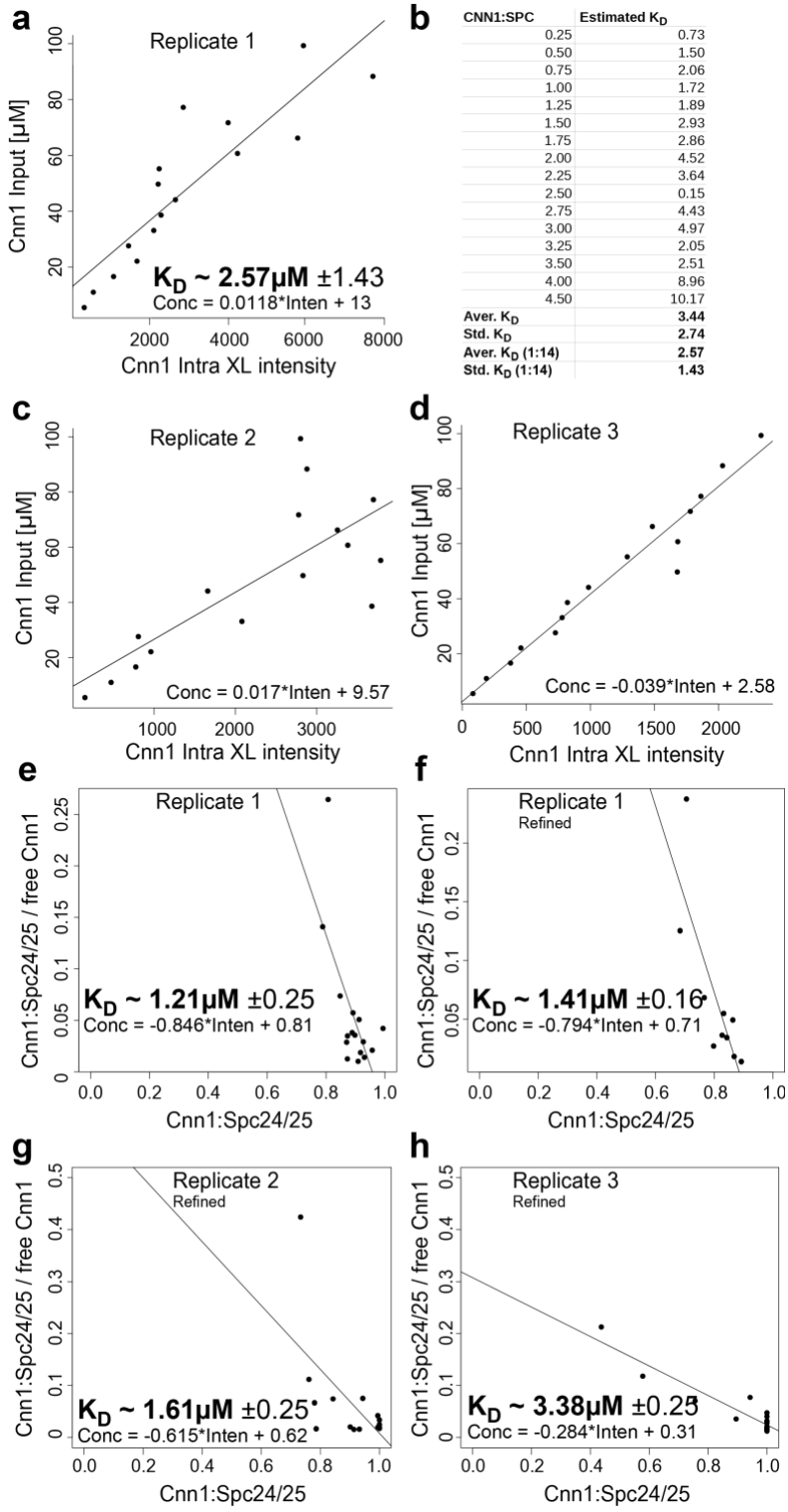

Figure 15. The Linear Regression Model and *Scatchard* Plot yielded Comparable K_D Estimation Values for Cnn1$^{64-80}$:Spc24/25 Interaction.

A constant molar concentration of Spc24/25 complex was titrated against increasing amounts of the Cnn1$^{64-80}$ peptide. After feature extraction, the intensities of site-site crosslinks were summarized and used to interpolate crosslink intensities and protein concentrations. Apparent K_D values were calculated based on the concentration of the formed complex estimated from the linear regression and averaged across molar ratios of the titration steps from 3 biological replicates (a) (c) and (d). Using the linear regression model a K_D value was estimated for each step of the titration (b). By excluding titration steps that exceeded twice the standard deviation (Std. K_D) the estimation of K_D was further refined (b). Estimation of apparent K_D values of the Cnn1$^{60-84}$:Spc24/25 interaction by the *Scatchard* plot (e) is refined when excluding values exceeding twice the standard deviation (f) in three biological replicates (g) and (h).

Figure 16

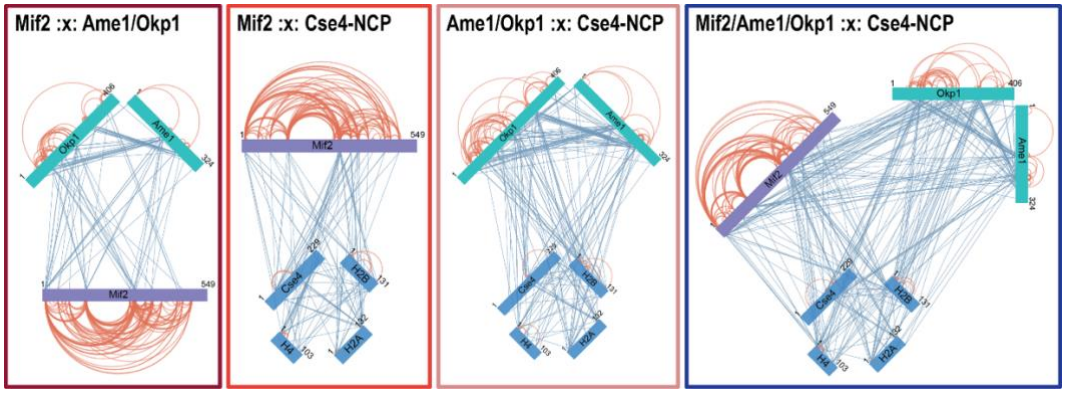

Figure 16. Schematic Representation of Crosslink Restraints on Mif2, Ame1/Okp1 and Cse4-NCP Complexes Applied for the Estimation of Apparent K_D Values.

All crosslink restraints which were reproducibly identified in all replicates of the individual Mif2:Ame1/Okp1, Mif2:Cse4-NCP, Ame1/Okp1:Cse4-NCP and Mif2:Ame1/Okp1:Cse4-NCP titrations are visualized by network plots. The crosslink restraints were identified by xQuest and MS1 intensities (raw intensity) were extracted by the TOPP-qXL pipeline (M8).

Figure 17 - Figure 24 Intra- and Inter-Protein Crosslink Intensities of Cse4-NCP Titration with Mif2.

The intensities of crosslinks detected in each of the three replicates were extracted by the TOPP-qXL pipeline (M8). The intensities of the identified peptide-peptide crosslinks were summarized to protein site-site crosslink intensities. The intra-protein crosslink intensities of the constant interactor were used to normalize intensities between replicates and showed the reproducible quantification of the subunits across the titration series. The sum of the raw intensities of the indicated intra- or inter-protein crosslinks of the individual molar ratios were plotted before and after normalization. The intra-protein crosslink intensities of the titrated interactor were applied to calculate a linear regression on the input concentrations. The linear regression model was used to recalculate the input concentrations and to interpolate the concentration of the formed complex from the inter-protein crosslink intensities. Plots in Figure 17 - Figure 24 were generated accordingly.

Figure 17

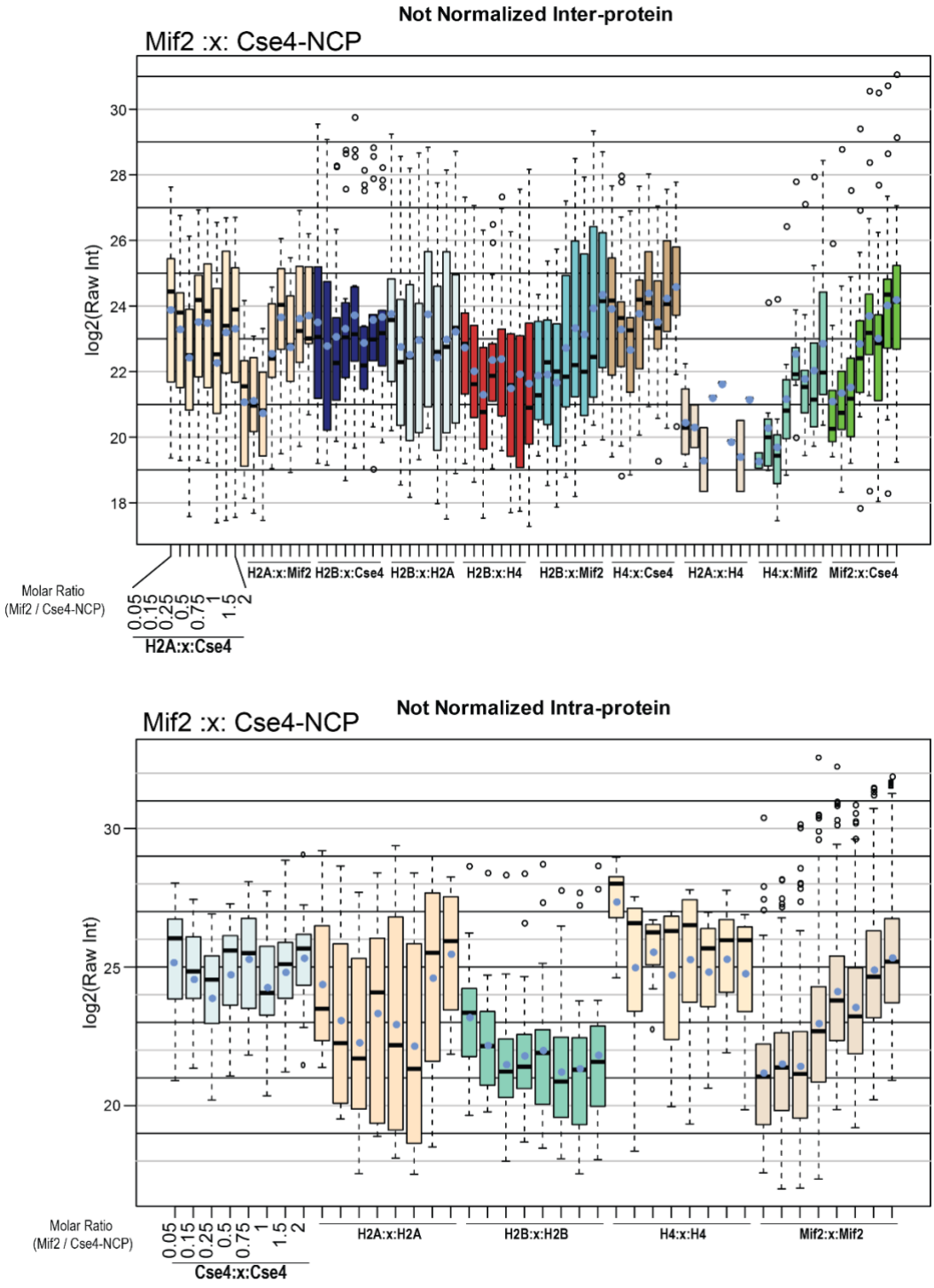

Figure 17. Intra- and Inter-Protein Crosslink Intensities of Cse4-NCP Titrated with Mif2.

The plot was generated before normalization as described.

Figure 18

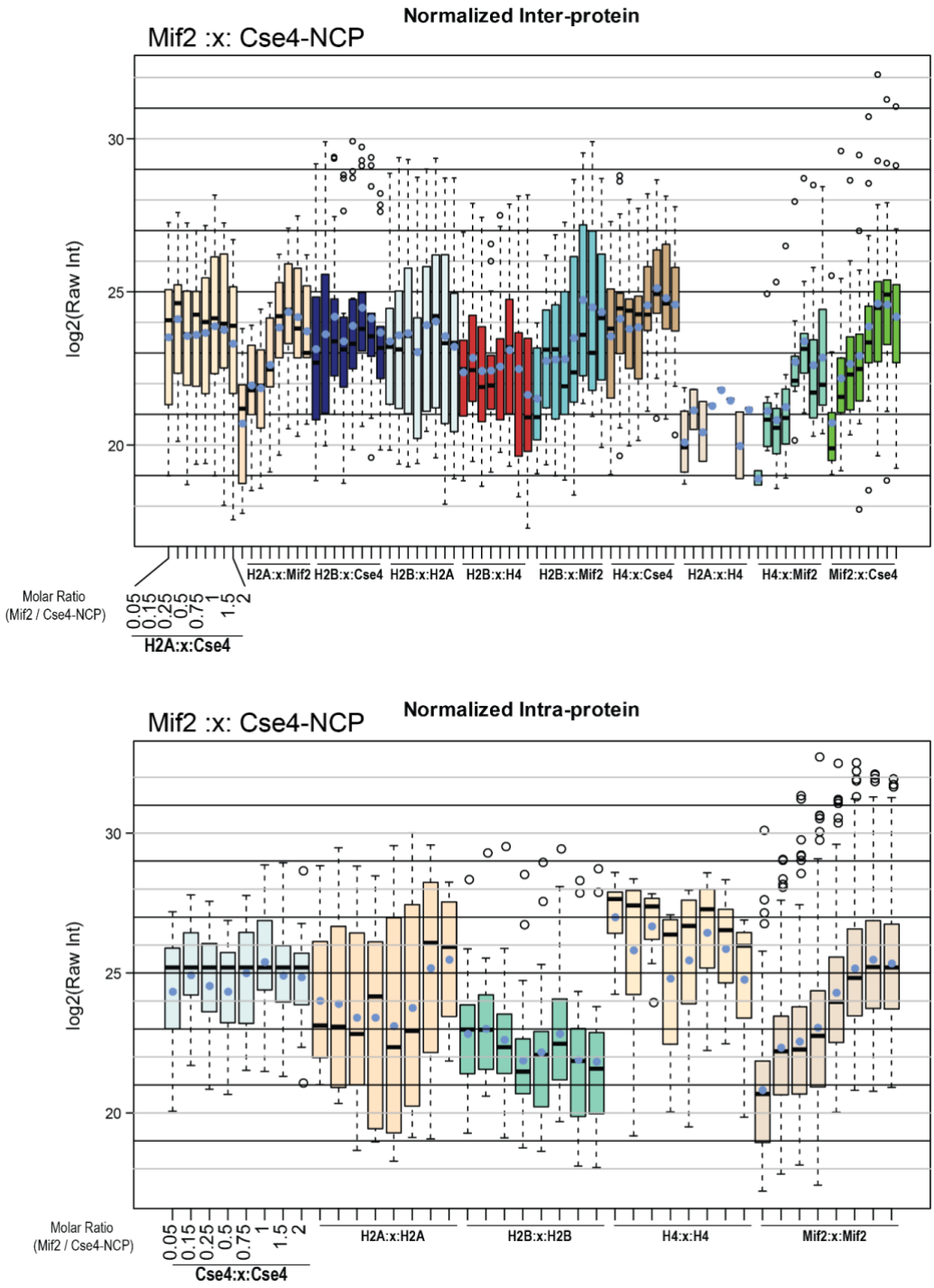

Figure 18. Intra- and Inter-Protein Crosslink Intensities of Cse4-NCP Titrated with Mif2.

The plot was generated after normalization as described.

Figure 19

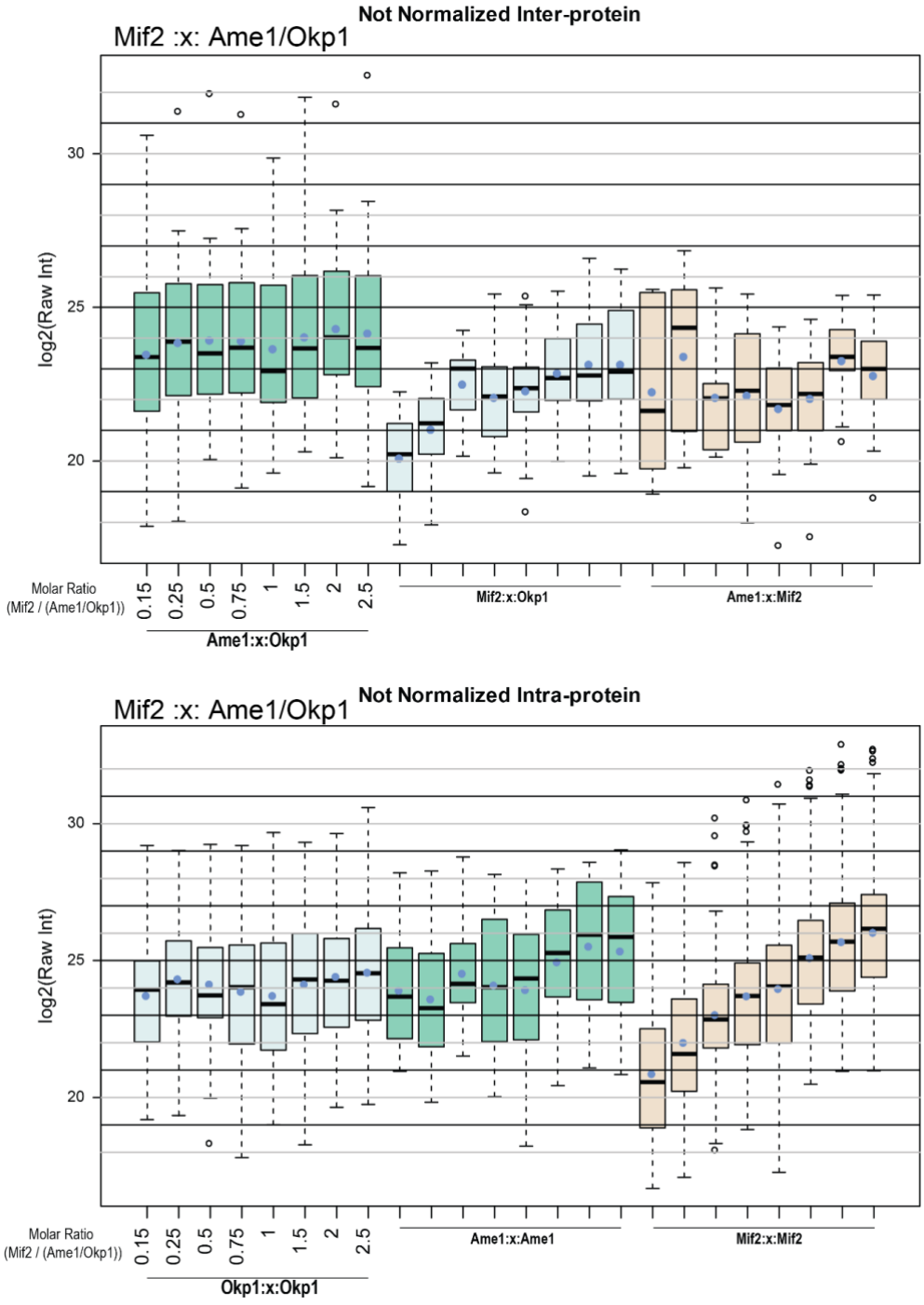

Figure 19. Intra- and Inter-Protein Crosslink Intensities of Cse4-NCP Titrated with Mif2.

The plot was generated after normalization as described.

Figure 20

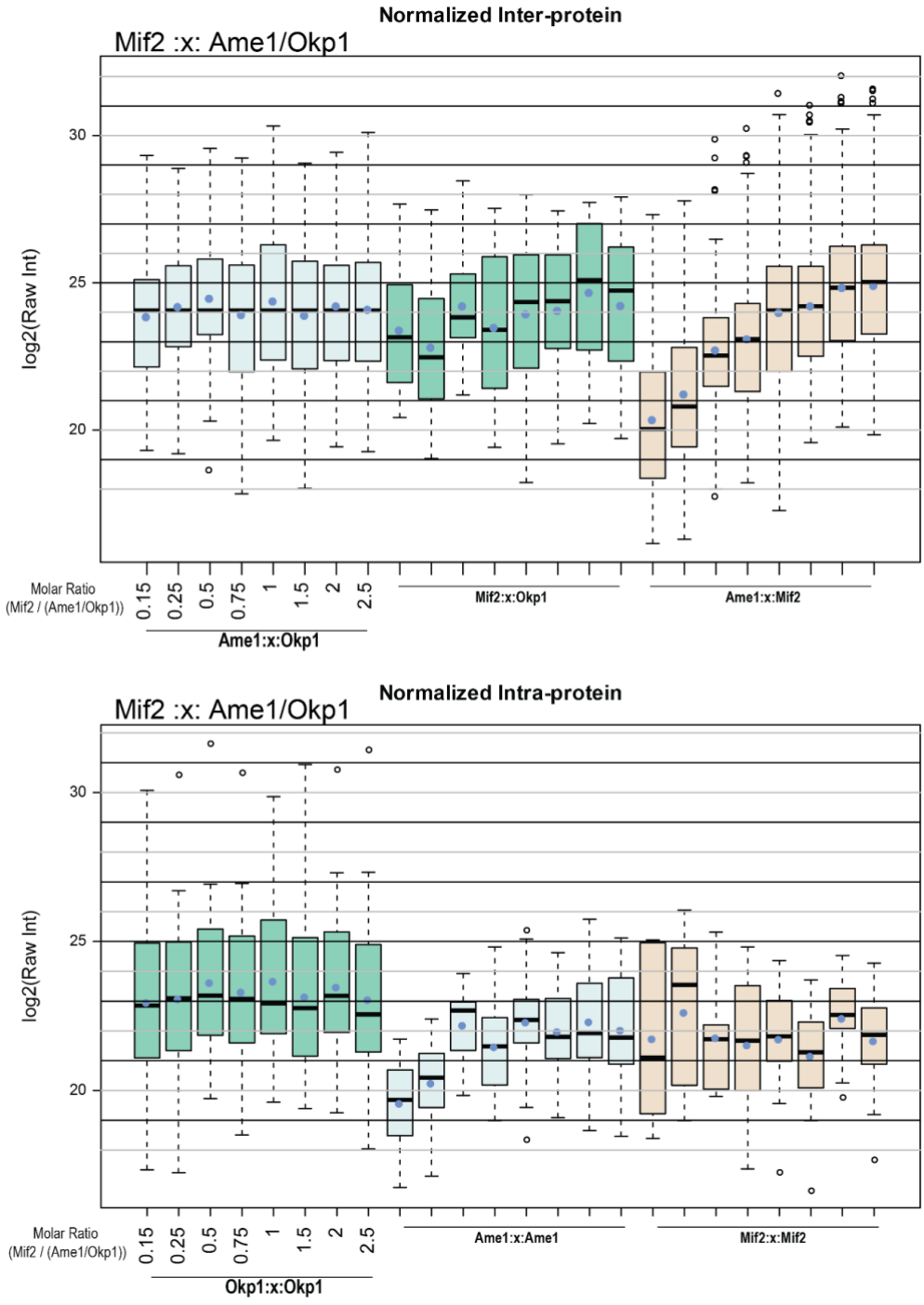

Figure 20. Intra- and Inter-Protein Crosslink Intensities of Cse4-NCP Titrated with Mif2.

The plot was generated after normalization as described.

Figure 21

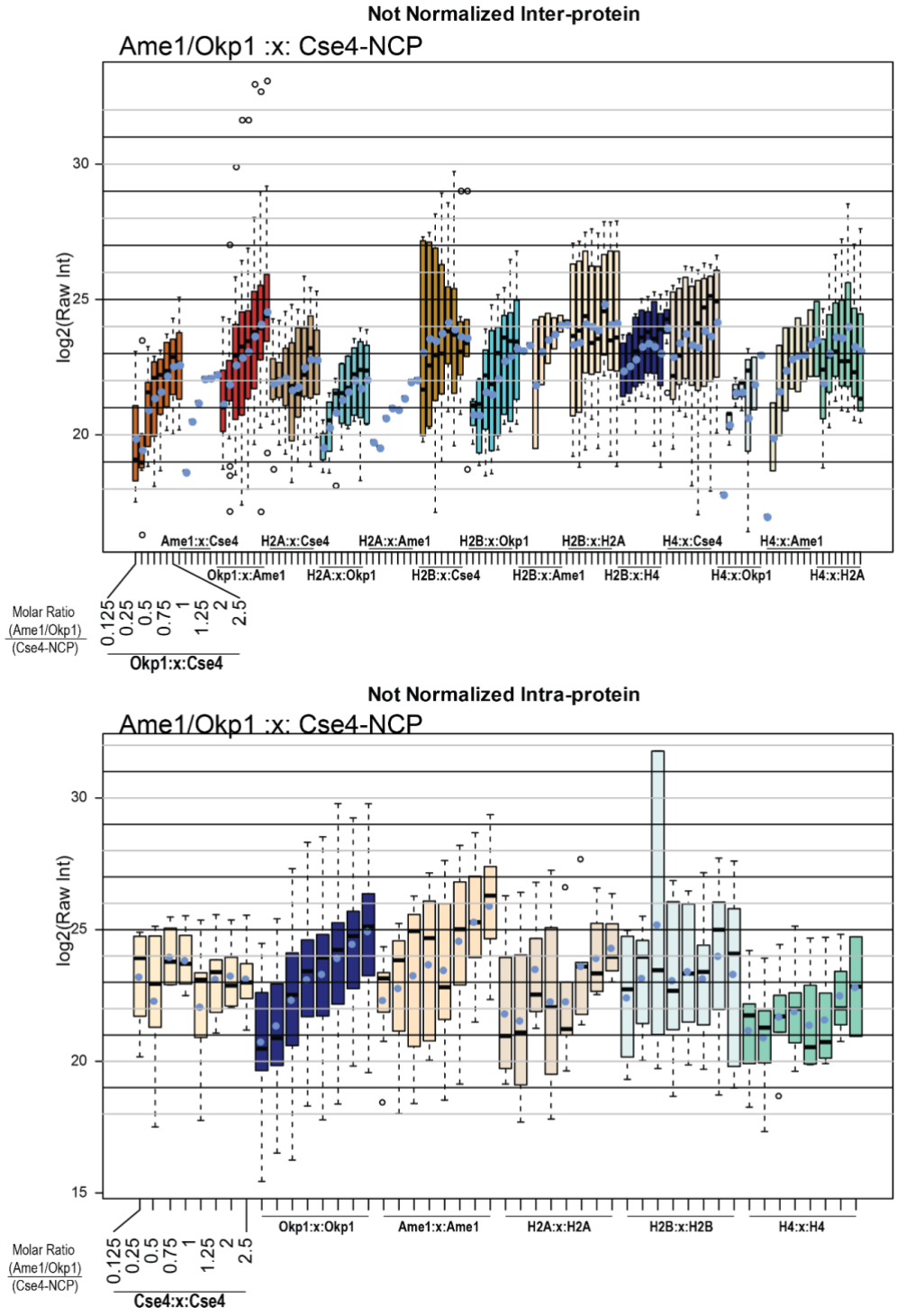

Figure 21. Intra- and Inter-Protein Crosslink Intensities of Cse4-NCP Titrated with Mif2.

The plot was generated after normalization as described.

Figure 22

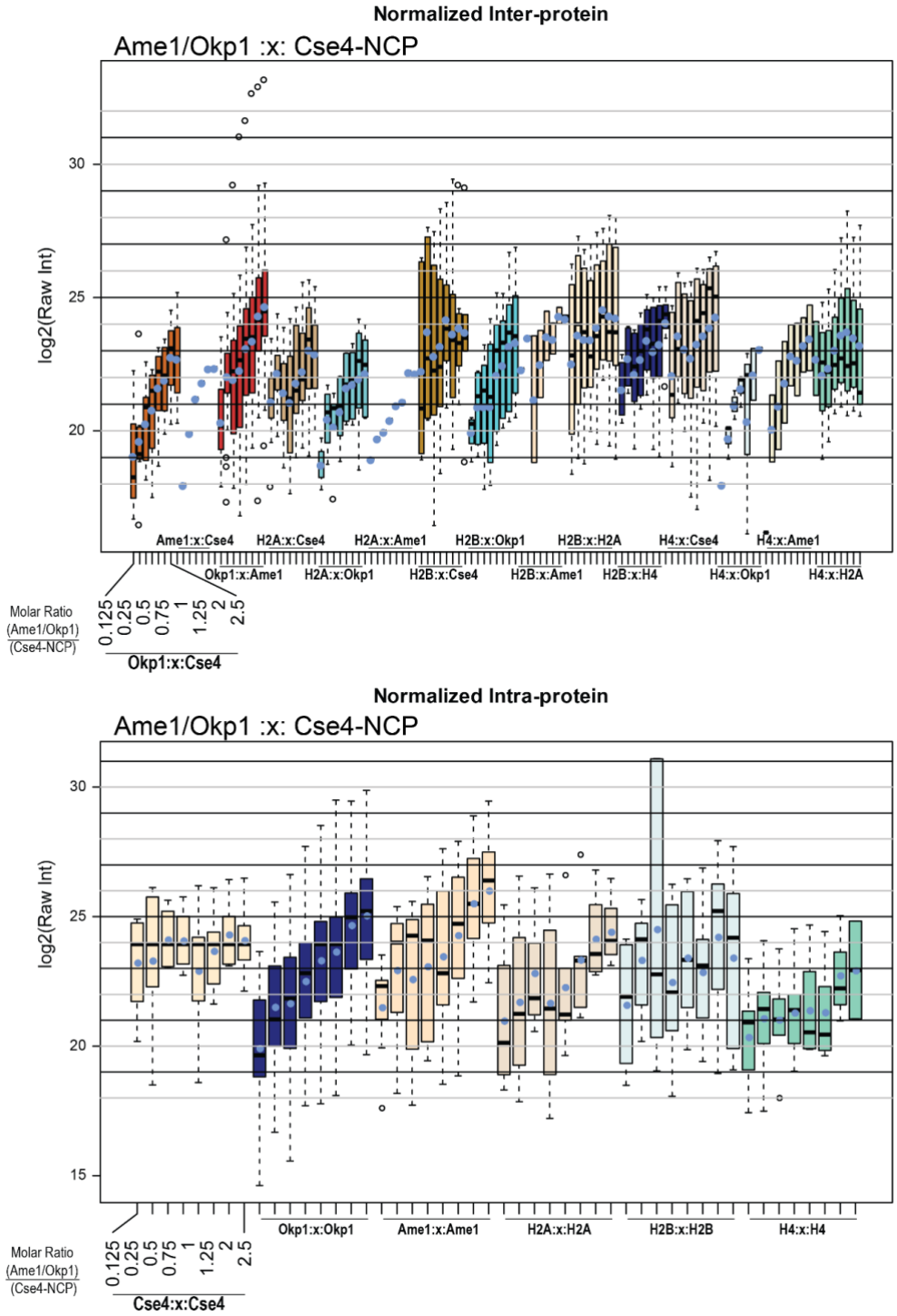

Figure 22. Intra- and Inter-Protein Crosslink Intensities of Cse4-NCP Titrated with Mif2.

The plot was generated after normalization as described.

Figure 23

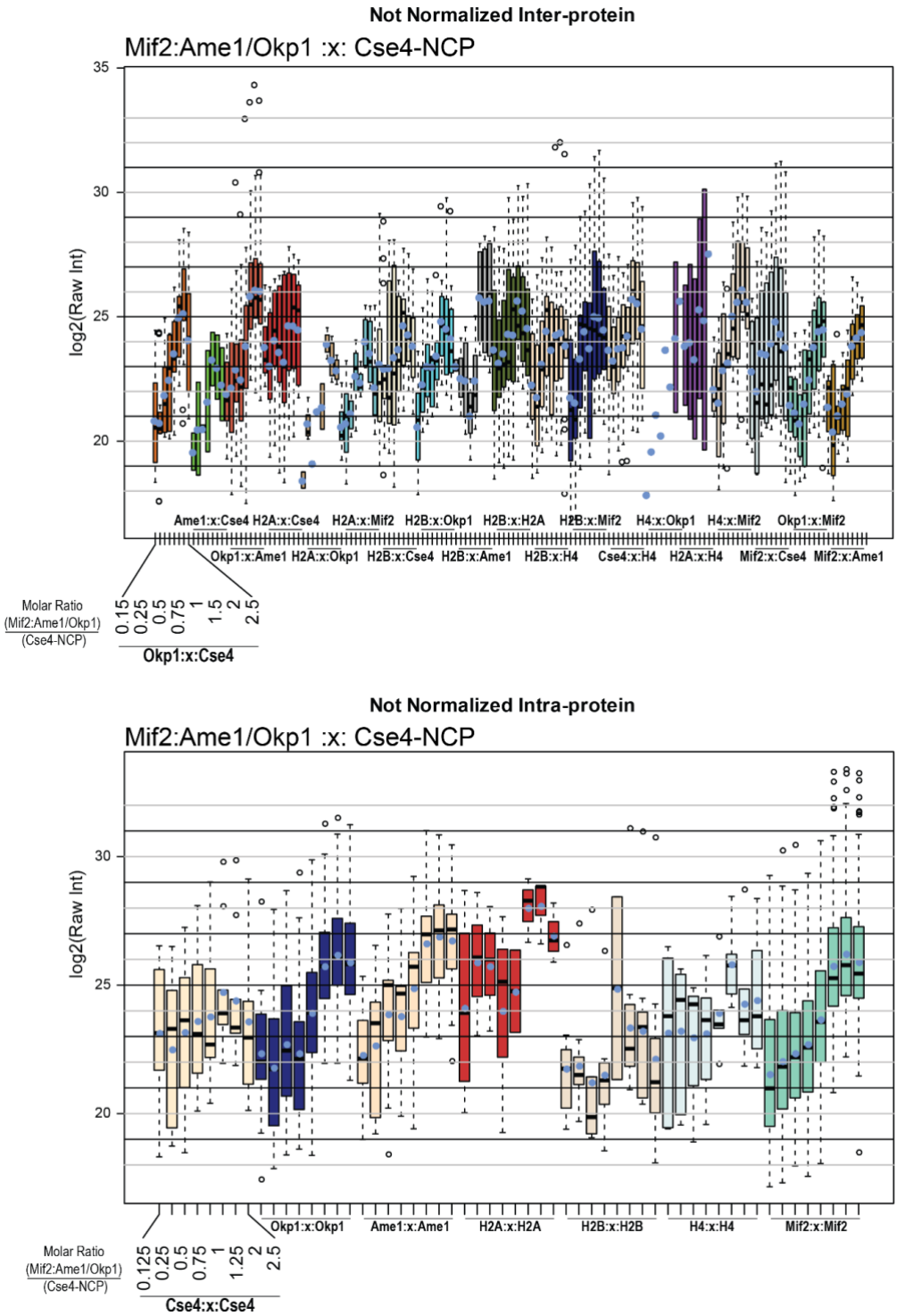

Figure 23. Intra- and Inter-Protein Crosslink Intensities of Cse4-NCP Titrated with Mif2.

The plot was generated after normalization as described.

Figure 24

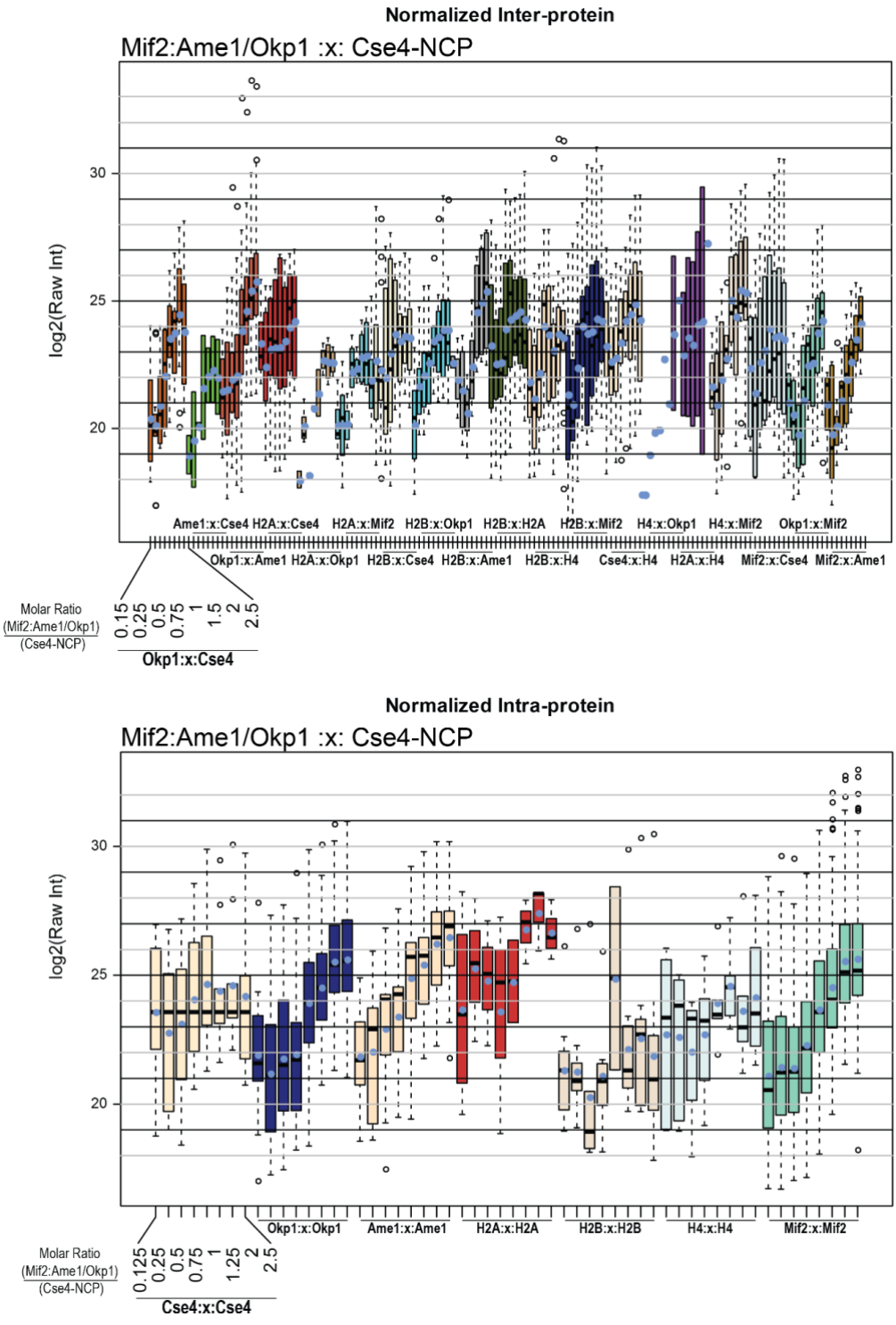

Figure 24. Intra- and Inter-Protein Crosslink Intensities of Cse4-NCP Titrated with Mif2:Ame1/Okp1.

The plot was generated after normalization as described.

Figure 25

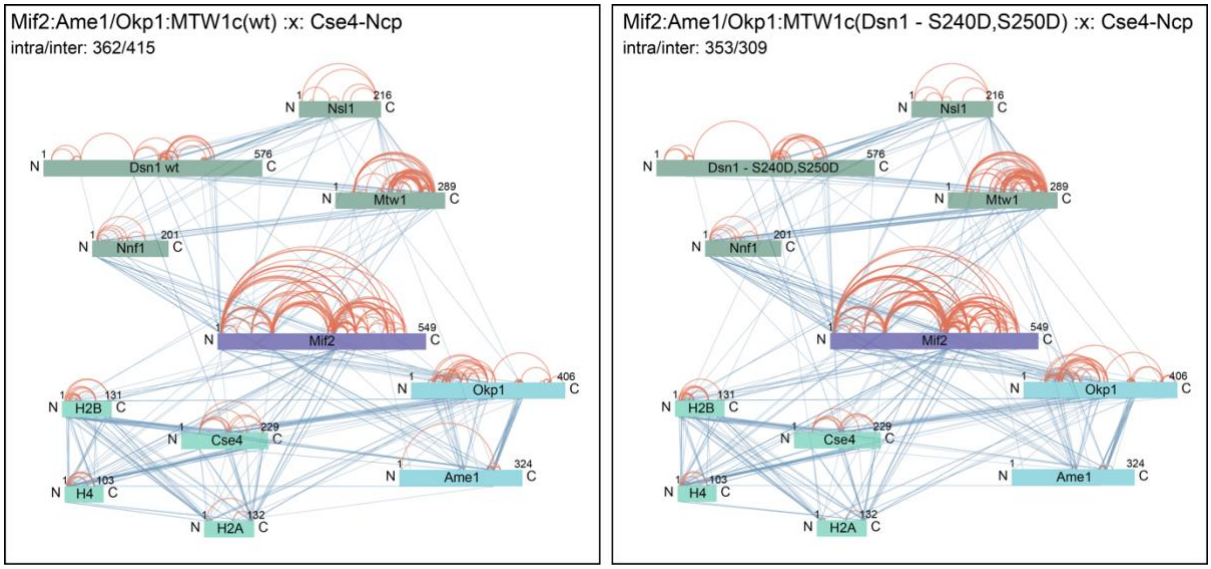

Figure 25. Comparison of Crosslink-Derived Restraints Detected on MTW1c:Mif2:Ame1/Okp1:Cse4-NCP Complexes Containing Either Dsn1^{wt} or the Dsn1^{S240D,S250D} Mutant.

Intra- and inter-protein crosslinks that were reproducibly identified in 2 replicates of the individual titration were visualized as network plot by xVis (Grimm et al., 2015). The crosslink restraints were identified using the xQuest software (Walzthoeni et al., 2012).

Figure 26

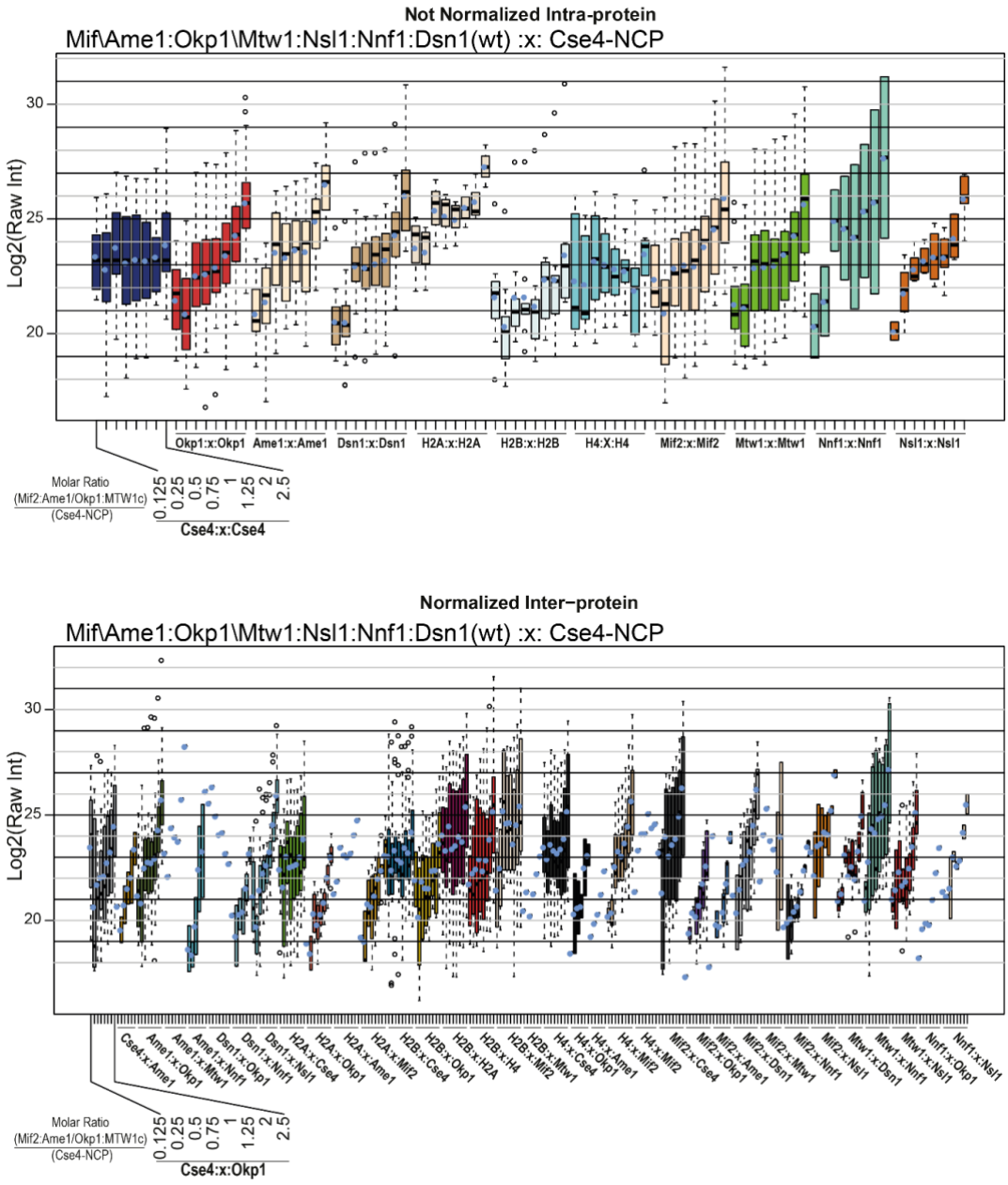

Figure 26. Intra- and Inter-Protein Crosslink Intensities of Cse4-NCP Titrated with MTW1c(Dsn1^{wt}):Mif2:Ame1/Okp1.

The plot was generated after normalization as described in Figure 17.

Figure 27

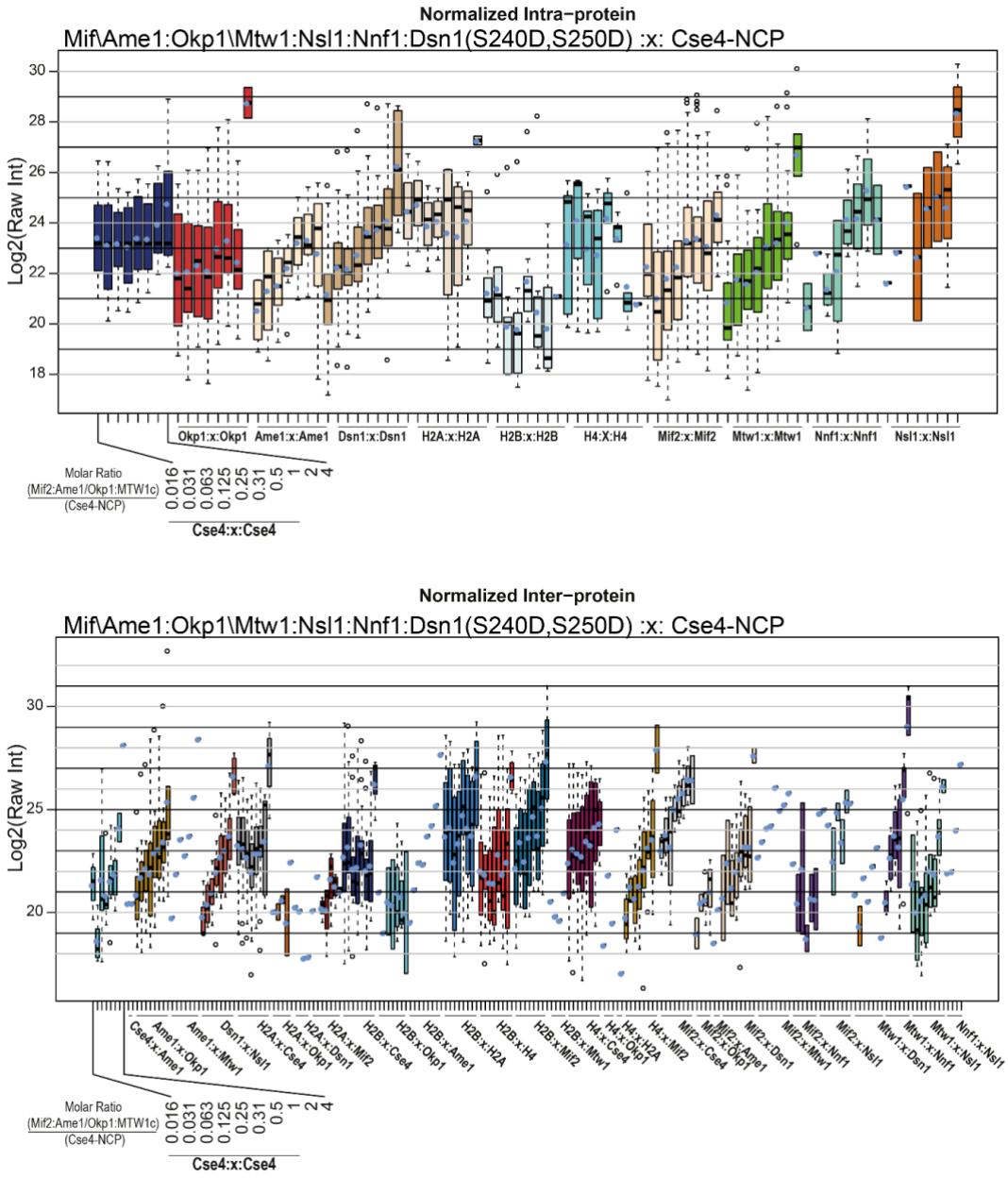

Figure 27. Intra- and Inter-Protein Crosslink Intensities of Cse4-NCP Titrated with MTW1c(Dsn1^{S240D,S250D}):Mif2:Ame1/Okp1. The plot was generated after normalization as described in Figure 17.

Figure 28

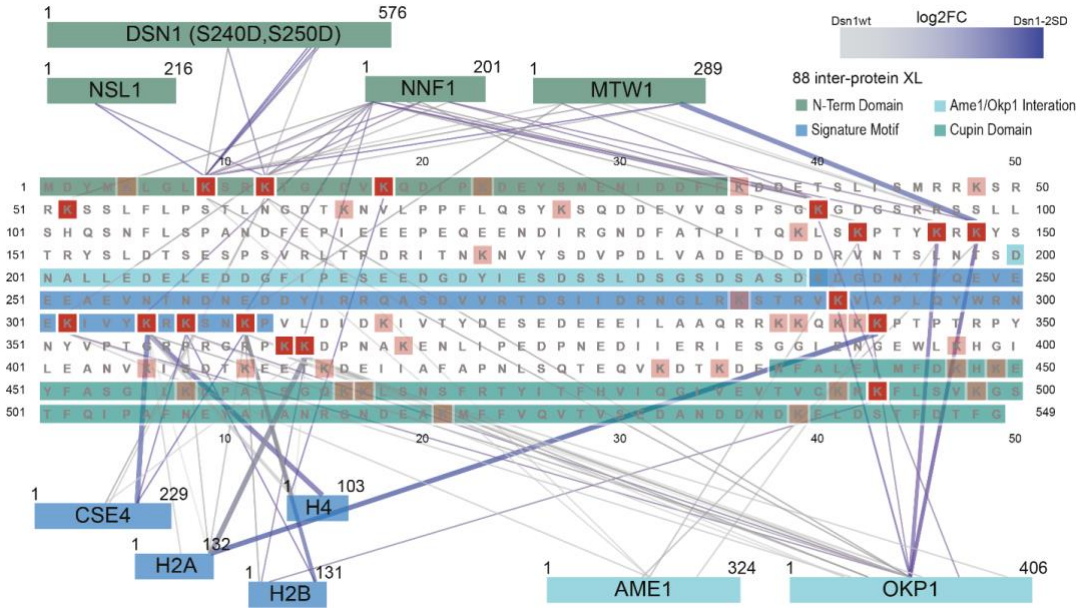

Figure 28. Schematic Representation of the Mif2 Amino Acid Sequence Indicating the Lysines Crosslinked to MTW1c, Mif2, Ame1/Okp1 and Cse4-NCP.

Crosslink intensities were extracted and quantified with our quantification workflow (M7, M8). The intensities of site-site crosslinks from Cse4-NCP titrated with MTW1c(wt):Mif2:Ame1/Okp1 or MTW1c(Dsn1^{S240D,S250D}):Mif2:Ame1/Okp1 were log2 transformed and the fold change (log2FC) of each restraint was calculated. Crosslinks were assigned to a color code (gray – no increase in intensity; blue – increase in intensity) and mapped on the amino acid sequence of Mif2. Crosslinked lysines are indicated in red, lysines that are not involved in crosslinks are light red. The Mif2 N-terminal domain (green) interacts with the MTW1c, the Ame1/Okp1 interaction domain is indicated in light blue, Cse4-NCP bind to the signature motif of Mif2 (depicted in blue) and the C-terminal Mif2 cupin domain is indicated in turquoise. The comparison of MTW1c(wt) to MTW1c (Dsn1^{S240D,S250D}) showed an increase of intensity of crosslinks that are within or close to the binding domains of the Mif2 interacting protein complexes.

Figure 29

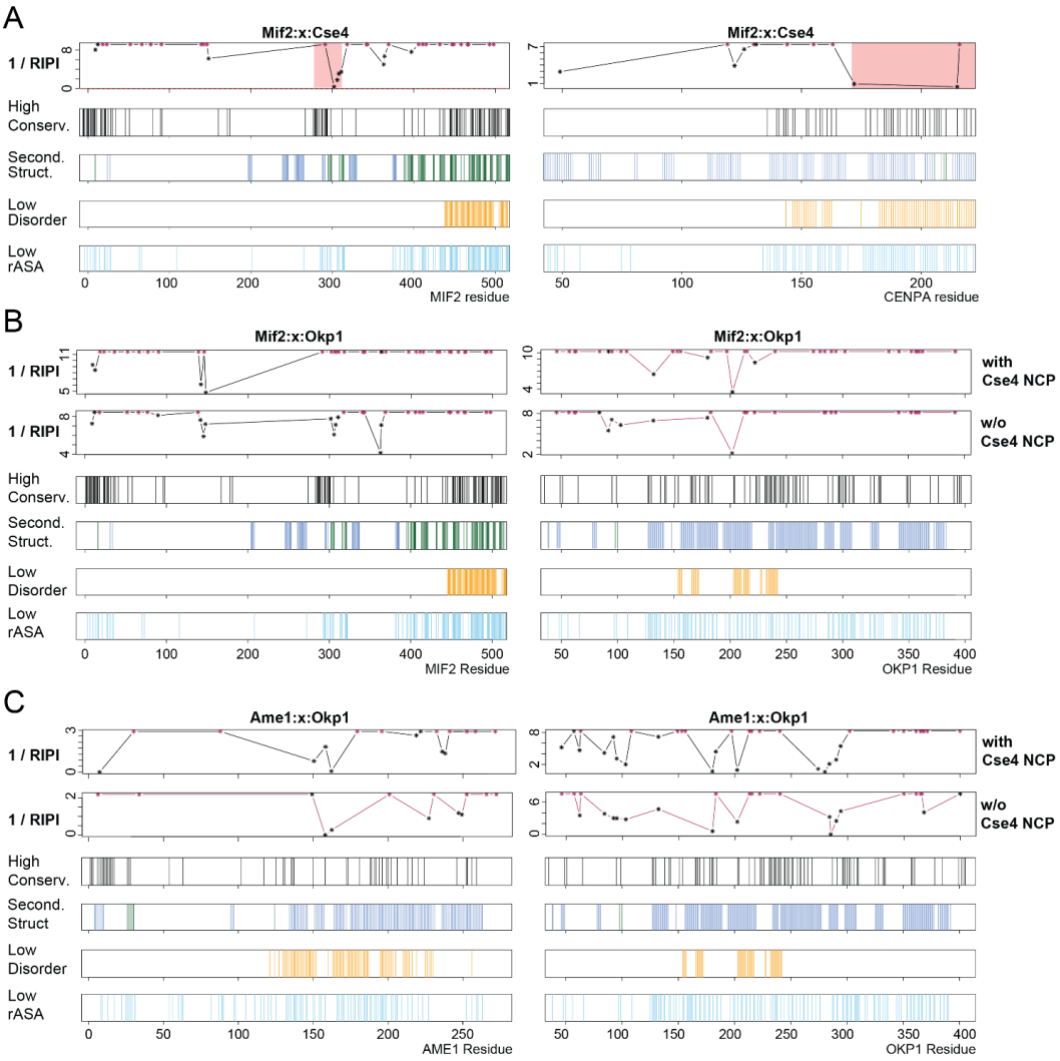

Figure 29. RIPI Analysis of the Mif2:Cse4, Mif2:Okp1 and Ame1:Okp1 Contacts to Identify the Binding Interfaces.

The Mif2:Cse4-NCP, Ame1/Okp1:Cse4-NCP and Mif2:Ame1/Okp1:Cse4-NCP complexes were analyzed by quantitative XLMS (Figure 6c). Crosslink intensities were extracted using the TOPP-qXL quantification pipeline (M8). The RIPI was calculated as described in Figure 17 (M10). The inverse of the RIPI was plotted in the respective first panel of each protein:protein interaction. (A) The sequence areas of the Mif2 and Cse4 interface is indicated by a drop of the inversed RIPI. The previously reported binding sites on Mif2$^{285\text{-}311}$ (signature motif) (Hornung et al., 2014, Kato et al., 2013) and the Cse4 loop L1 and C-terminus (Kato et al., 2013, Xiao et al., 2017) are indicated as red boxes. (B) (C) The Mif2:Okp1 and Ame1:Okp1 interfaces were analyzed in the presence or absence of the Cse4-NCP using the quantitative XLMS

datasets of the Ame1/Okp1:Cse4-NCP and Mif2:Ame1/Okp1:Cse4-NCP complexes. In the absence of Cse4-NCP the RIPI indicated that the Okp1 binding site is formed by the Mif2 residues 320-380 close to the signature motif. In the presence of Cse4-NCP the putative Okp1 binding site is indicated between Mif2 residues 150-250.

Figure 30

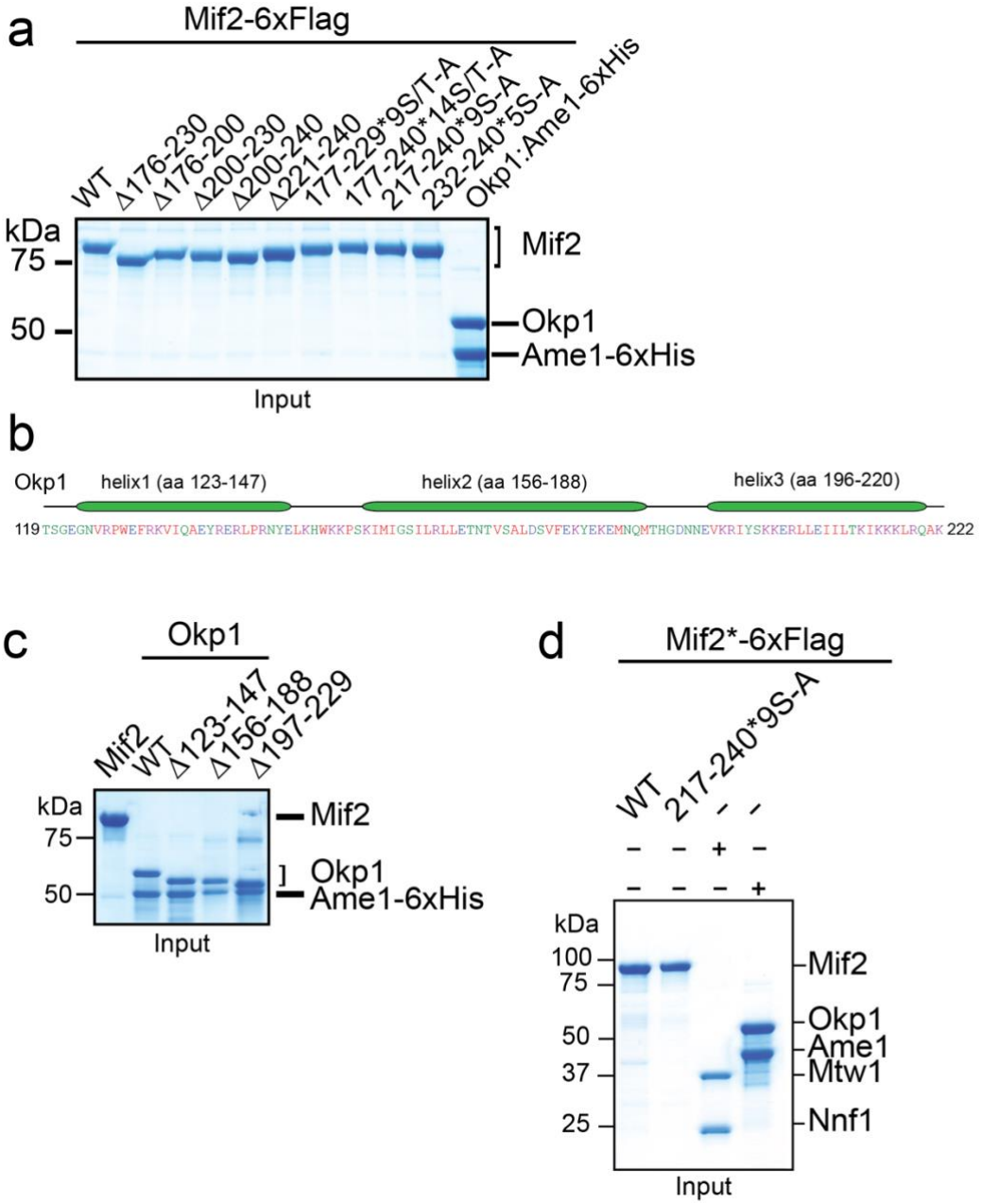

Figure 30. Input Protein Levels in Mif2:Ame1/Okp1 Binding Assays. **a**, The protein input levels for testing the interaction of Mif2-6xHis-6xFlag wild-type (wt), Mif2-deletion or -phospho-ablative mutants with Ame1-6xHis/Okp1 shown in Figure 7a were analyzed by Coomassie stained SDS-PAGE. **b**, Prediction of 3 alpha helical motifs in the Okp1 core domain (Hornung et al., 2014) using JPred (Drozdetskiy et al., 2015). **c, d**, The protein input levels of the binding assays shown in Figure 7c and f were visualized by SDS-PAGE and Coomassie staining.

Figure 31

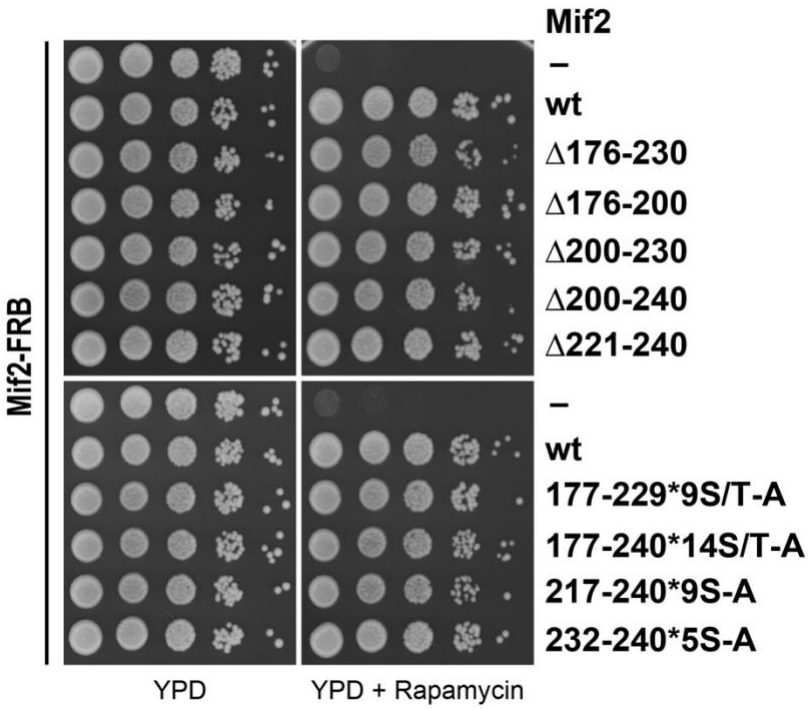

Figure 31. Cell Viability Assay of Mif2 Deletion and Phospho-Ablative Mutants in Budding Yeast Using the Anchor-Away System. The Mif2 wild-type and indicated mutant proteins were ectopically expressed in a Mif2 anchor-away strain (*Mif2-FRB*) and yeast cell growth was assessed in 1:10 serial dilutions on YPD medium at 30 °C in the absence and presence of rapamycin.

Figure 32

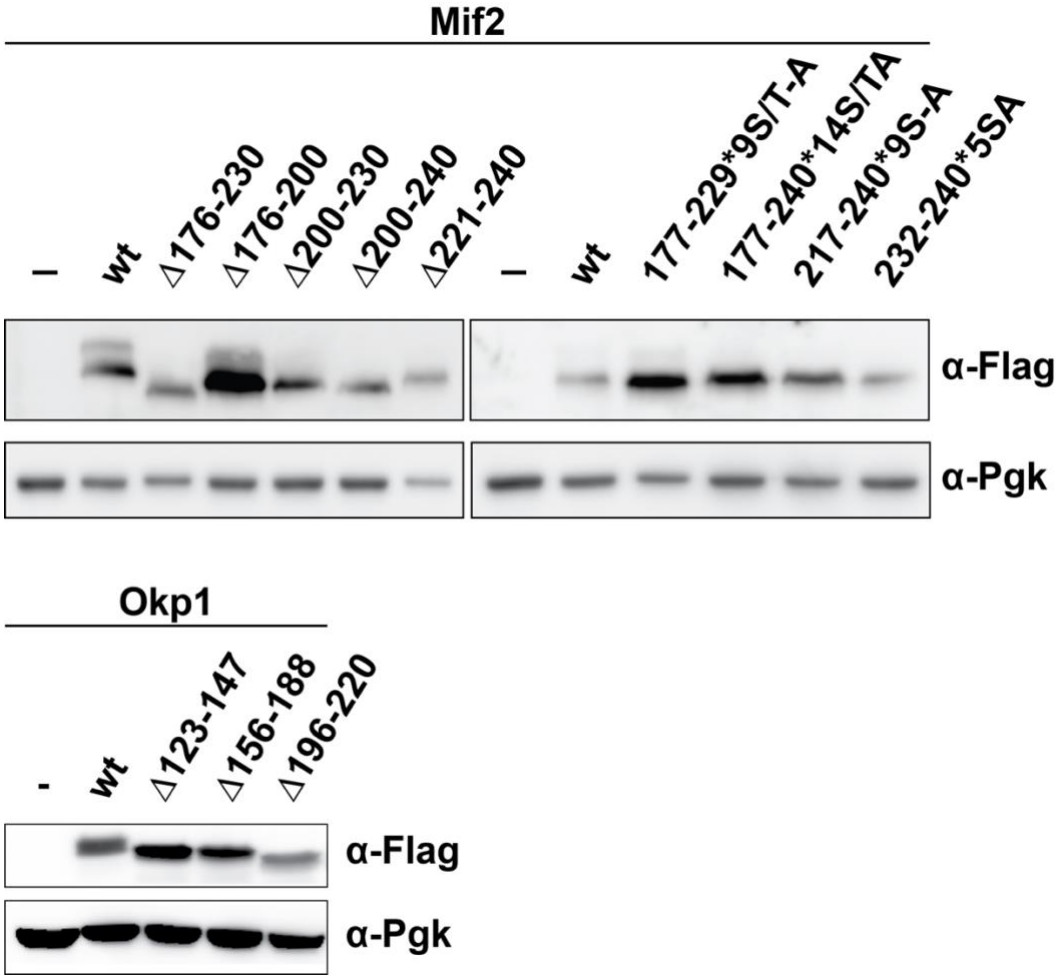

Figure 32. Western Blot Analysis of Ectopically Expressed Mif2 and Okp1 Wild-Type and Mutant Proteins in Yeast Cells.

Western blot analysis visualizing the levels of the ectopically expressed proteins in the yeast strains spotted in the cell viability assays. (A) Western blot of the expression of 7xFlag-tagged Mif2 wildtype (wt) and mutant proteins in the *Mif2-FRB/Dsn1S240A-S250A-S264A* background shown in Figure 7B. (B) Western blot of the expression of 7xFlag-tagged Okp1 wt and helix deletion mutants in the *Okp1-FRB* background shown in Figure 7D. Pgk1 levels are shown as loading control.

Figure 33

Figure 33. Phylogenetic Conservation of the Mif2^{CENP-C} and Okp1^{CENP-Q} Binding interface.

Multiple sequence alignments of the *S. cerevisiae* Mif2 and Okp1 amino acid sequences with their indicated mammalian orthologues were conducted using Clustal Omega (https://www.ebi.ac.uk/Tools/msa/clustalo/).

4.6 Discussion

Integrative structural biology applied XLMS to determine spatial proximity and protein connectivity at the domain level. Quantification of chemical crosslinking derived distance restraints has been initially used to detect conformational changes of protein complexes (O'Reilly and Rappsilber, 2018). In my thesis, I aimed to demonstrate the applicability of protein crosslink intensities to approximate binding affinities. The RNA polymerase datasets analysis indicated that shorter Euclidean distances of site-site crosslinks coincide with higher inter-protein crosslink intensities. This implied that inter-protein crosslinks of high intensity relative to the sum of all detected crosslink intensities are in proximity of the residues and may guide the identification of binding interfaces. Furthermore, this observation bears great potential for biological and functional modeling, even in *de novo* structural analysis of protein complexes. I applied the quantitative workflow, described by Victor Solis-Mezzarino (doctoral thesis, LMU), to estimate binding affinities of up to 11-budding yeast kinetochore proteins and their interaction sites (Solis-Mezarino, 2019).

To investigate the molecular mechanism of a protein complex, the interaction strength of its subunit contacts is a fundamental determinant to characterize its biological function. Most protein complexes are dynamically modulated by co-factors and PTMs to perform their often spatiotemporally regulated role. Thus far, biophysical methods to measure protein affinities focus on binary protein contacts that depend on the preparation of highly concentrated and homogenous protein or peptide samples, bulky fluorescent tags, or protein immobilization, therefore steric alteration, including crowding effects or masking of binding interfaces. Strikingly, all known methods to measure protein-protein affinity lack the ability to determine affinities of individual contacts in macromolecular complexes simultaneously and thus cannot study the cooperativity of interactions during assembly.

Based on inter-protein crosslink intensities acquired by in vitro titration experiments, I have assessed the concentration of the formed complex in the steady state equilibrium, which facilitated the estimation of apparent K_D values in multi-subunit complexes. Thereby, when introducing the crosslinker, the protein-protein interaction is stabilized by the covalent binding and therefore resembles a snapshot of the equilibrium at the time before quenching the crosslink reaction.

To preserve the equilibrium at a certain time, I kept the reaction time of each titration point long enough to ensure that the crosslink reaction was successful and short enough not to shift the equilibrium to either side. This step might be critical as too short reaction times might lead to an incomplete reaction with the proteins, especially within their interaction sites, and too long reaction times may lead to "over-crosslinking," where -due to the long reaction time- lysines that are incidentally in the proximity of the reactive site of the crosslinker are nonspecifically crosslinked and thus impact on the equilibrium. The reaction speed can be influenced by time and crosslinker concentration, and therefore each experiment was titrated for each crosslinker concentration in a reaction time of 2 minutes. As chemical labeling might also affect biophysical properties of the protein and are dependent on the presence of primary amine groups, I decided on a label-free quantification and an adequate number of titration points in order to interpolate protein concentrations from MS1 peak intensities. By using light and heavy labeled crosslinker, mixed in a 1:1 molar ratio, I ruled out irregular behavior of the reactant by only using crosslink spectra that were identified with both crosslinker species.

In this work, I have demonstrated the capacity of quantitative crosslinking and mass spectrometry to estimate K_D values ranging from 6 to 0.015 µM and which enabled the detection of a ~200-fold change in binding affinity. The three most commonly used technologies to measure the K_D of protein interactions are Surface Plasmon Resonance (SPR), Isothermal Titration Calorimetry (ITC), and fluorescence-based methods, such as Fluorescence Polarization (FP) and Fluorescence Resonance Energy Transfer (FRET). Advantages and disadvantages exist for all of these methods. For example, ITC measurements require large and highly concentrated protein amounts, proper orientation of the immobilized subunit has to be assured to allow binding in SPR or proper orientation of the fluorophores in FRET. In addition, obligatory labeling may change the molecular properties of the subunits. In SPR, the interaction is not measured in solution but on a surface, where non-specific interactions can occur. ITC has limited sensitivity (K_D range 0.1-10µM) and is best suited for measuring the biophysical properties of small molecules and peptides. None of these methods can measure large protein complexes under native conditions. qXLMS does not have the capability of measuring thermodynamic parameters or physical properties of the reaction and is based on statistical models that are only estimations of the forward reaction of the steady state equilibrium and, therefore, the apparent K_D of a protein

interaction. However, thus far, qXLMS is the sole opportunity to gain mechanistic insights into the dynamics of large protein assemblies and their everchanging degrees of stability to fulfill their biological functions. This was demonstrated on the highly conserved and essential macromolecular kinetochore complex (Musacchio and Desai, 2017).

Its complexity, size, and the predominance of elongated proteins have limited the structural and biophysical analysis of the kinetochore. The regulated and timely buildup of the kinetochore at centromeric chromatin ensures the fidelity of chromosome segregation by connecting chromosomes and spindle microtubules. In order to bi-orient chromosomes on the mitotic spindle, the kinetochore has to transmit forces of ~10 pN by forming a load-bearing attachment to spindle microtubules and a high-affinity link to the centromeric nucleosome, marked by the histone H3 variant CENP-A^{Cse4} (Gennerich et al., 2007, Mallik et al., 2004, Toba et al., 2006, Yardimci et al., 2008). Whereas the human kinetochore assembly is temporally regulated, establishing a microtubule attachment site in mitosis, budding yeast kinetochores are built up and attached to a single microtubule almost throughout the entire cell cycle (Biggins, 2013). In both species, phosphorylation by mitotic kinases has been shown to stabilize the kinetochore to withstand the pulling forces of the depolymerizing microtubules (Akiyoshi et al., 2009). If these phosphorylation events are responsible for a high-affinity binding between the kinetochore and centromeric chromatin upon the onset of anaphase is currently unknown.

To determine the apparent K_D values of the individual interactions that assemble the kinetochore on the octameric CENP-A^{Cse4} nucleosomal core particle (CENP-A^{Cse4}-NCP), I *in vitro* reconstituted various kinetochore complexes of up to 11 recombinant proteins, which were purified from *E. coli* except for CENP-C^{Mif2}, which was isolated from insect cells. I first tested the interaction between CENP-C^{Mif2} and CENP-U^{Ame1}/-Q^{Okp1}, which directly bind CENP-A^{Cse4}-NCP by immobilizing CENP-C^{Mif2} on solid-phase and found that this interaction was lost upon dephosphorylation of CENP-C^{Mif2}. *In vitro* phosphorylation by different mitotic kinases showed that phosphorylation of CENP-C^{Mif2} by Plk1^{CDC5} restored CENP-U ^{Ame1}/-Q^{Okp1} binding to levels detected with insect cell phosphorylated CENP-C^{Mif2} (Figure 5). This suggests that Plk1^{Cdc5} activity is required during CCAN establishment of budding yeast kinetochores to stabilize the CENP-U^{Ame1}/-Q^{Okp1} interaction. Mps1 and Plk1^{Cdc5} have a very similar consensus sequence and act cooperatively in SAC signaling in humans (von Schubert et al., 2015). I observed a

similar effect on restoring CENP-C^{Mif2} binding to CENP-U ^{Ame1}/-Q^{Okp1} for Mps1 and Plk1^{Cdc5} phosphorylation. However, CENP-C^{Mif2} bound CENP-U ^{Ame1}/-Q^{Okp1} levels were highest when phosphorylating CENP-C^{Mif2} with Plk1^{Cdc5}, compared to the other mitotic kinases and combinations thereof (Figure 5).

To compare protein affinities measured for binary interactions with those measured within a multi-subunit protein complex context, I measured the binary interactions by titrating constant amounts of CENP-A^{Cse4}-NCPs with increasing concentrations of CENP-C^{Mif2} or CENP-U^{Ame1}/-Q^{Okp1} or incubated a constant amount of CENP-U/-Q$^{Ame1/Okp1}$ with increasing concentrations of CENP-C^{Mif2}, respectively. These binary interaction affinities were then compared to the K_D values of the interactions in the CENP-C^{Mif2}: CENP-U ^{Ame1}/-Q^{Okp1}: CENP-A^{Cse4}-NCP complex. The K_D values were determined by the steady state equilibrium equation calculating the mean of the K_D values of each titration step. The affinities ranged from 3 to 6 µM for the binary interactions and were increased by 6-fold for the CENP-C^{Mif2}: CENP-A^{Cse4}-NCP interaction and by 10-fold for the CENP-U ^{Ame1}/-Q^{Okp1}: CENP-A^{Cse4}-NCP and CENP-C^{Mif2}: CENP-U ^{Ame1}/-Q^{Okp1} interactions in the CENP-C^{Mif2}: CENP-U ^{Ame1}/-Q^{Okp1}: CENP-A^{Cse4}-NCP complex (Figure 5). Taken together, this shows that putative phosphorylation of the inner kinetochore CENP-C^{Mif2} subunit by Plk1^{Cdc5} raises its affinity to the centromeric nucleosome by ~10-fold.

Restricting the inter-protein crosslinks to the subset that intersected with the CENP-C$^{Mif2(285-311)}$ signature motif which directly binds the CENP-A^{Cse4} C-terminus, resulted in a K_D value of ~0.9 µM for the binary interaction, which dropped by a factor of 30 upon the cooperative binding of CENP-C^{Mif2} and Ame1/Okp1 to the Cse4-NCP (Figure 5). ITC measurements of the CENP-C$^{Mif2(285-311)}$ peptide with the CENP-A^{Cse4}-NCP yielded a K_D of ~0.5 µM similar to our quantitative XLMS determined value, once inter-protein crosslinks were restricted to the minimal binding interface (Kato et al., 2013). This indicates that estimation of the apparent K_D by crosslink intensities has a sufficient sensitivity that is capable of estimating equivalent measurements to thermodynamic based methods of dissociation constants determination. Furthermore, it represents a more holistic approach to characterize protein-protein interactions in the context of larger protein assemblies.

As cryo-EM studies are not capable of resolving the localization of CENP-C^{Mif2} on CENP-A^{Cse4}, I analyzed the crosslinks between these proteins in order to further

characterize this pivotal interaction. The most intense crosslinks within the interaction site of CENP-C^{Mif2} and CENP-A^{Cse4} were on CENP-C^{Mif2} K302, K306, K308, and K311 (Figure 28). All of these crosslinks exclusively interact with K172 of CENP-A^{Cse4}, which is in the L1-loop and not resolved in the cryo-EM structures (Figure 8) (Ali-Ahmad et al., 2019, Yan et al., 2019). Furthermore, no crosslinks were found that showed an interaction of CENP-C^{Mif2} with the C-terminal end of CENP-A^{Cse4}. Besides the CENP-C^{Mif2} interaction with CENP-A^{Cse4}, also crosslinks with low intensity were found to CENP-U^{Ame1} and CENP-Q^{Okp1} (Figure 16, Figure 28). Lysines interacting with the CENP-A^{Cse4}-NCP are also involved in forming intra-protein crosslinks within CENP-C^{Mif2,} indicating increased flexibility of CENP-C^{Mif2}. However, intra-protein crosslinks are generally at a lower intensity. The increase of crosslink intensity upon interaction with the centromeric nucleosome may imply a conformational change in CENP-C^{Mif2} upon binding of the CENP-A^{Cse4}-NCP, as has been recently shown (Killinger et al., 2020).

CENP-C^{Mif2}, which seems to have a pivotal role in the assembly of the inner kinetochore, is also binding to the outer kinetochore MIS12^{MTW1} complex. The interaction of the CENP-C^{Mif2} N-terminus with the MIS12^{MTW1} complex is well described by cryo-EM analysis (Dimitrova et al., 2016). As a second receptor for MIS12^{MTW1} complex interaction, the N-terminus of CENP-U^{Ame1} also binds an equivalent CENP-C^{Mif2} motif. This equivalency was demonstrated by swapping the N-termini of Ame1$^{Mif2\text{-}N}$ and CENP-C^{Mif2}, where Ame1$^{Mif2\text{-}N}$ was capable of rescuing the lethality induced by deletion of the Ame1 N-terminus (Killinger et al., 2020). Whether the two proteins bind cooperatively or competitively to the MIS12^{MTW1} complex was a matter of debate (Hornung et al., 2014, Killinger et al., 2020, Dimitrova et al., 2016). When the CENP-C^{Mif2} N-terminal binding site was purified from *E.coli* and pre-bound to the MIS12^{MTW1} complex, the binding was competed with increasing amounts of a CENP-U^{Ame1} N-terminal peptide (Killinger et al., 2020). However, phosphorylated CENP-C^{Mif2} was capable of binding the MIS12^{MTW1} complex cooperatively with CENP-U^{Ame1} (Figure 7e), while the cooperative interaction was lost in a phospho-ablative mutant of CENP-C^{Mif2}. This indicates that phosphorylation of CENP-C^{Mif2} facilitates cooperative binding of CENP-C^{Mif2} and CENP-U^{Ame1} to the MIS12^{MTW1}complex, probably by inducing a conformational change of the N-terminus of CENP-C^{Mif2}. I titrated increasing amounts of an equimolar mixture of MIS12^{MTW1}complex:CENP-C^{Mif2}: CENP-U^{Ame1} /-Q^{Okp1} to CENP-A^{Cse4}-NCP to investigate whether two AuroraB^{Ipl1} phosphorylation sites (S240 and S250) on the MIS12^{MTW1}complex subunit Dsn1 have an impact on

the centromere binding affinity of this 11-protein budding yeast kinetochore complex. While the K_D of wildtype Dsn1 containing MIS12^{MTW1}complex did not change the affinity of CENP-A^{Cse4}-NCP binding, the addition of the phosphomimetic MIS12^{MTW1}(Dsn1$^{S240D, S250D}$) complex yielded an increase of ~200 fold. Thus, both phosphorylation events contribute synergistically to the cooperative stabilization of the kinetochore at the centromeric nucleosome. Since in the qXLMS based K_D measurements presented here and in ITC experiments, the affinity of the CENP-U^{Ame1} binding site was lower compared to the CENP-C^{Mif2} binding site of the MIS12^{MTW1} complex, it remains elusive whether CENP-C^{Mif2} engages in intermolecular interactions resulting in conformational changes or CENP-U^{Ame1} masks the MIS12^{MTW1} complex binding site for CENP-C^{Mif2} (Killinger et al., 2020).

Based on inter-protein crosslink intensities, we have identified the CENP-C^{Mif2}:/ CENP-Q^{Okp1} interface using the highest Relative Interface Propensity Index (RIPI). Binding regions were indicated as a drop of the inverse of the RIPI; here, the inter-protein crosslink intensities are higher than the sum of all intensities, which results in high RIPI values (Figure 6 and Figure 29). Considering the degree of conservation, secondary structure prediction, relative accessible surface area, and degree of disorder of the protein structure, the interface on CENP-C^{Mif2} was predicted between aa 176-230 and between aa 196-220 on CENP-Q^{Okp1} (Figure 6 and Figure 29). Furthermore, I demonstrated that phospho-ablative mutations in the predicted CENP-C^{Mif2} interaction region and in the MIS12^{MTW1} complex subunit Dsn1 lead to synthetic lethality *in vivo,* indicating that the induced cooperativity by these particular sites is essential for cell viability (Figure 7).

CENP-C^{Mif2} was described as the cornerstone for kinetochore assembly. However, due to its high flexibility and the presence of disordered regions, neither crystal structures nor cryo-electron microscopy structures have been solved yet (Lampert and Westermann, 2011). In an attempt to map the topological arrangement of CENP-C^{Mif2} and, in particular, how it is positioned at centromeric chromatin reaching to the outer kinetochore, I gathered the crosslink data of the interconnectivity of 11 yeast kinetochore proteins with recent cryo-EM structures (Figure 8). Particularly interesting is a helix-turn-helix motif in CENP-Q^{Okp1}, where the first helix (aa 161-188) is responsible for the interaction with the N-terminal tail of CENP-A^{Cse4} and the second helix (aa 196-217) induced the binding with CENP-C^{Mif2} (Figure 8). This model gives functional insight into how phosphorylation induces the cooperative binding of these proteins.

Although human and budding yeast kinetochores differ in subunit connectivity, the human MIS12 complex has been implicated in CENP-A stabilization at centromeres suggesting that similar phosphorylation events might induce cooperative stabilization of human kinetochores. The yeast Mif2: Okp1 interface is partially conserved in their human orthologues CENP-C: CENP-Q, and a single nucleotide polymorphism in this region (CENP-C T667K) has been found in malignant hepatic cancer cells (Wu et al., 2014). As Ame1/Okp1, together with Mif2, are the only essential CCAN proteins in budding yeast and have functions comparable to vertebrate CENP-L/-N and CENP-C, their functional conservation is very likely. Therefore, it would be interesting to further characterize the functional conservation of CENP-L/-N and CENP-Q/-U between yeast and human and the mechanism which establishes high-affinity microtubule binding upon the onset of anaphase.

In this part of my thesis, I was able to demonstrate the estimation of dissociation constants on various protein interactions (Figure 3 , Figure 5, Figure 6). qXLMS also allows the quantification of multivalent interactions within a protein complex. Furthermore, PTMs at or around the contact interface can be quantified, which allows the evaluation of the effect of PTMs on the affinity of protein interactions. qXLMS can detect changes in these complex and sophisticated structures and thus may reveal the crosstalk of multi-subunit protein complexes while maintained in its native state. Although the cell cycle dependent CCAN reorganization has not been comprehensively understood yet, it might be related to the dynamic (re)localization of the conserved CCAN subunits in kinetochores. In fact, electron microscopy observation suggests that during mitosis, the CCAN subunits change their distribution in the kinetochore when microtubule tension is applied. How the kinetochore structure is rearranged and what is the significance of this remodeling are future questions to be addressed.

5. A Time-Resolved Proteomic Analysis of the Human Centromeric Chromatin

5.1 Introduction

5.1.1 The Eukaryotic Cell Cycle

The extraordinary trait of life is its capacity to proliferate and pass on the genetic information from generation to the next. In eukaryotes, the cell cycle consists of four distinguished steps: G1-, S- and G2-phase, followed by mitosis. The fundamental elements that drive the progression of the cell-cycle are cyclins (Evans et al., 1983). These act as a regulatory subunit and activate cyclin-dependent kinases (CDKs), the "engine" of the cell cycle (Ubersax et al., 2003, Sullivan and Morgan, 2007). Hence, the oscillating protein levels of cyclins, which are determined by gene expression and degradation through ubiquitin-mediated proteolysis, result in distinct CDK activities (Peters, 2006). This interplay between cyclin production and degradation, along with the activation of CDKs, initiates and regulates different cell-cycle specific events to take place in an orderly manner (Martinez-Alonso and Malumbres, 2020). Cell cycle-progression happens in waves of transcription (Simon et al., 2001, Pramila et al., 2006, Lee et al., 2002). The next wave of transcription forms a continuous regulatory network in which each wave is triggered by the previous one and contains activators for the next wave (Simon et al., 2001, Pramila et al., 2006, Lee et al., 2002). For example, the deactivation of CDKs is needed in mitosis for spindle disassembly, cytokinesis, and the transition into the G1-phase (Martinez-Alonso and Malumbres, 2020).

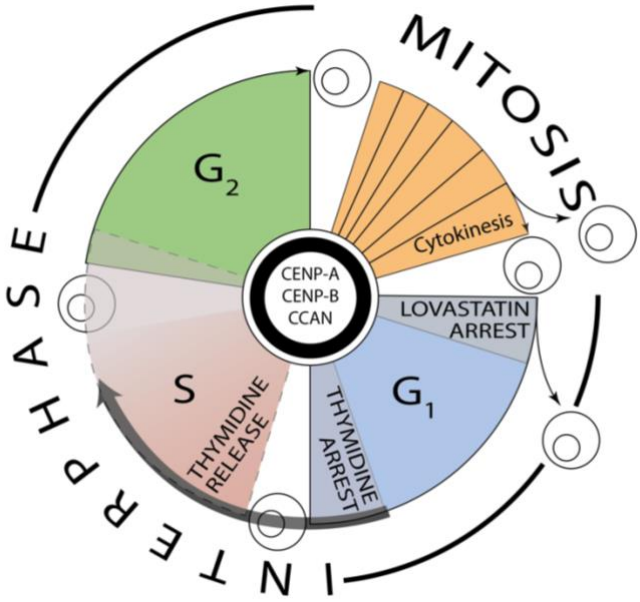

Figure 34. Schematic Overview of the Cell Cycle and Arrest or Arrest/Release Strategies.

The composition of the kinetochore is precisely timed over the cell cycle. In S-phase, chromosomes are duplicated by DNA replication, and centromere proteins are dynamically recruited and evicted to and from the centromeric chromatin. These processes can be tracked by the addition of chemical compounds to capture the cell in distinct cell cycle moments. For cell cycle arrest, I used Lovastatin, which leads, upon addition, to the accumulation of the CDK inhibitors p21 and p27 and, therefore, a G1-phase arrest. When adding thymidine, the cells arrest in G1/S-phase transition by inhibition of ribonucleotide reductase and therefore stalling the replication machinery by inhibition of dCTP synthesis. The cells can be released of this arrest by washing out thymidine and the addition of dCTP.

Throughout G1-phase, the cells commit to fate decisions, grow, and prepare for entering S-phase by synthesizing precursor proteins needed for DNA-synthesis. During every round of cell division, cells decide to either continue dividing or withdraw from the cell cycle to enter into the quiescent state (G_0) by a mechanism identified as 'restriction point' (R-point) control (Foster et al., 2010). Throughout G1-Phase, cyclin-D accumulates and forms a complex with CDK4/6, which creates a positive feedback loop to initiate the expression of S-phase genes (Bertoli et al., 2013). After passing the R-point, the cell is committed to the cell cycle, and irreversibly progresses through DNA synthesis or S-phase (Bertoli et al., 2013). Here, the replication machinery duplicates the DNA of each sister chromatid. Activation of the pre-replication complexes (pre-RC), which is assembled during

the G1-phase, enables the unwinding of small stretches of parental DNA by MCM (minichromosome maintenance protein complex) helicase (Hammond et al., 2017). The phosphorylation-induced activation of replication protein A (RPA) leads to its binding to ssDNA and therefore primes the replication fork for loading of replicative DNA polymerases and PCNA (Boehm et al., 2016). This completes the activation of replication forks, and DNA synthesis starts (Boehm et al., 2016). Since new DNA must be packaged into nucleosomes to function appropriately, the synthesis of canonical histones occurs simultaneously with DNA replication (Annunziato, 2005, Alabert and Groth, 2012). This high demand for canonical histones is, on the one hand, provided by increasing synthesis of new canonical histones, organized as multiple copies in gene-clusters, that only transcribe during S-phase (Hammond et al., 2017). In addition to increased transcription of histone genes, genes of canonical histones lack polyadenylated tails and instead possess a conserved supply regulating stem-loop structure at the 3' end (Marzluff et al., 2008). On the other hand, parental histones, produced by the cell during replication, are rapidly recycled into nucleosomes behind the replication fork (Hammond et al., 2017). MCM helicase translocation along the leading strand most likely mediates the recycling of these histones, which disrupts parental nucleosome octamers, following the release of H3-H4 and H2A-H2B subunits (Hammond et al., 2017, Petryk et al., 2018). Chromatin assembly factors (CAFs) are reassembling the nucleosomes behind the replication fork in a process that is not fully understood.

With the completion of DNA duplication, the cell enters a short phase of rapid growth and protein synthesis, termed G2-phase. As some cell types directly proceed from S-phase to mitosis, G2-phase is not a fundamental part of the cell cycle progression (Liskay, 1977). However, double-strand breaks, which occur during DNA-replication, might be repaired by homologous recombination using the intact sister chromatid during this subphase of the interphase (Burgoyne et al., 2007). A threshold level of the activated cyclin-B1/CDK1 complex determines the entry into mitosis after the G2-phase (Stark and Taylor, 2006, Martinez-Alonso and Malumbres, 2020). The protein levels of cyclin B1 remain suppressed throughout G1 and S phases and start rising after DNA replication (Dimova et al., 2012, Martinez-Alonso and Malumbres, 2020). A positive feedback loop of CDK1 with Cdc25 phosphatases, also involving Polo-like kinase (PLK1), leads to the transition into mitosis (Martinez-Alonso and Malumbres, 2020).

At the end of S-phase, each sister chromatid only holds half the epigenetic modifications that were present in the parental chromatid (Hammond et al., 2017). Accordingly, the cell must use this partial set of instructions to restore functional chromatin domains (like, e.g., centromeres) before entering mitosis.

5.1.2 Histone Inheritance During Replication

What has arisen from more recent studies is the observation that chromatin states harbor epigenetic information, which is propagated between cell divisions to maintain cellular identity and which also defines centromere integrity and function (Hammond et al., 2017). In S-phase, the chromatin disassembles prior to DNA replication in order to allow replication fork passage (Hammond et al., 2017). Histone chaperones, epigenetic readers, and writers, along with chromatin remodelers, follow the replication fork and reassemble chromatin after replication (Hammond et al., 2017). The influence of the cell cycle on chromatin structure and composition still remains elusive, despite long-standing efforts to solve the question, how these processes are orchestrated. The maintenance of characteristic chromatin traits is especially crucial for functional domains like the centromere.

Behind the replication fork, two pathways of histone deposition have to happen simultaneously in distinct processes: 1. reassembly of evicted parental histones and 2. incorporation of newly synthesized histones (Petryk et al., 2018, Yu et al., 2018, Stewart-Morgan et al., 2020, Alabert and Groth, 2012). CAF1 is a histone chaperone that directly interacts with new histones and the replication fork via the processivity clamp PCNA (Shibahara and Stillman, 1999, Moggs et al., 2000). This pathway of new histone deposition demonstrates a close link to DNA replication.

DNA replication happens through distinct mechanisms for the leading and the lagging strand (Ransom et al., 2010, Probst et al., 2009). Likewise, to prevent the dilution of epigenetic features, the redeposition of parental histones happens from independent types of machineries, near the leading and lagging strand after the replisome (Ransom et al., 2010, Probst et al., 2009). In this process, as mentioned earlier, the conserved N-terminal tail of MCM2 from the MCM helicase complex binds and evicts parental H3-H4 dimers and tetramers (Huang et al., 2015). The deletion of this N-terminal histone binding domain leads to chromatin assembly defects in yeast (Huang et al., 2015). Novel deep sequencing techniques identified a nearly equal distribution of parental histones to the leading and lagging strand after the replisome (Petryk et al., 2018). When the histone binding properties of

MCM2 is abolished by the deletion of the N-terminus, parental histones strongly prefer the leading strand—hence showing an apparent defect in lagging strand histone recycling (Petryk et al., 2018).

Similarly, after detaching one of the core lagging strand polymerases (Polα) from the MCM helicase, lagging strand histone recycling fails (Gan et al., 2018). Whether the N-terminal truncation of MCM2 disrupted the interaction of the lagging strand DNA replication machinery or impaired a histone specific H3-H4 recycling is not known (Gan et al., 2018). Two non-catalytical subunits of the core leading strand enzyme Polε, POLE3-POLE4, have been shown to harbor histone chaperone properties for histone H3-H4 (Bellelli et al., 2018). Likewise, the deletion of the yeast homologs showed impaired, leading strand parental histone recycling (Yu et al., 2018). This evidence led to the assumption that parental histone distribution happens in a semi-conservative manner, guided by a specialized type of machinery (Bellelli et al., 2018).

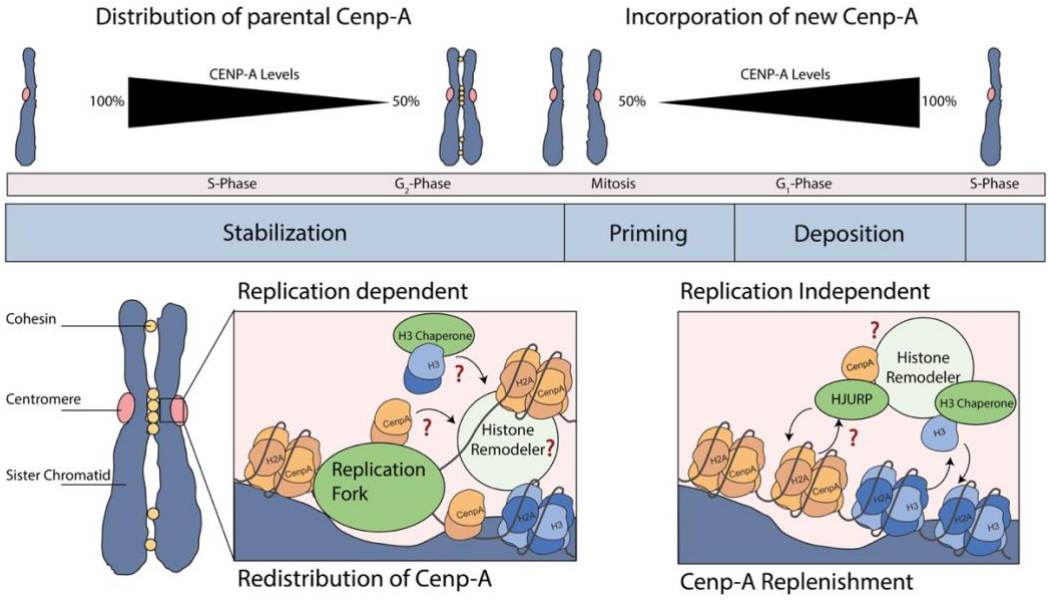

Figure 35. Identifying the CENP-A Loading Machinery Assembled on Centromeric Chromatin.

During S-Phase, CENP-A levels are halved and do not rise until G1-phase, although protein synthesis of CENP-A peaks in G2-phase. However, loading of CENP-A is replication-independent and restricted to early G1-phase, which is possibly regulated by the CENP-A specific chaperone HJURP, and cell cycle-regulated post-translational modifications. During S-phase, nucleosomes are disassembled in front of the DNA replication machinery and reincorporated into chromatin behind the replication fork. The underlying processes to maintain chromatin domains is vastly unknown.

The necessity for such machinery becomes even more apparent in terms of specialized chromatin domains like the centromere, which is characterized by the presence of CENP-A nucleosomes. Throughout DNA replication, parental CENP-A-H4 histones are distributed equally to the leading and lagging strand after the replisome (Jansen et al., 2007, Dunleavy et al., 2011, Ross et al., 2016). Recent data showed that CENP-A deposition happens at the same DNA locations in the centromere over several cell cycles (Nechemia-Arbely et al., 2019). Whether the CENP-A specific chaperone HJURP is capable of mediating the redeposition by itself or if this mechanism necessitates a distinct type of machinery is unclear. Furthermore, the centromeric histone CENP-A is atypical, as most histone variants express from one or two gene copies throughout the cell cycle. CENP-A expression levels peak in G2-phase, but histone incorporation exclusively happens in early G1-phase (Foltz et al., 2009, Heun et al., 2006, Shelby et al., 1997, Jansen et al., 2007). It seems extraordinary that during mitosis, where CENP-A establishes the physical link between depolymerizing spindle microtubules and DNA, the centromere only harbors half of the maximum CENP-A levels (Ross et al., 2016, Jansen et al., 2007).

5.1.3 The CENP-A Deposition Pathway during G1-Phase

For stable centromeric chromatin inheritance over many cell cycles, the CENP-A deposition machinery must ensure exact deposition at the site of pre-existing centromeres. This process occurs in three distinct steps, each involving a specific protein complex (Stellfox et al., 2013). I. The priming of centromeric chromatin in order to create a predisposed state of chromatin (Stellfox et al., 2013, Moree et al., 2011). II. Deposition of new histones by CENP-A specific proteins (Barnhart et al., 2011, Stellfox et al., 2013, Dunleavy et al., 2009, Foltz et al., 2009, Shuaib et al., 2010). III. Maturation of the nascent centromeric chromatin by the reestablishment of the centromeric environment and stabilization of nucleosomes by histone remodeling (Stellfox et al., 2013, Lagana et al., 2010, Perpelescu et al., 2009).

Towards the end of mitosis, when CDK1 levels decrease, the MIS18 complex (consisting of Mis18α, Mis18β, Mis18BP1, RbAp46, RbAp48) is localized to centromeres and associates with CENP-A nucleosomes in a phosphorylation-dependent manner (Stellfox et al., 2013, Silva et al., 2012, Moree et al., 2011, Dambacher et al., 2012). Under this condition, Mis18α, Mis18β, and Mis18BP1 are dependent on each other for centromere targeting (Fujita et al., 2007, Hayashi et

al., 2004). Knockdown experiments showed the requirement of all three proteins along with RbAp46 RbAp48 for the deposition of newly synthesized CENP-A (Fujita et al., 2007). The CENP-A specific chaperone HJURP is also a necessary and sufficient player in histone deposition, as it localizes to centromeres specifically at G1-phase and is capable of generating neocentromeres upon ectopic localization (Barnhart et al., 2011, Dunleavy et al., 2009, Foltz et al., 2009). Knockdown of the MIS18 complex members Mis18α and Mis18BP1 results in loss of centromeric HJURP, which underlines the importance of the MIS18 complex in CENP-A deposition (Barnhart et al., 2011).

Since the deposition of CENP-A appears to be phosphorylation-dependent, the APC/C targeted degradation of B-type cyclins after anaphase onset is capable of temporal regulation of CENP-A deposition (Castro et al., 2005, Erhardt et al., 2008, Grosskortenhaus and Sprenger, 2002). The coupling of the deposition machinery to the CCAN might regulate the spatial regulation of CENP-A deposition (Stellfox et al., 2013). In particular, as confirmed in *Xenopus* egg extracts, the MIS18 complex interacts with the CCAN protein CENP-C to initiate CENP-A deposition (Moree et al., 2011). However, the ectopic localization of CENP-C did not recruit the MIS18 complex and initiated CENP-A deposition (Moreno-Moreno et al., 2006, Heun et al., 2006). The lack of ectopic MIS18 complex initiated CENP-A deposition was leading to the assumption that the deposition pathway is more complex and not fully understood.

Priming of centromeric chromatin is an acetylation dependent mechanism. The Mis18 complex promotes H3.3 acetylation by the recruitment of acetyltransferase KAT7, which earmarks H3.3 histones for chromatin eviction (Ohzeki et al., 2016, Srivastava and Foltz, 2018, Stellfox et al., 2013). Accordingly, after knockdown of MIS18 complex members, the deposition of CENP-A could be restored by trichostatin A treatment, increasing the overall acetylation state by histone deacetylase (HDAC) inhibition (Fujita et al., 2007). The exchange mechanism of histone H3.3 eviction and CENP-A deposition is not known. Known histone H3 variants associate with distinct histone chaperones to define the location and timing of histone remodeling (Zink and Hake, 2016). Likewise, CENP-A and histone H4 form a pre-nucleosomal complex with HJURP that localizes to centromeres during G1-phase and which was sufficient to assemble nucleosomes *in vitro* (Shuaib et al., 2010, Bernad et al., 2011, Foltz et al., 2009, Dunleavy et al., 2009).

Equally, the recruitment of HJURP to non-centromeric sites leads to CENP-A incorporation into chromatin. However, the formation of the pre-nucleosomal CENP-A/ H4/ HJURP complex excludes tetramer formation as well as DNA interactions (Barnhart et al., 2011, Bernad et al., 2011, Dunleavy et al., 2009, Shuaib et al., 2010). Hence, CENP-A incorporation requires a stepwise conformational change and nucleosome assembly mediated by a histone remodeling machinery (Stellfox et al., 2013). Besides, CENP-A deposition takes place at a highly condensed chromatin state, right after mitosis (Cuylen and Haering, 2011). Even though depletion of structural maintenance of chromosomes protein 2 (SMC2) leads to a reduced CENP-A incorporation, there is no evidence of a link between chromosome condensation and centromere maintenance (Samoshkin et al., 2009). Condensin may maintain the higher-order structure of chromatin (Yong-Gonzalez et al., 2007, Verdaasdonk and Bloom, 2011, Fazzio and Panning, 2010). However, whether this rigid chromatin environment might necessitate an ATP-dependent CENP-A histone remodeler in order to exchange earmarked H3.3 histones with CENP-A remains to be identified. Finally, the RSF complex (Rsf1 and Snf2h) and Mgc-RacGap stabilize newly deposited CENP-A nucleosomes (Perpelescu et al., 2009, Lagana et al., 2010). This maturation process helps to generate centromeric chromatin sufficiently stable to support kinetochore assembly and chromosome segregation during mitosis (Perpelescu et al., 2009, Lagana et al., 2010, Nechemia-Arbely et al., 2012). The cell cycle dependent deposition of CENP-A nucleosomes, as well as the maintenance of centromere identity, are fundamental processes for cell viability that demand a detailed understanding of the proteinaceous environment of centromeric chromatin.

5.2 Aims of the Work

Centromere identity in nearly all eukaryotes is epigenetically defined and based on the physical properties of CENP-A containing nucleosomes. During DNA replication CENP-A levels at each daughter centromere are halved. The directed redistribution of CENP-A nucleosomes may require a specific deposition machinery like histone-modifying enzymes, chromatin remodelers and other structural and regulatory proteins. Furthermore, the approximate twofold dilution requires the replenishment of the CENP-A pool to maintain CENP-A levels and centromere identity. The current hypothesis assumes that the gaps resulting from the distribution of CENP-A nucleosomes to daughter centromeres in S-phase are filled by H3 nucleosomes, which serve as placeholders for CENP-A deposition. Centromere propagation by maintaining a constant number of CENP-A nucleosomes through generations suggests that CENP-A itself templates the incorporation of new CENP-A histones at the exit of mitosis. The molecular basis of the remarkable accuracy of the underlying CENP-A replenishment mechanism has not yet been fully understood. Preexisting CENP-A nucleosomes and CENP-C recruit the MIS18 complex that, together with acetyltransferases, marks H3.3 nucleosomes for replacement by new CENP-A nucleosomes. Recognition of the spatial proximity between the CENP-A and an H3.3 nucleosome may be accomplished by the CCAN protein CENP-C and post-translational histone modifications. In addition to selectively assemble and stabilize the kinetochore on CENP-A nucleosomes, the CCAN proteins might have a role in recruiting the replacement machinery which directs the exchange of the neighboring H3.3 nucleosome.

In this project I aimed to identify key proteins that establish the molecular bases of the mechanisms that redistribute CENP-A after replication and facilitate its deposition at the M/G1 transition. Notably, the redistribution of CENP-A after replication fork passage and the histone remodeling in G1-phase is enigmatic. Previous studies tried to tackle these questions by cell biological assays and fluorescence microscopy. The identification of time-resolved cell cycle specific protein interactions of CENP-A might be instrumental to assess the importance of these candidate proteins by cell biology. In this work, I established the time-resolved analysis of CENP-A copurifying protein complexes to monitor quantitative alterations of centromere-associated proteins. I aimed to address the following questions:

- How is the centromere associated proteome changing throughout the cell cycle?

- What are the candidate proteins necessary for CENP-A partitioning to sister chromatids subsequent to DNA replication?

- Is there a CENP-A specific histone remodeler and what CENP-A specific chromatin remodelers may have a role in CENP-A deposition and maintenance?

5.3 Results

Although CENP-A has been subjected to intense studies for the past decade, little is known about modulation and mechanisms of CENP-A itself and interacting partners. To identify the CENP-A interactome in a comprehensive manner, I established a cell cycle arrest release protocol followed by chromatin-immunoprecipitation (ChIP) of Micrococcal Nuclease (MNase) digested chromatin to obtain mono- or oligonucleosomes. To purify the low abundant CENP-A histone from centromeric chromatin, doxycycline-inducible stable HeLa cell lines expressing either N-terminal Flag-HA-6xHis (pEWS-Nfl) CENP-A or histone H3.3 were established. Here the Flp-IN-T-REx expression system was used, which incorporates the gene of interest (GOI) at a single loci that showed near endogenous expression levels (Tighe et al., 2004). The expression of pEWS-CENP-A and pEWS-H3.3 was confirmed in a protein immunoblot against HA-antibody from whole-cell extracts, comparing induced and non-induced asynchronously cycling cells. Chromatin-associated proteins are tightly interacting with DNA and have to be solubilized by DNA digestion. I used controlled incomplete MNase digestion. MNase is a calcium-dependent endonuclease that cuts in the linker regions between nucleosomes in chromatin. Partial digestion with MNase results in a periodic pattern, resembling the spacing of nucleosomes. Since the size of centromeric chromatin varies between a single nucleosome and several hundred, I titrated the MNase amount to obtain either mostly mononucleosomes or ~30N oligonucleosomes. To assess the quality of chromatin, the DNA was deproteinized and analyzed by agarose gel electrophoresis.

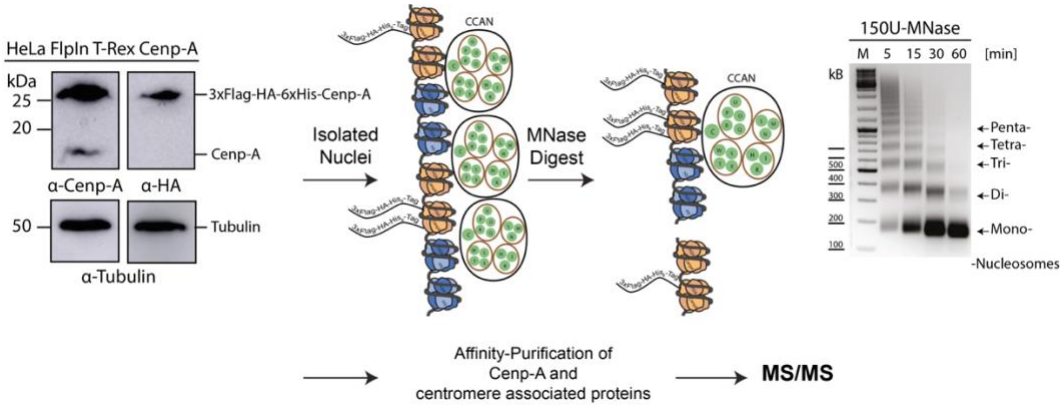

Figure 36. Workflow of CENP-A and H3.3 Purification from MNase Digested Nuclei.

CENP-A/H3.3 was expressed in HeLa FlpIN T-Rex cells using a Doxycycline inducible cell expression system. The expression was confirmed by western blot (M.18). Nuclei were isolated, and the DNA was digested with MNase, which selectively cuts the DNA regions between nucleosomes. The time of MNase digestion was titrated to obtain mononucleosomes or oligonucleosomes. Subsequently, CENP-A or H3.3 were purified by tandem affinity purification and subjected to tryptic digest for tandem mass spectrometry analysis.

5.3.1 Oligo-Nucleosome Chromatin Immunoprecipitation (ChIP) Can Purify Human Centromeres

CENP-A, as the epigenetic mark of centromere identity, is the most upstream component of kinetochore assembly. Accordingly, the CCAN proteins should be interacting with CENP-A throughout the cell cycle. By tandem affinity purification of CENP-A, either solubilized as mononucleosomes or in larger stretches of oligonucleosomes, I compared whether chromatin immunoprecipitation ChIP) a single CENP-A nucleosome is sufficient to stabilize the CCAN in such a manner that it is detectable by tandem mass spectrometry (MS/MS). The low abundance of CENP-A and expression levels of the system require to take a total cell mass of $1 \cdot 10^9$—$4 \cdot 10^9$ cells.

The overall protein identifications (IDs) of three biological replicates is comparable, as there were 735 IDs in the oligonucleosome ChIP sample versus 703 IDs in the mononucleosome ChIP sample (excluding Razor- and potential contaminant proteins). Out of the 386 IDs common to both experiments, CENP-

A as the bait protein was the only protein of the inner kinetochore that was identified in the mononucleosome preparation. In contrast, all CCAN proteins, CENP-B, and CENP-A were identified in the oligo-nucleosome sample (Figure 37). Taken together, since proteins associated with kinetochores, the cell cycle, or DNA replication were only found in the oligo-nucleosome ChIP, only oligo-nucleosome preparations (~10-30 meres) were used in further experiments.

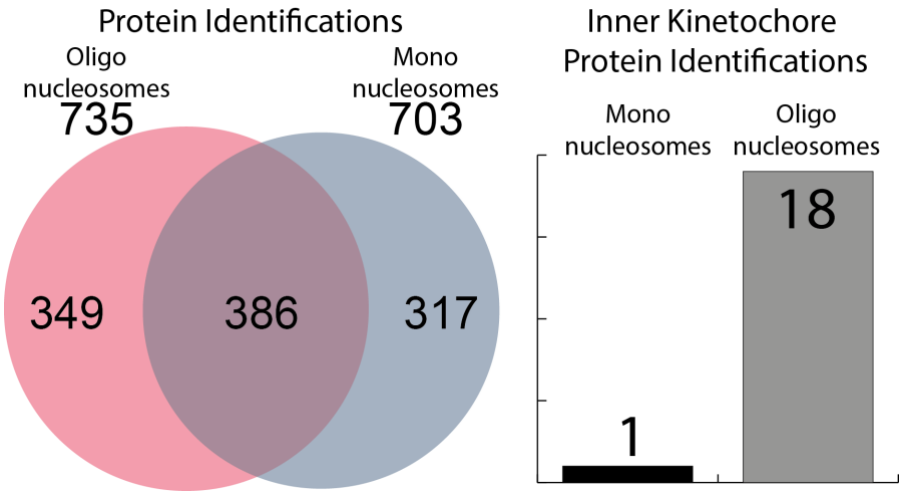

Figure 37. Oligonucleosome Purification Achieves a Higher Quality of Inner Kinetochore Proteins.

Comparing oligo- and mononucleosome purification indicates that oligonucleosomes maintain centromere protein distribution. While the total number of protein identifications remains relatively similar, the number of centromere and especially kinetochore proteins is higher when purifying larger stretches of centromeric chromatin. The Venn diagram shows total protein identifications in both experiments. The bar plot indicates the identification of CENP-A, CENP-B, and CCAN proteins.

5.3.2 The Cell Cycle can be Resolved by Distinct Arrest Release Protocols

Over the course of the cell cycle, centromeric chromatin is dynamically modified, especially during S-phase, where CENP-A is equally distributed between sister chromatids. In addition, the deposition of CENP-A during G1-phase is dependent on important cell cycle driving mechanisms and PTMs. To identify the cell cycle stage-specific CENP-A associated proteome, I performed oligo-nucleosome CENP-A-ChIP experiments from HeLa cells arrested at the following cell cycle

stages: 1. Early G1 phase (lovastatin arrest), 2. G1- to S-phase transition (21 h thymidine arrest), 3. early S-phase (21 h thymidine arrest/2 h after wash and deoxycytidine release), 4. mid-S-phase (21 h thymidine arrest/3 h after wash and deoxycytidine release), 5. late S-phase (21 h thymidine arrest/4 h after wash and deoxycytidine release), 6. Early G2-phase (21 h thymidine arrest/6 h after wash and deoxycytidine release) (Figure 34, Figure 38, Material and Methods).

For each cell cycle stage, the CENP-A associated interactome was identified by tandem MS from three biological replicates.

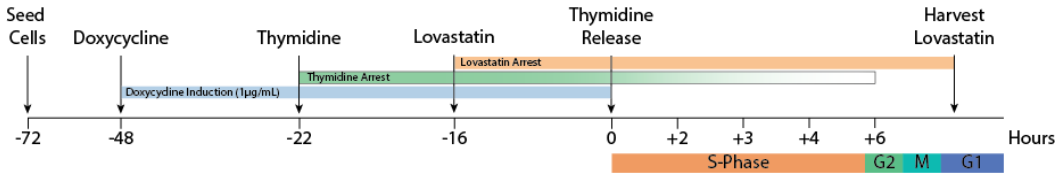

Figure 38. Timing of the Induction of Protein Expression and Cell Arrest Protocols.

HeLa FlpIN T-Rex cells, either expressing CENP-A or H3.3, were seeded 72 hours in advance. The Protein expression was induced 48 hours before either harvest or release. Cells were Either Thymidine arrested for 22 hours or Lovastatin arrested for 16 hours. (Deoxy-) thymidine is a nucleoside composed of the pentose sugar deoxyribose, joined to the pyrimidine base thymine that can, by (tri-) phosphorylation, be converted to deoxythymidine triphosphate (dTTP). This is one of the four nucleoside triphosphates that are used in the *in vivo* synthesis of DNA. By adding an excess of thymidine, dTTP becomes an allosteric inhibitor of the ribonucleotide reductase, which eventually leads to a depletion of dCTP and stalls the DNA replication machinery. The cell cycle was restored with the washout of thymidine in the culture medium and the addition of 24µM deoxycytidine after the thymidine block. To capture the cells in different cell cycle states, the cells were harvested either 21h after the addition of 2mM Thymidine for G1 to S-Phase transition, 2h after release for early S-Phase, 3h for mid-S-phase, 4h for late S-phase or after 6 hours for early G2-phase (Ma and Poon, 2011). Lovastatin reduces the proteasome activity, leading to an accumulation of CDK inhibitors p21 and p27 and to subsequent G1-phase arrest, as seen in cells of different cancer lines. The morphology of the cells changed to an elongated tapered shape. Similar to the thymidine arrest, the cells were harvested by trypsinization, and the flag-fusion CENP-A containing nucleosomes were tandem purified as oligonucleosomes in triplicates (Ma and Poon, 2011).

After establishing the arrest and arrest-release protocols to capture HeLa cells in distinct cell cycle stages, I purified CENP-A as described previously.

5.3.3 Analysis of G1-Arrested Cells Provides Insight into CENP-A Maintenance

CENP-A maintenance is vital for faithful chromosome segregation and cell viability. The incorporation of newly synthesized CENP-A histones is a key process of centromeric inheritance and is restricted to early G1-phase. Although some components involved in these mechanisms are identified, the putative specific chromatin remodeler and the factors mediating centromere specificity, required for discrete nucleosome disassembly and exchange of histone H3 variant by CENP-A are not identified. In order to analyze the protein environment of centromeres during G1-phase, Hela cells were arrested by the addition of Lovastatin and oligo-nucleosome ChIP purifications, using either CENP-A or histone H3.3 as bait was performed and analyzed by tandem MS. The Intensity Based Absolute Quantification (iBAQ) values were extracted, and the abundance (fold change [log2]) and significance (adjusted P-value [-log10]) of the identified proteins in three biological replicates were visualized in a volcano plot. The iBAQ values estimate the absolute amount of each identified protein by incorporation of individual peptide MS signals and theoretical peptides and subsequently normalize by the number of observable peptides of the protein.

During G1-phase, 388 proteins were identified to be significantly enriched for CENP-A over histone H3.3 in all three biological replicates (excluding Razor- and potential contaminant proteins). Amongst the most significant and abundant proteins, all of the previously described CCAN proteins of the human kinetochore were identified. Also, the CENP-A specific chaperone HJURP was identified, which indicated sufficiently high sensitivity. As a histone-modifying protein, the histone deacetylase HDAC4 was highly enriched for CENP-A interaction in G1-Phase. Also, various other chromatin-modifying proteins show significant enrichment for CENP-A, including the E3 ubiquitin-protein ligase UHRF1 that contains PHD and RING finger domains. Most histones are recruited and incorporated into chromatin by specialized protein environments that include histone chaperones interacting with histone remodeling complexes. Purification of such proteins is in the nature of ChIP experiments. However, the

ATP-dependent helicase SWI/SNF-related matrix-associated actin-dependent regulator of chromatin subfamily A member 5 (SMARCA5 also Snf2h) is a central player in various histone remodeling complexes and was specifically enriched in CENP-A ChIP experiments during G1 (Figure 39). Histone or nucleosome specificity for most histone remodelers is achieved by interaction with a specific protein network. In the pulldown experiments presented in this work, most abundant for CENP-A interactions were proteins associated with the Wich chromatin remodeling complex (Figure 39). In particular, these proteins are Baz1b, which forms the core of the Wich-complex in association with Snf2h (Bozhenok et al., 2002). Associated with this complex are a number of proteins that are summarized as the B-WICH-complex (Bozhenok et al., 2002). Additional chromatin factors enriched in CENP-A ChIP experiments are the histone H2A, H2B chaperoning Fact-Complex (SP16H and SSRP1), the heterochromatin associated nucleophosmin (NPM), Chromatin accessibility complex protein 1 (Chrac1), and SWI/SNF complex subunit SMARCC1 (SMCR1). Furthermore, AT-rich DNA sequence binding proteins were enriched like, e.g., DNA-binding protein SATB1. Also, several transcription factors were co-immunoprecipitated with CENP-A during G1. Most prominent were Lin37, ZBTB9, JUNB, and ERR2. Furthermore, I also identified proteins that were previously described to be involved in the CENP-A deposition process, like RbAp46/48 or Rsf1 (Stellfox et al., 2013).

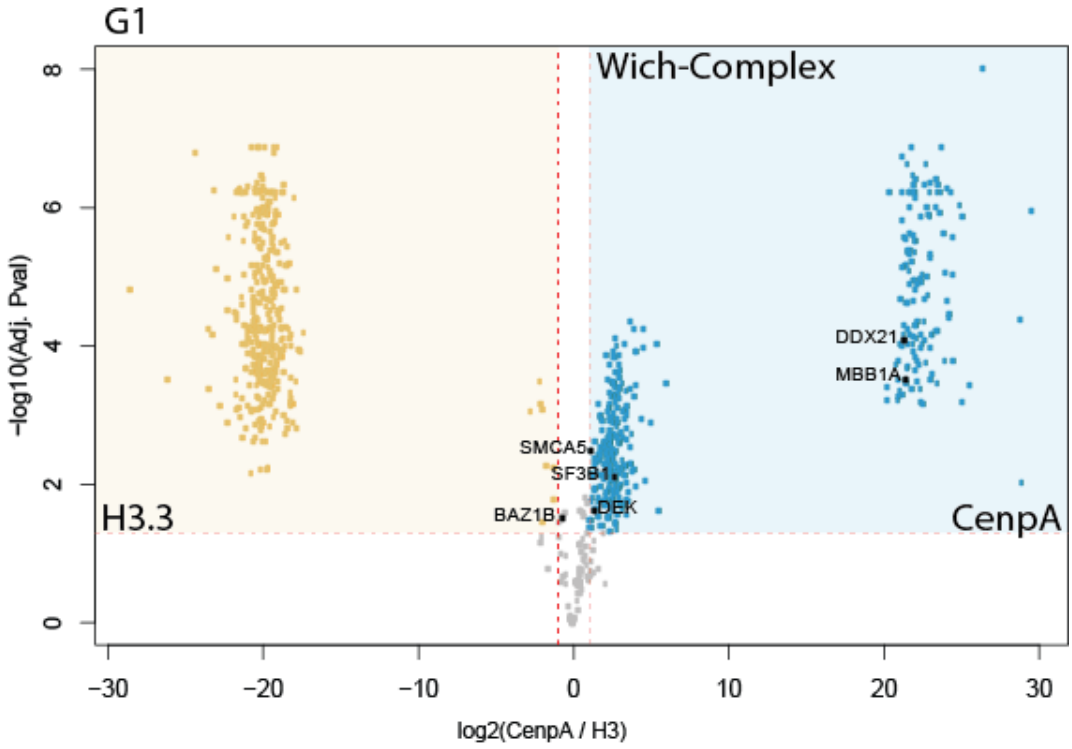

Figure 39. Comparison of Protein Identifications Purified from H3.3 vs. CENP-A Oligonucleosomes From G1 Arrested Cells.

Cells were arrested in G1-phase, nuclei were extracted, oligonucleosomes were purified and analyzed as described (M22, M23, M25, M26, M27, and M28). Proteins were identified with MaxQuant from three biological replicates. In the volcano plot, the significance, tested by a two-sample t-test, is plotted versus the $\log_2$ transformed fold change of intensity. Proteins enriched in H3.3 ChIP experiments (yellow) were compared to proteins enriched in CENP-A ChIP experiments (blue). Proteins that were significant for neither pull-down or below a threshold of 2 are gray. Highlighted are proteins of the B-WICH chromatin remodeling complex: SMCA5 (p-val: 0.00332/FC: 1.188), BAZ1B (p-val: 0.03119/FC: -0.659), DEK (p-val: 0.02474/FC: 1.427), SF3B1 (p-val: 0.00812/FC: 2.697), DDX21 (p-val: 0.0000084/FC: 21.396), MBB1A (p-val: 0.000298/FC: 21.48711).

These data reveal a significant difference for the proteins quantified from ChIP experiments of CENP-A and H3.3 oligonucleosomes.

5.3.4 The CENP-A Proteome at the Beginning of DNA-Replication (G1- to S-Phase Transition)

To analyze the CENP-A specific proteome during initiation of DNA-replication, HeLa cells were single thymidine arrested and treated as described earlier. CENP-A ChIP experiments are tested against H3.3 pull-downs and quantified for significance and abundance illustrated as a volcano plot (Figure 40). The analysis identified 758 proteins in three biological replicates in CENP-A ChIP experiments. 197 proteins were significantly enriched in CENP-A ChIP samples, of which 137 were identified in all three CENP-A replicates. The majority of the protein identifications (557 IDs) were found in both (CENP-A and H3.3) pull-down experiments.

The most abundant proteins in CENP-A experiments were again the CENP-A chaperone HJURP, the CCAN members. Some of the proteins, significantly enriched during early G1-phase, were also identified during late G1 to S-phase transition, however not of particular significance for either histone, such as NPM. This protein is directly interacting with nucleophosmin-3 (NPM3), which was specifically found in CENP-A pull-downs. Also, the unknown transcription factor ZBTB9 was highly abundant and significantly enriched in CENP-A experiments. Additionally, the transcription factor JUNB was identified again. However, most of the identifications that overlap with those identified in G1-phase were not significantly enriched in CENP-A ChIP experiments since most were more general chromatin interacting proteins.

Of the chromatin-modifying proteins, the most prominent CENP-A interactors were Kat6b, a Histone Acetyl Transferase (HAT), which has a histone H3 acetyltransferase activity and Chromodomain-Helicase-DNA-binding protein 7 (CHD7), a transcription regulator, that also has ATP binding properties and may be involved in higher-order chromatin structure. Another transcription factor, Negative Cofactor 2 Beta (NC2B), is also a component of the ATAC complex, a complex with histone acetyltransferase activity on histones H3 and non-histone proteins. Also, a significant interaction of the DNA methylation proteins DNA (cytosine-5)-Methyltransferase 3a and b (DNMT3A/B) was observed, which are required for genome-wide de novo methylation and are essential for the establishment of DNA methylation patterns (Figure 40).

Most members of the putative replicative helicase MCM complex were identified in CENP-A and H3.3 ChIP experiments but MCM4 was exclusively identified in CENP-A experiments. The mitotic kinase PLK1 plays a major part during G2/M-transition as well as during mitosis. Also, in single thymidine arrested HeLa cells with induced CENP-A expression, the kinase was significantly enriched.

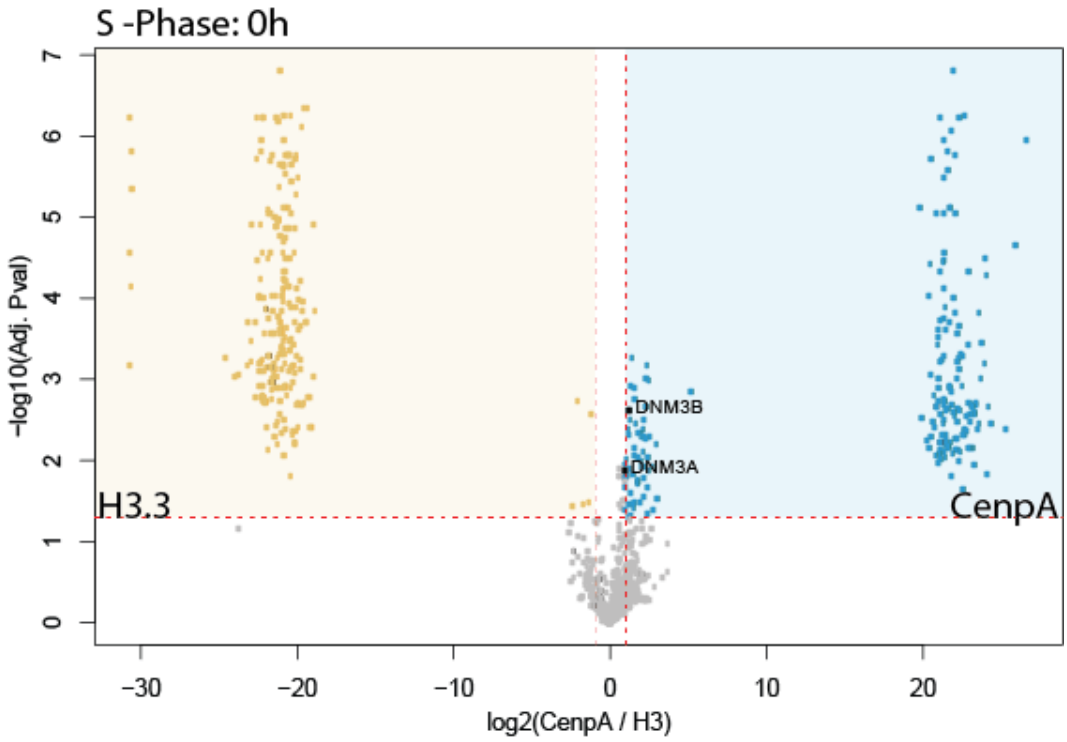

Figure 40. Comparison of Changes in Protein Identifications Purified from H3.3 vs. CENP-A Oligonucleosomes from Cells in G1- to S-phase transition.

Three replicates of thymidine arrested cells expressing either CENP-A or H3.3 were purified from MNase digested nuclei. The ChIP purified proteins were identified by MaxQuant, analyzed in R, and visualized as a volcano plot. Here, the significance of a protein identification was tested in a two-sample t-test and plotted versus the fold-change of the respective protein. Proteins enriched in H3.3 ChIP triplicates are yellow, Proteins enriched in CENP-A ChIP triplicates are blue, and proteins below a 2-fold threshold are grayed out. Highlighted here are the de-novo methyltransferases DNMT3A (p-val: 0.0137/FC: 0.987) and DNMT3B (p-val: 0.00245/FC 1.286)

In summary, the CENP-A associated proteins identified during G1- to S-phase transition expressing CENP-A were primarily associated with either chromatin or

the kinetochore. Interestingly, the function of most of the novel identifications in the interactome of centromeres is largely unknown.

5.3.5 The CENP-A Associated Proteome During Early S-Phase

By the release of single thymidine arrested HeLa cells into dCTP, the cells actively and synchronously replicate DNA. I employed the previously described protocol to capture this early state of DNA replication and analyze the proteome at the centromere by comparing CENP-A against H3.3 ChIP experiments using tandem mass spectrometry. In early S-phase, 678 proteins were identified in CENP-A pull-down experiments. 197 of these were statistically significantly enriched, whereas 159 of these were only identified in the CENP-A replicates.

Most abundant and significant in CENP-A ChIP experiments compared to histone H3.3 were the CCAN proteins and HJURP. Similar in terms of abundance and significance in CENP-A experiments is again transcription factor ZBTB9. Several other transcription factors were enriched in CENP-A pull-downs; among these are zinc finger protein ZN562, steroid hormone receptor ERR2, or transcription initiation protein NC2B, and transcription regulation protein Max.

There are several chromatin-modifying proteins identified as significant for CENP-A interaction. Amidst these is histone H3.3 chaperone Death domain-associated protein 6 (DAXX) and the transcriptional regulator ATRX, which has ATP-dependent DNA translocase activity and catalyzes the replication-independent deposition of histone H3.3 in heterochromatin domains. CENP-A pull-downs from cells in G1- to S-phase transition showed enrichment for CHD7, whereas those cells in early S-phase additionally showed significant enrichment of CHD2, -6, -7, -8, and -9 over histone variant H3.3.

Analysis of the dataset also showed significant enrichment of Chromatin accessibility complex protein 1 (Chrac1) and an accessory subunit of the DNA polymerase epsilon complex (DPOE3). These two proteins form a complex that binds naked DNA, which can then be incorporated into chromatin by association with Acf1 (ATP-dependent chromatin-remodeling protein) and Snf2h, resembling the Chrac-complex. Acf1 and Snf2h were also identified as all CENP-A ChIP replicates, yet not with high abundance and significance.

The DNA mismatch repair proteins MSH2 and MSH6 were also enriched in CENP-A ChIP experiments compared to histone H3.3 in all three biological replicates. These proteins are recruited to chromatin in G1- and early S-phase via its PWWP domain that specifically binds trimethylated histone H3 on lysine 36 (H3K36me3). In this cell cycle stage, again, Plk1 was significantly enriched for CENP-A interaction as well as the E3 ubiquitin-protein ligase Trim21.

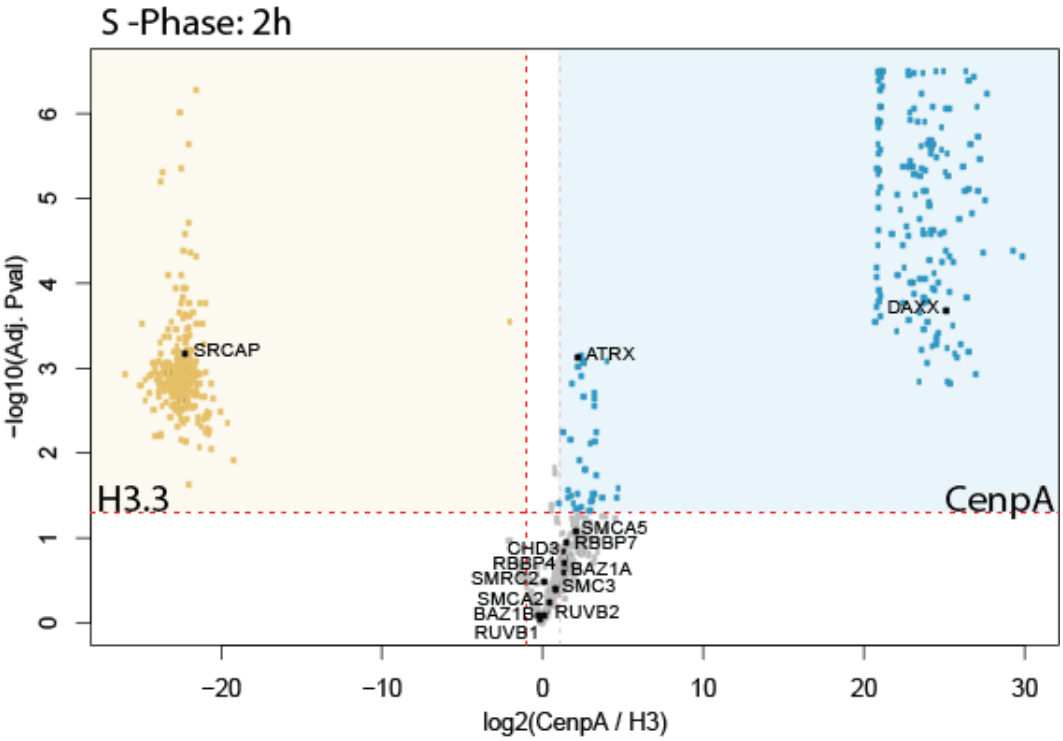

Figure 41. Chromatin Factors are Enriched at Centromeric Chromatin in Early S-Phase.

Protein intensities of three biological replicates were extracted from the analysis of ChIP experiments of cells expressing either H3.3 or CENP-A that were arrested with thymidine and released for 2 hours before harvesting. Protein abundances in CENP-A were averaged, and the significance of their FC to the three biological replicates of H3.3 were assessed by a two-sample t-test. The resulting adj. p-val was plotted versus the respective FC in a volcano plot. The proteins two-fold enriched in H3.3 are indicated in yellow and in CENP-A ChIP experiments in blue, respectively. Highlighted are chromatin interacting proteins involved in remodeling processes. DAXX (p-val: 0.00021/ FC: 25.1823), ATRX (p-val: 0.00074/ FC: 2.2881), DPOE3 (p-val: 0.3476/ FC: 1.323), CHRC1 (p-val: 0.0310/ FC: 2.2154), MSH2(p-val: 1.42E-06/ FC:

24.8661), MSH6(p-val: 4.92E-06/ FC: 25.1049), ZBTB9 (p-val: 26.7088/ FC: 2,26E-06), ZN562(p-val: 5,19E-06/ FC: 23.1856).

Taken together in early S-phase, several chromatin factors were significantly enriched in centromeric chromatin as represented by CENP-A ChIP experiments, in comparison to chromatin domains that harbor histone variant H3.3.

5.3.6 The CENP-Associated Proteome in Mid S-Phase

To further characterize the centromere during active DNA replication, HeLa cells either expressing histone variant CENP-A or H3.3 were harvested after 3 hours of release. Overall, 855 proteins were identified in the three biological replicates of CENP-A ChIP samples. 476 proteins were significantly enriched in CENP-A ChIP samples over H3.3 ChIP samples, and 376 of these were unique for the CENP-A interactome. Amidst the most abundant and significant proteins in the CENP-A ChIP replicates compared to histone variant H3.3 are the CCAN proteins and HJURP along with transcription factor ZBTB9 and transcription initiation protein NC2B. The histone H3.3 chaperone DAXX was again more abundant in CENP-A experiments. Also, NPM3, which showed histone chaperone function before, and mitotic kinase Plk1 was identified (Chang et al., 1998, Ito et al., 1996). Chromatin modifying proteins like CHD were not significantly enriched in CENP-A experiments in comparison to H3.3. The E3 ubiquitin-protein ligase CUL4b was exclusively identified in CENP-A ChIP experiments as well as ubiquitin carboxyl-terminal hydrolase 10 (UBP10), which is able to remove conjugated ubiquitin from target proteins.

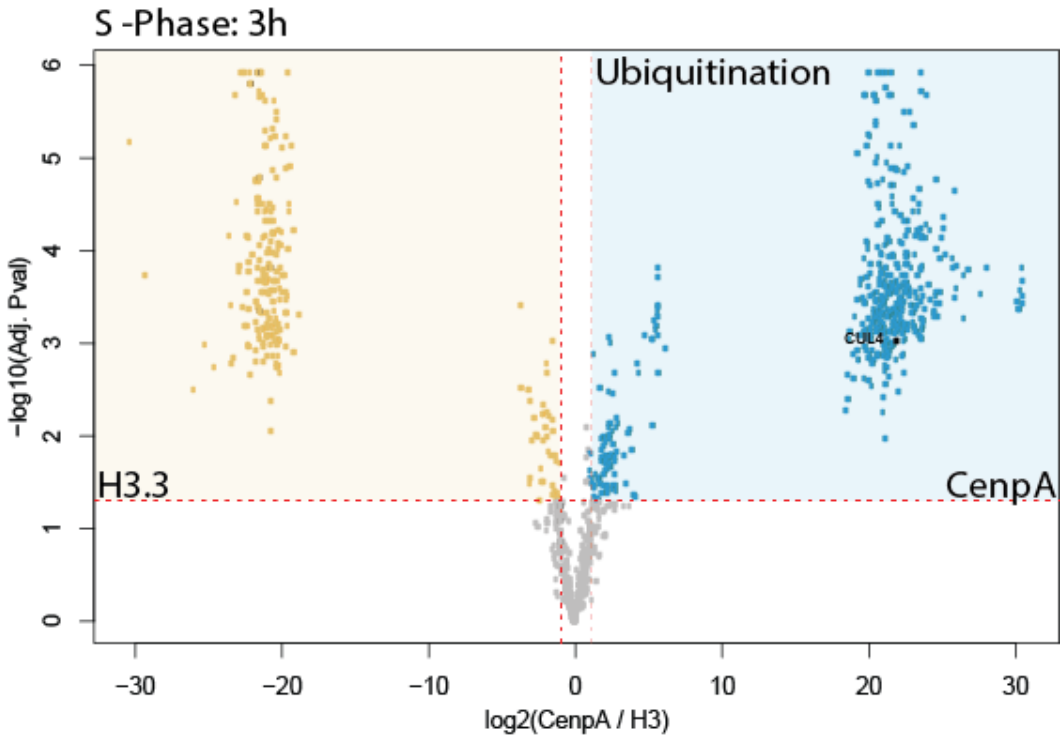

Figure 42. Ubiquitin ligases are Enriched at Centromeric Chromatin in Mid S-Phase.

Cells, released in S-phase for 3 hours, expressing either H3.3 or CENP-A, were analyzed by ChIP and MS/MS. Protein intensities of three biological replicates were extracted, and protein abundances in CENP-A ChIP samples were averaged, and the significance of their FC to the three biological replicates of H3.3 ChIP samples were assessed by a two-sample t-test. The resulting adj. p-val was plotted versus the respective FC in a volcano plot. The proteins two-fold enriched in H3.3 are indicated in yellow and in CENP-A ChIP experiments in blue, respectively. Highlighted is the E3-ubiquitin ligase CUL4 (p-val: 0.00095/FC: 21.955).

HeLa cells in mid-S-phase showed a significant increase of CENP-A associated proteins involved in ubiquitination and de-ubiquitination. Whether the identified candidates are of functional relevance for a certain centromeric environment has to be further elucidated.

5.3.7 The CENP-A Associated Proteome in Late S-Phase

DNA replication is an essential event occurring once per cell cycle and which necessitates specialized protein-protein interactions that are spatiotemporally organized. Here I analyzed the proteome of the specific chromatin domain of the

centromere by comparing the histone variants CENP-A against H3.3 during a late stage of transcription. In three biological replicates of HeLa cells that were released from a single thymidine arrest for 4 hours, I was able to identify 508 proteins interacting with CENP-A. Of these, 223 were significantly enriched in CENP-A experiments, and 48 were exclusive for CENP-A interaction.

Most significantly enriched in CENP-A ChIP experiments compared to histone H3.3 were the 16 CCAN proteins as well as HJURP and the putative transcription factor ZBTB9. Also, several other transcription factors were enriched in CENP-A ChIP experiments compared to H3.3. Among these were again Nc2b and ZN562. Also, Plk1 was again among the most abundant and significant protein identifications in CENP-A pull-down experiments.

Among the chromatin-modifying proteins identified as statistically enriched in CENP-A ChIP experiments over H3.3 were NPM3, NPM, Histone-lysine N-methyltransferase SETDB1, and H3.3 chaperone DAXX. The catalytic component of the DAXX: ATRX complex, however, was not significantly enriched. The centromere binding proteins RbAp46/48 were again more abundant and significant in CENP-A experiments. After release into S-phase for 4 hours, the ATPase Snf2h, along with Acf1, as members of the Chrac-complex, were of high abundance (Figure 43). The Wich-complex member Baz1b was highly abundant in CENP-A, however not statistically significant in three biological replicates. Likewise, the chromatin assembly factor (CAF1) was equally abundant in CENP-A, and H3.3 replicates. Evaluation of the dataset also showed a high abundance and significance for MSH2 and Trim21. There is also a slightly higher abundance for PCNA in CENP-A experiments, indicating an active DNA-replicating state. For all other arrested or arrest-release states in S-phase, PCNA was more abundant in H3.3 experiments, indicating an active replication of the centromere during late S-phase, which should be reflected by a 4 hours release (Nechemia-Arbely et al., 2019).

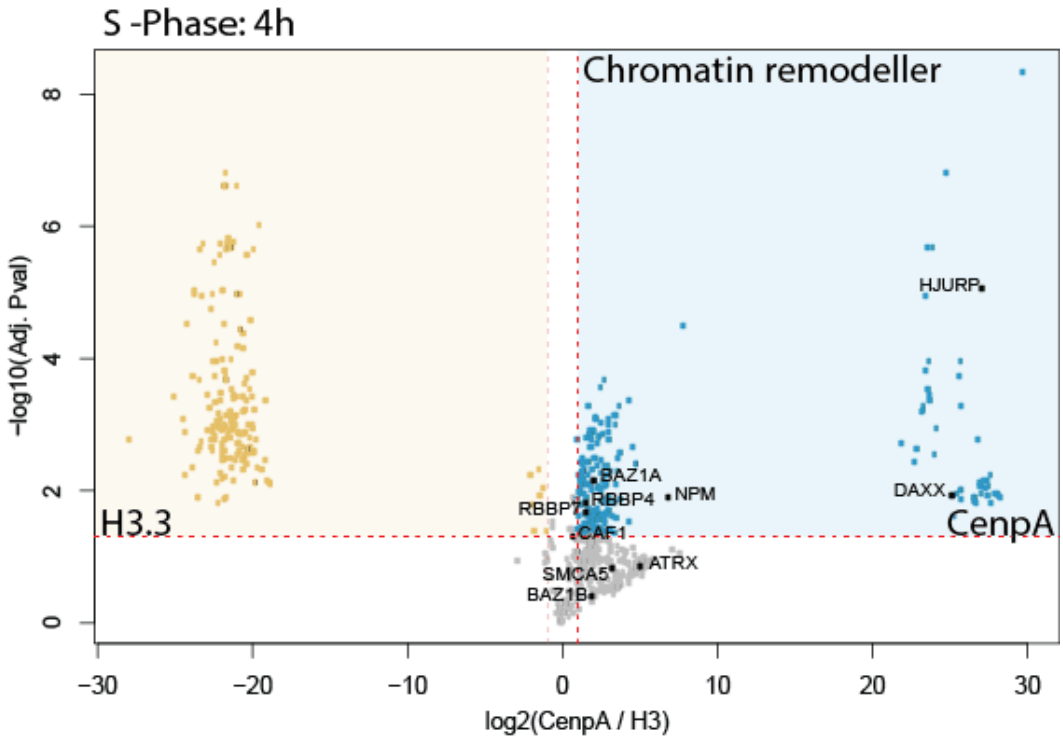

Figure 43. Chromatin Remodeling Factors are Enriched at Centromeric Chromatin in Late S-Phase.

Cells, released to S-phase for 4 hours, expressing either H3.3 or CENP-A, were analyzed by ChIP and MS/MS. Protein intensities of three biological replicates were extracted, and protein abundances in CENP-A samples were averaged, and the significance of their FC to the three biological replicates of H3.3 samples were assessed by a two-sample t-test. The resulting adj. p-val was plotted versus the respective FC in a volcano plot. The proteins two-fold enriched in H3.3 are indicated in yellow and in CENP-A ChIP experiments in blue, respectively. Highlighted are proteins involved in chromatin remodeling: HJURP (p-val: 8.7E-06 /FC: 27.142), BAZ1A (p-val: 0.00685 /FC: 2.093), BAZ1B (p-val: 0.4057 /FC: 1.950), SMCA5 (p-val: 0.151 /FC: 3.247), RBBP4 (p-val: 0.0151 /FC: 1.584), RBBP7 (p-val: 0.02076 /FC: 1.582), NPM (p-val: 0.0127 /FC: 6.868), DAXX (p-val: 0.012 /FC: 25.207), ATRX (p-val: 0.142 /FC: 5.073), CAF1 (p-val: 0.159 /FC: 1.037).

In summary, in late S-phase, there were several chromatin-modifying proteins enriched in CENP-A ChIP experiments in comparison to H3.3. Some of them act in remodeling complexes, which are potential candidates to promote a redistribution of CENP-A histones after the replication fork, probably in an

interplay with CAF1 (Petryk et al., 2018). Whether these can be validated is a matter of further research.

5.3.8 The CENP-A Associated Proteome in Early G2-Phase

After DNA replication, the cell prepares for cell division during G2-phase. I analyzed this particular stage by the release of single thymidine arrested cells for 6 hours. According to this protocol, cells should be in the transition from S- to G2-phase or in an early G2-phase. In total, 665 proteins were identified in the three biological replicates of CENP-A experiments. Of these compared to H3.3-ChIP experiments, 137 were of statistical significance, and 99 were unique for CENP-A nucleosome interaction.

The most significantly enriched proteins were the CCAN proteins and HJURP, as well as the putative transcription factor ZBTB9 (Figure 44). In addition, Plk1, which has a significant role in centromeres during G2/M-transition, was enriched. In contrast, CHD proteins were most dominantly found in H3.3 but not in CENP-A pull-down experiments.

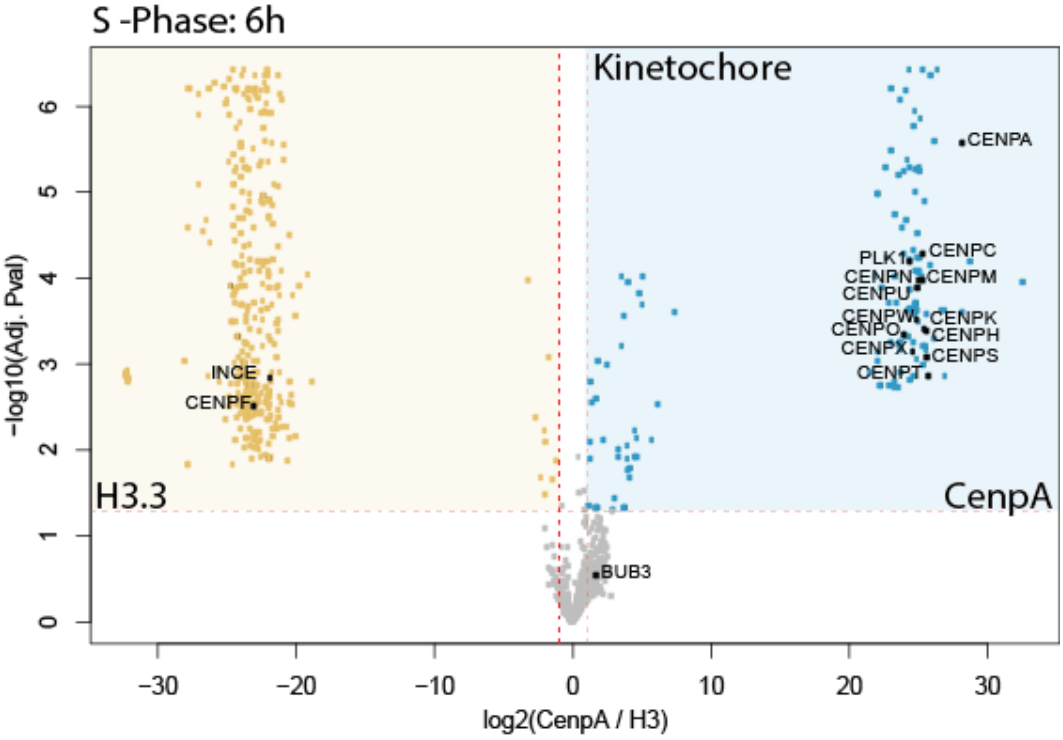

Figure 44. CCAN is Enriched at Centromeric Chromatin Over the Cell Cycle.

Cells released in S-phase for 6 hours, expressing either H3.3 or CENP-A, were analyzed by ChIP, followed by MS/MS. Protein intensities of three biological replicates were extracted, and protein abundances in CENP-A experiments were averaged, and the significance of their FC to the three biological replicates of H3.3 experiments were assessed by a two-sample t-test. The resulting adj. p-val was plotted versus the respective FC in a volcano plot. The proteins two-fold enriched in H3.3 are indicated in yellow and in CENP-A ChIP experiments in blue, respectively. Highlighted are kinetochore proteins.

Strikingly, also in early G2-phase, the putative transcription factor ZBTB9 showed high abundance and significant enrichment in CENP-A pull-down samples. The analysis of the spatiotemporal dynamics of the human centromere identified a variety of chromatin-modifying proteins, transcription factors, and other effector proteins. However, their relevance for CENP-A maintenance and inheritance has to be further investigated.

5.3.9 The Time Course of the Inner Kinetochore

CCAN proteins remain associated with centromeric chromatin over the course of the cell cycle. Likewise, CCAN protein intensities remained relatively stable compared to the CENP-A histone. Besides the inner kinetochore proteins, only a few proteins were identified in all experiments that have a statistical significance for CENP-A. Comparably abundant to other CCAN proteins was the transcription factor ZBTB9, which was found in all ChIP experiments of CENP-A. Most protein interactions happen exclusively during a particular phase of the cell cycle, reflecting the complex nature of dynamic protein-protein interactions, higher-order chromatin states, and posttranslational modifications.

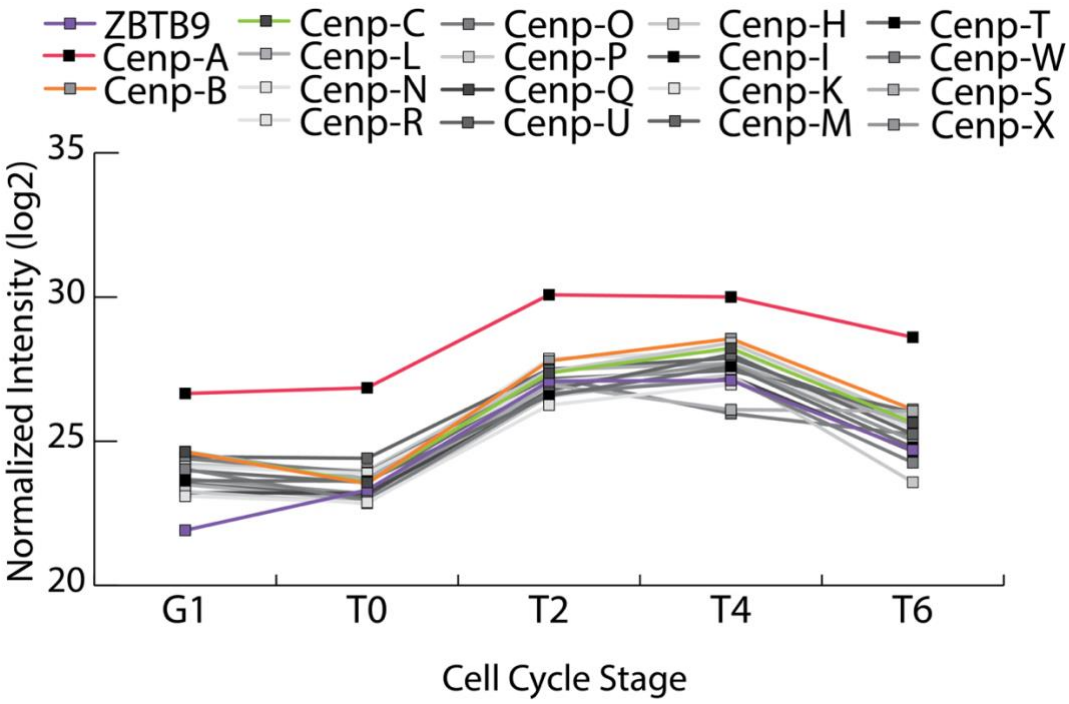

Figure 45. The Time-Resolved Abundance of Inner Kinetochore Proteins.

The log2 transformed intensities of inner kinetochore proteins from ChIP purifications of three replicates from MNase digested nuclei of cell cycle arrested cells expressing CENP-A were plotted in a line plot. The intensities of inner kinetochore proteins are comparably high with respect to CENP-A intensity (red). ZBTB9 (purple), a virtually uncharacterized protein, shows similar distribution with respect to the other CCAN components.

In this part of my thesis, I presented a time-resolved cell cycle-specific proteomic analysis of the human centromere to identify candidate proteins involved in maintaining the sophisticated environment of this specific chromatin domain. I used distinct cell cycle arrest and arrest-release protocols to capture synchronized HeLa cells at time-points during the cell cycle. Amongst the known CENP-A interacting proteins, I was able to identify several novel members of the centromeric interactome. Selected candidates will be analyzed for their relevance in centromere maintenance in the future.

5.4 Discussion

The self-templated duplication of centromeric chromatin that is independent of DNA sequence features requires distinct protein interactions to provide stable transmission across multiple cell division cycles. Despite intense research, crucial steps in this process have not been comprehensively understood. In this work, I analyzed the proteome specifically associated with- CENP-A in a cell cycle-dependent manner to further characterize how CENP-A is (1.) assembled into chromatin, (2.) stably transmitted during DNA replication, and (3.) which proteins are necessary to promote centromere identity. To gain insight, I performed a comprehensive analysis, comparing CENP-A containing oligonucleosomes with H3.3 oligo-nucleosomes to identify chromatin-associated proteins required for maintaining centromeric chromatin at discrete cell cycle moments.

Among the top-ranking interactors, I found proteins involved in centromere and kinetochore function as expected. These imply all CCAN proteins. The functionality of the CCAN is dependent on centromeric chromatin and vice versa. Assembly of CENP-A is dependent on the CCAN proteins, which was shown in multiple studies (Hori et al., 2013, Dambacher et al., 2012, Moree et al., 2011, Carroll et al., 2009). Most importantly, an intact CCAN is required to prevent CENP-A eviction induced by disruptive stress such as DNA replication. Accordingly, CENP-C as the cornerstone and central hub of the inner kinetochore stabilizes CENP-A nucleosomes, as shown both *in vivo* and *in vitro* (Falk et al., 2015, Klare et al., 2015). The constitutive association of the CCAN was confirmed by the ChIP experiments performed in this work. The relative abundance of all components remained stable in comparison to CENP-A levels for all monitored time points. Moreover, the identification of all inner kinetochore proteins indicates that my pull-down experiments are capable of snapshotting the stably associated protein environment of centromeric chromatin. A constitutively associated protein network such as the CCAN particularly serves two purposes. Maintaining pre-assembled CENP-A providing a template for CENP-A replenishment during G1-Phase and counteracting neocentromere formation induced by CENP-A misplacement. On this note, to avoid an excess of CENP-A containing nucleosomes, CENP-A protein-degradation may need to be regulated by an yet unknown mechanism (Hoffmann et al., 2016, Lomonte et al., 2001, Mitra et al., 2020b). Chromatin regulatory proteins such as chromatin remodelers,

chromatin readers and writers, transcription factors, or histone chaperones might also depend on this centromere proximal protein network to achieve CENP-A specificity. Therefore, this work also aimed to expand the view on proteins interacting with centromeric chromatin.

Some ATP dependent motors and other chromatin remodeling factors that play an integral role in nucleic-acid biology were particularly enriched in CENP-A ChIP experiments over H3.3. Especially abundant among proteins selectively isolated with CENP-A in early G1-phase arrested HeLa cells and in late stages of DNA replication was SMARCA5 as part of the SWI/SNF-subfamily of helicase proteins. Motors of this subfamily can catalyze a variety of nucleosome structure changes and are organized in large, multi-subunit complexes (Kadoch and Crabtree, 2015). In the presence of free DNA, SWI/SNF ATPases can transfer the entire histone octamer to an acceptor DNA, however only disassemble nucleosomes in the presence of specific histone chaperones (Lorch et al., 2006, Lorch et al., 1999). Thereby the proteins associated with the ATP-dependent motor proteins define the functionality and specificity of the remodeling complexes. In my CENP-A pull-down experiments of early G1-phase arrested cells, proteins of the B-WICH complex (SMARCA5, BAZ1B, NM1, DDX21, DEK, SF3B1, MBB1A) were specifically enriched. This chromatin remodeler has also been found to be abundant at heterochromatin (Bozhenok et al., 2002). In particular, BAZ1B was found to be enriched at metaphase chromosomes, which distinguishes it from other remodeling factor subunits that are excluded from condensed chromosomes (Bozhenok et al., 2002). Furthermore, BAZ1B was shown to bind acetylated histone H3 on lysine 14 (H3K14ac) (Fujiki et al., 2005). This histone acetylation mark is particularly important for H3/CENP-A turnover/exchange and mediated by histone acetyltransferase KAT7 that directly interacts with Mis18BP and positively regulates CENP-A replenishment in G1-phase (Ohzeki et al., 2016). Ectopic tethering of KAT7 recruited RSF chromatin remodeling complex, which also purifies with CENP-A nucleosomes, as shown before (Perpelescu et al., 2009). RSF1 and KAT7 tethering was sufficient to assemble overexpressed CENP-A to an ectopic alphoid^{tetO} DNA site; however, it failed to mediate de novo endogenous CENP-A assembly (Shono et al., 2015). The data presented here, strongly suggests that the RSF complex acts in a multistep mechanism together with B-WICH to promote the exchange of earmarked histone H3 with nascent CENP-A. However, this has to be validated in an *in vivo* experiment that monitors CENP-A incorporation after B-WICH knock-down. Furthermore, the HAT KAT6B which is

specifically enriched in thymidine arrested cells in my experiments also harbors a potential role in acetylating H3 histones to promote CENP-A exchange.

Recent publications showed that the polymerase epsilon complex accessory proteins POLE3 and POLE4 possess histone H3-H4 chaperone activity and facilitate nucleosome reassembly after the replication fork during DNA replication (Bellelli et al., 2018). A potential role for the leading strand polymerase epsilon complex (POLε) has been proposed multiple times (Iida and Araki, 2004, Tackett et al., 2005, Li et al., 2011, He et al., 2017). In my experiments, I also observed an enrichment of POLε subunits with CENP-A, which implies that the cells were actively replicating and confirmed the involvement of POLε. Interestingly, I also detected Chrac1 along with BAZ1A and SMARCA5 during S-phase, resembling the CHRAC-complex (SMARCA5, BAZ1A, DPOE3, Chrac1), which also has been proposed to be involved in chromatin inheritance before (Iida and Araki, 2004). POLε and the CHRAC remodeling complex have been proposed to interact with each other to maintain and inherit proper chromatin states during DNA replication in yeast (Iida and Araki, 2004). In *Drosophila*, DPOE3 was proposed to functionally and physically interact with CENP-A, as depletion of DPOE3 resulted in ectopic translocation of CENP-A to sites of DNA repair, which caused chromosome segregation defects (Mathew et al., 2014). The histone fold domains of DPOE3 have similarities with those of CENP-T/-W and enable the CHRAC complex to slide nucleosomes (Nishino et al., 2012, Hartlepp et al., 2005). However, the POLε and CHRAC complexes act independently from each other (Iida and Araki, 2004). As Chrac1 and POLE4 share some sequence homology, it is feasible that POLE3 and Chrac1 form a centromere-specific complex acting with POLε and the CHRAC complex to redistribute CENP-A after the replication fork. My data provides additional evidence that both protein complexes are involved in chromatin inheritance during DNA replication. Whether Chrac1 provides CENP-A specificity to either of these protein complexes has to be investigated.

Incorporation of replication-independent histone variant H3.3 depends on HIRA and the ATPase activity of CHD1 in euchromatin and DAXX: ATRX in heterochromatic regions (Konev et al., 2007, Lewis et al., 2010, Zink and Hake, 2016). However, CENP-A mistargeting to ectopic sites leading to the formation of neocentromeres is mediated by DAXX upon overexpression of CENP-A (Lacoste et al., 2014). The enrichment of DAXX for CENP-A can hence be explained as an effect of tetracycline induced overexpression. It also cannot be ruled out that

DAXX binding of CENP-A might fulfill a role in CENP-A handling during DNA-replication since the centromere-specific chaperone HJURP is low abundant.

In mammalian cells, the knock-down of CHD1 has also been associated with centromere function as it led to a decrease of CENP-A (Okada et al., 2009). The CHD chromatin remodeler family consists of 9 proteins subdivided into 3 classes (class I: CHD1/2; class II: CHD3/4/5; class III: CHD6/7/8/9). They all contain two chromodomains tandemly arranged in the N-terminus (Marfella and Imbalzano, 2007). Class I CHD proteins have AT-rich DNA binding affinity, Class II proteins contain PHD-finger domains that recognize methylation marks, the C-terminal BRK region of class III CHD proteins is still not fully understood (Rother and van Attikum, 2017). CHD2, which was significantly enriched in CENP-A pulldowns from cells arrested at the G1- to S-phase transition and in early S-phase, was shown to be involved in histone H3.3 deposition (Adam et al., 2013, Siggens et al., 2015). The class III CHD proteins that were all specifically enriched for CENP-A after 2 hours release from thymidine are very variable, and CHD8 also had an impact on CENP-A maintenance in a microscopy-based genetic screen (Mitra et al., 2020a). The CHD family is highly conserved, yet the function of these proteins remains widely unknown. Notably, the SNF2-like ATPase domain, their chromatin recognition patterns, and the connection with CENP-A maintenance make them interesting candidates whose specific role in CENP-A deposition has to be addressed.

ATP hydrolysis may be an important hallmark to exchange histone variants. The abundant phosphoprotein NPM1 acts as a chaperone for histone H2B, H3, and H4 and can bind ATP. In *Drosophila*, NPM1 can also function as a chromatin remodeler, and its specific association with CENP-A hints at a functional relevance in CENP-A maintenance (Ito et al., 1996, Chang et al., 1998). In my pull-down experiments, NPM1 was enriched but not very significant for CENP-A interaction. This is not surprising considering the histone H3 chaperone activity of NPM1. However, NPM1 was already identified as a direct interactor of CENP-A with unknown function and a promising candidate for centromere anchoring (Foltz et al., 2006). NPM1 functions in a variety of cellular processes, including DNA repair, transcription, ribosome biogenesis, or centrosome duplication, and is predominantly located to the nucleolus (Lindstrom, 2011). A hypothesis of how NPM1 is able to act in such a diverse manner is that it is regulated by PTMs, variants, or through interaction with other proteins, including members of the

NPM family (Frehlick et al., 2007). In a yeast two-hybrid screen, a major binding partner of NPM1 was its protein family member nucleoplasmin 3 (NPM3) (Huang et al., 2005). NPM3 was highly abundant and significant for CENP-A in my experiments, especially during DNA-replication. Interestingly, when NPM1 is in complex with NPM3, the ribosomal biogenesis activities of NPM1 are decreased. Whether the histone chaperoning properties of the NPM1-NPM3 complex are increased upon interaction is not known. In *Drosophila,* the oligomerization of NPM homologs is necessary for centromere targeting (Anselm et al., 2018). Here, the proteins show a distinct pattern, filling the loci in between CENP-A containing chromatin domains, which revealed distinct centromeric subdomains (Anselm et al., 2018). The functionality and influence of these observations is matter of ongoing research and should be addressed in future experiments.

Related to chromatin remodelers are proteins involved in transcriptional regulation. Among the most significant and abundant interactors of CENP-A over the time-course of my pull-down experiments was ZBTB9, a zinc-finger and BTB domain-containing protein. Though highly conserved, not much is known about this protein. In my ChIP experiments, it showed a very high significance for CENP-A and similar abundances as the CCAN members (Figure 45). BTB domains are very common for zinc finger motif-containing proteins and mostly induce protein dimerization. Many of the proteins containing a BTB domain are transcriptional regulators, acting on chromatin structure (Zollman et al., 1994). The zinc finger motif, first identified as DNA sequence binding, are small protein motifs that exist in a large variety (Klug, 2010). A vast majority of zinc finger motifs function as interaction modules that bind RNA, DNA, amino acids, or other small molecules (Klug, 2010). Their modular organization and variations in structure primarily serve to alter the binding specificity of the protein containing these motifs (Klug, 2010). Between the N-terminal BTB domain and the C-terminal Zinc finger motif, ZBTB9 contains a stretch of acidic amino acids that might mediate an interaction with basic proteins such as histones. Thus far, the only protein of human inner kinetochores that is capable of binding DNA in a sequence-specific manner is CENP-B, which binds a 17 bp DNA motif, called 'CENP-B box,' that exists in every other α-satellite DNA (Tanaka et al., 2001). The DNA-binding domain of CENP-B is located in the N-terminus, while the C-terminal end of the protein consists of highly acidic amino acids (Tanaka et al., 2001). While unconfirmed, it is very likely that this domain of CENP-B mediates the direct interaction with the N-terminal tail of CENP-A (Fachinetti et al., 2015). Like CENP-B, ZBTB9 has, therefore, the

potential to recruit histones in a DNA sequence-specific manner to support centromere stabilization downstream of CENP-B dependent CENP-A recruitment, especially in chromatin domains lacking 'CENP-B-boxes'. Thus, it is very tempting to further validate ZBTB9 sequence and interaction specificity by pull down experiments and EMSA to test α-satellite DNA specificity. Furthermore, it would be interesting to knock down ZBTB9 by RNAi and investigate CENP-A incorporation and maintenance over the cell cycle. Using high resolution microscopy, it would be feasible to investigate the localization of ZBTB9 to see whether it is a constitutive interactor of human inner kinetochores.

A second zinc finger motif-containing protein, ZN562, is particularly interesting as it is highly significant and enriched during DNA-replication and in late S-phase, when centromeres are replicated (Nechemia-Arbely et al., 2019). Remarkably, CENP-A is retained to the exact sites of α-satellite DNA before and after replication (Nechemia-Arbely et al., 2019). Hence, DNA-replication not only functions to duplicate the genetic information but retains the specificity of chromatin domains by removing CENP-A from ectopic sites during early and mid-S-phase (Nechemia-Arbely et al., 2019). Ectopic sites of CENP-A incorporation would cause major problems for the cells, as shown in multiple cancer cell lines (Hasson et al., 2013, Zhang et al., 2016, Sun et al., 2016). These chromatin sites containing CENP-A nucleosomes were also able to recruit CCAN components and act as functional centromeres during mitosis, which are therefore not solely responsible for retaining CENP-A during S-phase (Lacoste et al., 2014, Gascoigne et al., 2011, Van Hooser et al., 2001). The mechanism of how this highly specific retention of centromeric proteins is achieved is not comprehensively understood. Thus far, it has been shown that knock-down of the CENP-A chaperone HJURP in early S-Phase reduces CENP-A retention during replication (Zasadzinska et al., 2018). HJURP also interacts with MCM2 of the MCM complex in a histone independent manner, indicating a co-chaperone function during DNA-replication. MCM2 was shown to evict the histone dimers H3-H4 as well as CENP-A-H4 and promote parental histone positioning to the lagging strand after the replication fork in cooperation with ASF1 (Petryk et al., 2018, Huang et al., 2015). Since neither of these proteins has centromere specificity and HJURP binds CENP-A and not centromeric DNA, the uncharacterized protein ZN562 with its zinc finger motif could provide protein and/or DNA sequence specificity to achieve this accuracy of CENP-A redeposition.

Another protein that was significantly enriched for CENP-A in my pull-down experiments was NC2B, also known as DR1, which acts in several protein complexes. DR1 forms a heterodimer with DRAP1, which can associate with TATA-box Binding Protein (TBP) to repress the transcription of class II genes (Goppelt et al., 1996). Thereby, the DR1/DRAP1 heterodimer has a direct binding affinity for DNA and can affect the DNA conformation via histone fold domains. In the absence of DRAP1, DR1 also interacts with the ATAC complex, which has histone H3 acetylation activity (Wang et al., 2008). In vitro, the ATAC complex preferentially acetylates both free and nucleosomal histone H3. However, it has no activity towards H4 (Wang et al., 2008). Interactors of the ATAC complex are, among others, DPOE3 and DPOE4 (Wang et al., 2008). Thus, the DPOE3/DPOE4 or DPOE3/Chrac1 histone fold dimers may act in either of the Polε, ATAC, or CHRAC complexes in DNA, centromere, and/or nucleosome specific manner (Wang et al., 2008). Furthermore, ADA3 of the ATAC complex is a direct interactor of CENP-B and has a role in centromere regulation (Mohibi et al., 2015). Knock down of ADA3 may result in a change of the acetylation state of histone H3 and non-histone proteins and therefore impairs CENP-A incorporation in G1 (Mohibi et al., 2015). Since NC2B is enriched in single thymidine arrested and released HeLa cells, expressing CENP-A, over the course of DNA-replication, I hypothesize that the ATAC complex acts complementary to the association of KAT7 with the MIS18 complex and acetylates histone H3 for CENP-A deposition. As a histone "reader" and "writer," ATAC may maintain the acetylation marks during DNA-replication. This is underlined by the direct interaction of ATAC with CENP-B, which resulted in CENP-B diminishing and chromosome segregation defects upon ATAC knock down in mouse embryonic fibroblasts and immortalized breast cancer cells (Mohibi et al., 2015). Whether the ATAC complex also has an impact on histone redeposition during DNA-replication or modifies kinetochore proteins is not known.

An interesting candidate involved in acetylation patterns and recruitment of chromatin remodeling complexes that is enriched for CENP-A ChIP experiments during G1-phase is the AT-rich DNA sequence binding protein - SATB1 (Yasui et al., 2002). In particular, it was shown that in vitro SATB1 directly interacts with BAZ1A and SMARCA5 and is, therefore, a targeting factor of the CHRAC complex specific proteins (Yasui et al., 2002). Bearing this feature, it is assumed that SATB1 links higher-order chromatin packing to gene regulation by guiding several chromatin remodeling factors to entry sites of chromatin at regions with high base

unpairing propensity for a mechanism of global transcriptional regulation (Yasui et al., 2002). Therefore, it might also direct higher-order chromatin structure formation in the centromeric region. SATB1 also recruits HDACs to maintain a hypoacetylated state of the chromatin, which is required for constitutive heterochromatin (Yasui et al., 2002, Casas-Delucchi et al., 2012). While kinetochore architecture and microtubule attachment are well studied, less is known about centromere organization and chromatin structure. In fact, centromeres have been described to be distinct from bulk chromatin structures and are forming a linear chromatin structure termed 'centrochromatin' (Sullivan and Karpen, 2004, Lam et al., 2006, Bergmann et al., 2011). Whether this distinct higher-order chromatin structure of centromeres enables to withstand the forces of chromosome segregation is unknown as well as how this chromatin structure is established. Whether SATB1 plays a role in this organizational process remains to be investigated.

The transcriptional repressor SETDB1 was significantly enriched for CENP-A in late S-phase (Wang et al., 2000). SETDB1 acts as a histone methyltransferase that specifically tri-methylates lysine 9 of histone H3 (H3K9me3), which is a mark of silent chromatin (Martins et al., 2016). In particular, the centromeric domain is flanked by pericentromeric heterochromatin that is enriched for H3K9me3 (Martins et al., 2016, Sullivan and Karpen, 2004). H3K9me3 induces transcriptional repression by recruitment of heterochromatin factor HP1, which also is abundant in my experiments. HP1 generates a highly compact chromatin structure, most likely by linking several nucleosomes, in a process that is not comprehensively understood (Jenuwein and Allis, 2001). Previous studies reported that tethering of SETDB1 to alphoid^{tetO}-HAC sites reduced CENP-A levels (Shono et al., 2015, Cardinale et al., 2009, Nakano et al., 2008, Ohzeki et al., 2012). A similar reduction of CENP-A levels was observed for HDAC4, which was highly enriched and significant for CENP-A in G1-phase in my experiments (Shono et al., 2015, Hassig and Schreiber, 1997). As mentioned earlier, histone acetylation is an important mark for centromere maintenance and histone turnover during G1-phase. HDAC4 might, therefore, be involved in these critical roles of CENP-A inheritance. Interestingly, a microscopy-based genetic screen of CENP-A also identified HDAC4 as an important factor in CENP-A maintenance of 'old' nucleosomes at the centromere (Mitra et al., 2020a). This suggests an unknown role in CENP-A maintenance for these chromatin-modifying proteins that might be investigated in future experiments.

In addition to transcription factors, I found several chromatin-modifying proteins enriched in centromere ChIP experiments. Importantly, for CENP-A deposition, the MIS18 complex has been shown to directly interact with CENP-C, DNMT3A, and DNMT3B and to enhance DNA methylation within centromeric chromatin and CENP-A assembly (Gopalakrishnan et al., 2009). DNA methylation as a heritable mark of transcriptional repression and has also been shown to be important for chromatin structure and genome stability, especially during mitosis (Gopalakrishnan et al., 2009). Methylation is generally mediated by the genome-wide collaboration of the three DNA-methyltransferases DNMT1, DNMT3A, and DNMT3B (Goll and Bestor, 2005). In my experiments, DNMT3A and B were significant for CENP-A interaction in early S-Phase. This aligns with the observation that DNMT3B is interacting with the CCAN protein CENP-C (Gopalakrishnan et al., 2009). The knock down of either protein resulted in increased chromosome misalignment and transcription of the centromeric DNA region (Gopalakrishnan et al., 2009). Also, cancer cells showed elevated expression of alternatively spliced DNMT3 versions that lack the N-terminal CENP-C binding region (Ostler et al., 2007). This could result in altered methylation patterns, which in turn causes genomic instabilities, predisposing to cancer. Epigenetic determination of the centromere plays a pivotal role in cell viability since α-satellite DNA lacks consensus sequences. Bearing in mind that methylation patterns of both, DNA and histones, are important for genomic stability transcriptional regulation and chromatin structure, DNMT3A, and B de-novo methylation might be of significant importance to establish a dense centromeric chromatin structure by recruiting factors like condensin or HP1 (Gopalakrishnan et al., 2009).

Besides the MIS18 complex and CENP-C, DNMT3A and B may be recruited by UHRF1, which is slightly enriched with CENP-A in my experiments and has a role in the progression of replication of heterochromatic DNA regions in S-Phase (Arima et al., 2004, Papait et al., 2007, Bonapace et al., 2002). UHRF1 is an E3 ubiquitin ligase, bridging DNA methylation, and chromatin modification and ensures faithful propagation of DNA methylation patterns through DNA replication (Bostick et al., 2007). The role of UHRF1 is presumably to restore a heterochromatic state important for the higher-order structure of 'centrochromatin' after replication fork passage (Arima et al., 2004, Bonapace et al., 2002, Papait et al., 2007).

CENP-A ubiquitination on lysine 124 (CENP-AK124ub) is an important histone maintenance mark and indispensable for cell viability (Niikura et al., 2019). This histone mark was found to be mediated by the CUL4A-RBX1-COPS8 E3-ubiquitin ligase complex by RNAi mediated knock down experiments (Niikura et al., 2015). The CENP-AK124ub is epigenetically inherited through dimerization in a templated process after new CENP-A is deposited and before the next round of deposition in G1-phase (Niikura et al., 2016). In my experiments, CUL4A and B were identified in H3.3 and CENP-A experiments. However, CUL4B was significantly enriched in CENP-A pull-down experiments in mid-S-phase after 3 hours of release before replication of the centromere. CUL4A and CUL4B share ~84% sequence identity and act in the same pathways, which suggests redundant or overlapping function (Higa et al., 2003). Both, CUL4A and CUL4B interact with RBX1/ROC1 via their C-terminal RING domains. Here, CUL4 is thought to be a scaffold protein that acts in multiple cullin-RING-based E3 ubiquitin-protein ligase complexes. With the N-terminal region, the CUL4 proteins interact with several adaptor proteins that achieve substrate specificity. One of these is DNA damage-binding protein 1 (DDB1), which was shown to be constitutively associated with centromeric DNA in a proteomic analysis (Obuse et al., 2004). However, knock down of DDB1 did not affect CENP-A maintenance in HeLa cells (Niikura et al., 2015). In contrast, the depletion of COPS8 resulted in reduced CENP-A localization (Niikura et al., 2016, Niikura et al., 2015). As CUL4A and B are constitutively associated with H3.3 as well as CENP-A, I hypothesize that CENP-A along with histone H2A, H3, and H4 is ubiquitinated during S-phase, since a ubiquitination activity of the CUL4 proteins was also observed on these histones (Guerrero-Santoro et al., 2008, Wang et al., 2006). The ubiquitination of CENP-A is conserved in budding yeast, which is mediated by the E3 RING finger ligase Psh1 (Hewawasam et al., 2010). Given the importance of this mark, in budding yeast, ubiquitination underlies a control mechanism that involves ubiquitin protease Ubp8 (Canzonetta et al., 2015). Correspondingly, there are observations that suggest a similar control mechanism in humans, as CENP-A K124 is acetylated at the transition from G1-/S-phase (Bui et al., 2012). This covalent modification might “prime” CENP-A for the ubiquitination mark and blocks lysine 124 for ubiquitination before the next G1-phase (Niikura et al., 2015). As lysine 124 is acetylated at the transition of G1-/S-phase, this would necessitate a ubiquitin protease similar to budding yeast (Bui et al., 2012, Canzonetta et al., 2015). A candidate for de-ubiquitination that is specifically enriched with CENP-

A in my experiments is USP10, a hydrolase that can remove conjugated ubiquitin from target proteins.

Ordered nucleosome disassembly and reconstruction is a required trait during DNA replication. To achieve this, several chromatin acting factors are necessary. Among these factors are histone chaperones, by promoting specific histone-DNA and histone-histone interactions in an ATP-independent manner. While an intact nucleosome is stable enough to halt transcription and replication machineries at the DNA elongation step during S-phase, histones have to be evicted before and reassembled after the passage of replication forks (Bondarenko et al., 2006). The pivotal histone chaperone Facilitates Chromatin Transcription (FACT) was initially identified in HeLa cells and is conserved in all eukaryotes (Gurova et al., 2018). Human FACT is a heterodimer comprised of the multi-domain proteins SPT16 (Suppressor of Ty 16) and SSRP1 (Structure-Specific Recognition Protein 1) (Orphanides et al., 1999). Initially, FACT was identified for its role during transcription, to allow RNA polymerase II (RNAPII) to progress through nucleosomes while preserving nucleosome integrity (Belotserkovskaya et al., 2003). In *Drosophila,* RNAPII was required for CENP-A deposition (Chen et al., 2015). In this process, FACT interacts with CAL1 (the functional HJURP homolog in *Drosophila*) to drive the DNA-sequence independent transcription of RNAPII (Chen et al., 2015). In earlier pull-down experiments as well as my time resolved analysis, FACT was stably associated with CENP-A nucleosomes (Foltz et al., 2006). In my experiments, the interaction was most significant during G1-phase, when CENP-A is deposited and most abundant in late S-phase, when the centromeric chromatin is replicated. In budding yeast, FACT facilitates PTM of CENP-A. In *Drosophila*, it probably has a direct role in CENP-A deposition, while in chicken, it is required for CENP-A localization (Okada et al., 2009, Deyter and Biggins, 2014, Chen et al., 2015). This indicates that FACT has a conserved role during CENP-A deposition and redistribution (Chen et al., 2015). Furthermore, it appears that FACT has a role in restricting CENP-A occupancy to centromeres (Choi et al., 2012, Deyter and Biggins, 2014). FACT can interact with the H3-H4 tetramer with several domains and increases nucleosome accessibility, even in the absence of H2A and H2B (Xin et al., 2009). Most likely, FACT acts as a nucleosome destabilizer to allow RNAPII passage, which in turn interacts with the CENP-A specific histone chaperone (Hondele and Ladurner, 2013). However, which of these features would enable FACT to discriminate between histone variants and especially centromeric nucleosomes is an intriguing question to be tackled in

future experiments. It also remains elusive whether the transcripts of RNAPII produced during CENP-A maintenance are a byproduct of chromatin re-organization or are important specifiers of centromeric identity (Quenet and Dalal, 2014, Rosic et al., 2014, Topp et al., 2004).

Finally, the mismatch repair proteins MSH2 and MSH6 were highly abundant and significant, especially in early S-phase in my ChIP experiments. These proteins also led to a reduced CENP-A maintenance in a recent microscopy-based RNAi screen (Mitra et al., 2020a). MSH2 forms a heterodimeric complex with MSH6, which is the most abundant mismatch-binding factor and also known as MutSα as part of the post-replicative DNA mismatch repair system (MMR) (Jiricny, 2006). Interestingly, MutSα has been shown to exclude nucleosomes and to counteract histone H3 chaperones HIRA and CAF1 chromatin assembly activity in *Xenopus* egg extracts (Terui et al., 2018). This could potentially exclude the replication-independent histone deposition from centromeric chromatin and support the cell cycle-specific deposition of CENP-A exclusively during early G1-phase. Whether the MutSα specifically interacts with the centromere may be validated either by ChIP-seq of MSH2 or MSH6 or a centromere-specific qPCR. Also, it would be interesting to investigate whether a conditional knock down of MSH2 or MSH6 results in atypical CENP-A deposition or loss of centromeric identity.

The setup of the CENP-A specific interactome presented herein allows to differentiate between different cell cycle stages and, therefore, between proteins associated with CENP-A during the deposition in G1-phase and DNA-replication in late S-phase (4hours after thymidine release). I, therefore, summarized and incorporated the candidates identified in this study in the CENP-A deposition and redistribution pathway in the following model, which is based on the prevailing literature (Figure 46). After mitosis, when CDK activity decreases, the Mis18 complex is recruited to centromeres by association with CENP-C and leads to acetylation of CENP-A proximal histone H3 by Kat7 and potentially Kat6b and the ATAC complex. The acetylation mark of H3K14ac is recognized by BAZ1B, which assembles the B-WICH complex, potentially exchanging H3 for CENP-A. These nucleosomes are subsequently stabilized and spaced by the RSF complex.

At the beginning of S-phase, while CDK activity is still low, DNMT3A/B associate with the MIS18 complex to methylate centromeric DNA to establish a transcriptionally repressed state that also induces the higher-order structure of

'centrochromatin.' As S-phase commences, also PTMs of centromeric histones are propagated, priming the chromatin state for inheritance during DNA replication. Among these may be ubiquitination by CUL4, acetylation by the ATAC complex, or ATP-dependent remodeling by NPM1-NPM3 and other chromatin factors. When the replication machinery arrives at the centromere, the nucleosomes are disassembled in a process that involves the MCM2-7 helicase. The chromatin is disrupted by ATP-dependent remodeling complexes and the MCM2-7 helicase, which results in the eviction of parental histones. The disassembly of chromatin may be aided by the interaction of histone chaperones FACT and ASF1 with the MCM2-7 complex, which also results in the separation of H2A-H2B dimers and $(H3\text{-}H4)_2$ tetramers. In this process, ASF1 is chaperoning H3-H4, splits tetramers into dimers, and associates them to CAF1 for deposition to either the leading or lagging strand after the replication fork. CAF1 is tethered to either strand by interaction with PCNA. A semi-conservative deposition of parental histones may be promoted by MCM2, and, speculatively for CENP-A, the CHRAC chromatin remodeling complex, which might be tethered to the replication fork directly. Newly synthesized H3-H4 dimers are likewise delivered to CAF1 by ASF1. For H2A-H2B, FACT would facilitate the retention of parental histone dimers, and NAP1 handles newly synthesized H2A-H2B dimers. The epigenetic marks of centromeric chromatin are restored by the interplay of several chromatin factors, which eventually reestablish the higher-order chromatin structure of the 'centrochromatin.'

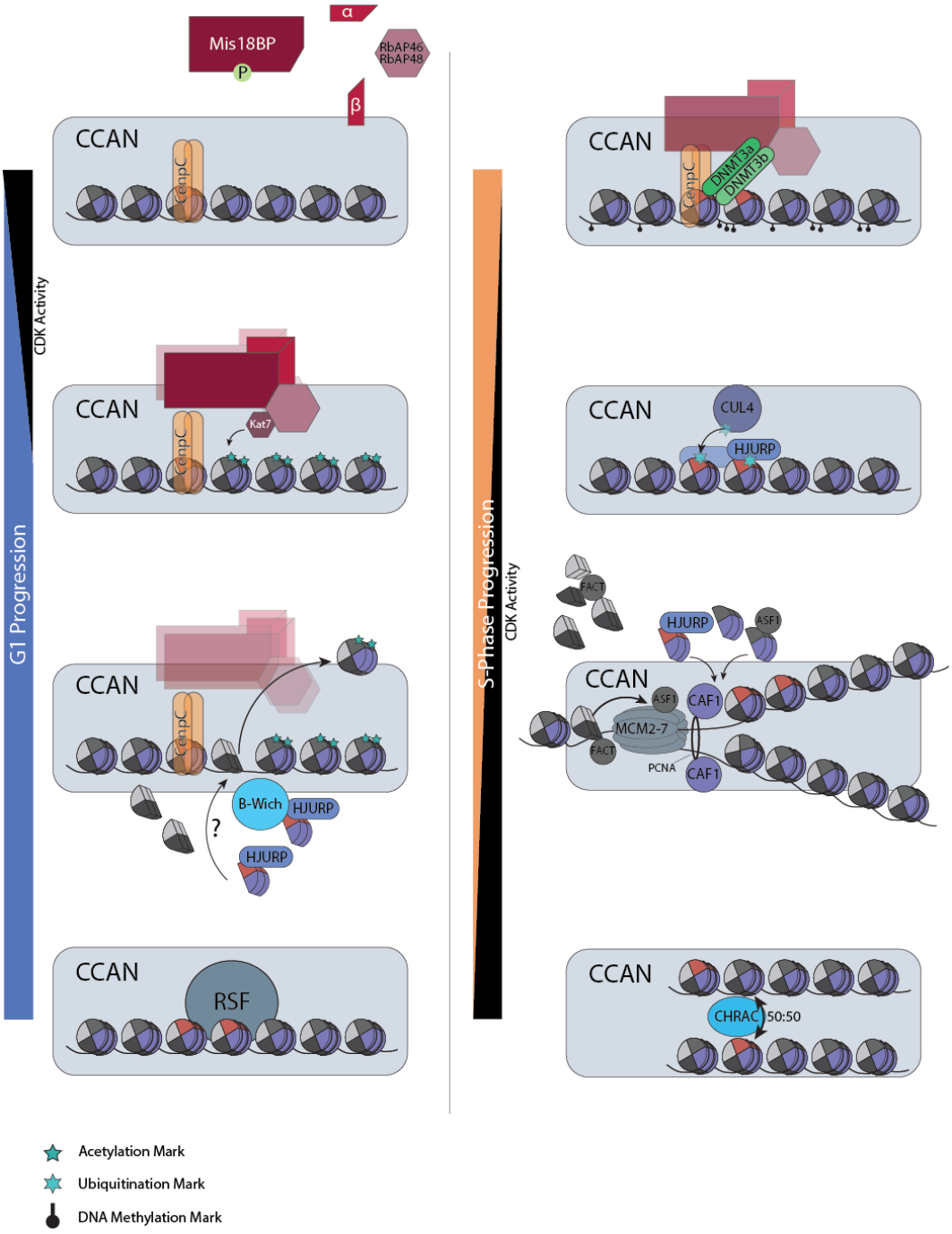

Figure 46. Schematic Overview of the CENP-A Deposition and Redistribution Pathway in G1 and S-phase, Respectively.

Towards the end of mitosis, when CDK levels begin to drop, the MIS18 complex assembles on CENP-C. Acetyltransferases like Kat7 and potentially KAT6B are recruited to earmark histone H3.3 in the vicinity of CENP-A containing nucleosomes. The acetyl mark of histone H3.3 recruits chromatin remodeling machineries like B-WICH that promotes the exchange of histone H3 for CENP-A. Afterward, RSF and Mgc-RacGap stabilize and space the

deposition of the new CENP-A at the centromere. Subsequently, the chromatin has to be organized in a translationally repressed, heterochromatic state, probably by centromere-specific PTMs. The important ubiquitination mark of CENP-A K124ub is mediated and maintained by CUL4 during early S-phase. When the replication machinery arrives, nucleosomes are disassembled before and reassembled into chromatin after the replication fork. This happens in a semi-conservative manner distributing the histone dimers to the leading and lagging strand in a process that is not well understood but potentially involves the Chrac chromatin remodeling complex.

It should be noted that the candidates reported in this part of my thesis remain to be validated for their role in CENP-A dynamics before a putative function or mechanism can be claimed in centromere biology. Therefore, I propose a microscopy-based RNAi screen of the candidates presented in this work (Bodor et al., 2014). Analyzing the CENP-A associated proteins *in vivo* by knock down experiments would further reveal the importance of centromere associated proteins in chromatin biology and will help to understand the impact of the CENP-A protein environment comprehensively. In this part of my thesis, I presented the identification of a variety of proteins that previously have only vaguely been associated with centromere function or CENP-A maintenance. These candidates act selectively for CENP-A while some bind constitutively, and some bind the centromeric region at distinct moments during the cell cycle. This underlines the dynamic nature of centromeric chromatin. The identification of these CENP-A interacting proteins serves as a source for further investigation to elucidate the dynamics of CENP-A deposition, maintenance, and centromeric inheritance.

5.5 Materials and Methods

5.5.1 Materials

5.5.1.1 Devices

Description	Supplier
-20°C freezer	Liebherr
-80°C freezer	Eppendorf
4°C fridge	Liebherr
37°C incubator (bacteria)	Binder
37°C (human cells)	Thermo
Centrifuges	5424R, Eppendorf
	5810R, Eppendorf
	EvolutionRC, Sorvall
Cell Counter	Vi-Cell XR, Beckmann Coulter
Chromatography Systems	Äkta Pure25, GE-Healthcare
	Äkta micro, GE-Healthcare
	Äkta start, GE-Healthcare
	Äkta explorer10, GE-Healthcare
	Easy-nLC 1000, Thermo
Developer machine	Amersham Imager 600, GE-Healthcare
Dounce homogenizer	Satorius
Gel documentation system	Intas GelDoc
Hood	BDK
Incubation shaker (37°C)	New Brunswick
Magnetic separation rack	NEB/ Permagen

Mass Spectrometer	Orbitrap Elite, Thermo
Mini Trans Blot cell	BioRad
pH meter	Mettler
Pipetboy	Integra
Pipettes	Gilson
Protein gel chamber	BioRad
Rotating wheel	Sunlab
Scales	Sartorius
Sonicator	Branson
Spectrophotometer	NanoDrop 2000c, Thermo
Thermomixer Eppendorf	Thermomixer comfort, Thermomixer C, Eppendorf
Vortex	Bender&Hobein AG

5.5.1.2 Chemicals and Consumables

Description	Supplier
1.5 ml reaction tubes	Sarstedt
2 ml reaction tubes	Sarstedt
1.5 ml low binding tubes (DNA and protein)	Sarstedt
15 ml and 50 ml tubes	Sarstedt
Acetic acid	Sigma-Aldrich
Acetonitrile	Honeywell
Agarose	Biozym
Ampicillin (Amp)	Roth
Blasticidin S HCl	Thermo
LB Agar	VWR

BSA 98%	Sigma-Aldrich
C_{18} cartridges, Sep-Pak	Waters
$CaCl_2$	Sigma-Aldrich
Cell culture plates	Thermo
Complete Protease Inhibitor Cocktails Tablets (PI)	Roche
Coomassie Brilliant Blue	Sigma-Aldrich
Cryovials	Th.Geyer
Developer	AGFA
Deoxycytidine	Sigma
DMEM	Thermo
DMSO	Sigma-Aldrich
DNA oligonucleotides	Sigma-Aldrich, Metabion
dNTP mix	NEB
DTT	Roth
Dynabeads Protein G	Thermo
ECL Western Blotting detection reagents	Amersham
EDTA	Roth
EGTA	Roth
Ethanol, absolute	Roth
FCS	Thermo
Filter paper Whatman 3MM	Whatman
Filter tips	Star Lab
Formic Acid	Fisher
Formaldehyde (37%)	Roth
GelRed	Biotrend
Glycerol	Roth

Glycine	VWR
Halt™ phosphatase inhibitor	Thermo
HEPES	Sigma-Aldrich
Hygromycin B	Thermo
IPTG	Roth
Isoamyl alcohol	Merck
Kanamycin sulfate (Kan)	Roth
KCl	Roth
Lipofectamine LTX	Thermo
Lovastatin	Selleckchem
MaXtract High Density Column	Qiagen
ß-mercaptoethanol	Sigma
Methanol	Sigma
$MgCl_2$	Roth
NaCl	Roth
NP-40	Sigma
Opti-MEM Reduced-Serum Medium	Thermo
Phenol/chloroform/isoamylalcohol	Roth
Pipette tips	Star Lab
Ponceau S solution	Sigma
Protein gels - precast	BioRad
Nitrocellulose Transfer Membrane	Merck
Silver nitrate	Roth
Sodium Dodecyl Sulfate (SDS)	Serva
Thymidine	Roth
Trifluoroacetic acid (TFA)	Thermo

Tris	Roth
Triton X-100	Sigma
Trypsin/EDTA (cell culture)	Sigma/ Thermo
Tween20	Sigma
Water (MS-grade)	Honeywell/ Fisher
X-ray films	Amersham
Zeocin	Thermo

5.5.1.3 Kits, Enzymes, Markers and Antibodies

Description	Supplier
50 bp ladder	NEB
1 kb ladder	NEB
Broad range Protein Marker	NEB
Gateway BP clonase enzyme mix	Thermo
Gateway LR clonase II enzyme mix	Thermo
Gel extraction Kit	Macherey-Nagel
Midiprep Kit	Macherey-Nagel
Micrococcal nuclease (MNase)	Roche
NucleoSpin® Plasmid EasyPure Kit	Macherey-Nagel
Lysyl Endopeptidase (LysC)	Wako
Phusion High Fidelity DNA polymerase	NEB
Proteinase K	Thermo
RNase A	Thermo
Trypsin	Promega
Q5 DNA Polymerase	NEB
Q5 site-directed mutagenesis kit	NEB
Restriction endonucleases	NEB

Taq DNA Polymerase	NEB

5.5.1.3.1 Antibodies

Name (product #)	Supplier	Application	Dilution
Mouse α-CENP-A (ab13939)	Abcam	WB	1:10000
Mouse α-HA (11583816001)	Roche	WB	1:8000
Mouse α-Tubulin (T6199)	Sigma	WB	1:2000
α-mouse IgG-HRP (SC2005)	Santa Cruz	WB	1:10000
Mouse α-Flag M2 (F1804)	Sigma	IP (see M23)	1:2.5

5.5.1.4 Plasmids

Name	Source	Description	Marker
pOG44	Thermo	Expression of Flp recombinase	Amp
pDONOR221	Thermo	Entry plasmid for gateway cloning	Kan
pDONOR221-CENP-A	this thesis	Entry plasmid carrying full length CENP-A	Kan
pDONOR221-H3.3	this thesis	Entry plasmid carrying full length H3.3	Kan
pEWS	Herzog et al.	Expression plasmid for FlpIN T-Rex system (Thermo) N-term Twin-Strep-HA-tag-6xHis-GOI	Amp
pEWS-Nfl	this thesis	modified from pEWS N-term 6xFlag-tag-HA-tag-6xHis-GOI	Amp
pEWS-Nfl-CENP-A	this thesis	Expression plasmid, carrying full length CENP-A in frame	Amp
pEWS-Nfl-H3.3	this thesis	Expression plasmid,	Amp

		carrying full length H3.3 in frame

5.5.1.5 Oligonucleotides

Name	3'-Sequence-5'	Description
OGH18	TAAAGATGATGATGATAAAGATTATAAAGATG ATGATGATAAAGGACATCACCATCACCATCAC	Forward Primer Introduction of 3xFlag in pEWS
OGH19	TAATCTTTATCATCATCATCTTTATAATCCGCGC CTCCGGCGCCACCGGCATAGTCAGGAACATC	Reverse Primer Introduction of 3xFlag in pEWS
OGH141	GGGGACAAGTTTGTACAAAAAAGCAGGCTTAG CTCGTACCAAGCAGACTGC	Forward Primer Cloning of H3.3 into pDONR221
OGH142	GGGGACCACTTTGTACAAGAAAGCTGGGTCTT ACGCCCTCTCCCCACG	Reverse Primer Cloning of H3.3 into pDONR221
OGH145	TCTCCGTCGTCAGGATCATCCCACCACCACCAC CACCACGGATC	Forward Primer Cloning of CENP-A into pDONR221
OGH146	CCGCCGTCGTCGACAAGCCGGCATGGTGGCCT TAAGTTAAACG	Reverse Primer Cloning of CENP-A into pDONR221

5.5.1.6 Cell Lines, Yeast- and Bacterial-Strains

5.5.1.7 Human Cell Lines

Cell line	Origin	Source
HeLa FlpIN T-Rex	cervical cancer	Thermo
1B12 – Nfl-CENP-A	cervical cancer	this thesis
4C07 – Nfl-H3.3	cervical cancer	this thesis

5.5.1.8 *E.coli* Strains

Strain	Genotype	Supplier
E.coli DH5a	*fhuA2 Δ(argF-lacZ)U169 phoA glnV44 Φ80 Δ(lacZ)M15 gyrA96 recA1 relA1 endA1 thi-1 hsdR17*	NEB
E.coli DH5a-T1^{R}	F- φ80lacZΔM15 Δ(lacZYA-argF)U169 recA1 endA1 hsdR17(rk - , mk +) phoA supE44 thi-1 gyrA96 relA1 tonA	Thermo

5.5.1.9 Software

Application	Software
Image Processing	Adobe Photoshop CS6
	Adobe Illustrator CS6
Primer Design	Benchling (web-browser based)
Protein identification	MaxQuant (vers.1.6.5.0)
	Xquest (vers.1.2.3)
	OpenMS (vers.2.1.0)
Statistical Analysis	R Studio / R (3.0.2)
Sequence Alignment	ClustalW, ClustalOmega

5.5.1.10 Buffers

Ampicillin stock solution	100 mg/ml Ampicillin (1000x)
Blocking solution	5% Milk powder (w/v)
	TBS + 0.1 % Tween20
Coomassie staining solution	10% Acetic acid (v/v)
	50% Methanol (v/v)

	0.1% Coomassie Brilliant Blue (w/v)
Coomassie destaining solution	10% Acetic acid (v/v)
	30% Methanol (v/v)
4x Laemmli loading buffer	250 mM Tris
(adjust pH to 6.8 with HCl)	40% Glycerol (v/v)
	8% SDS (w/v)
	20% beta-Mercaptoethanol (v/v)
	0.01% Bromphenol blue
SDS-PAGE running buffer	25 mM Tris
	192 mM Glycine
	0.1% SDS (w/v)
LB Agar plates	1.5% LB Agar
LB medium	1.0% Tryptone (w/v)
	0.5% yeast extract (w/v)
	1.0% NaCl (w/v)
Phosphate buffered saline (PBS)	140 mM NaCl
	2.7 mM KCl
	10 mM Na2HPO4
	1.8 mM KH2PO4
TBE	45 mM Tris
	45 mM Boric acid
	1 mM EDTA
Transfer Buffer (SDS gel electrophoresis)	48 mM Tris
	39 mM Glycine
	0.0375% SDS (w/v)
	20% Methanol (v/v)

TE	10 mM Tris
	1 mM EDTA

5.5.2 Methods

5.5.3 Molecular Biology Methods

M14. Mutagenesis of pEWS to Generate pEWS-Nfl

The pEWS plasmid was used to substitute the N-terminal twin strep-tag for a N-terminal 3xFlag-Tag with the Q5 site-directed mutagenesis kit (NEB). Primer pairs, carrying the desired substitution were used for PCR amplification with the following conditions:

Table 1: Composition of reagents for site-directed mutagenesis.

Template (25 ng/µl)	1 µl
Primer fwd (10 µM)	1.25 µl
Primer rev (10 µM)	1.25 µl
Q5 Hot Start High-Fidelity 2X Master Mix	12.5 µl
H_2O	9 µl
Total volume	25 µl

Table 2: Conditions for site-directed mutagenesis of pEWS

	Temperature	Duration	Cycles
Initial denaturation	98°C	30 s	1
Denaturation	98°C	10 s	25
Annealing	57°C	1 min	
Elongation	72°C	3:30 min	
Final Elongation	72°C	5 min	1

After PCR, 1 µl of the PCR product were subjected to KLD reaction mix (NEB) in order to eliminate the parental template DNA not carrying the mutation. Next, 5µL of the KLD treated DNA was transformed into competent *E. coli* DH5a-T1^R cells. Finally, the isolated DNA of several clones was analyzed by sequencing (Eurofins) and the obtained DNA sequence was investigated by the ClustalW sequence alignment program in order to determine whether it contains the desired mutation.

M15. Cloning of CENP-A and H3.3 into Entry Vector pEWS-Nfl

In order to clone histone variants H3.3 and CENP-A into pEWS-Nfl, the vector used for expression in HeLa FlpIN T-Rex cells, the DNA was amplified with primers containing attL overhangs for gateway cloning (see Table 3, Table 4 and 6.1.1.5), and cloned into pDONR221 entry vector (Thermo).

Table 3: Reagents used for PCR to clone CENP-A and H3.3 into entry vector pDONR221.

CENP-A / H3.3 (1ng/µl)	1 µl
5x HF buffer	10 µl
dNTPs	1 µl
Primer fwd (10 µM)	0.5 µl
Primer rev (10 µM)	0.5 µl
Polymerase (Q5)	0.5 µl
H_2O	36.5 µl
Total volume	50 µl

Table 4: PCR conditions for amplification of Entry mutant constructs.

	Temperature	Duration	Cycles
Initial denaturation	95°C	30 s	1
Denaturation	95°C	30 s	30
Annealing	55°C	1 min	
Elongation	72°C	1 min	
Final elongation	72°C	7 min	1

Obtained PCR products were PCR purified and subjected to Gateway Cloning according to the manufacturer's protocol. Briefly, 50-150 ng of the purified PCR

product was mixed with 150 ng of pDONR221 vector and filled up to 8 µl with TE buffer. 2 µl of BP Clonase enzyme mix (Thermo) was added to this mixture and incubated at 25°C for 1 hour. Afterward, 1 µl of Proteinase K was added and incubated at 37°C for 10 minutes. Finally, 2 µl of the final mix was transformed into competent *E. coli* cells. DNA of the received bacterial clones was isolated with the NucleoSpin Plasmid EasyPure Kit, sent for sequencing (Eurofins), and analyzed with the help of the ClustalW sequence alignment program.

Positive entry clones were subsequently used to generate expression plasmids. To do this, 50-150ng of entry vector was mixed with 150ng of pEWS-Nfl expression vector and filled to 8µL with TE buffer. 2µL of LR clonase II enzyme mix (Thermo) was added to this mixture, briefly mixed, and incubated for 1 hour at room temperature. Subsequently, 1µL of Proteinase K was added and incubated at 37°C for 1 minute. 2µL of the LR reaction was transformed into 50µL competent *E. coli* cells. DNA of the received bacterial clones was isolated with the NucleoSpin Plasmid EasyPure Kit, sent for sequencing, and analyzed with the help of the ClustalW sequence alignment program. Positive clones were used to transfect HeLa FlpIN T-Rex cells.

5.5.4 Biochemical and Cell Biology Methods

M16. SDS-Polyacrylamide Gel Electrophoresis (SDS-PAGE)

Proteins were separated with 4-20% precast gels from BioRad by SDS-polyacrylamide gel electrophoresis. NEB and BioRad broad range marker were used to determine the size of the respective proteins. Before loading, samples were boiled 5-10 min at 95°C in 4x Loading Dye and then ran for approximately 1.5 hours at 150-235 V. Afterwards, the gel was either used for Coomassie staining, Silver staining, or subsequent immunoblotting.

M17. Coomassie Staining of Polyacrylamide Gels

In order to visualize proteins separated by SDS-PAGE, the polyacrylamide gel was stained for 1 hour or overnight in the Coomassie staining solution. Subsequently, the gel was destained in destaining solution or water until the protein bands became apparent. After washing the destained gel with water, it was scanned.

M18. Silver Staining of Polyacrylamide Gels

To visualize proteins that were separated by SDS-PAGE, the gel was fixed in a fixing solution for 20 minutes. Subsequently, the gel was washed twice in 50% ethanol, twice in 30% ethanol, and incubated in 0.02% sodium thiosulfate. The gel was washed three times with water for 1 minute and stained with silver nitrate for 20 minutes. Finally, the gel was developed by the addition of developing solution until the protein bands are sufficiently visible. The reaction was stopped by adding 10% acetic acid, and the gel was stored in water.

Fixing Solution:	45%	Methanol (v/v)
	10%	Acetic Acid (v/v)
Sodium Thiosulfate:	0.8mM	Sodium thiosulfate
Silver Nitrate:	12mM	Silver nitrate
	0.04%	Formaldehyde (v/v)
Developer:	1.5%	Sodium carbonate (w/v)
	0.016mM	Sodium thiosulfate
	0.03%	Formaldehyde (v/v)

M19. Immunoblotting

Polyacrylamide gels were blotted onto a nitrocellulose membrane with a wet blotting device. The polyacrylamide gel, a nitrocellulose membrane, and Whatman papers were equilibrated for 5 min in transfer buffer prior to the formation of a blotting sandwich in the following order: Whatman paper, membrane, gel, additional Whatman paper. The sandwich was blotted for 1.5 hours at 400 mA at 4°C. Subsequently, the membrane was blocked for at least 1 hour in blocking solution. The primary antibody was diluted in a blocking solution (see 6.1.1.3.1 for details) and incubated overnight at 4°C, followed by three washing steps à 10 min with TBS-T the next day. After washing, the membrane was incubated with the secondary antibody diluted in blocking solution (see 6.1.1.3.1 for details) and incubated for 1 hour at room temperature (RT). Afterward, the membrane was again washed three times with TBS-T. Next, respective proteins were detected by incubation with ECL detection reagent for 2-10 min. The bands were developed in

Amersham Imager600 (GE-Healthcare) blot documentation system in auto exposure mode.

M20. Generation of FlpIN T-Rex HeLa cells expressing H3.3 or CENP-A

HeLa FlpIN T-Rex cells were cultured, cells cultivated in Dulbecco's modified Eagle medium (DMEM) plus 10% FCS and 4 µg/mL Blasticidin and 10 µg/mL Zeocin (before transfection) at 37°C and 5% CO2. To establish FlpIN T-Rex HeLa cell lines stably expressing 6xFlag-Ha-6xHis-tagged histone proteins, 1.5 x 10^5 cells were seeded into 6-well plates without antibiotics. The following day, the cells should have reached a confluency of approximately 70%. 1 µL (80ng/µL) pEWS and 1 µL (720ng/µL) pOG44 (Thermo) plasmid DNA was mixed with 0.8µL Plus reagent (Thermo). 3 µL Lipofectamine (Thermo) was mixed with 97 µl Opti-MEM (Thermo) before this transfection mix was added to the plasmid DNA and incubated for 30-45minutes at room temperature. Additionally, one negative control sample was set up that contained water instead of plasmid DNA. Subsequently, the transfection mix was added dropwise to the cells. The plates were mildly shaken to distribute the transfection mix into the cell medium, and the cells were then incubated for 48 hours. The cells were trypsinized and transferred to a T75 cell culture flask. The following day, cells were selected by the addition of 200 µg/mL Hygromycin and 4 µg/mL Blasticidin. The medium was changed every 2-3 days. When colonies appeared, the cells were trypsinized, singularized, and transferred to a 150mm dish. The cells were grown to confluency, split once 1:8, and after reaching 70-90% confluency, the cells were back frozen until further use. To do so, trypsinized cells were resuspended in FCS + 10% DMSO. Usually, 1 x10^7 cells were resuspended in 3 ml FCS + 10% DMSO and separated into three 1 ml aliquots, transferred to cryovials, and frozen at -80°C. For long term storage, cells were relocated to liquid nitrogen. In the case of thawing, the frozen cells were put into a 37°C water bath for quick melting, transferred to a 150 mm dish, and 20 ml DMEM + FCS was added.

M21. Protein expression and purification from FlpIN T-Rex HeLa cells

Three days before harvest, the cells were seeded with ~30% confluency. A 2 mg/mL doxycycline stock solution was prepared in 95% ethanol. For induction, a 20 µg/mL working solution was prepared in DMEM. After 24 hours, protein expression was induced at ~50% by the addition of doxycycline working solution to a final concentration of 1 µg/mL. The cells were incubated to a 95-100% confluency and harvested by trypsinization.

M22. Cell Cycle Arrest and Arrest/Release of FlpIN T-Rex HeLa cells

To synchronize cells by single thymidine block, the cells were grown to a confluency of ~40-50% before thymidine was added to a final concentration of 2mM. The cells were incubated for 21 hours before either harvesting (S0h) or release. To release the cells, the medium was aspirated, and the cells were washed twice with PBS. Subsequently, DMEM containing 24 µM deoxycytidine was added for release. The cells were incubated either for 2, 3, 4, or 6 hours before harvesting.

Synchronization of HeLa cells in early G1-phase was performed with Lovastatin. Before synchronization, lovastatin was activated by dissolving 52 mg in 1.04 mL ethanol. 813 µL sodium hydroxide (1M) was added and neutralized with HCl (1M) to reach pH 7.2. The solution was filled to 13 mL for a 10mM lovastatin stock. To synchronize cells, the cells were grown to a confluency of ~40-50% before lovastatin was added to a final concentration of 20 µM. The cells were incubated for 24 hours before harvesting. Cells were harvested by trypsinization and collected on ice. The cells were counted, and $8 \cdot 10^7$ were aliquoted. The cell aliquots were washed twice with PBS and snap-frozen until further use.

M23. Coupling of Flag-M2 Antibody to Magnetic Beads

To couple Flag-M2 Antibody (Sigma-Aldrich) to magnetic beads, 5mL of Dynabeads Protein-G (novex) were pipetted in a 50mL falcon. The beads were washed with HEPES-buffer (25mM HEPES pH 8; 150 mM KCl; 5% Glycerol (v/v); 0.02% NP-40), collected on a magnetic rack, and the supernatant was aspirated. 40mL HEPES-buffer containing 2mL of Flag-M2 antibody were pipetted to the beads and incubated for 30minutes on a rotation wheel at room temperature. The beads were collected on a magnetic rack, the supernatant was aspirated, and the beads were washed with 50mL 0.2M Borate (pH 9). Subsequently, the beads were crosslinked by adding 50mL Borate (pH 9) containing 250mg DMP (Thermo) and incubation for 30min at RT in the dark. The solution was split in half, and the reaction was quenched by adding 6.25mL 1M Tris (pH 7.5) and incubated for 5minutes. The beads were collected on a magnetic rack, washed with wash buffer (50mM Tris (pH7.5); 150mM KCl; 5% Glycerol (w/v); 0.02% NP-40) for 15minutes. The beads were pooled and collected on a magnetic rack before the supernatant was aspirated, and 5mL of storage buffer (50mM Tris (pH 7.5); 150mM KCl; 50% Glycerol (w/v); 0.02% sodium azide) was added and stored at 4°C.

M24. Oligonucleosome Preparation

The implemented protocol was initially developed by (Sansoni et al., 2014). HeLa FlpIN T-Rex cells were harvested, counted with the cell counter, and aliquots of $8 \cdot 10^7$ cells were separated into 15 ml falcon tubes, frozen in liquid nitrogen, and stored until further use at -80°C. All the following steps were done on ice. A total cell count of $1\text{-}4 \cdot 10^9$ cells were thawed in Aliquots and lysed for 10 min with 5 ml PBS + 0.3% Triton X-100 + complete protease inhibitors (PI) at 4°C. Nuclei were pelleted by centrifugation for 5 min at 2000 rpm and washed in 6 ml PBS + PI. Nuclei were resuspended in 500 µl EX100 buffer, $CaCl_2$ was added to a final concentration of 2 mM, and the mixture was transferred to a low-binding reaction tube. 150 U micrococcal nuclease (MNase) was added to each of the reaction mixes and incubated for 16-18h min at 4°C, ~1400rpm. Adding EGTA to a final concentration of 10 mM and 0.05% Tween-20 stopped the reaction. Afterward, the samples were centrifuged for 30 min at 21130 rcf; the supernatant (S1) was joined and used for subsequent analysis (M25). First, 25 µl of S1 were boiled for 5 min at 95°C in 4x loading dye to serve as input. Second, 25 µl of S1 were subjected to DNA extraction (see M25). Finally, the rest was used for chromatin immunoprecipitation (ChIP) (see M26).

EX100 buffer: 10 mM HEPES pH 7.6

100 mM KCl

1.5 mM $MgCl_2$

0.5 mM EGTA

10% (v/v) Glycerol

10 mM β-Glycerol phosphate

prior to use: 1 mM DTT

1 x Protease inhibitor

M25. Purification of MNase Digested DNA

In order to determine the MNase digestion degree, DNA was extracted from the S1 fraction obtained after MNase digestion (see M24). Initially, nucleic acids were isolated by phenol/chloroform/isoamyl alcohol extraction, followed by the DNA precipitation by ethanol. First, 175 µl 5 mM Tris-HCl was added to 25 µl S1, then

400 µl phenol/chloroform/isoamyl alcohol (ratio 25:24:1) were added, the mixture was vortexed and transferred to maXtract tubes (Qiagen). The aqueous and organic phases were separated by centrifugation at 13 000 rcf. The aqueous phase containing nucleic acids was used for subsequent DNA precipitation: after the addition of glycogen to reach a final concentration of 200 µg/ml, sodium acetate (final concentration 0.3 M), and 500 µl 100% ethanol, the DNA was precipitated for at least 20 min at -20°C. Centrifugation for 20 min at 20000 rcf at 4°C pelleted the DNA. The pellet was washed twice with 500 µl 70% ethanol and dried at RT for at least 10 min. After drying, the DNA pellet was resuspended in 30 µl double distilled water (ddH_2O). The DNA concentration was analyzed by the Nanodrop spectrophotometer (Thermo). 500 ng DNA were analyzed regarding the digestion degree on a 2% agarose gel.

M26. Chromatin Immunoprecipitation (ChIP) of Oligonucleosomes

Oligonucleosomes from HeLa FlpIN T-Rex cells were prepared as described in M20, M21, M22, and M24 and then subjected to immunoprecipitation. All the following steps were done on ice or at 4°C. A total cell count of $1\text{-}2 \cdot 10^9$ were used for immunoprecipitation with 100µl slurry Flag-M2 conjugated magnetic beads (M23). First, 100 µl slurry of Flag-M2 beads were equilibrated in EX100 buffer containing 0.05% Tween-20 in a protein and DNA low-binding tube. Next, the S1 fraction containing the oligonucleosomes was added to the Flag-M2 magnetic beads and incubated for 2.5 hours at 4°C on a rotation wheel. The mixture was then magnetically separated, and the supernatant was kept as “non-bound.” The beads were washed once in 5 ml wash buffer 1 for 5 min and twice in 1mL to transfer in a 2mL low binding tube. After washing beads were magnetically separated, the supernatant was removed, and the bound proteins were eluted with 200µl Elution buffer for 2.5 hours at 4°C on a rotation wheel. The mixture was then magnetically separated, and 10µl of the supernatant was kept as “Flag eluate.” The remaining eluate was added to 30µl of Ni-NTA slurry (Qiagen), prewashed twice with wash buffer 1, and incubated for 2 hours at 4°C on a rotation wheel. The Ni-NTA beads were washed once in 1 ml wash buffer 1 for 5 min and twice in 500µl wash buffer 2. Finally, 30µl of wash buffer 2 was added, 10µl was saved for analysis on a silver-stained SDS-PAGE gel (see M16), and 20µl were subjected to protein digest.

Wash buffer 1: 10 mM Tris pH 7.5

150 mM KCl

5% Glycerol

0.05% Tween-20

prior to use: 1 mM DTT

1 x CPI

Elution buffer 1: 10 mM Tris pH 7.5

150 mM KCl

5% Glycerol

0.05% Tween-20

1mg/ml Flag peptide

Wash buffer 2: 10 mM Tris pH 7.5

150 mM KCl

5% Glycerol

M27. On-Bead Tryptic Digest

Immunoprecipitated proteins were subjected to on-bead tryptic digestion. To do so, the beads were incubated for 20 minutes at 25°C in wash buffer 2. Subsequently, the sample was denatured by the addition of two sample volumes of 8M urea (Sigma). The sample was reduced by adding 5mM tris(2-carboxyethyl)phosphine (TCEP, Thermo) for 15 minutes at 35°C shaking and alkylated by addition of 10mM iodoacetamide for 30 minutes at room temperature in the dark. Proteins were digested with lysyl endopeptidase (Wako) at an enzyme: substrate ratio of 1:50 (w/w) at 35°C for 2 hours. The sample was diluted with 50mM ammonium bicarbonate to a urea concentration of 1M, 1/50 (w/w) trypsin (Promega) was added and then incubated at 35°C, shaking overnight. The next morning concentrated trifluoroacetic acid (TFA) was added to the reaction to stop the tryptic digest to a final concentration of 1%, and acetonitrile was added to a final concentration of 3%. The pH was checked with an indicator strip (Merck) to be around pH 2 and proceeded to peptide clean-up.

M28. Peptide Clean-Up

Tryptic digested peptides were purified by solid-phase extraction (SPE) using C_{18} cartridges (Sep-Pak, Waters). The columns were activated by the addition of 1mL 100% acetonitrile and washed twice with 3% acetonitrile, 0.2% formic acid before applying the sample twice. The column was washed with 3% acetonitrile, 0.2% formic acid, and the peptides were eluted by adding 400µL of 60% acetonitrile, 0.2% formic acid twice. The eluate was lyophilized in a SpeedVac and sored at -20°C until further use.

M29. Protein analysis and mass spectrometry

Liquid chromatography coupled to mass spectrometry (LC-MS/MS) analysis was carried out on a Thermo Nano UHPLC 1000 connected to a Thermo Orbitrap Elite mass spectrometer, equipped with a standard nanoelectrospray source. Lyophilized samples were reconstituted in the mobile phase (water/acetonitrile/formic acid, 97/3/0.1). 3.5µL of the digest was injected onto an Acclaim PepMap™ RSLC 15cm x 75µm I.D. (Thermo). Peptides were separated at a flow rate of 0.3 µL/min, ramping a gradient from 5% to 35% mobile phase B (water/acetonitrile/formic acid, 2:98:0.1). The mobile phase was directly applied to the mass spectrometer. The spray voltage was adjusted to 1.6-1.9 kV and the capillary temperature to 220°C. Data acquisition was performed in 'data-dependent mode.' Precursor ion scan acquired data at 120.000 resolution in the range of m/z 250-1800 with an AGC target of 1E06 and an injection time of 20 ms. Top10 ion spectra were selected for fragmentation with an isolation window of 5 m/z and fragmented by CID (Collision Induced Dissociation) with a normalized collision energy of 35 % and an activation *q* of 0.25. Dynamic exclusion was activated with a repeat count of 1, an exclusion duration of 30 seconds, a list size of 500, and a mass window of ±50 ppm. MS^2 spectra were acquired at 10.000 resolution with an AGC target value of 1E04 ions and 120 ms injection time.

M30. Raw Data analysis

RAW data files were searched against the UniProtKB human proteome database (Swissprot date of download: July 3rd, 2019) and a database containing frequently detected contaminants, using the MaxQuant software (vers.1.6.5.0). Two missed cleavages and a protein false discovery rate of 1 % were set as analysis parameters. Carbamidomethylation of cysteine residues was defined as fixed modification and methionine oxidation and N-terminal acetylation as variable modifications. Label-

free quantification (LFQ) was set to a minimum ratio count of 1, and Raw files of the same cell cycle arrest were analyzed using the match between runs option.

5.5.5 Bioinformatic Analysis

M31. Oligonucleosome ChIP Data analysis

Protein intensities obtained by the software suite MaxQuant of 3 biological replicates were extracted, merged by protein name, and loaded to the statistical analysis environment Rstudio (vers.1.1.463). Proteins detected in a single replicate were eliminated as well as hits to the reverse database, contaminants, proteins with one or less razor. Unique peptides and single peptide identifications present in at least 1 triplicate were included. LFQ intensities were normalized to the peptide count, and $\log_2$ transformed. Missing values in the data matrix were assigned to values representing a normal distribution close to the detection limit of the mass spectrometer. Protein abundances in the CENP-A pulldowns were averaged, and the significance of their fold-changes (FC) to the 3 Histone H3.3 experiments were assessed by a two-sample t-test. Protein identifications were identified as true if their enrichment to H3.3 was at least two-fold. Respective p-values were plotted against their FC differences in volcano plots.

6. References

ADAM, S., POLO, S. E. & ALMOUZNI, G. 2013. Transcription recovery after DNA damage requires chromatin priming by the H3.3 histone chaperone HIRA. *Cell,* 155**,** 94-106.

AEBERSOLD, R. & MANN, M. 2003. Mass spectrometry-based proteomics. *Nature,* 422**,** 198-207.

AHMAD, K. & HENIKOFF, S. 2002. Epigenetic consequences of nucleosome dynamics. *Cell,* 111**,** 281-4.

AKIYOSHI, B., NELSON, C. R. & BIGGINS, S. 2013. The aurora B kinase promotes inner and outer kinetochore interactions in budding yeast. *Genetics,* 194**,** 785-9.

AKIYOSHI, B., NELSON, C. R., RANISH, J. A. & BIGGINS, S. 2009. Quantitative proteomic analysis of purified yeast kinetochores identifies a PP1 regulatory subunit. *Genes & development,* 23**,** 2887-2899.

ALABERT, C. & GROTH, A. 2012. Chromatin replication and epigenome maintenance. *Nat Rev Mol Cell Biol,* 13**,** 153-67.

ALDRUP-MACDONALD, M. E. & SULLIVAN, B. A. 2014. The past, present, and future of human centromere genomics. *Genes (Basel),* 5**,** 33-50.

ALEXANDROV, I., KAZAKOV, A., TUMENEVA, I., SHEPELEV, V. & YUROV, Y. 2001. Alpha-satellite DNA of primates: old and new families. *Chromosoma,* 110**,** 253-66.

ALI-AHMAD, A., BILOKAPIC, S., SCHAFER, I. B., HALIC, M. & SEKULIC, N. 2019. CENP-C unwraps the human CENP-A nucleosome through the H2A C-terminal tail. *EMBO Rep,* 20**,** e48913.

ALKAN, C., CARDONE, M. F., CATACCHIO, C. R., ANTONACCI, F., O'BRIEN, S. J., RYDER, O. A., PURGATO, S., ZOLI, M., DELLA VALLE, G., EICHLER, E. E. & VENTURA, M. 2011. Genome-wide characterization of centromeric satellites from multiple mammalian genomes. *Genome Res,* 21**,** 137-45.

ANEDCHENKO, E. A., SAMEL-POMMERENCKE, A., TRAN NGUYEN, T. M., SHAHNEJAT-BUSHEHRI, S., POPSEL, J., LAUSTER, D., HERRMANN, A., RAPPSILBER, J., CUOMO, A., BONALDI, T. & EHRENHOFER-MURRAY, A. E. 2019. The kinetochore module Okp1(CENP-Q)/Ame1(CENP-U) is a reader for N-terminal modifications on the centromeric histone Cse4(CENP-A). *EMBO J,* 38.

ANNUNZIATO, A. T. 2005. Split decision: what happens to nucleosomes during DNA replication? *J Biol Chem,* 280**,** 12065-8.

ANSELM, E., THOMAE, A. W., JEYAPRAKASH, A. A. & HEUN, P. 2018. Oligomerization of Drosophila Nucleoplasmin-Like Protein is required for its centromere localization. *Nucleic Acids Res,* 46**,** 11274-11286.

ARIMA, Y., HIROTA, T., BRONNER, C., MOUSLI, M., FUJIWARA, T., NIWA, S., ISHIKAWA, H. & SAYA, H. 2004. Down-regulation of nuclear protein ICBP90 by p53/p21Cip1/WAF1-dependent DNA-damage checkpoint signals contributes to cell cycle arrest at G1/S transition. *Genes Cells,* 9**,** 131-42.

BANTSCHEFF, M., SCHIRLE, M., SWEETMAN, G., RICK, J. & KUSTER, B. 2007. Quantitative mass spectrometry in proteomics: a critical review. *Anal Bioanal Chem,* 389**,** 1017-31.

BARNHART, M. C., KUICH, P. H., STELLFOX, M. E., WARD, J. A., BASSETT, E. A., BLACK, B. E. & FOLTZ, D. R. 2011. HJURP is a CENP-A chromatin assembly factor sufficient to form a functional de novo kinetochore. *J Cell Biol,* 194**,** 229-43.

BASILICO, F., MAFFINI, S., WEIR, J. R., PRUMBAUM, D., ROJAS, A. M., ZIMNIAK, T., DE ANTONI, A., JEGANATHAN, S., VOSS, B., VAN GERWEN, S., KRENN, V., MASSIMILIANO, L., VALENCIA, A., VETTER, I. R., HERZOG, F., RAUNSER, S., PASQUALATO, S. & MUSACCHIO, A. 2014. The pseudo GTPase CENP-M drives human kinetochore assembly. *Elife,* 3**,** e02978.

BELLELLI, R., BELAN, O., PYE, V. E., CLEMENT, C., MASLEN, S. L., SKEHEL, J. M., CHEREPANOV, P., ALMOUZNI, G. & BOULTON, S. J. 2018. POLE3-POLE4 Is a Histone H3-H4 Chaperone that Maintains Chromatin Integrity during DNA Replication. *Mol Cell,* 72**,** 112-126 e5.

BELOTSERKOVSKAYA, R., OH, S., BONDARENKO, V. A., ORPHANIDES, G., STUDITSKY, V. M. & REINBERG, D. 2003. FACT facilitates transcription-dependent nucleosome alteration. *Science,* 301**,** 1090-3.

BERGMANN, J. H., RODRIGUEZ, M. G., MARTINS, N. M., KIMURA, H., KELLY, D. A., MASUMOTO, H., LARIONOV, V., JANSEN, L. E. & EARNSHAW, W. C. 2011. Epigenetic engineering shows H3K4me2 is required for HJURP targeting and CENP-A assembly on a synthetic human kinetochore. *EMBO J,* 30**,** 328-40.

BERNAD, R., SANCHEZ, P., RIVERA, T., RODRIGUEZ-CORSINO, M., BOYARCHUK, E., VASSIAS, I., RAY-GALLET, D., ARNAOUTOV, A., DASSO, M., ALMOUZNI, G. & LOSADA, A. 2011. Xenopus HJURP and condensin II are required for CENP-A assembly. *J Cell Biol,* 192**,** 569-82.

BERTOLI, C., SKOTHEIM, J. M. & DE BRUIN, R. A. 2013. Control of cell cycle transcription during G1 and S phases. *Nat Rev Mol Cell Biol,* 14**,** 518-28.

BIGGINS, S. 2013. The composition, functions, and regulation of the budding yeast kinetochore. *Genetics,* 194**,** 817-46.

BLACK, B. E. & CLEVELAND, D. W. 2011. Epigenetic centromere propagation and the nature of CENP-a nucleosomes. *Cell,* 144**,** 471-9.

BLEES, A., JANULIENE, D., HOFMANN, T., KOLLER, N., SCHMIDT, C., TROWITZSCH, S., MOELLER, A. & TAMPE, R. 2017. Structure of the human MHC-I peptide-loading complex. *Nature,* 551**,** 525-528.

BLOWER, M. D. & KARPEN, G. H. 2001. The role of Drosophila CID in kinetochore formation, cell-cycle progression and heterochromatin interactions. *Nat Cell Biol,* 3**,** 730-9.

BODOR, D. L., MATA, J. F., SERGEEV, M., DAVID, A. F., SALIMIAN, K. J., PANCHENKO, T., CLEVELAND, D. W., BLACK, B. E., SHAH, J. V. & JANSEN, L. E. 2014. The quantitative architecture of centromeric chromatin. *Elife,* 3**,** e02137.

BOEHM, E. M., GILDENBERG, M. S. & WASHINGTON, M. T. 2016. The Many Roles of PCNA in Eukaryotic DNA Replication. *Enzymes,* 39**,** 231-54.

BONAPACE, I. M., LATELLA, L., PAPAIT, R., NICASSIO, F., SACCO, A., MUTO, M., CRESCENZI, M. & DI FIORE, P. P. 2002. Np95 is regulated by E1A during mitotic reactivation of terminally differentiated cells and is essential for S phase entry. *J Cell Biol,* 157**,** 909-14.

BONDARENKO, V. A., STEELE, L. M., UJVARI, A., GAYKALOVA, D. A., KULAEVA, O. I., POLIKANOV, Y. S., LUSE, D. S. & STUDITSKY, V. M. 2006. Nucleosomes can form a polar barrier to transcript elongation by RNA polymerase II. *Mol Cell,* 24**,** 469-79.

BOSTICK, M., KIM, J. K., ESTEVE, P. O., CLARK, A., PRADHAN, S. & JACOBSEN, S. E. 2007. UHRF1 plays a role in maintaining DNA methylation in mammalian cells. *Science,* 317**,** 1760-4.

BOZHENOK, L., WADE, P. A. & VARGA-WEISZ, P. 2002. WSTF-ISWI chromatin remodeling complex targets heterochromatic replication foci. *EMBO J,* 21**,** 2231-41.

BROWN, M. T. 1995. Sequence similarities between the yeast chromosome segregation protein Mif2 and the mammalian centromere protein CENP-C. *Gene,* 160**,** 111-6.

BROWN, M. T., GOETSCH, L. & HARTWELL, L. H. 1993. MIF2 is required for mitotic spindle integrity during anaphase spindle elongation in Saccharomyces cerevisiae. *J Cell Biol,* 123**,** 387-403.

BUI, M., DIMITRIADIS, E. K., HOISCHEN, C., AN, E., QUENET, D., GIEBE, S., NITA-LAZAR, A., DIEKMANN, S. & DALAL, Y. 2012. Cell-cycle-dependent structural transitions in the human CENP-A nucleosome in vivo. *Cell,* 150**,** 317-26.

BURGOYNE, P. S., MAHADEVAIAH, S. K. & TURNER, J. M. 2007. The management of DNA double-strand breaks in mitotic G2, and in mammalian meiosis viewed from a mitotic G2 perspective. *Bioessays,* 29**,** 974-86.

CAMPBELL, C. S. & DESAI, A. 2013. Tension sensing by Aurora B kinase is independent of survivin-based centromere localization. *Nature,* 497**,** 118-21.

CANZONETTA, C., VERNARECCI, S., IULIANI, M., MARRACINO, C., BELLONI, C., BALLARIO, P. & FILETICI, P. 2015. SAGA DUB-Ubp8 Deubiquitylates Centromeric Histone Variant Cse4. *G3 (Bethesda),* 6**,** 287-98.

CARDINALE, S., BERGMANN, J. H., KELLY, D., NAKANO, M., VALDIVIA, M. M., KIMURA, H., MASUMOTO, H., LARIONOV, V. & EARNSHAW, W. C. 2009. Hierarchical inactivation of a synthetic human kinetochore by a chromatin modifier. *Mol Biol Cell,* 20**,** 4194-204.

CARROLL, C. W., SILVA, M. C., GODEK, K. M., JANSEN, L. E. & STRAIGHT, A. F. 2009. Centromere assembly requires the direct recognition of CENP-A nucleosomes by CENP-N. *Nat Cell Biol,* 11**,** 896-902.

CASAS-DELUCCHI, C. S., VAN BEMMEL, J. G., HAASE, S., HERCE, H. D., NOWAK, D., MEILINGER, D., STEAR, J. H., LEONHARDT, H. & CARDOSO, M. C. 2012. Histone hypoacetylation is required to maintain late replication timing of constitutive heterochromatin. *Nucleic Acids Res,* 40**,** 159-69.

CASTRO, A., BERNIS, C., VIGNERON, S., LABBE, J. C. & LORCA, T. 2005. The anaphase-promoting complex: a key factor in the regulation of cell cycle. *Oncogene,* 24**,** 314-25.

CHAMBERS, M. C., MACLEAN, B., BURKE, R., AMODEI, D., RUDERMAN, D. L., NEUMANN, S., GATTO, L., FISCHER, B., PRATT, B., EGERTSON, J., HOFF, K., KESSNER, D., TASMAN, N., SHULMAN, N., FREWEN, B., BAKER, T. A., BRUSNIAK, M. Y., PAULSE, C., CREASY, D., FLASHNER, L., KANI, K., MOULDING, C., SEYMOUR, S. L., NUWAYSIR, L. M., LEFEBVRE, B., KUHLMANN, F., ROARK, J., RAINER, P., DETLEV, S., HEMENWAY, T., HUHMER, A., LANGRIDGE, J., CONNOLLY, B., CHADICK, T., HOLLY, K., ECKELS, J., DEUTSCH, E. W., MORITZ, R. L., KATZ, J. E., AGUS, D. B., MACCOSS, M., TABB, D. L. & MALLICK, P. 2012. A cross-platform toolkit for mass spectrometry and proteomics. *Nat Biotechnol,* 30**,** 918-20.

CHANG, J. H., LIN, J. Y., WU, M. H. & YUNG, B. Y. 1998. Evidence for the ability of nucleophosmin/B23 to bind ATP. *Biochem J,* 329 (Pt 3)**,** 539-44.

CHAVEZ, J. D. & BRUCE, J. E. 2019. Chemical cross-linking with mass spectrometry: a tool for systems structural biology. *Curr Opin Chem Biol,* 48**,** 8-18.

CHEESEMAN, I. M. & DESAI, A. 2008. Molecular architecture of the kinetochore-microtubule interface. *Nat Rev Mol Cell Biol,* 9**,** 33-46.

CHEESEMAN, I. M., NIESSEN, S., ANDERSON, S., HYNDMAN, F., YATES, J. R., 3RD, OEGEMA, K. & DESAI, A. 2004. A conserved protein network controls assembly of the outer kinetochore and its ability to sustain tension. *Genes Dev,* 18**,** 2255-68.

CHEN, C. C., BOWERS, S., LIPINSZKI, Z., PALLADINO, J., TRUSIAK, S., BETTINI, E., ROSIN, L., PRZEWLOKA, M. R., GLOVER, D. M., O'NEILL, R. J. & MELLONE, B. G. 2015. Establishment of Centromeric Chromatin by the CENP-A Assembly Factor CAL1 Requires FACT-Mediated Transcription. *Dev Cell,* 34**,** 73-84.

CHOI, E. S., STRALFORS, A., CATANIA, S., CASTILLO, A. G., SVENSSON, J. P., PIDOUX, A. L., EKWALL, K. & ALLSHIRE, R. C. 2012. Factors that promote H3 chromatin integrity during transcription prevent promiscuous deposition of CENP-A(Cnp1) in fission yeast. *PLoS Genet,* 8**,** e1002985.

CHOO, K. H., VISSEL, B., NAGY, A., EARLE, E. & KALITSIS, P. 1991. A survey of the genomic distribution of alpha satellite DNA on all the human chromosomes, and derivation of a new consensus sequence. *Nucleic Acids Res,* 19**,** 1179-82.

CIFERRI, C., PASQUALATO, S., SCREPANTI, E., VARETTI, G., SANTAGUIDA, S., DOS REIS, G., MAIOLICA, A., POLKA, J., DE LUCA, J. G., DE WULF, P., SALEK, M., RAPPSILBER, J., MOORES, C. A., SALMON, E. D. & MUSACCHIO, A. 2008. Implications for kinetochore-microtubule attachment from the structure of an engineered Ndc80 complex. *Cell,* 133**,** 427-39.

CLARKE, L. 1998. Centromeres: proteins, protein complexes, and repeated domains at centromeres of simple eukaryotes. *Curr Opin Genet Dev,* 8**,** 212-8.

CLARKE, L. & CARBON, J. 1980. Isolation of a yeast centromere and construction of functional small circular chromosomes. *Nature,* 287**,** 504-9.

CLEVELAND, D. W., MAO, Y. & SULLIVAN, K. F. 2003. Centromeres and kinetochores: from epigenetics to mitotic checkpoint signaling. *Cell,* 112**,** 407-21.

COHEN, R. L., ESPELIN, C. W., DE WULF, P., SORGER, P. K., HARRISON, S. C. & SIMONS, K. T. 2008. Structural and functional dissection of Mif2p, a conserved DNA-binding kinetochore protein. *Mol Biol Cell,* 19**,** 4480-91.

COHEN-FIX, O., PETERS, J. M., KIRSCHNER, M. W. & KOSHLAND, D. 1996. Anaphase initiation in Saccharomyces cerevisiae is controlled by the APC-dependent degradation of the anaphase inhibitor Pds1p. *Genes Dev,* 10**,** 3081-93.

COMBES, G., ALHARBI, I., BRAGA, L. G. & ELOWE, S. 2017. Playing polo during mitosis: PLK1 takes the lead. *Oncogene,* 36**,** 4819-4827.

COX, J. & MANN, M. 2008. MaxQuant enables high peptide identification rates, individualized p.p.b.-range mass accuracies and proteome-wide protein quantification. *Nat Biotechnol,* 26**,** 1367-72.

CUMBERLEDGE, S. & CARBON, J. 1987. Mutational analysis of meiotic and mitotic centromere function in Saccharomyces cerevisiae. *Genetics,* 117**,** 203-12.

CUYLEN, S. & HAERING, C. H. 2011. Deciphering condensin action during chromosome segregation. *Trends Cell Biol,* 21**,** 552-9.

DAMBACHER, S., DENG, W., HAHN, M., SADIC, D., FROHLICH, J., NUBER, A., HOISCHEN, C., DIEKMANN, S., LEONHARDT, H. & SCHOTTA, G. 2012. CENP-C facilitates the recruitment of M18BP1 to centromeric chromatin. *Nucleus,* 3**,** 101-10.

DE ROP, V., PADEGANEH, A. & MADDOX, P. S. 2012. CENP-A: the key player behind centromere identity, propagation, and kinetochore assembly. *Chromosoma,* 121**,** 527-38.

DE WULF, P., MCAINSH, A. D. & SORGER, P. K. 2003. Hierarchical assembly of the budding yeast kinetochore from multiple subcomplexes. *Genes Dev,* 17**,** 2902-21.

DELUCA, J. G., GALL, W. E., CIFERRI, C., CIMINI, D., MUSACCHIO, A. & SALMON, E. D. 2006. Kinetochore microtubule dynamics and attachment stability are regulated by Hec1. *Cell,* 127**,** 969-82.

DEYTER, G. M. & BIGGINS, S. 2014. The FACT complex interacts with the E3 ubiquitin ligase Psh1 to prevent ectopic localization of CENP-A. *Genes Dev,* 28**,** 1815-26.

DIMITROVA, Y. N., JENNI, S., VALVERDE, R., KHIN, Y. & HARRISON, S. C. 2016. Structure of the MIND Complex Defines a Regulatory Focus for Yeast Kinetochore Assembly. *Cell,* 167**,** 1014-1027 e12.

DIMOVA, N. V., HATHAWAY, N. A., LEE, B. H., KIRKPATRICK, D. S., BERKOWITZ, M. L., GYGI, S. P., FINLEY, D. & KING, R. W. 2012. APC/C-mediated multiple monoubiquitylation provides an alternative degradation signal for cyclin B1. *Nat Cell Biol,* 14**,** 168-76.

DOMON, B. & AEBERSOLD, R. 2006. Mass spectrometry and protein analysis. *Science,* 312**,** 212-7.

DROZDETSKIY, A., COLE, C., PROCTER, J. & BARTON, G. J. 2015. JPred4: a protein secondary structure prediction server. *Nucleic Acids Res,* 43**,** W389-94.

DUBOIS, M. L., BASTIN, C., LEVESQUE, D. & BOISVERT, F. M. 2016. Comprehensive Characterization of Minichromosome Maintenance Complex (MCM) Protein Interactions Using Affinity and Proximity Purifications Coupled to Mass Spectrometry. *J Proteome Res,* 15**,** 2924-34.

DUNLEAVY, E. M., ALMOUZNI, G. & KARPEN, G. H. 2011. H3.3 is deposited at centromeres in S phase as a placeholder for newly assembled CENP-A in G(1) phase. *Nucleus,* 2**,** 146-57.

DUNLEAVY, E. M., ROCHE, D., TAGAMI, H., LACOSTE, N., RAY-GALLET, D., NAKAMURA, Y., DAIGO, Y., NAKATANI, Y. & ALMOUZNI-PETTINOTTI, G. 2009. HJURP is a cell-cycle-dependent maintenance and deposition factor of CENP-A at centromeres. *Cell,* 137**,** 485-97.

EARNSHAW, W. C. & ROTHFIELD, N. 1985. Identification of a family of human centromere proteins using autoimmune sera from patients with scleroderma. *Chromosoma,* 91**,** 313-21.

ELIUK, S. & MAKAROV, A. 2015. Evolution of Orbitrap Mass Spectrometry Instrumentation. *Annu Rev Anal Chem (Palo Alto Calif),* 8**,** 61-80.

EMANUELE, M. J., LAN, W., JWA, M., MILLER, S. A., CHAN, C. S. & STUKENBERG, P. T. 2008. Aurora B kinase and protein phosphatase 1 have opposing roles in modulating kinetochore assembly. *J Cell Biol,* 181**,** 241-54.

ERHARDT, S., MELLONE, B. G., BETTS, C. M., ZHANG, W., KARPEN, G. H. & STRAIGHT, A. F. 2008. Genome-wide analysis reveals a cell cycle-

dependent mechanism controlling centromere propagation. *J Cell Biol,* 183**,** 805-18.

EVANS, T., ROSENTHAL, E. T., YOUNGBLOM, J., DISTEL, D. & HUNT, T. 1983. Cyclin: a protein specified by maternal mRNA in sea urchin eggs that is destroyed at each cleavage division. *Cell,* 33**,** 389-96.

FACHINETTI, D., HAN, J. S., MCMAHON, M. A., LY, P., ABDULLAH, A., WONG, A. J. & CLEVELAND, D. W. 2015. DNA Sequence-Specific Binding of CENP-B Enhances the Fidelity of Human Centromere Function. *Dev Cell,* 33**,** 314-27.

FALK, S. J., GUO, L. Y., SEKULIC, N., SMOAK, E. M., MANI, T., LOGSDON, G. A., GUPTA, K., JANSEN, L. E., VAN DUYNE, G. D., VINOGRADOV, S. A., LAMPSON, M. A. & BLACK, B. E. 2015. Chromosomes. CENP-C reshapes and stabilizes CENP-A nucleosomes at the centromere. *Science,* 348**,** 699-703.

FALK, S. J., LEE, J., SEKULIC, N., SENNETT, M. A., LEE, T. H. & BLACK, B. E. 2016. CENP-C directs a structural transition of CENP-A nucleosomes mainly through sliding of DNA gyres. *Nat Struct Mol Biol,* 23**,** 204-208.

FAZZIO, T. G. & PANNING, B. 2010. Condensin complexes regulate mitotic progression and interphase chromatin structure in embryonic stem cells. *J Cell Biol,* 188**,** 491-503.

FISCHBOCK-HALWACHS, J., SINGH, S., POTOCNJAK, M., HAGEMANN, G., SOLIS-MEZARINO, V., WOIKE, S., GHODGAONKAR-STEGER, M., WEISSMANN, F., GALLEGO, L. D., ROJAS, J., ANDREANI, J., KOHLER, A. & HERZOG, F. 2019. The COMA complex interacts with Cse4 and positions Sli15/Ipl1 at the budding yeast inner kinetochore. *Elife,* 8.

FISCHER, L., CHEN, Z. A. & RAPPSILBER, J. 2013. Quantitative cross-linking/mass spectrometry using isotope-labelled cross-linkers. *J Proteomics,* 88**,** 120-8.

FOE, I. T., FOSTER, S. A., CHEUNG, S. K., DELUCA, S. Z., MORGAN, D. O. & TOCZYSKI, D. P. 2011. Ubiquitination of Cdc20 by the APC occurs through an intramolecular mechanism. *Curr Biol,* 21**,** 1870-7.

FOLEY, E. A. & KAPOOR, T. M. 2013. Microtubule attachment and spindle assembly checkpoint signalling at the kinetochore. *Nat Rev Mol Cell Biol,* 14**,** 25-37.

FOLTZ, D. R., JANSEN, L. E., BAILEY, A. O., YATES, J. R., 3RD, BASSETT, E. A., WOOD, S., BLACK, B. E. & CLEVELAND, D. W. 2009. Centromere-specific assembly of CENP-a nucleosomes is mediated by HJURP. *Cell,* 137**,** 472-84.

FOLTZ, D. R., JANSEN, L. E., BLACK, B. E., BAILEY, A. O., YATES, J. R., 3RD & CLEVELAND, D. W. 2006. The human CENP-A centromeric nucleosome-associated complex. *Nat Cell Biol,* 8**,** 458-69.

FOSTER, D. A., YELLEN, P., XU, L. & SAQCENA, M. 2010. Regulation of G1 Cell Cycle Progression: Distinguishing the Restriction Point from a Nutrient-Sensing Cell Growth Checkpoint(s). *Genes Cancer,* 1**,** 1124-31.

FOSTER, S. A. & MORGAN, D. O. 2012. The APC/C subunit Mnd2/Apc15 promotes Cdc20 autoubiquitination and spindle assembly checkpoint inactivation. *Mol Cell,* 47**,** 921-32.

FRASCHINI, R., BERETTA, A., SIRONI, L., MUSACCHIO, A., LUCCHINI, G. & PIATTI, S. 2001. Bub3 interaction with Mad2, Mad3 and Cdc20 is mediated by WD40 repeats and does not require intact kinetochores. *EMBO J,* 20**,** 6648-59.

FREHLICK, L. J., EIRIN-LOPEZ, J. M. & AUSIO, J. 2007. New insights into the nucleophosmin/nucleoplasmin family of nuclear chaperones. *Bioessays,* 29**,** 49-59.

FUJIKI, R., KIM, M. S., SASAKI, Y., YOSHIMURA, K., KITAGAWA, H. & KATO, S. 2005. Ligand-induced transrepression by VDR through association of WSTF with acetylated histones. *EMBO J,* 24**,** 3881-94.

FUJITA, Y., HAYASHI, T., KIYOMITSU, T., TOYODA, Y., KOKUBU, A., OBUSE, C. & YANAGIDA, M. 2007. Priming of centromere for CENP-A recruitment by human hMis18alpha, hMis18beta, and M18BP1. *Dev Cell,* 12**,** 17-30.

FUKAGAWA, T. & BROWN, W. R. 1997. Efficient conditional mutation of the vertebrate CENP-C gene. *Hum Mol Genet,* 6**,** 2301-8.

FUKAGAWA, T. & EARNSHAW, W. C. 2014. The centromere: chromatin foundation for the kinetochore machinery. *Dev Cell,* 30**,** 496-508.

FUKAGAWA, T., MIKAMI, Y., NISHIHASHI, A., REGNIER, V., HARAGUCHI, T., HIRAOKA, Y., SUGATA, N., TODOKORO, K., BROWN, W. & IKEMURA, T. 2001. CENP-H, a constitutive centromere component, is required for centromere targeting of CENP-C in vertebrate cells. *EMBO J,* 20**,** 4603-17.

FUKAGAWA, T., PENDON, C., MORRIS, J. & BROWN, W. 1999. CENP-C is necessary but not sufficient to induce formation of a functional centromere. *EMBO J,* 18**,** 4196-209.

FUNABIKI, H., YAMANO, H., KUMADA, K., NAGAO, K., HUNT, T. & YANAGIDA, M. 1996. Cut2 proteolysis required for sister-chromatid seperation in fission yeast. *Nature,* 381**,** 438-41.

FURUYAMA, S. & BIGGINS, S. 2007. Centromere identity is specified by a single centromeric nucleosome in budding yeast. *Proc Natl Acad Sci U S A,* 104**,** 14706-11.

GAN, H., SERRA-CARDONA, A., HUA, X., ZHOU, H., LABIB, K., YU, C. & ZHANG, Z. 2018. The Mcm2-Ctf4-Polalpha Axis Facilitates Parental Histone H3-H4 Transfer to Lagging Strands. *Mol Cell,* 72**,** 140-151 e3.

GASCOIGNE, K. E. & CHEESEMAN, I. M. 2013. CDK-dependent phosphorylation and nuclear exclusion coordinately control kinetochore assembly state. *J Cell Biol,* 201**,** 23-32.

GASCOIGNE, K. E., TAKEUCHI, K., SUZUKI, A., HORI, T., FUKAGAWA, T. & CHEESEMAN, I. M. 2011. Induced ectopic kinetochore assembly bypasses the requirement for CENP-A nucleosomes. *Cell,* 145**,** 410-22.

GENNERICH, A., CARTER, A. P., RECK-PETERSON, S. L. & VALE, R. D. 2007. Force-induced bidirectional stepping of cytoplasmic dynein. *Cell,* 131**,** 952-65.

GERARD, A., KOUNDRIOUKOFF, S., RAMILLON, V., SERGERE, J. C., MAILAND, N., QUIVY, J. P. & ALMOUZNI, G. 2006. The replication kinase Cdc7-Dbf4 promotes the interaction of the p150 subunit of chromatin assembly factor 1 with proliferating cell nuclear antigen. *EMBO Rep,* 7**,** 817-23.

GIBSON, D. G., YOUNG, L., CHUANG, R. Y., VENTER, J. C., HUTCHISON, C. A., 3RD & SMITH, H. O. 2009. Enzymatic assembly of DNA molecules up to several hundred kilobases. *Nat Methods,* 6**,** 343-5.

GLOTZER, M., MURRAY, A. W. & KIRSCHNER, M. W. 1991. Cyclin is degraded by the ubiquitin pathway. *Nature,* 349**,** 132-8.

GOLL, M. G. & BESTOR, T. H. 2005. Eukaryotic cytosine methyltransferases. *Annu Rev Biochem,* 74**,** 481-514.

GOPALAKRISHNAN, S., SULLIVAN, B. A., TRAZZI, S., DELLA VALLE, G. & ROBERTSON, K. D. 2009. DNMT3B interacts with constitutive centromere protein CENP-C to modulate DNA methylation and the histone code at centromeric regions. *Hum Mol Genet,* 18**,** 3178-93.

GOPPELT, A., STELZER, G., LOTTSPEICH, F. & MEISTERERNST, M. 1996. A mechanism for repression of class II gene transcription through specific binding of NC2 to TBP-promoter complexes via heterodimeric histone fold domains. *EMBO J,* 15**,** 3105-16.

GORDON, D. J., RESIO, B. & PELLMAN, D. 2012. Causes and consequences of aneuploidy in cancer. *Nat Rev Genet,* 13**,** 189-203.

GOSHIMA, G., KIYOMITSU, T., YODA, K. & YANAGIDA, M. 2003. Human centromere chromatin protein hMis12, essential for equal segregation, is independent of CENP-A loading pathway. *J Cell Biol,* 160**,** 25-39.

GRADY, D. L., RATLIFF, R. L., ROBINSON, D. L., MCCANLIES, E. C., MEYNE, J. & MOYZIS, R. K. 1992. Highly conserved repetitive DNA sequences are present at human centromeres. *Proc Natl Acad Sci U S A,* 89**,** 1695-9.

GRIMM, M., ZIMNIAK, T., KAHRAMAN, A. & HERZOG, F. 2015. xVis: a web server for the schematic visualization and interpretation of crosslink-derived spatial restraints. *Nucleic Acids Res,* 43**,** W362-9.

GROSSKORTENHAUS, R. & SPRENGER, F. 2002. Rca1 inhibits APC-Cdh1(Fzr) and is required to prevent cyclin degradation in G2. *Dev Cell,* 2**,** 29-40.

GUERRERO-SANTORO, J., KAPETANAKI, M. G., HSIEH, C. L., GORBACHINSKY, I., LEVINE, A. S. & RAPIC-OTRIN, V. 2008. The cullin 4B-based UV-damaged DNA-binding protein ligase binds to UV-damaged chromatin and ubiquitinates histone H2A. *Cancer Res,* 68**,** 5014-22.

GUIMARAES, G. J., DONG, Y., MCEWEN, B. F. & DELUCA, J. G. 2008. Kinetochore-microtubule attachment relies on the disordered N-terminal tail domain of Hec1. *Curr Biol,* 18**,** 1778-84.

GUNJAN, A., PAIK, J. & VERREAULT, A. 2005. Regulation of histone synthesis and nucleosome assembly. *Biochimie,* 87**,** 625-35.

GUROVA, K., CHANG, H. W., VALIEVA, M. E., SANDLESH, P. & STUDITSKY, V. M. 2018. Structure and function of the histone chaperone FACT - Resolving FACTual issues. *Biochim Biophys Acta Gene Regul Mech*.

GUSE, A., CARROLL, C. W., MOREE, B., FULLER, C. J. & STRAIGHT, A. F. 2011. In vitro centromere and kinetochore assembly on defined chromatin templates. *Nature,* 477**,** 354-8.

HAMMOND, C. M., STROMME, C. B., HUANG, H., PATEL, D. J. & GROTH, A. 2017. Histone chaperone networks shaping chromatin function. *Nat Rev Mol Cell Biol,* 18**,** 141-158.

HARA, M. & FUKAGAWA, T. 2020. Dynamics of kinetochore structure and its regulations during mitotic progression. *Cell Mol Life Sci*.

HARTLEPP, K. F., FERNANDEZ-TORNERO, C., EBERHARTER, A., GRUNE, T., MULLER, C. W. & BECKER, P. B. 2005. The histone fold subunits of Drosophila CHRAC facilitate nucleosome sliding through dynamic DNA interactions. *Mol Cell Biol,* 25**,** 9886-96.

HARUKI, H., NISHIKAWA, J. & LAEMMLI, U. K. 2008. The anchor-away technique: rapid, conditional establishment of yeast mutant phenotypes. *Mol Cell,* 31**,** 925-32.

HASSIG, C. A. & SCHREIBER, S. L. 1997. Nuclear histone acetylases and deacetylases and transcriptional regulation: HATs off to HDACs. *Curr Opin Chem Biol,* 1**,** 300-8.

HASSON, D., PANCHENKO, T., SALIMIAN, K. J., SALMAN, M. U., SEKULIC, N., ALONSO, A., WARBURTON, P. E. & BLACK, B. E. 2013. The octamer is the major form of CENP-A nucleosomes at human centromeres. *Nat Struct Mol Biol,* 20**,** 687-95.

HAYASHI, T., FUJITA, Y., IWASAKI, O., ADACHI, Y., TAKAHASHI, K. & YANAGIDA, M. 2004. Mis16 and Mis18 are required for CENP-A loading and histone deacetylation at centromeres. *Cell,* 118**,** 715-29.

HE, H., LI, Y., DONG, Q., CHANG, A. Y., GAO, F., CHI, Z., SU, M., ZHANG, F., BAN, H., MARTIENSSEN, R., CHEN, Y. H. & LI, F. 2017. Coordinated regulation of heterochromatin inheritance by Dpb3-Dpb4 complex. *Proc Natl Acad Sci U S A,* 114**,** 12524-12529.

HEEGER, S., LEISMANN, O., SCHITTENHELM, R., SCHRAIDT, O., HEIDMANN, S. & LEHNER, C. F. 2005. Genetic interactions of separase regulatory subunits reveal the diverged Drosophila Cenp-C homolog. *Genes Dev,* 19**,** 2041-53.

HEGEMANN, J. H. & FLEIG, U. N. 1993. The centromere of budding yeast. *Bioessays,* 15**,** 451-60.

HEMMERICH, P., WEIDTKAMP-PETERS, S., HOISCHEN, C., SCHMIEDEBERG, L., ERLIANDRI, I. & DIEKMANN, S. 2008. Dynamics of inner kinetochore assembly and maintenance in living cells. *J Cell Biol,* 180**,** 1101-14.

HENIKOFF, S., AHMAD, K. & MALIK, H. S. 2001. The centromere paradox: stable inheritance with rapidly evolving DNA. *Science,* 293**,** 1098-102.

HERZOG, F., KAHRAMAN, A., BOEHRINGER, D., MAK, R., BRACHER, A., WALZTHOENI, T., LEITNER, A., BECK, M., HARTL, F. U., BAN, N., MALMSTROM, L. & AEBERSOLD, R. 2012. Structural probing of a protein phosphatase 2A network by chemical cross-linking and mass spectrometry. *Science,* 337**,** 1348-52.

HEUN, P., ERHARDT, S., BLOWER, M. D., WEISS, S., SKORA, A. D. & KARPEN, G. H. 2006. Mislocalization of the Drosophila centromere-specific histone CID promotes formation of functional ectopic kinetochores. *Dev Cell,* 10**,** 303-15.

HEWAWASAM, G., SHIVARAJU, M., MATTINGLY, M., VENKATESH, S., MARTIN-BROWN, S., FLORENS, L., WORKMAN, J. L. & GERTON, J. L. 2010. Psh1 is an E3 ubiquitin ligase that targets the centromeric histone variant Cse4. *Mol Cell,* 40**,** 444-54.

HEWITT, L., TIGHE, A., SANTAGUIDA, S., WHITE, A. M., JONES, C. D., MUSACCHIO, A., GREEN, S. & TAYLOR, S. S. 2010. Sustained Mps1 activity is required in mitosis to recruit O-Mad2 to the Mad1-C-Mad2 core complex. *J Cell Biol,* 190**,** 25-34.

HIGA, L. A., MIHAYLOV, I. S., BANKS, D. P., ZHENG, J. & ZHANG, H. 2003. Radiation-mediated proteolysis of CDT1 by CUL4-ROC1 and CSN complexes constitutes a new checkpoint. *Nat Cell Biol,* 5**,** 1008-15.

HINSHAW, S. M. & HARRISON, S. C. 2019. The structure of the Ctf19c/CCAN from budding yeast. *Elife,* 8.

HOFFMANN, S., DUMONT, M., BARRA, V., LY, P., NECHEMIA-ARBELY, Y., MCMAHON, M. A., HERVE, S., CLEVELAND, D. W. & FACHINETTI, D. 2016. CENP-A Is Dispensable for Mitotic Centromere Function after Initial Centromere/Kinetochore Assembly. *Cell Rep,* 17**,** 2394-2404.

HOLDING, A. N. 2015. XL-MS: Protein cross-linking coupled with mass spectrometry. *Methods,* 89**,** 54-63.

HOLLAND, S., IOANNOU, D., HAINES, S. & BROWN, W. R. 2005. Comparison of Dam tagging and chromatin immunoprecipitation as tools for the identification of the binding sites for S. pombe CENP-C. *Chromosome Res,* 13**,** 73-83.

HOLLOWAY, S. L., GLOTZER, M., KING, R. W. & MURRAY, A. W. 1993. Anaphase is initiated by proteolysis rather than by the inactivation of maturation-promoting factor. *Cell,* 73**,** 1393-402.

HONDELE, M. & LADURNER, A. G. 2013. Catch me if you can: how the histone chaperone FACT capitalizes on nucleosome breathing. *Nucleus,* 4**,** 443-9.

HORI, T., AMANO, M., SUZUKI, A., BACKER, C. B., WELBURN, J. P., DONG, Y., MCEWEN, B. F., SHANG, W. H., SUZUKI, E., OKAWA, K., CHEESEMAN, I. M. & FUKAGAWA, T. 2008. CCAN makes multiple contacts with centromeric DNA to provide distinct pathways to the outer kinetochore. *Cell,* 135**,** 1039-52.

HORI, T., SHANG, W. H., TAKEUCHI, K. & FUKAGAWA, T. 2013. The CCAN recruits CENP-A to the centromere and forms the structural core for kinetochore assembly. *J Cell Biol,* 200**,** 45-60.

HORNUNG, P., MAIER, M., ALUSHIN, G. M., LANDER, G. C., NOGALES, E. & WESTERMANN, S. 2011. Molecular architecture and connectivity of the budding yeast Mtw1 kinetochore complex. *J Mol Biol,* 405**,** 548-59.

HORNUNG, P., TROC, P., MALVEZZI, F., MAIER, M., DEMIANOVA, Z., ZIMNIAK, T., LITOS, G., LAMPERT, F., SCHLEIFFER, A., BRUNNER, M., MECHTLER, K., HERZOG, F., MARLOVITS, T. C. & WESTERMANN, S. 2014. A cooperative mechanism drives budding yeast kinetochore assembly downstream of CENP-A. *J Cell Biol,* 206**,** 509-24.

HOWMAN, E. V., FOWLER, K. J., NEWSON, A. J., REDWARD, S., MACDONALD, A. C., KALITSIS, P. & CHOO, K. H. 2000. Early disruption of centromeric chromatin organization in centromere protein A (Cenpa) null mice. *Proc Natl Acad Sci U S A,* 97**,** 1148-53.

HUANG, H., STROMME, C. B., SAREDI, G., HODL, M., STRANDSBY, A., GONZALEZ-AGUILERA, C., CHEN, S., GROTH, A. & PATEL, D. J. 2015. A unique binding mode enables MCM2 to chaperone histones H3-H4 at replication forks. *Nat Struct Mol Biol,* 22**,** 618-26.

HUANG, N., NEGI, S., SZEBENI, A. & OLSON, M. O. 2005. Protein NPM3 interacts with the multifunctional nucleolar protein B23/nucleophosmin and inhibits ribosome biogenesis. *J Biol Chem,* 280**,** 5496-502.

IACOBUCCI, C., PIOTROWSKI, C., AEBERSOLD, R., AMARAL, B. C., ANDREWS, P., BERNFUR, K., BORCHERS, C., BRODIE, N. I., BRUCE, J. E., CAO, Y., CHAIGNEPAIN, S., CHAVEZ, J. D., CLAVEROL, S., COX, J., DAVIS, T., DEGLIESPOSTI, G., DONG, M. Q., EDINGER, N., EMANUELSSON, C., GAY, M., GOTZE, M., GOMES-NETO, F., GOZZO, F. C., GUTIERREZ, C., HAUPT, C., HECK, A. J. R., HERZOG, F., HUANG, L., HOOPMANN, M. R., KALISMAN, N., KLYKOV, O., KUKACKA, Z., LIU, F., MACCOSS, M. J., MECHTLER, K., MESIKA, R., MORITZ, R. L., NAGARAJ, N., NESATI, V., NEVES-FERREIRA, A. G. C., NINNIS, R., NOVAK, P., O'REILLY, F. J., PELZING, M., PETROTCHENKO, E., PIERSIMONI, L., PLASENCIA, M., PUKALA, T., RAND, K. D., RAPPSILBER, J., REICHMANN, D., SAILER, C., SARNOWSKI, C. P., SCHELTEMA, R. A., SCHMIDT, C., SCHRIEMER, D. C., SHI, Y., SKEHEL, J. M., SLAVIN, M., SOBOTT, F., SOLIS-MEZARINO, V., STEPHANOWITZ, H., STENGEL, F., STIEGER, C. E., TRABJERG, E., TRNKA, M., VILASECA, M., VINER, R., XIANG, Y., YILMAZ, S., ZELTER, A., ZIEMIANOWICZ, D., LEITNER, A. & SINZ, A. 2019. First Community-Wide, Comparative Cross-Linking Mass Spectrometry Study. *Anal Chem,* 91**,** 6953-6961.

IIDA, T. & ARAKI, H. 2004. Noncompetitive counteractions of DNA polymerase epsilon and ISW2/yCHRAC for epigenetic inheritance of telomere position effect in Saccharomyces cerevisiae. *Mol Cell Biol,* 24**,** 217-27.

IKENO, M., MASUMOTO, H. & OKAZAKI, T. 1994. Distribution of CENP-B boxes reflected in CREST centromere antigenic sites on long-range alpha-satellite DNA arrays of human chromosome 21. *Hum Mol Genet,* 3**,** 1245-57.

ISHII, K., OGIYAMA, Y., CHIKASHIGE, Y., SOEJIMA, S., MASUDA, F., KAKUMA, T., HIRAOKA, Y. & TAKAHASHI, K. 2008. Heterochromatin integrity affects chromosome reorganization after centromere dysfunction. *Science,* 321**,** 1088-91.

ITO, T., TYLER, J. K., BULGER, M., KOBAYASHI, R. & KADONAGA, J. T. 1996. ATP-facilitated chromatin assembly with a nucleoplasmin-like protein from Drosophila melanogaster. *J Biol Chem,* 271**,** 25041-8.

JANSEN, L. E., BLACK, B. E., FOLTZ, D. R. & CLEVELAND, D. W. 2007. Propagation of centromeric chromatin requires exit from mitosis. *J Cell Biol,* 176**,** 795-805.

JENNEBACH, S., HERZOG, F., AEBERSOLD, R. & CRAMER, P. 2012. Crosslinking-MS analysis reveals RNA polymerase I domain architecture and basis of rRNA cleavage. *Nucleic Acids Res,* 40**,** 5591-601.

JENUWEIN, T. & ALLIS, C. D. 2001. Translating the histone code. *Science,* 293**,** 1074-80.

JIRICNY, J. 2006. The multifaceted mismatch-repair system. *Nat Rev Mol Cell Biol,* 7**,** 335-46.

JOUKOV, V. & DE NICOLO, A. 2018. Aurora-PLK1 cascades as key signaling modules in the regulation of mitosis. *Sci Signal,* 11.

KADOCH, C. & CRABTREE, G. R. 2015. Mammalian SWI/SNF chromatin remodeling complexes and cancer: Mechanistic insights gained from human genomics. *Sci Adv,* 1**,** e1500447.

KAMAKAKA, R. T. & BIGGINS, S. 2005. Histone variants: deviants? *Genes Dev,* 19**,** 295-310.

KANG, Y. H., PARK, J. E., YU, L. R., SOUNG, N. K., YUN, S. M., BANG, J. K., SEONG, Y. S., YU, H., GARFIELD, S., VEENSTRA, T. D. & LEE, K. S. 2006. Self-regulated Plk1 recruitment to kinetochores by the Plk1-PBIP1 interaction is critical for proper chromosome segregation. *Mol Cell,* 24**,** 409-22.

KASINATH, V., FAINI, M., POEPSEL, S., REIF, D., FENG, X. A., STJEPANOVIC, G., AEBERSOLD, R. & NOGALES, E. 2018. Structures of human PRC2 with its cofactors AEBP2 and JARID2. *Science,* 359**,** 940-944.

KATO, H., JIANG, J., ZHOU, B. R., ROZENDAAL, M., FENG, H., GHIRLANDO, R., XIAO, T. S., STRAIGHT, A. F. & BAI, Y. 2013. A conserved mechanism for centromeric nucleosome recognition by centromere protein CENP-C. *Science,* 340**,** 1110-3.

KETEL, C., WANG, H. S., MCCLELLAN, M., BOUCHONVILLE, K., SELMECKI, A., LAHAV, T., GERAMI-NEJAD, M. & BERMAN, J. 2009. Neocentromeres form efficiently at multiple possible loci in Candida albicans. *PLoS Genet,* 5**,** e1000400.

KILLINGER, K., BOHM, M., STEINBACH, P., HAGEMANN, G., BLUGGEL, M., JANEN, K., HOHOFF, S., BAYER, P., HERZOG, F. & WESTERMANN, S. 2020. Auto-inhibition of Mif2/CENP-C ensures centromere-dependent kinetochore assembly in budding yeast. *EMBO J,* 39**,** e102938.

KIM, E. M. & BURKE, D. J. 2008. DNA damage activates the SAC in an ATM/ATR-dependent manner, independently of the kinetochore. *PLoS Genet,* 4**,** e1000015.

KING, R. W., PETERS, J. M., TUGENDREICH, S., ROLFE, M., HIETER, P. & KIRSCHNER, M. W. 1995. A 20S complex containing CDC27 and CDC16 catalyzes the mitosis-specific conjugation of ubiquitin to cyclin B. *Cell,* 81**,** 279-88.

KLARE, K., WEIR, J. R., BASILICO, F., ZIMNIAK, T., MASSIMILIANO, L., LUDWIGS, N., HERZOG, F. & MUSACCHIO, A. 2015. CENP-C is a blueprint for constitutive centromere-associated network assembly within human kinetochores. *J Cell Biol,* 210**,** 11-22.

KLINE, S. L., CHEESEMAN, I. M., HORI, T., FUKAGAWA, T. & DESAI, A. 2006. The human Mis12 complex is required for kinetochore assembly and proper chromosome segregation. *J Cell Biol,* 173**,** 9-17.

KLUG, A. 2010. The discovery of zinc fingers and their applications in gene regulation and genome manipulation. *Annu Rev Biochem,* 79**,** 213-31.

KONEV, A. Y., TRIBUS, M., PARK, S. Y., PODHRASKI, V., LIM, C. Y., EMELYANOV, A. V., VERSHILOVA, E., PIRROTTA, V., KADONAGA, J. T., LUSSER, A. & FYODOROV, D. V. 2007. CHD1 motor protein is required for deposition of histone variant H3.3 into chromatin in vivo. *Science,* 317**,** 1087-90.

KOPS, G. J., KIM, Y., WEAVER, B. A., MAO, Y., MCLEOD, I., YATES, J. R., 3RD, TAGAYA, M. & CLEVELAND, D. W. 2005. ZW10 links mitotic checkpoint signaling to the structural kinetochore. *J Cell Biol,* 169**,** 49-60.

KRENN, V., OVERLACK, K., PRIMORAC, I., VAN GERWEN, S. & MUSACCHIO, A. 2014. KI motifs of human Knl1 enhance assembly of comprehensive spindle checkpoint complexes around MELT repeats. *Curr Biol,* 24**,** 29-39.

KURSEL, L. E. & MALIK, H. S. 2016. Centromeres. *Curr Biol,* 26**,** R487-R490.

KWON, M. S., HORI, T., OKADA, M. & FUKAGAWA, T. 2007. CENP-C is involved in chromosome segregation, mitotic checkpoint function, and kinetochore assembly. *Mol Biol Cell,* 18**,** 2155-68.

LACOSTE, N., WOOLFE, A., TACHIWANA, H., GAREA, A. V., BARTH, T., CANTALOUBE, S., KURUMIZAKA, H., IMHOF, A. & ALMOUZNI, G. 2014. Mislocalization of the centromeric histone variant CenH3/CENP-A in human cells depends on the chaperone DAXX. *Mol Cell,* 53**,** 631-44.

LAGANA, A., DORN, J. F., DE ROP, V., LADOUCEUR, A. M., MADDOX, A. S. & MADDOX, P. S. 2010. A small GTPase molecular switch regulates epigenetic centromere maintenance by stabilizing newly incorporated CENP-A. *Nat Cell Biol,* 12**,** 1186-93.

LAM, A. L., BOIVIN, C. D., BONNEY, C. F., RUDD, M. K. & SULLIVAN, B. A. 2006. Human centromeric chromatin is a dynamic chromosomal domain that can spread over noncentromeric DNA. *Proc Natl Acad Sci U S A,* 103**,** 4186-91.

LAMPERT, F. & WESTERMANN, S. 2011. A blueprint for kinetochores — new insights into the molecular mechanics of cell division. *Nature Reviews Molecular Cell Biology,* 12**,** 407-412.

LAMPSON, M. A. & CHEESEMAN, I. M. 2011. Sensing centromere tension: Aurora B and the regulation of kinetochore function. *Trends Cell Biol,* 21**,** 133-40.

LAMPSON, M. A., RENDUCHITALA, K., KHODJAKOV, A. & KAPOOR, T. M. 2004. Correcting improper chromosome-spindle attachments during cell division. *Nat Cell Biol,* 6**,** 232-7.

LARA-GONZALEZ, P., WESTHORPE, F. G. & TAYLOR, S. S. 2012. The spindle assembly checkpoint. *Curr Biol,* 22**,** R966-80.

LAWRIMORE, J., BLOOM, K. S. & SALMON, E. D. 2011. Point centromeres contain more than a single centromere-specific Cse4 (CENP-A) nucleosome. *J Cell Biol,* 195**,** 573-82.

LEE, T. I., RINALDI, N. J., ROBERT, F., ODOM, D. T., BAR-JOSEPH, Z., GERBER, G. K., HANNETT, N. M., HARBISON, C. T., THOMPSON, C. M., SIMON, I., ZEITLINGER, J., JENNINGS, E. G., MURRAY, H. L., GORDON, D. B., REN, B., WYRICK, J. J., TAGNE, J. B., VOLKERT, T. L., FRAENKEL, E., GIFFORD, D. K. & YOUNG, R. A. 2002. Transcriptional regulatory networks in Saccharomyces cerevisiae. *Science,* 298**,** 799-804.

LEITNER, A. 2016. Cross-linking and other structural proteomics techniques: how chemistry is enabling mass spectrometry applications in structural biology. *Chem Sci,* 7**,** 4792-4803.

LERA, R. F., NORMAN, R. X., DUMONT, M., DENNEE, A., MARTIN-KOOB, J., FACHINETTI, D. & BURKARD, M. E. 2019. Plk1 protects kinetochore-centromere architecture against microtubule pulling forces. *EMBO Rep,* 20**,** e48711.

LERA, R. F., POTTS, G. K., SUZUKI, A., JOHNSON, J. M., SALMON, E. D., COON, J. J. & BURKARD, M. E. 2016. Decoding Polo-like kinase 1 signaling along the kinetochore-centromere axis. *Nat Chem Biol,* 12**,** 411-8.

LEWIS, P. W., ELSAESSER, S. J., NOH, K. M., STADLER, S. C. & ALLIS, C. D. 2010. Daxx is an H3.3-specific histone chaperone and cooperates with ATRX in replication-independent chromatin assembly at telomeres. *Proc Natl Acad Sci U S A,* 107**,** 14075-80.

LI, F., MARTIENSSEN, R. & CANDE, W. Z. 2011. Coordination of DNA replication and histone modification by the Rik1-Dos2 complex. *Nature,* 475**,** 244-8.

LINDSTROM, M. S. 2011. NPM1/B23: A Multifunctional Chaperone in Ribosome Biogenesis and Chromatin Remodeling. *Biochem Res Int,* 2011**,** 195209.

LISKAY, R. M. 1977. Absence of a measurable G2 phase in two Chinese hamster cell lines. *Proc Natl Acad Sci U S A,* 74**,** 1622-5.

LIU, Z., SUN, Q. & WANG, X. 2017. PLK1, A Potential Target for Cancer Therapy. *Transl Oncol,* 10**,** 22-32.

LOCKE, D. P., HILLIER, L. W., WARREN, W. C., WORLEY, K. C., NAZARETH, L. V., MUZNY, D. M., YANG, S. P., WANG, Z., CHINWALLA, A. T., MINX, P., MITREVA, M., COOK, L., DELEHAUNTY, K. D., FRONICK, C., SCHMIDT, H., FULTON, L. A., FULTON, R. S., NELSON, J. O., MAGRINI, V., POHL, C., GRAVES, T. A., MARKOVIC, C., CREE, A., DINH, H. H., HUME, J., KOVAR, C. L., FOWLER, G. R., LUNTER, G., MEADER, S., HEGER, A., PONTING, C. P., MARQUES-BONET, T., ALKAN, C., CHEN, L., CHENG, Z., KIDD, J. M., EICHLER, E. E., WHITE, S., SEARLE, S., VILELLA, A. J., CHEN, Y., FLICEK, P., MA, J., RANEY, B., SUH, B., BURHANS, R., HERRERO, J., HAUSSLER, D., FARIA, R., FERNANDO, O., DARRE, F., FARRE, D., GAZAVE, E., OLIVA, M., NAVARRO, A., ROBERTO, R., CAPOZZI, O., ARCHIDIACONO, N., DELLA VALLE, G., PURGATO, S., ROCCHI, M., KONKEL, M. K., WALKER, J. A., ULLMER, B., BATZER, M. A., SMIT, A. F., HUBLEY, R., CASOLA, C., SCHRIDER, D. R., HAHN, M. W., QUESADA, V., PUENTE, X. S., ORDONEZ, G. R., LOPEZ-OTIN, C., VINAR, T., BREJOVA, B., RATAN, A., HARRIS, R. S., MILLER, W., KOSIOL, C., LAWSON, H. A., TALIWAL, V., MARTINS, A. L., SIEPEL, A., ROYCHOUDHURY, A., MA, X., DEGENHARDT, J., BUSTAMANTE, C. D., GUTENKUNST, R. N., MAILUND, T., DUTHEIL, J. Y., HOBOLTH, A., SCHIERUP, M. H., RYDER, O. A., YOSHINAGA, Y., DE JONG, P. J., WEINSTOCK, G. M., ROGERS, J., MARDIS, E. R., GIBBS, R. A., et al. 2011. Comparative and demographic analysis of orang-utan genomes. *Nature,* 469**,** 529-33.

LOMONTE, P., SULLIVAN, K. F. & EVERETT, R. D. 2001. Degradation of nucleosome-associated centromeric histone H3-like protein CENP-A induced by herpes simplex virus type 1 protein ICP0. *J Biol Chem,* 276**,** 5829-35.

LORCH, Y., MAIER-DAVIS, B. & KORNBERG, R. D. 2006. Chromatin remodeling by nucleosome disassembly in vitro. *Proc Natl Acad Sci U S A,* 103**,** 3090-3.

LORCH, Y., ZHANG, M. & KORNBERG, R. D. 1999. Histone octamer transfer by a chromatin-remodeling complex. *Cell,* 96**,** 389-92.

LUGER, K., MADER, A. W., RICHMOND, R. K., SARGENT, D. F. & RICHMOND, T. J. 1997. Crystal structure of the nucleosome core particle at 2.8 A resolution. *Nature,* 389**,** 251-60.

LUO, X. & YU, H. 2008. Protein metamorphosis: the two-state behavior of Mad2. *Structure,* 16**,** 1616-25.

LY, P., BRUNNER, S. F., SHOSHANI, O., KIM, D. H., LAN, W., PYNTIKOVA, T., FLANAGAN, A. M., BEHJATI, S., PAGE, D. C., CAMPBELL, P. J. & CLEVELAND, D. W. 2019. Chromosome segregation errors generate a diverse spectrum of simple and complex genomic rearrangements. *Nat Genet,* 51**,** 705-715.

MA, H. T. & POON, R. Y. 2011. Synchronization of HeLa cells. *Methods Mol Biol,* 761**,** 151-61.

MACIEJOWSKI, J., GEORGE, K. A., TERRET, M. E., ZHANG, C., SHOKAT, K. M. & JALLEPALLI, P. V. 2010. Mps1 directs the assembly of Cdc20 inhibitory complexes during interphase and mitosis to control M phase timing and spindle checkpoint signaling. *J Cell Biol,* 190**,** 89-100.

MALIK, H. S. & HENIKOFF, S. 2003. Phylogenomics of the nucleosome. *Nat Struct Biol,* 10**,** 882-91.

MALLIK, R., CARTER, B. C., LEX, S. A., KING, S. J. & GROSS, S. P. 2004. Cytoplasmic dynein functions as a gear in response to load. *Nature,* 427**,** 649-52.

MALUREANU, L. A., JEGANATHAN, K. B., HAMADA, M., WASILEWSKI, L., DAVENPORT, J. & VAN DEURSEN, J. M. 2009. BubR1 N terminus acts as a soluble inhibitor of cyclin B degradation by APC/C(Cdc20) in interphase. *Dev Cell,* 16**,** 118-31.

MALVEZZI, F., LITOS, G., SCHLEIFFER, A., HEUCK, A., MECHTLER, K., CLAUSEN, T. & WESTERMANN, S. 2013. A structural basis for kinetochore recruitment of the Ndc80 complex via two distinct centromere receptors. *EMBO J,* 32**,** 409-23.

MANUELIDIS, L. 1978. Chromosomal localization of complex and simple repeated human DNAs. *Chromosoma,* 66**,** 23-32.

MARFELLA, C. G. & IMBALZANO, A. N. 2007. The Chd family of chromatin remodelers. *Mutat Res,* 618**,** 30-40.

MARGUERON, R. & REINBERG, D. 2010. Chromatin structure and the inheritance of epigenetic information. *Nat Rev Genet,* 11**,** 285-96.

MARTINEZ-ALONSO, D. & MALUMBRES, M. 2020. Mammalian cell cycle cyclins. *Semin Cell Dev Biol*.

MARTINS, N. M., BERGMANN, J. H., SHONO, N., KIMURA, H., LARIONOV, V., MASUMOTO, H. & EARNSHAW, W. C. 2016. Epigenetic engineering shows that a human centromere resists silencing mediated by H3K27me3/K9me3. *Mol Biol Cell,* 27**,** 177-96.

MARZLUFF, W. F. & DURONIO, R. J. 2002. Histone mRNA expression: multiple levels of cell cycle regulation and important developmental consequences. *Curr Opin Cell Biol,* 14**,** 692-9.

MARZLUFF, W. F., WAGNER, E. J. & DURONIO, R. J. 2008. Metabolism and regulation of canonical histone mRNAs: life without a poly(A) tail. *Nat Rev Genet,* 9**,** 843-54.

MASKELL, D. P., HU, X. W. & SINGLETON, M. R. 2010. Molecular architecture and assembly of the yeast kinetochore MIND complex. *J Cell Biol,* 190**,** 823-34.

MATHEW, V., PAULEAU, A. L., STEFFEN, N., BERGNER, A., BECKER, P. B. & ERHARDT, S. 2014. The histone-fold protein CHRAC14 influences chromatin composition in response to DNA damage. *Cell Rep,* 7**,** 321-330.

MCGREW, J., DIEHL, B. & FITZGERALD-HAYES, M. 1986. Single base-pair mutations in centromere element III cause aberrant chromosome segregation in Saccharomyces cerevisiae. *Mol Cell Biol,* 6**,** 530-8.

MCKINLEY, K. L., SEKULIC, N., GUO, L. Y., TSINMAN, T., BLACK, B. E. & CHEESEMAN, I. M. 2015. The CENP-L-N Complex Forms a Critical Node

in an Integrated Meshwork of Interactions at the Centromere-Kinetochore Interface. *Mol Cell,* 60**,** 886-98.

MELUH, P. B. & KOSHLAND, D. 1995. Evidence that the MIF2 gene of Saccharomyces cerevisiae encodes a centromere protein with homology to the mammalian centromere protein CENP-C. *Mol Biol Cell,* 6**,** 793-807.

MENDIBURO, M. J., PADEKEN, J., FULOP, S., SCHEPERS, A. & HEUN, P. 2011. Drosophila CENH3 is sufficient for centromere formation. *Science,* 334**,** 686-90.

MITRA, S., BODOR, D. L., DAVID, A. F., ABDUL-ZANI, I., MATA, J. F., NEUMANN, B., REITHER, S., TISCHER, C. & JANSEN, L. E. T. 2020a. Genetic screening identifies a SUMO protease dynamically maintaining centromeric chromatin. *Nat Commun,* 11**,** 501.

MITRA, S., SRINIVASAN, B. & JANSEN, L. E. T. 2020b. Stable inheritance of CENP-A chromatin: Inner strength versus dynamic control. *J Cell Biol,* 219.

MOGGS, J. G., GRANDI, P., QUIVY, J. P., JONSSON, Z. O., HUBSCHER, U., BECKER, P. B. & ALMOUZNI, G. 2000. A CAF-1-PCNA-mediated chromatin assembly pathway triggered by sensing DNA damage. *Mol Cell Biol,* 20**,** 1206-18.

MOHIBI, S., SRIVASTAVA, S., WANG-FRANCE, J., MIRZA, S., ZHAO, X., BAND, H. & BAND, V. 2015. Alteration/Deficiency in Activation 3 (ADA3) Protein, a Cell Cycle Regulator, Associates with the Centromere through CENP-B and Regulates Chromosome Segregation. *J Biol Chem,* 290**,** 28299-310.

MOORE, L. L. & ROTH, M. B. 2001. HCP-4, a CENP-C-like protein in Caenorhabditis elegans, is required for resolution of sister centromeres. *J Cell Biol,* 153**,** 1199-208.

MOREE, B., MEYER, C. B., FULLER, C. J. & STRAIGHT, A. F. 2011. CENP-C recruits M18BP1 to centromeres to promote CENP-A chromatin assembly. *J Cell Biol,* 194**,** 855-71.

MORENO-MORENO, O., TORRAS-LLORT, M. & AZORIN, F. 2006. Proteolysis restricts localization of CID, the centromere-specific histone H3 variant of Drosophila, to centromeres. *Nucleic Acids Res,* 34**,** 6247-55.

MULLER, F., FISCHER, L., CHEN, Z. A., AUCHYNNIKAVA, T. & RAPPSILBER, J. 2018. On the Reproducibility of Label-Free Quantitative Cross-Linking/Mass Spectrometry. *J Am Soc Mass Spectrom,* 29**,** 405-412.

MUSACCHIO, A. & DESAI, A. 2017. A Molecular View of Kinetochore Assembly and Function. *Biology (Basel),* 6.

MUSACCHIO, A. & SALMON, E. D. 2007. The spindle-assembly checkpoint in space and time. *Nat Rev Mol Cell Biol,* 8**,** 379-93.

NAGPAL, H., HORI, T., FURUKAWA, A., SUGASE, K., OSAKABE, A., KURUMIZAKA, H. & FUKAGAWA, T. 2015. Dynamic changes in CCAN organization through CENP-C during cell-cycle progression. *Mol Biol Cell,* 26**,** 3768-76.

NAKANO, M., CARDINALE, S., NOSKOV, V. N., GASSMANN, R., VAGNARELLI, P., KANDELS-LEWIS, S., LARIONOV, V., EARNSHAW, W. C. & MASUMOTO, H. 2008. Inactivation of a human kinetochore by specific targeting of chromatin modifiers. *Dev Cell,* 14**,** 507-22.

NECHEMIA-ARBELY, Y., FACHINETTI, D. & CLEVELAND, D. W. 2012. Replicating centromeric chromatin: spatial and temporal control of CENP-A assembly. *Exp Cell Res,* 318**,** 1353-60.

NECHEMIA-ARBELY, Y., MIGA, K. H., SHOSHANI, O., ASLANIAN, A., MCMAHON, M. A., LEE, A. Y., FACHINETTI, D., YATES, J. R., 3RD, REN, B. & CLEVELAND, D. W. 2019. DNA replication acts as an error correction mechanism to maintain centromere identity by restricting CENP-A to centromeres. *Nat Cell Biol,* 21**,** 743-754.

NG, R. & CARBON, J. 1987. Mutational and in vitro protein-binding studies on centromere DNA from Saccharomyces cerevisiae. *Mol Cell Biol,* 7**,** 4522-34.

NIIKURA, Y., KITAGAWA, R., FANG, L. & KITAGAWA, K. 2019. CENP-A Ubiquitylation Is Indispensable to Cell Viability. *Dev Cell,* 50**,** 683-689 e6.

NIIKURA, Y., KITAGAWA, R. & KITAGAWA, K. 2016. CENP-A Ubiquitylation Is Inherited through Dimerization between Cell Divisions. *Cell Rep,* 15**,** 61-76.

NIIKURA, Y., KITAGAWA, R., OGI, H., ABDULLE, R., PAGALA, V. & KITAGAWA, K. 2015. CENP-A K124 Ubiquitylation Is Required for CENP-A Deposition at the Centromere. *Dev Cell,* 32**,** 589-603.

NISHINO, T., TAKEUCHI, K., GASCOIGNE, K. E., SUZUKI, A., HORI, T., OYAMA, T., MORIKAWA, K., CHEESEMAN, I. M. & FUKAGAWA, T. 2012. CENP-T-W-S-X forms a unique centromeric chromatin structure with a histone-like fold. *Cell,* 148**,** 487-501.

O'REILLY, F. J. & RAPPSILBER, J. 2018. Cross-linking mass spectrometry: methods and applications in structural, molecular and systems biology. *Nat Struct Mol Biol,* 25**,** 1000-1008.

OBUSE, C., YANG, H., NOZAKI, N., GOTO, S., OKAZAKI, T. & YODA, K. 2004. Proteomics analysis of the centromere complex from HeLa interphase cells: UV-damaged DNA binding protein 1 (DDB-1) is a component of the CEN-complex, while BMI-1 is transiently co-localized with the centromeric region in interphase. *Genes Cells,* 9**,** 105-20.

OEGEMA, K., DESAI, A., RYBINA, S., KIRKHAM, M. & HYMAN, A. A. 2001. Functional analysis of kinetochore assembly in Caenorhabditis elegans. *J Cell Biol,* 153**,** 1209-26.

OHZEKI, J., BERGMANN, J. H., KOUPRINA, N., NOSKOV, V. N., NAKANO, M., KIMURA, H., EARNSHAW, W. C., LARIONOV, V. & MASUMOTO, H. 2012. Breaking the HAC Barrier: histone H3K9 acetyl/methyl balance regulates CENP-A assembly. *EMBO J,* 31**,** 2391-402.

OHZEKI, J., NAKANO, M., OKADA, T. & MASUMOTO, H. 2002. CENP-B box is required for de novo centromere chromatin assembly on human alphoid DNA. *J Cell Biol,* 159**,** 765-75.

OHZEKI, J., SHONO, N., OTAKE, K., MARTINS, N. M., KUGOU, K., KIMURA, H., NAGASE, T., LARIONOV, V., EARNSHAW, W. C. & MASUMOTO, H. 2016. KAT7/HBO1/MYST2 Regulates CENP-A Chromatin Assembly by Antagonizing Suv39h1-Mediated Centromere Inactivation. *Dev Cell,* 37**,** 413-27.

OKADA, M., OKAWA, K., ISOBE, T. & FUKAGAWA, T. 2009. CENP-H-containing complex facilitates centromere deposition of CENP-A in cooperation with FACT and CHD1. *Mol Biol Cell,* 20**,** 3986-95.

OLSEN, J. V., ONG, S. E. & MANN, M. 2004. Trypsin cleaves exclusively C-terminal to arginine and lysine residues. *Mol Cell Proteomics,* 3**,** 608-14.

OLSZAK, A. M., VAN ESSEN, D., PEREIRA, A. J., DIEHL, S., MANKE, T., MAIATO, H., SACCANI, S. & HEUN, P. 2011. Heterochromatin boundaries are hotspots for de novo kinetochore formation. *Nat Cell Biol,* 13**,** 799-808.

ONG, S. E., KRATCHMAROVA, I. & MANN, M. 2003. Properties of 13C-substituted arginine in stable isotope labeling by amino acids in cell culture (SILAC). *J Proteome Res,* 2**,** 173-81.

ONG, S. E. & MANN, M. 2005. Mass spectrometry-based proteomics turns quantitative. *Nat Chem Biol,* 1**,** 252-62.

ORPHANIDES, G., WU, W. H., LANE, W. S., HAMPSEY, M. & REINBERG, D. 1999. The chromatin-specific transcription elongation factor FACT comprises human SPT16 and SSRP1 proteins. *Nature,* 400**,** 284-8.

OSTLER, K. R., DAVIS, E. M., PAYNE, S. L., GOSALIA, B. B., EXPOSITO-CESPEDES, J., LE BEAU, M. M. & GODLEY, L. A. 2007. Cancer cells express aberrant DNMT3B transcripts encoding truncated proteins. *Oncogene,* 26**,** 5553-63.

OVERLACK, K., BANGE, T., WEISSMANN, F., FAESEN, A. C., MAFFINI, S., PRIMORAC, I., MULLER, F., PETERS, J. M. & MUSACCHIO, A. 2017. BubR1 Promotes Bub3-Dependent APC/C Inhibition during Spindle Assembly Checkpoint Signaling. *Curr Biol,* 27**,** 2915-2927 e7.

PALMER, D. K., O'DAY, K., WENER, M. H., ANDREWS, B. S. & MARGOLIS, R. L. 1987. A 17-kD centromere protein (CENP-A) copurifies with nucleosome core particles and with histones. *J Cell Biol,* 104**,** 805-15.

PAN, J. & CHEN, R. H. 2004. Spindle checkpoint regulates Cdc20p stability in Saccharomyces cerevisiae. *Genes Dev,* 18**,** 1439-51.

PAPAIT, R., PISTORE, C., NEGRI, D., PECORARO, D., CANTARINI, L. & BONAPACE, I. M. 2007. Np95 is implicated in pericentromeric heterochromatin replication and in major satellite silencing. *Mol Biol Cell,* 18**,** 1098-106.

PEKGOZ ALTUNKAYA, G., MALVEZZI, F., DEMIANOVA, Z., ZIMNIAK, T., LITOS, G., WEISSMANN, F., MECHTLER, K., HERZOG, F. & WESTERMANN, S. 2016. CCAN Assembly Configures Composite Binding

Interfaces to Promote Cross-Linking of Ndc80 Complexes at the Kinetochore. *Curr Biol,* 26**,** 2370-8.

PENTAKOTA, S., ZHOU, K., SMITH, C., MAFFINI, S., PETROVIC, A., MORGAN, G. P., WEIR, J. R., VETTER, I. R., MUSACCHIO, A. & LUGER, K. 2017. Decoding the centromeric nucleosome through CENP-N. *Elife,* 6.

PERPELESCU, M., NOZAKI, N., OBUSE, C., YANG, H. & YODA, K. 2009. Active establishment of centromeric CENP-A chromatin by RSF complex. *J Cell Biol,* 185**,** 397-407.

PESENTI, M. E., PRUMBAUM, D., AUCKLAND, P., SMITH, C. M., FAESEN, A. C., PETROVIC, A., ERENT, M., MAFFINI, S., PENTAKOTA, S., WEIR, J. R., LIN, Y. C., RAUNSER, S., MCAINSH, A. D. & MUSACCHIO, A. 2018. Reconstitution of a 26-Subunit Human Kinetochore Reveals Cooperative Microtubule Binding by CENP-OPQUR and NDC80. *Mol Cell,* 71**,** 923-939 e10.

PETERS, J. M. 2006. The anaphase promoting complex/cyclosome: a machine designed to destroy. *Nat Rev Mol Cell Biol,* 7**,** 644-56.

PETROVIC, A., KELLER, J., LIU, Y., OVERLACK, K., JOHN, J., DIMITROVA, Y. N., JENNI, S., VAN GERWEN, S., STEGE, P., WOHLGEMUTH, S., ROMBAUT, P., HERZOG, F., HARRISON, S. C., VETTER, I. R. & MUSACCHIO, A. 2016. Structure of the MIS12 Complex and Molecular Basis of Its Interaction with CENP-C at Human Kinetochores. *Cell,* 167**,** 1028-1040 e15.

PETROVIC, A., PASQUALATO, S., DUBE, P., KRENN, V., SANTAGUIDA, S., CITTARO, D., MONZANI, S., MASSIMILIANO, L., KELLER, J., TARRICONE, A., MAIOLICA, A., STARK, H. & MUSACCHIO, A. 2010. The MIS12 complex is a protein interaction hub for outer kinetochore assembly. *J Cell Biol,* 190**,** 835-52.

PETRYK, N., DALBY, M., WENGER, A., STROMME, C. B., STRANDSBY, A., ANDERSSON, R. & GROTH, A. 2018. MCM2 promotes symmetric inheritance of modified histones during DNA replication. *Science,* 361**,** 1389-1392.

PINSKY, B. A., KUNG, C., SHOKAT, K. M. & BIGGINS, S. 2006. The Ipl1-Aurora protein kinase activates the spindle checkpoint by creating unattached kinetochores. *Nat Cell Biol,* 8**,** 78-83.

PIRAS, F. M., NERGADZE, S. G., MAGNANI, E., BERTONI, L., ATTOLINI, C., KHORIAULI, L., RAIMONDI, E. & GIULOTTO, E. 2010. Uncoupling of satellite DNA and centromeric function in the genus Equus. *PLoS Genet,* 6**,** e1000845.

PLOHL, M., MESTROVIC, N. & MRAVINAC, B. 2014. Centromere identity from the DNA point of view. *Chromosoma,* 123**,** 313-25.

PLUTA, A. F., MACKAY, A. M., AINSZTEIN, A. M., GOLDBERG, I. G. & EARNSHAW, W. C. 1995. The centromere: hub of chromosomal activities. *Science,* 270**,** 1591-4.

POWERS, A. F., FRANCK, A. D., GESTAUT, D. R., COOPER, J., GRACYZK, B., WEI, R. R., WORDEMAN, L., DAVIS, T. N. & ASBURY, C. L. 2009. The Ndc80 kinetochore complex forms load-bearing attachments to dynamic microtubule tips via biased diffusion. *Cell,* 136**,** 865-75.

PRAMILA, T., WU, W., MILES, S., NOBLE, W. S. & BREEDEN, L. L. 2006. The Forkhead transcription factor Hcm1 regulates chromosome segregation genes and fills the S-phase gap in the transcriptional circuitry of the cell cycle. *Genes Dev,* 20**,** 2266-78.

PROBST, A. V., DUNLEAVY, E. & ALMOUZNI, G. 2009. Epigenetic inheritance during the cell cycle. *Nat Rev Mol Cell Biol,* 10**,** 192-206.

PRZEWLOKA, M. R., VENKEI, Z., BOLANOS-GARCIA, V. M., DEBSKI, J., DADLEZ, M. & GLOVER, D. M. 2011. CENP-C is a structural platform for kinetochore assembly. *Curr Biol,* 21**,** 399-405.

QI, W., TANG, Z. & YU, H. 2006. Phosphorylation- and polo-box-dependent binding of Plk1 to Bub1 is required for the kinetochore localization of Plk1. *Mol Biol Cell,* 17**,** 3705-16.

QUENET, D. & DALAL, Y. 2014. A long non-coding RNA is required for targeting centromeric protein A to the human centromere. *Elife,* 3**,** e03254.

RANSOM, M., DENNEHEY, B. K. & TYLER, J. K. 2010. Chaperoning histones during DNA replication and repair. *Cell,* 140**,** 183-95.

REGNIER, V., VAGNARELLI, P., FUKAGAWA, T., ZERJAL, T., BURNS, E., TROUCHE, D., EARNSHAW, W. & BROWN, W. 2005. CENP-A is required for accurate chromosome segregation and sustained kinetochore association of BubR1. *Mol Cell Biol,* 25**,** 3967-81.

RIEDER, D., TRAJANOSKI, Z. & MCNALLY, J. G. 2012. Transcription factories. *Front Genet,* 3**,** 221.

RISCHITOR, P. E., MAY, K. M. & HARDWICK, K. G. 2007. Bub1 is a fission yeast kinetochore scaffold protein, and is sufficient to recruit other spindle checkpoint proteins to ectopic sites on chromosomes. *PLoS One,* 2**,** e1342.

ROSIC, S., KOHLER, F. & ERHARDT, S. 2014. Repetitive centromeric satellite RNA is essential for kinetochore formation and cell division. *J Cell Biol,* 207**,** 335-49.

ROSS, J. E., WOODLIEF, K. S. & SULLIVAN, B. A. 2016. Inheritance of the CENP-A chromatin domain is spatially and temporally constrained at human centromeres. *Epigenetics Chromatin,* 9**,** 20.

ROSSI, A. M. & TAYLOR, C. W. 2011. Analysis of protein-ligand interactions by fluorescence polarization. *Nat Protoc,* 6**,** 365-87.

ROST, H. L., SACHSENBERG, T., AICHE, S., BIELOW, C., WEISSER, H., AICHELER, F., ANDREOTTI, S., EHRLICH, H. C., GUTENBRUNNER, P., KENAR, E., LIANG, X., NAHNSEN, S., NILSE, L., PFEUFFER, J., ROSENBERGER, G., RURIK, M., SCHMITT, U., VEIT, J., WALZER, M., WOJNAR, D., WOLSKI, W. E., SCHILLING, O., CHOUDHARY, J. S., MALMSTROM, L., AEBERSOLD, R., REINERT, K. & KOHLBACHER, O.

2016. OpenMS: a flexible open-source software platform for mass spectrometry data analysis. *Nat Methods,* 13**,** 741-8.

ROTHER, M. B. & VAN ATTIKUM, H. 2017. DNA repair goes hip-hop: SMARCA and CHD chromatin remodellers join the break dance. *Philos Trans R Soc Lond B Biol Sci,* 372.

ROUT, M. P. & SALI, A. 2019. Principles for Integrative Structural Biology Studies. *Cell,* 177**,** 1384-1403.

SAITOH, H., TOMKIEL, J., COOKE, C. A., RATRIE, H., 3RD, MAURER, M., ROTHFIELD, N. F. & EARNSHAW, W. C. 1992. CENP-C, an autoantigen in scleroderma, is a component of the human inner kinetochore plate. *Cell,* 70**,** 115-25.

SALIMIAN, K. J., BALLISTER, E. R., SMOAK, E. M., WOOD, S., PANCHENKO, T., LAMPSON, M. A. & BLACK, B. E. 2011. Feedback control in sensing chromosome biorientation by the Aurora B kinase. *Curr Biol,* 21**,** 1158-65.

SAMOSHKIN, A., ARNAOUTOV, A., JANSEN, L. E., OUSPENSKI, I., DYE, L., KARPOVA, T., MCNALLY, J., DASSO, M., CLEVELAND, D. W. & STRUNNIKOV, A. 2009. Human condensin function is essential for centromeric chromatin assembly and proper sister kinetochore orientation. *PLoS One,* 4**,** e6831.

SANSONI, V., CASAS-DELUCCHI, C. S., RAJAN, M., SCHMIDT, A., BONISCH, C., THOMAE, A. W., STAEGE, M. S., HAKE, S. B., CARDOSO, M. C. & IMHOF, A. 2014. The histone variant H2A.Bbd is enriched at sites of DNA synthesis. *Nucleic Acids Res,* 42**,** 6405-20.

SANTAGUIDA, S., TIGHE, A., D'ALISE, A. M., TAYLOR, S. S. & MUSACCHIO, A. 2010. Dissecting the role of MPS1 in chromosome biorientation and the spindle checkpoint through the small molecule inhibitor reversine. *J Cell Biol,* 190**,** 73-87.

SAURIN, A. T. 2018. Kinase and Phosphatase Cross-Talk at the Kinetochore. *Front Cell Dev Biol,* 6**,** 62.

SCATCHARD, G. 1949. THE ATTRACTIONS OF PROTEINS FOR SMALL MOLECULES AND IONS. *Ann NY Acad Sci***,** 660-672.

SCHINDELIN, J., ARGANDA-CARRERAS, I., FRISE, E., KAYNIG, V., LONGAIR, M., PIETZSCH, T., PREIBISCH, S., RUEDEN, C., SAALFELD, S., SCHMID, B., TINEVEZ, J. Y., WHITE, D. J., HARTENSTEIN, V., ELICEIRI, K., TOMANCAK, P. & CARDONA, A. 2012. Fiji: an open-source platform for biological-image analysis. *Nat Methods,* 9**,** 676-82.

SCHLEIFFER, A., MAIER, M., LITOS, G., LAMPERT, F., HORNUNG, P., MECHTLER, K. & WESTERMANN, S. 2012. CENP-T proteins are conserved centromere receptors of the Ndc80 complex. *Nat Cell Biol,* 14**,** 604-13.

SCHMIDT, C. & URLAUB, H. 2017. Combining cryo-electron microscopy (cryo-EM) and cross-linking mass spectrometry (CX-MS) for structural elucidation of large protein assemblies. *Curr Opin Struct Biol,* 46**,** 157-168.

SCHMIDT, C., ZHOU, M., MARRIOTT, H., MORGNER, N., POLITIS, A. & ROBINSON, C. V. 2013. Comparative cross-linking and mass spectrometry of an intact F-type ATPase suggest a role for phosphorylation. *Nat Commun,* 4**,** 1985.

SCHUELER, M. G., HIGGINS, A. W., RUDD, M. K., GUSTASHAW, K. & WILLARD, H. F. 2001. Genomic and genetic definition of a functional human centromere. *Science,* 294**,** 109-15.

SCHUELER, M. G. & SULLIVAN, B. A. 2006. Structural and functional dynamics of human centromeric chromatin. *Annu Rev Genomics Hum Genet,* 7**,** 301-13.

SCREPANTI, E., DE ANTONI, A., ALUSHIN, G. M., PETROVIC, A., MELIS, T., NOGALES, E. & MUSACCHIO, A. 2011. Direct binding of Cenp-C to the Mis12 complex joins the inner and outer kinetochore. *Curr Biol,* 21**,** 391-8.

SHANG, W. H., HORI, T., MARTINS, N. M., TOYODA, A., MISU, S., MONMA, N., HIRATANI, I., MAESHIMA, K., IKEO, K., FUJIYAMA, A., KIMURA, H., EARNSHAW, W. C. & FUKAGAWA, T. 2013. Chromosome engineering allows the efficient isolation of vertebrate neocentromeres. *Dev Cell,* 24**,** 635-48.

SHANG, W. H., HORI, T., TOYODA, A., KATO, J., POPENDORF, K., SAKAKIBARA, Y., FUJIYAMA, A. & FUKAGAWA, T. 2010. Chickens possess centromeres with both extended tandem repeats and short non-tandem-repetitive sequences. *Genome Res,* 20**,** 1219-28.

SHELBY, R. D., VAFA, O. & SULLIVAN, K. F. 1997. Assembly of CENP-A into centromeric chromatin requires a cooperative array of nucleosomal DNA contact sites. *J Cell Biol,* 136**,** 501-13.

SHIBAHARA, K. & STILLMAN, B. 1999. Replication-dependent marking of DNA by PCNA facilitates CAF-1-coupled inheritance of chromatin. *Cell,* 96**,** 575-85.

SHIM, Y., DUAN, M. R., CHEN, X., SMERDON, M. J. & MIN, J. H. 2012. Polycistronic coexpression and nondenaturing purification of histone octamers. *Anal Biochem,* 427**,** 190-2.

SHONO, N., OHZEKI, J., OTAKE, K., MARTINS, N. M., NAGASE, T., KIMURA, H., LARIONOV, V., EARNSHAW, W. C. & MASUMOTO, H. 2015. CENP-C and CENP-I are key connecting factors for kinetochore and CENP-A assembly. *J Cell Sci,* 128**,** 4572-87.

SHUAIB, M., OUARARHNI, K., DIMITROV, S. & HAMICHE, A. 2010. HJURP binds CENP-A via a highly conserved N-terminal domain and mediates its deposition at centromeres. *Proc Natl Acad Sci U S A,* 107**,** 1349-54.

SIEVERS, F., WILM, A., DINEEN, D., GIBSON, T. J., KARPLUS, K., LI, W., LOPEZ, R., MCWILLIAM, H., REMMERT, M., SODING, J., THOMPSON, J. D. & HIGGINS, D. G. 2011. Fast, scalable generation of high-quality protein multiple sequence alignments using Clustal Omega. *Mol Syst Biol,* 7**,** 539.

SIGGENS, L., CORDEDDU, L., RONNERBLAD, M., LENNARTSSON, A. & EKWALL, K. 2015. Transcription-coupled recruitment of human CHD1 and CHD2 influences chromatin accessibility and histone H3 and H3.3 occupancy at active chromatin regions. *Epigenetics Chromatin,* 8**,** 4.

SILVA, M. C., BODOR, D. L., STELLFOX, M. E., MARTINS, N. M., HOCHEGGER, H., FOLTZ, D. R. & JANSEN, L. E. 2012. Cdk activity couples epigenetic centromere inheritance to cell cycle progression. *Dev Cell,* 22**,** 52-63.

SIMON, I., BARNETT, J., HANNETT, N., HARBISON, C. T., RINALDI, N. J., VOLKERT, T. L., WYRICK, J. J., ZEITLINGER, J., GIFFORD, D. K., JAAKKOLA, T. S. & YOUNG, R. A. 2001. Serial regulation of transcriptional regulators in the yeast cell cycle. *Cell,* 106**,** 697-708.

SMITH, S. & STILLMAN, B. 1989. Purification and characterization of CAF-I, a human cell factor required for chromatin assembly during DNA replication in vitro. *Cell,* 58**,** 15-25.

SMITS, A. H. & VERMEULEN, M. 2016. Characterizing Protein-Protein Interactions Using Mass Spectrometry: Challenges and Opportunities. *Trends Biotechnol,* 34**,** 825-834.

SOLIS-MEZARINO, V. 2019. *Characterization of Protein Interactions by Mass Spectrometry and Bioinformatics*. PhD Dissertation, Ludwig-Maximilians Universität München.

SRIVASTAVA, S. & FOLTZ, D. R. 2018. Posttranslational modifications of CENP-A: marks of distinction. *Chromosoma,* 127**,** 279-290.

STARK, G. R. & TAYLOR, W. R. 2006. Control of the G2/M transition. *Mol Biotechnol,* 32**,** 227-48.

STELLFOX, M. E., BAILEY, A. O. & FOLTZ, D. R. 2013. Putting CENP-A in its place. *Cell Mol Life Sci,* 70**,** 387-406.

STEWART-MORGAN, K. R., PETRYK, N. & GROTH, A. 2020. Chromatin replication and epigenetic cell memory. *Nat Cell Biol,* 22**,** 361-371.

STILLMAN, B. 1986. Chromatin assembly during SV40 DNA replication in vitro. *Cell,* 45**,** 555-65.

STOLER, S., KEITH, K. C., CURNICK, K. E. & FITZGERALD-HAYES, M. 1995. A mutation in CSE4, an essential gene encoding a novel chromatin-associated protein in yeast, causes chromosome nondisjunction and cell cycle arrest at mitosis. *Genes Dev,* 9**,** 573-86.

SUDAKIN, V., CHAN, G. K. & YEN, T. J. 2001. Checkpoint inhibition of the APC/C in HeLa cells is mediated by a complex of BUBR1, BUB3, CDC20, and MAD2. *J Cell Biol,* 154**,** 925-36.

SUDAKIN, V., GANOTH, D., DAHAN, A., HELLER, H., HERSHKO, J., LUCA, F. C., RUDERMAN, J. V. & HERSHKO, A. 1995. The cyclosome, a large complex containing cyclin-selective ubiquitin ligase activity, targets cyclins for destruction at the end of mitosis. *Mol Biol Cell,* 6**,** 185-97.

SUIJKERBUIJK, S. J., VLEUGEL, M., TEIXEIRA, A. & KOPS, G. J. 2012. Integration of kinase and phosphatase activities by BUBR1 ensures

formation of stable kinetochore-microtubule attachments. *Dev Cell,* 23**,** 745-55.

SULLIVAN, B. A. & KARPEN, G. H. 2004. Centromeric chromatin exhibits a histone modification pattern that is distinct from both euchromatin and heterochromatin. *Nat Struct Mol Biol,* 11**,** 1076-83.

SULLIVAN, M. & MORGAN, D. O. 2007. Finishing mitosis, one step at a time. *Nat Rev Mol Cell Biol,* 8**,** 894-903.

SUN, X., CLERMONT, P. L., JIAO, W., HELGASON, C. D., GOUT, P. W., WANG, Y. & QU, S. 2016. Elevated expression of the centromere protein-A(CENP-A)-encoding gene as a prognostic and predictive biomarker in human cancers. *Int J Cancer,* 139**,** 899-907.

TACKETT, A. J., DILWORTH, D. J., DAVEY, M. J., O'DONNELL, M., AITCHISON, J. D., ROUT, M. P. & CHAIT, B. T. 2005. Proteomic and genomic characterization of chromatin complexes at a boundary. *J Cell Biol,* 169**,** 35-47.

TAKAHASHI, K., CHEN, E. S. & YANAGIDA, M. 2000. Requirement of Mis6 centromere connector for localizing a CENP-A-like protein in fission yeast. *Science,* 288**,** 2215-9.

TAKEUCHI, K., NISHINO, T., MAYANAGI, K., HORIKOSHI, N., OSAKABE, A., TACHIWANA, H., HORI, T., KURUMIZAKA, H. & FUKAGAWA, T. 2014. The centromeric nucleosome-like CENP-T-W-S-X complex induces positive supercoils into DNA. *Nucleic Acids Res,* 42**,** 1644-55.

TANAKA, Y., NUREKI, O., KURUMIZAKA, H., FUKAI, S., KAWAGUCHI, S., IKUTA, M., IWAHARA, J., OKAZAKI, T. & YOKOYAMA, S. 2001. Crystal structure of the CENP-B protein-DNA complex: the DNA-binding domains of CENP-B induce kinks in the CENP-B box DNA. *EMBO J,* 20**,** 6612-8.

TERUI, R., NAGAO, K., KAWASOE, Y., TAKI, K., HIGASHI, T. L., TANAKA, S., NAKAGAWA, T., OBUSE, C., MASUKATA, H. & TAKAHASHI, T. S. 2018. Nucleosomes around a mismatched base pair are excluded via an Msh2-dependent reaction with the aid of SNF2 family ATPase Smarcad1. *Genes Dev,* 32**,** 806-821.

THOMPSON, A., SCHAFER, J., KUHN, K., KIENLE, S., SCHWARZ, J., SCHMIDT, G., NEUMANN, T., JOHNSTONE, R., MOHAMMED, A. K. & HAMON, C. 2003. Tandem mass tags: a novel quantification strategy for comparative analysis of complex protein mixtures by MS/MS. *Anal Chem,* 75**,** 1895-904.

TIGHE, A., JOHNSON, V. L. & TAYLOR, S. S. 2004. Truncating APC mutations have dominant effects on proliferation, spindle checkpoint control, survival and chromosome stability. *J Cell Sci,* 117**,** 6339-53.

TIPTON, A. R., WANG, K., OLADIMEJI, P., SUFI, S., GU, Z. & LIU, S. T. 2012. Identification of novel mitosis regulators through data mining with human centromere/kinetochore proteins as group queries. *BMC Cell Biol,* 13**,** 15.

TOBA, S., WATANABE, T. M., YAMAGUCHI-OKIMOTO, L., TOYOSHIMA, Y. Y. & HIGUCHI, H. 2006. Overlapping hand-over-hand mechanism of single

molecular motility of cytoplasmic dynein. *Proc Natl Acad Sci U S A,* 103**,** 5741-5.

TOMKIEL, J., COOKE, C. A., SAITOH, H., BERNAT, R. L. & EARNSHAW, W. C. 1994. CENP-C is required for maintaining proper kinetochore size and for a timely transition to anaphase. *J Cell Biol,* 125**,** 531-45.

TOPP, C. N., ZHONG, C. X. & DAWE, R. K. 2004. Centromere-encoded RNAs are integral components of the maize kinetochore. *Proc Natl Acad Sci U S A,* 101**,** 15986-91.

TROWITZSCH, S., BIENIOSSEK, C., NIE, Y., GARZONI, F. & BERGER, I. 2010. New baculovirus expression tools for recombinant protein complex production. *J Struct Biol,* 172**,** 45-54.

TURCO, E., GALLEGO, L. D., SCHNEIDER, M. & KOHLER, A. 2015. Monoubiquitination of histone H2B is intrinsic to the Bre1 RING domain-Rad6 interaction and augmented by a second Rad6-binding site on Bre1. *J Biol Chem,* 290**,** 5298-310.

UBERSAX, J. A., WOODBURY, E. L., QUANG, P. N., PARAZ, M., BLETHROW, J. D., SHAH, K., SHOKAT, K. M. & MORGAN, D. O. 2003. Targets of the cyclin-dependent kinase Cdk1. *Nature,* 425**,** 859-64.

VAN HOOFF, J. J., TROMER, E., VAN WIJK, L. M., SNEL, B. & KOPS, G. J. 2017. Evolutionary dynamics of the kinetochore network in eukaryotes as revealed by comparative genomics. *EMBO Rep,* 18**,** 1559-1571.

VAN HOOSER, A. A., OUSPENSKI, II, GREGSON, H. C., STARR, D. A., YEN, T. J., GOLDBERG, M. L., YOKOMORI, K., EARNSHAW, W. C., SULLIVAN, K. F. & BRINKLEY, B. R. 2001. Specification of kinetochore-forming chromatin by the histone H3 variant CENP-A. *J Cell Sci,* 114**,** 3529-42.

VANOOSTHUYSE, V., VALSDOTTIR, R., JAVERZAT, J. P. & HARDWICK, K. G. 2004. Kinetochore targeting of fission yeast Mad and Bub proteins is essential for spindle checkpoint function but not for all chromosome segregation roles of Bub1p. *Mol Cell Biol,* 24**,** 9786-801.

VERDAASDONK, J. S. & BLOOM, K. 2011. Centromeres: unique chromatin structures that drive chromosome segregation. *Nat Rev Mol Cell Biol,* 12**,** 320-32.

VISSEL, B. & CHOO, K. H. 1987. Human alpha satellite DNA--consensus sequence and conserved regions. *Nucleic Acids Res,* 15**,** 6751-2.

VLEUGEL, M., TROMER, E., OMERZU, M., GROENEWOLD, V., NIJENHUIS, W., SNEL, B. & KOPS, G. J. 2013. Arrayed BUB recruitment modules in the kinetochore scaffold KNL1 promote accurate chromosome segregation. *J Cell Biol,* 203**,** 943-55.

VON SCHUBERT, C., CUBIZOLLES, F., BRACHER, J. M., SLIEDRECHT, T., KOPS, G. & NIGG, E. A. 2015. Plk1 and Mps1 Cooperatively Regulate the Spindle Assembly Checkpoint in Human Cells. *Cell Rep,* 12**,** 66-78.

WADE, C. M., GIULOTTO, E., SIGURDSSON, S., ZOLI, M., GNERRE, S., IMSLAND, F., LEAR, T. L., ADELSON, D. L., BAILEY, E., BELLONE, R. R., BLOCKER, H., DISTL, O., EDGAR, R. C., GARBER, M., LEEB, T.,

MAUCELI, E., MACLEOD, J. N., PENEDO, M. C., RAISON, J. M., SHARPE, T., VOGEL, J., ANDERSSON, L., ANTCZAK, D. F., BIAGI, T., BINNS, M. M., CHOWDHARY, B. P., COLEMAN, S. J., DELLA VALLE, G., FRYC, S., GUERIN, G., HASEGAWA, T., HILL, E. W., JURKA, J., KIIALAINEN, A., LINDGREN, G., LIU, J., MAGNANI, E., MICKELSON, J. R., MURRAY, J., NERGADZE, S. G., ONOFRIO, R., PEDRONI, S., PIRAS, M. F., RAUDSEPP, T., ROCCHI, M., ROED, K. H., RYDER, O. A., SEARLE, S., SKOW, L., SWINBURNE, J. E., SYVANEN, A. C., TOZAKI, T., VALBERG, S. J., VAUDIN, M., WHITE, J. R., ZODY, M. C., BROAD INSTITUTE GENOME SEQUENCING, P., BROAD INSTITUTE WHOLE GENOME ASSEMBLY, T., LANDER, E. S. & LINDBLAD-TOH, K. 2009. Genome sequence, comparative analysis, and population genetics of the domestic horse. *Science,* 326**,** 865-7.

WALZTHOENI, T., CLAASSEN, M., LEITNER, A., HERZOG, F., BOHN, S., FORSTER, F., BECK, M. & AEBERSOLD, R. 2012. False discovery rate estimation for cross-linked peptides identified by mass spectrometry. *Nat Methods,* 9**,** 901-3.

WALZTHOENI, T., JOACHIMIAK, L. A., ROSENBERGER, G., ROST, H. L., MALMSTROM, L., LEITNER, A., FRYDMAN, J. & AEBERSOLD, R. 2015. xTract: software for characterizing conformational changes of protein complexes by quantitative cross-linking mass spectrometry. *Nat Methods,* 12**,** 1185-90.

WAN, X., O'QUINN, R. P., PIERCE, H. L., JOGLEKAR, A. P., GALL, W. E., DELUCA, J. G., CARROLL, C. W., LIU, S. T., YEN, T. J., MCEWEN, B. F., STUKENBERG, P. T., DESAI, A. & SALMON, E. D. 2009. Protein architecture of the human kinetochore microtubule attachment site. *Cell,* 137**,** 672-84.

WANG, G., MA, A., CHOW, C. M., HORSLEY, D., BROWN, N. R., COWELL, I. G. & SINGH, P. B. 2000. Conservation of heterochromatin protein 1 function. *Mol Cell Biol,* 20**,** 6970-83.

WANG, H., ZHAI, L., XU, J., JOO, H. Y., JACKSON, S., ERDJUMENT-BROMAGE, H., TEMPST, P., XIONG, Y. & ZHANG, Y. 2006. Histone H3 and H4 ubiquitylation by the CUL4-DDB-ROC1 ubiquitin ligase facilitates cellular response to DNA damage. *Mol Cell,* 22**,** 383-94.

WANG, X., CIMERMANCIC, P., YU, C., SCHWEITZER, A., CHOPRA, N., ENGEL, J. L., GREENBERG, C., HUSZAGH, A. S., BECK, F., SAKATA, E., YANG, Y., NOVITSKY, E. J., LEITNER, A., NANNI, P., KAHRAMAN, A., GUO, X., DIXON, J. E., RYCHNOVSKY, S. D., AEBERSOLD, R., BAUMEISTER, W., SALI, A. & HUANG, L. 2017. Molecular Details Underlying Dynamic Structures and Regulation of the Human 26S Proteasome. *Mol Cell Proteomics,* 16**,** 840-854.

WANG, Y. L., FAIOLA, F., XU, M., PAN, S. & MARTINEZ, E. 2008. Human ATAC Is a GCN5/PCAF-containing acetylase complex with a novel NC2-like histone fold module that interacts with the TATA-binding protein. *J Biol Chem,* 283**,** 33808-15.

WAYE, J. S. & WILLARD, H. F. 1987. Nucleotide sequence heterogeneity of alpha satellite repetitive DNA: a survey of alphoid sequences from different human chromosomes. *Nucleic Acids Res,* 15**,** 7549-69.

WEI, R. R., AL-BASSAM, J. & HARRISON, S. C. 2007. The Ndc80/HEC1 complex is a contact point for kinetochore-microtubule attachment. *Nat Struct Mol Biol,* 14**,** 54-9.

WEI, R. R., SORGER, P. K. & HARRISON, S. C. 2005. Molecular organization of the Ndc80 complex, an essential kinetochore component. *Proc Natl Acad Sci U S A,* 102**,** 5363-7.

WEIR, J. R., FAESEN, A. C., KLARE, K., PETROVIC, A., BASILICO, F., FISCHBOCK, J., PENTAKOTA, S., KELLER, J., PESENTI, M. E., PAN, D., VOGT, D., WOHLGEMUTH, S., HERZOG, F. & MUSACCHIO, A. 2016. Insights from biochemical reconstitution into the architecture of human kinetochores. *Nature,* 537**,** 249-253.

WEISSMANN, F., PETZOLD, G., VANDERLINDEN, R., HUIS IN 'T VELD, P. J., BROWN, N. G., LAMPERT, F., WESTERMANN, S., STARK, H., SCHULMAN, B. A. & PETERS, J. M. 2016. biGBac enables rapid gene assembly for the expression of large multisubunit protein complexes. *Proc Natl Acad Sci U S A,* 113**,** E2564-9.

WELBURN, J. P., VLEUGEL, M., LIU, D., YATES, J. R., 3RD, LAMPSON, M. A., FUKAGAWA, T. & CHEESEMAN, I. M. 2010. Aurora B phosphorylates spatially distinct targets to differentially regulate the kinetochore-microtubule interface. *Mol Cell,* 38**,** 383-92.

WESTHORPE, F. G., FULLER, C. J. & STRAIGHT, A. F. 2015. A cell-free CENP-A assembly system defines the chromatin requirements for centromere maintenance. *J Cell Biol,* 209**,** 789-801.

WILLARD, H. F. & WAYE, J. S. 1987. Chromosome-specific subsets of human alpha satellite DNA: analysis of sequence divergence within and between chromosomal subsets and evidence for an ancestral pentameric repeat. *J Mol Evol,* 25**,** 207-14.

WU, T. J., SHAMSADDINI, A., PAN, Y., SMITH, K., CRICHTON, D. J., SIMONYAN, V. & MAZUMDER, R. 2014. A framework for organizing cancer-related variations from existing databases, publications and NGS data using a High-performance Integrated Virtual Environment (HIVE). *Database (Oxford),* 2014**,** bau022.

XIAO, H., WANG, F., WISNIEWSKI, J., SHAYTAN, A. K., GHIRLANDO, R., FITZGERALD, P. C., HUANG, Y., WEI, D., LI, S., LANDSMAN, D., PANCHENKO, A. R. & WU, C. 2017. Molecular basis of CENP-C association with the CENP-A nucleosome at yeast centromeres. *Genes Dev,* 31**,** 1958-1972.

XIN, H., TAKAHATA, S., BLANKSMA, M., MCCULLOUGH, L., STILLMAN, D. J. & FORMOSA, T. 2009. yFACT induces global accessibility of nucleosomal DNA without H2A-H2B displacement. *Mol Cell,* 35**,** 365-76.

XU, M., LONG, C., CHEN, X., HUANG, C., CHEN, S. & ZHU, B. 2010. Partitioning of histone H3-H4 tetramers during DNA replication-dependent chromatin assembly. *Science,* 328**,** 94-8.

XUE, L. C., DOBBS, D. & HONAVAR, V. 2011. HomPPI: a class of sequence homology based protein-protein interface prediction methods. *BMC Bioinformatics,* 12**,** 244.

YAN, K., YANG, J., ZHANG, Z., MCLAUGHLIN, S. H., CHANG, L., FASCI, D., EHRENHOFER-MURRAY, A. E., HECK, A. J. R. & BARFORD, D. 2019. Structure of the inner kinetochore CCAN complex assembled onto a centromeric nucleosome. *Nature,* 574**,** 278-282.

YANG, Y., HEFFERNAN, R., PALIWAL, K., LYONS, J., DEHZANGI, A., SHARMA, A., WANG, J., SATTAR, A. & ZHOU, Y. 2017. SPIDER2: A Package to Predict Secondary Structure, Accessible Surface Area, and Main-Chain Torsional Angles by Deep Neural Networks. *Methods Mol Biol,* 1484**,** 55-63.

YANG, Y., WU, F., WARD, T., YAN, F., WU, Q., WANG, Z., MCGLOTHEN, T., PENG, W., YOU, T., SUN, M., CUI, T., HU, R., DOU, Z., ZHU, J., XIE, W., RAO, Z., DING, X. & YAO, X. 2008. Phosphorylation of HsMis13 by Aurora B kinase is essential for assembly of functional kinetochore. *J Biol Chem,* 283**,** 26726-36.

YARDIMCI, H., VAN DUFFELEN, M., MAO, Y., ROSENFELD, S. S. & SELVIN, P. R. 2008. The mitotic kinesin CENP-E is a processive transport motor. *Proc Natl Acad Sci U S A,* 105**,** 6016-21.

YASUI, D., MIYANO, M., CAI, S., VARGA-WEISZ, P. & KOHWI-SHIGEMATSU, T. 2002. SATB1 targets chromatin remodelling to regulate genes over long distances. *Nature,* 419**,** 641-5.

YODA, K., ANDO, S., MORISHITA, S., HOUMURA, K., HASHIMOTO, K., TAKEYASU, K. & OKAZAKI, T. 2000. Human centromere protein A (CENP-A) can replace histone H3 in nucleosome reconstitution in vitro. *Proc Natl Acad Sci U S A,* 97**,** 7266-71.

YONG-GONZALEZ, V., WANG, B. D., BUTYLIN, P., OUSPENSKI, I. & STRUNNIKOV, A. 2007. Condensin function at centromere chromatin facilitates proper kinetochore tension and ensures correct mitotic segregation of sister chromatids. *Genes Cells,* 12**,** 1075-90.

YOO, T. Y., CHOI, J. M., CONWAY, W., YU, C. H., PAPPU, R. V. & NEEDLEMAN, D. J. 2018. Measuring NDC80 binding reveals the molecular basis of tension-dependent kinetochore-microtubule attachments. *Elife,* 7.

YU, C., GAN, H., SERRA-CARDONA, A., ZHANG, L., GAN, S., SHARMA, S., JOHANSSON, E., CHABES, A., XU, R. M. & ZHANG, Z. 2018. A mechanism for preventing asymmetric histone segregation onto replicating DNA strands. *Science,* 361**,** 1386-1389.

ZASADZINSKA, E., HUANG, J., BAILEY, A. O., GUO, L. Y., LEE, N. S., SRIVASTAVA, S., WONG, K. A., FRENCH, B. T., BLACK, B. E. & FOLTZ, D. R. 2018. Inheritance of CENP-A Nucleosomes during DNA Replication Requires HJURP. *Dev Cell,* 47**,** 348-362 e7.

ZHANG, G., LISCHETTI, T. & NILSSON, J. 2014. A minimal number of MELT repeats supports all the functions of KNL1 in chromosome segregation. *J Cell Sci,* 127**,** 871-84.

ZHANG, W., MAO, J. H., ZHU, W., JAIN, A. K., LIU, K., BROWN, J. B. & KARPEN, G. H. 2016. Centromere and kinetochore gene misexpression predicts cancer patient survival and response to radiotherapy and chemotherapy. *Nat Commun,* 7**,** 12619.

ZINK, L. M. & HAKE, S. B. 2016. Histone variants: nuclear function and disease. *Curr Opin Genet Dev,* 37**,** 82-89.

ZOLLMAN, S., GODT, D., PRIVE, G. G., COUDERC, J. L. & LASKI, F. A. 1994. The BTB domain, found primarily in zinc finger proteins, defines an evolutionarily conserved family that includes several developmentally regulated genes in Drosophila. *Proc Natl Acad Sci U S A,* 91**,** 10717-21.

7. Table of Figures

8. Abbreviations

Abbreviation	Explanation
AEBP2	Adipocyte Enhancer-Binding Protein 2
AP-MS	Affinity Purification Mass Spectrometry
APC	Anaphase-Promoting Complex
ASF1	Anti-Silencing Function Protein 1
ATP	Adenosine Triphosphate
ATPase	Adenosine Triphosphatase
ATRX	Alpha Thalassemia/Mental Retardation syndrome X-linked
BAZ1	Bromodomain Adjacent to Zinc Finger Domain
BS2G	Bis-Sulfosuccinimidyl Glutarate
BSA	Bovine Serum Albumin
BTB	Broad-Complex, Tramtrack and Bric a brac
CAF1	Chromatin Assembly Factor 1
CAL1	Chromosome Alignment Defect 1
CATD	CENP-A targeting domain
CCAN	Constitutive Centromere Associated Network
CDE	Centromere DNA Elements
CDK	Cyclin-dependent Kinase
CENP	Centromere Protein
CH	Calponin Homology
CHD	Chromodomain-Helicase-DNA-Binding Protein
ChIP	Chromatin-Immunoprecipitation
CHRAC	Chromatin Accessibility Complex
CID	Collision Induced Dissociation
COMA	Ctf19, Okp1, Mcm21, and Ame1
CPC	Chromosomal Passenger Complex
CSE4	Chromosome Segregation 4
DAXX	Death Domain-Associated Protein 6
DDB1	DNA Damage-Binding Protein 1
DDX21	DExD-Box Helicase 21
DMEM	Dulbecco's Modified Eagle's Medium
DMSO	Dimethyl Sulfoxide
DNA	Deoxyribonucleic Acid
DNMT	DNA-Methyltransferases
DPOE	DNA Polymerase Epsilon Complex
DR1	Down-Regulator of Transcription 1

Abbreviation	Explanation
DRAP1	DR1 Associated Protein 1
DTT	Dithiothreitol
dTTP	deoxythymidine triphosphate
EDTA	Ethylenediamine Tetraacetic Acid
EED	Embryonic Ectoderm Development
EGTA	Ethylene Glycol Tetraacetic Acid
EM	Electron Microscopy
EMSA	Electrophoretic Mobility Shift Assay
EZH2	Enhancer of Zeste 2 Polycomb Repressive Complex 2 Subunit
FACT	Facilitates Chromatin Transcription
FCS	Fetal Calf Serum
FRB	FKBP-Rapamycin Binding
FRET	Fluorescence Resonance Energy Transfer
GLEBS	Gle2-Binding-Sequence
GTPase	Guanosine Triphosphatase
HAT	Histone Acetyl Transferase
HCl	Hydrogen Chloride
HDAC	Histone Deacetylase
HEPES	N-2-hydroxyethylpiperazine-N-ethanesulfonic acid
HIRA	Histone Regulator A
HJURP	Holliday Junction Recognition Protein
HORs	Higher-Order Repeat
HP1	Heterochromatin Factor 1
HRP	Horseradish Peroxidase
iBAQ	Intensity Based Absolute Quantification
INCENP	Inner Centromere Protein
IP	Immunoprecipitation
IPTG	Isopropyl β- d-1-Thiogalactopyranoside
ITC	Isothermal Titration Calorimetry
JARID2	Jumonji and AT-Rich Interaction Domain Containing 2
KAT	K (lysine) Acetyltransferase
KMN	KNL1/MIS12/NDC80
KNL1	Kinetochore-Null Protein 1
LC-MS	Liquid Chromatography Mass Spectrometry
LFQ	Label-Free Quantification
Mad2	Mitotic Arrest Deficient 2
MCC	Mitotic Checkpoint Complex
MCM	Minichromosome Maintenance Complex
MELT	Methionine, Glutamic acid, Leucine, Threonine

Abbreviation	Explanation
MHC	Major Histocompatibility Complex
MMR	Mismatch Repair
MNase	Micrococcal Nuclease
MPS1	Monopolar spindle protein 1
MS	Mass Spectrometry
MSH	MutS Protein Homolog
NAP1	Nucleosome Assembly Protein 1
NC2B	Negative Cofactor 2-Beta
NCP	Nucleosome Core Particle
NHS	N-Hydroxysuccinimide
NPM	Nucleophosmin
PBD	Polo Box Domain
PBS	Phosphate Buffered Saline
PCNA	Proliferating Cell Nuclear Antigen
PCR	Polymerase Chain Reaction
PEST	Rich in Proline (P), Glutamic Acid (E), Serine (S), and Threonine (T)
PGK1	Phosphoglycerate Kinase 1
PHD	Plant Homeodomain
PLK1	Polo-Like Kinase 1
POL	Polymerase
PP	Protein Phosphatase1
PPIs	Protein-Protein Interactions
PRC2	Polycomb Repressive Complex 2
pre-RC	pre-Replication Complex
PTM	Post-Translational Modifications
qXLMS	Quantitative Mass Spectrometric Analysis of Crosslinked Proteins
rASA	Relative Accessible Surface Area
RbAp46/RBBP7	Retinoblastoma Binding Protein 7
RbAp48/RBBP4	Retinoblastoma Binding Protein 4
RBX1	Ring-Box 1
RING	Really Interesting New Gene
RIPI	Relative Interface Propensity Index
RacGap	Rac GTPase activating protein
RNA	Ribonucleic Acid
RNAi	RNA interference
RNAPII	RNA Polymerase II
RNase	Ribonuclease
RPA	Replication Protein A

Abbreviation	Explanation
RSF	Remodeling and Spacing Factor
RT	Room Temperature
RWD	domain in RING finger and WD repeat containing proteins
RZZ	Rod, Zwilch, ZW10
SAC	Spindle Assembly Checkpoint
SATB1	Special AT-Rich Sequence-Binding Protein 1
SD	Standard Deviation
SDS-PAGE	Sodium Dodecyl Sulfate Polyacrylamide Gel Electrophoresis
SEC	Size Exclusion Chromatography
SETDB1	SET Domain Bifurcated Histone Lysine Methyltransferase 1
SILAC	Stable Isotope Labeling By/With Amino Acids in Cell Culture
SMARCA5	SWI/SNF-Related Matrix-Associated Actin-Dependent Regulator of Chromatin Subfamily A Member 5
SMARCC1	SWI/SNF Related, Matrix Associated, Actin Dependent Regulator of Chromatin Subfamily C Member 1
SMC2	Structural Maintenance of Chromosomes Protein 2
SNF	Sucrose Nonfermenting
SPR	Surface Plasmon Resonance
SPT16	Suppressor of Ty 16
ssDNA	Single Stranded DNA
SSRP1	Structure-Specific Recognition Protein 1
SUZ12	Suppressor of Zeste 12 Protein Homolog
SWI/SNF	Switch/Sucrose Nonfermenting
TBP	TATA-Box Binding Protein
TOPP-qXL	The OpenMS Proteomics Pipeline-quantitative XLMS
UBP10	Ubiquitin Carboxyl-Terminal Hydrolase 10
UHRF1	Ubiquitin Like with PHD And Ring Finger Domains 1
USP10	Ubiquitin Specific Peptidase 10
WICH	WSTF-ISWI chromatin remodeling complex
XRCC5	X-Ray Repair Cross Complementing 5
Y2H	Yeast Two-Hybrid Screening
YPD	Yeast Extract-Peptone-Dextrose
ZBTB9	Zinc Finger and BTB Domain Containing 9
ZW10	Zeste-white 10

9. Acknowledgements

I want to express my deep gratitude to everyone who contributed to this work in some way or another:

A big thank you to Franz Herzog for giving me the opportunity to work in his laboratory on such an exciting topic. Thank you for the support and the trust you put in me over the past years. I am very grateful for the freedom you gave me to expand my knowledge and develop as a scientist. It was a real pleasure to be part of your team!

Many thanks to Stefan Westermann and all my dissertation committee members for taking the time to read and evaluate this thesis.

I like to thank all past and present members of the Herzog group for constructive feedback, lively discussions, and any support for experiments. I especially want to thank Victor Solis-Mezarino, a massive help with his bioinformatics and data analysis expertise, as well as encouragement and patience. Further, I want to thank Sylvia Singh for her critical reading and mad pipetting skills, discussions, and plenty of good advice that I got from her along the way. A big thank you also to Medini Ghodgaonkar-Steger, Josef Halwachs-Fischboeck, Mia Potocnjak, Chandni Kumar, and Tea Speljko. I enjoyed every day working with you!

During my doctoral studies, I was lucky to be part of the GRK1721. Therefore, I like to thank Karl-Peter Hopfner, Petra Runge-Wollmann, Beate Hafner, and all members of the GRK1721 Graduate Program for financial and ideational support during my PhD thesis. I gained much knowledge during Conferences, Retreats, and Summer Schools supported by the Graduate network; moreover, I grew personally as a graduate school member. It was a precious experience, and many thanks, Petra and Beate, for all your support and enthusiasm within the GRK1721.

Many thanks to all colleagues within the GeneCenter for sharing reagents, protocols, and experience. Especially Stephan Woike, who was always on point and gave significant input during "telephone conferences." It was great fun to work with you.

Of course, I want to thank my mother, grandparents, and family. Without your love and support, I would have never gotten to this point. I am more than thankful for all advice and sorry for the sleepless nights I might have caused you.

This work would have never been possible without my loving wife. Dear Lisa, thank you for your constant support and understanding along this journey. This may sound cheesy, but I can't wait for our future to begin!